predictive mineral discovery
COOPERATIVE RESEARCH CENTRE

pmd*CRC

Final Report

Fluid Chemical Paths in Ore Forming Processes

Fluids Project: F1/2

Editor: Prof. Nick Oliver

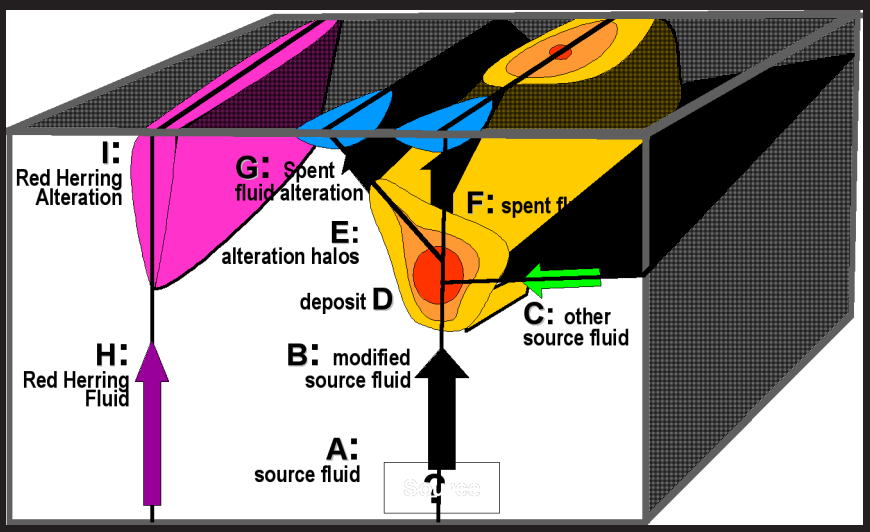

Key elements of a generic geochemical concept model (courtesy Dr Lesley Wyborn)

CSIRO · AMIRA INTERNATIONAL · Australian Government Geoscience Australia · MONASH University · THE UNIVERSITY OF MELBOURNE · JCU James Cook University · THE UNIVERSITY OF WESTERN AUSTRALIA

F1-2: Fluid Chemical Paths in Ore Forming Processes

Final Report (2002 – 2005)

Many ore discoveries followed industry's use of the inversion and rapid interpretation of aeromagnetic geophysical data. Very little such utilisation has ever occurred with geochemistry, because there is a perception that it is "disconnected from discovery". Our project was set up to change that perception. Our project considered all of the chemical source, transport and deposition issues for selected deposit styles in the industry-led environment of the CRC, attempting to contribute to a change in exploration practice that seeks process-driven target vectors rather than empirical "bullseyes". The project produced improved total system ore genesis models, a comprehensive up-to-date database and associated software tools for hydrothermal geochemistry modelling, and a range of short-course and poster-style deliverables.

The ***pmd****CRC* team for the F1/F2 project was as follows:

Role	Name	Affiliation
Program Coordinator:	Prof Nick Oliver	James Cook University
Project leader:	Prof Nick Oliver (until 2004); James Cleverley	James Cook University
Team Members:	Dr James Cleverley	James Cook University
	Dr Evgeniy Bastrakov	Geoscience Australia
	Dr Andy Wilde	Monash University
	Dr Michael Kühn	CSIRO
	Dr Peter Hornby	CSIRO
	Prof Bruce Hobbs	CSIRO
	Dr Rob Woodcock	CSIRO
Academic Contributors	Dr Yuri Shvarov	Moscow State University
	Dr Lesley Wyborn	Geoscience Australia
	Dr John Walshe	CSIRO
	Dr Andy Barnicoat	Geoscience Australia
	Dr Paul Roberts	CSIRO
	Dr Tim Baker	James Cook University
	Dr Mike Rubenach	James Cook University
	Dr Peter Neumayr	University of Western Australia
	Dr Alison Ord	CSIRO
	Dr Geordie Mark	Monash University
	Dr David Cooke	University of Tasmania
	Dr Joel Brügger	University of Adelaide / Museum of South Australia
	Dr Bear McPhail	Australian National University
	Dr Weiwha Liu	University of Adelaide
Industry Contributors	Mr Nick Fox	AngloGold
	Mr Abhen Pather	AngloGold
	Dr Doug Mason	Doug Mason & Co.
	Dr Ed Mikucki	Ed Mikucki & Associates
	Mr Greg Hall	Placer Dome Asia Pacific
	Dr Susan Dreiberg	Placer Dome Asia Pacific
PhD Student	Ms Martina Bertelli	James Cook University

Contents

Executive Summary: Lowering exploration risk through predictive geochemical modeling

Nicholas H. S. Oliver and James S. Cleverley

Introduction & goals

The gathering, processing and interpretation of aeromagnetic and structural data have already become standard tools in metalliferous exploration techniques. Now that new tools are available to simulate, replicate, and predict alteration patterns and geochemistry, there is potential for these techniques to complement or exceed the capacity of existing geophysical techniques. Alteration datasets are starting to be more widely used in exploration (e.g. PIMA, Aster, Hymap) but their potential is limited by uncertainty in connection between the data patterns and fluid/rock interactions that specifically vector towards mineralization. By coupling predicted geochemistry with:

1. forward modelled geophysics,
2. statistical treatment of alteration geochemistry datasets, and
3. geological and numerical simulations of fluid flow patterns,
   we aim to produce a predictive tool for mineral deposit exploration.

At the conclusion of the F1-2 project, we are in a position to:

1. Predict the processes that led to formation of certain mineral deposits.
2. Predict possible alteration assemblages and mineral paragenesis.
3. Understand which are the most important or effective processes in mineral deposit formation.
4. Start to build computer models of mineral deposit formation.

By the end of the CRC several companies should be routinely using these techniques to lower exploration risk, reduce expenditure, and shorten times towards discovery. Implementation of the techniques will require improved on-site and other training, semi-automated conversion of model results into 3D datasets and models, and persistent interchange between researchers and explorers.

Principles of the approach

Geochemical modeling is directed towards solution of the patterns and vectors indicated in the schematic figure. The purpose is to be able to take existing or new geochemical, petrographical and/or fluid inclusion datasets and identify fluid pathways of interest both to a total system understanding and also to specific patterns that provide spatial constraints on exploration lease potential (or lack thereof). Datasets routinely gathered by exploration companies are mostly perfectly suitable for inclusion into the modeling approach, which depends mostly on knowledge of whole-rock geochemistry and/or mineral assemblage data for less- and more-altered rocks. The starting point is a concept model, which is a spatially and temporally expressed geological visualization of the exploration model. The very least the geochemical modeling can achieve is to allow explorers

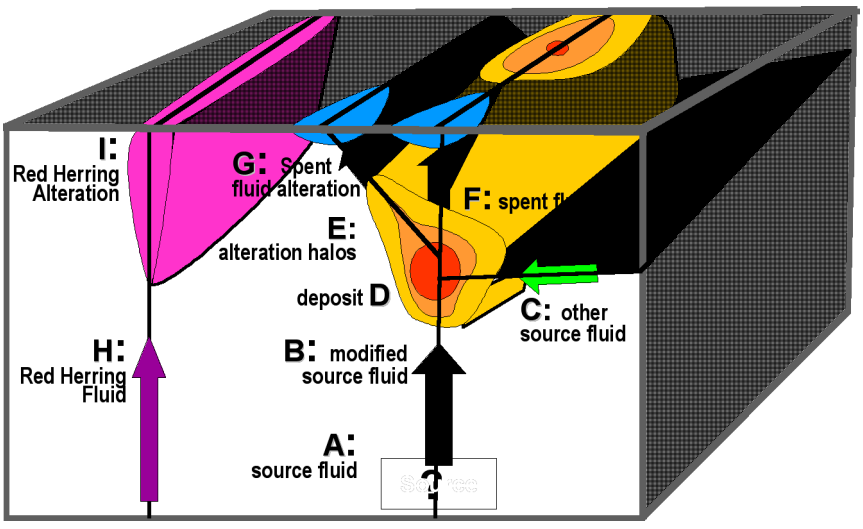

Figure 1. Key elements of a generic geochemical concept model (Figure courtesy Lesley Wyborn).

to produce better concept models, which in turn can assist refining exploration models.

What are concept models?

- Before computer modelling you need to know:
  - The problem that you are tackling,
  - What you hope to achieve and
  - Understand the limitations and assumptions
- Need to build concept models
  - Geological observation or Modelling cartoon
- Geochemical models are based on geological concept

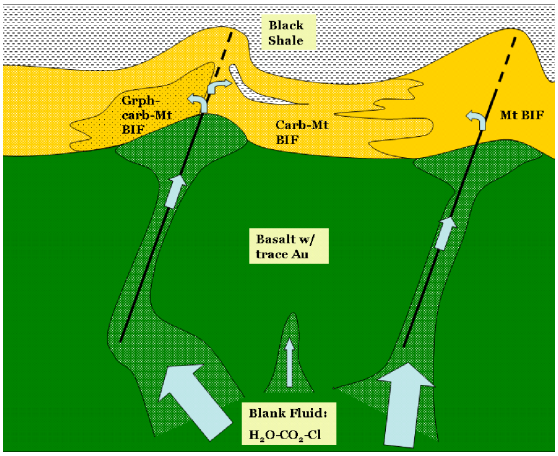

Figure 2. Geological/geochemical concept model pertinent to BIF-hosted lode gold deposits, specifying possible fluid flow paths, sources, alteration distributions and relationship to mineralisation.

What can the geochemical modelling do for exploration - summary

Output	Use for exploration
Replicated alteration zoning that matches known sequences and spatial patterning of observed alteration zoning around known mineral deposits	Verification or modification of existing concept model that can then be used to modify exploration model
Prediction of the type of alteration zonation that would be produced by spent ore fluids at lower P and T than the conditions of ore formation	Testable geochemical/alteration targets in rocks potentially lying above hidden orebodies
Prediction of types of alteration that may be produced by fluids that do not relate to ore-forming processes	Capacity to drop ground to focus on more prospective targets
Prediction of types of alteration, and their zonation, that would be produced in rocktypes other than the known ore hosts for a particular geological/geochemical concept model	Alternative targets not previously considered by earlier concept model
Replication of low grade and high grade parts of existing orebodies	Explanation for grade distribution that may enter into mine planning and brownfields exploration
Recognition of key ore-forming processes, e.g. fluid mixing versus wallrock reaction versus T gradients	Increase in confidence of detail of ore genesis model, allowing more reliable translation into exploration model, e.g. do we need to find two fluid pathways coinciding in order to get tonnes and grade?
For any of the above, extraction of information from models that can be used to calculate magnetic response, density, Aster or PIMA response, radiometric response	Potential for fusion of geochemical data into geophysical inversions using knowledge-based approach rather than just data-driven approach; capacity to better select targets under cover
Engagement of company staff with geochemical modellers and researchers	Stimulation of work environment and longer staff retention time
Improved understanding of geochemistry by exploration group	Encourage staff to broaden their thinking regarding ground selection, drill targets, ground dropping, and engagement with middle- to upper management with confidence

Filtering poor geological models (or tipping over barrows)

Long standing consensus on concept models, or highly persuasive personalities with strongly held views within research or exploration environments, do not necessarily permit positive changes in exploration practice. The geochemical modeling approach is a new way to open mental barriers and systematically test alternatives, without prejudice.

For example, the long-standing model for genesis of Archean lode gold deposits involves, in essence, regional metamorphism releasing basalt-equilibrated fluids into focused shear zones, whereupon reaction of these fluids (typically at lower P and T) with iron-rich wallrocks causes sulphidation of these rocks, destabilization of soluble gold sulphide species, and precipitation of gold. Expressed this way, the model necessitates exploration strategies focusing on 1) Basalt-bearing greenstone sequences, 2) evidence for

retrograde shearing, 3) particular structural sites, 4) iron-rich potential host rocks, and 5) the channeling of generic fluid sideways and upwards into specific structures.

Other models expand on or refute this concept, proposing that pre- to syn-tectonic granitoids provided a thermal structure in which cooler, denser fluid was drawn inwards towards hotter granite and/or granite gneiss cores during prograde metamorphism, and subsequently precipitated gold on a cooling path (Witt et al., 1997). Still other models have speculated that both heat and fluids were derived from granitoids, with reaction between oxidized granite-derived fluids and reduced rocks (or reduced fluids) causing gold precipitation (Neumayr et al., 2003; Walshe et al., 2003).

So how do we go about determining whether granitoids are important for gold or not? A relatively time-consuming and somewhat expensive method is to embark on a comprehensive geochronological program. A

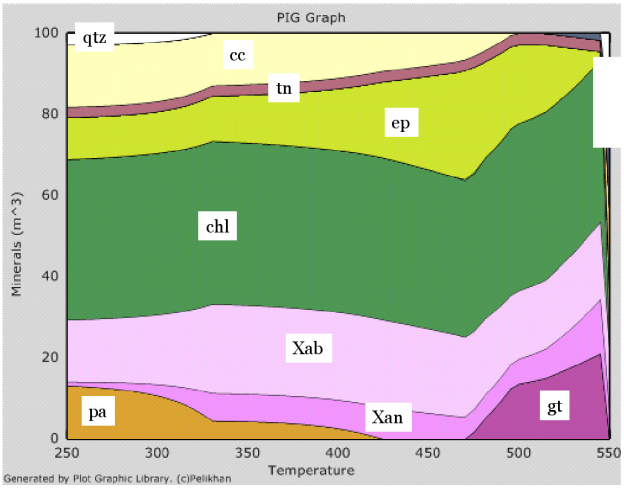

Figure 3. Case 1: Granites provided heat only and were not involved in fluid transfer. Here we took the assemblage known from the low temperature end for a series of basaltic conglomerates, and applied a thermal gradient from the right, without fluid infiltration (Xan = anorthite component of plagioclase, Xab = albite component, gt = garnet, pa = paragonite, chl = chlorite, ep = epidote, tn = titanite, cc = calcite, qtz = quartz). Heat source (syenite) is on the right. The pattern does not match observed field data (Wallaby, Yilgarn)

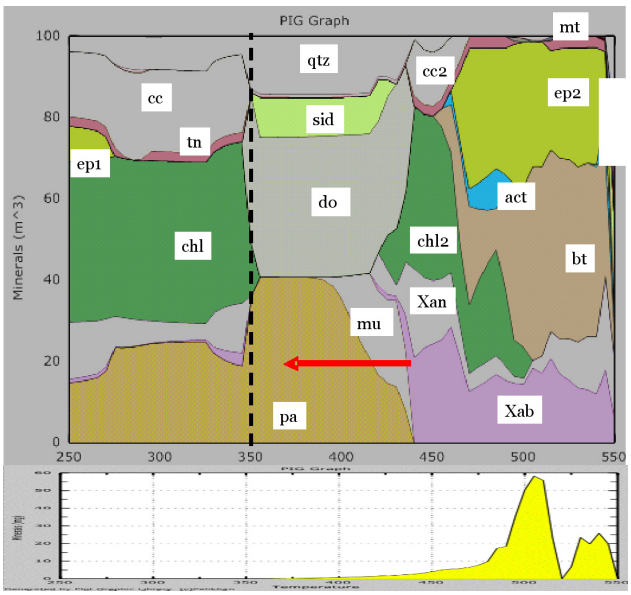

Figure 4. (upper), Case 2: Granitoid (syenite) provides thermal and fluid input. Here we derived a syenite-related fluid using the modelling code HCh, and then infiltrated that fluid (right to left) down the temperature gradient surrounding the intrusion. In this case, the model demonstrated that the syenite was responsible for much of the proximal alteration to the deposit. (bt = biotite, do = dolomite, sid = siderite, mu = muscovite, act = actinolite, mt = magnetite)

Figure 5. (lower) However, if it is assumed that both gold and sulphur are carried with the magmatic-related fluid, then gold dumps at high temperature, which is inconsistent with the known low-T gold association.

much simpler test is to construct geochemical models within which granites are important, or not, and see if the outcomes match the known distribution of mineral assemblages.

Fluid path and outflow modeling

Geochemical models have a capacity to predict alteration patterns in the fluid outflow parts of ore deposition. Naturally this presents some scope for detection of distal haloes, particularly above buried deposits.

In a second example, we simply took a lode gold fluid after it had dumped gold at 380°C, and ran it into the overlying rocks along a temperature gradient. However, we also looked at the lateral halo around the orebody at 380°C, and similarly ran those spent fluids (once they'd done their alteration work) into the overlying cooler rocks. Basically this is attempting to see what type of pattern at lower grade would correspond to a bullseye effect at depth:

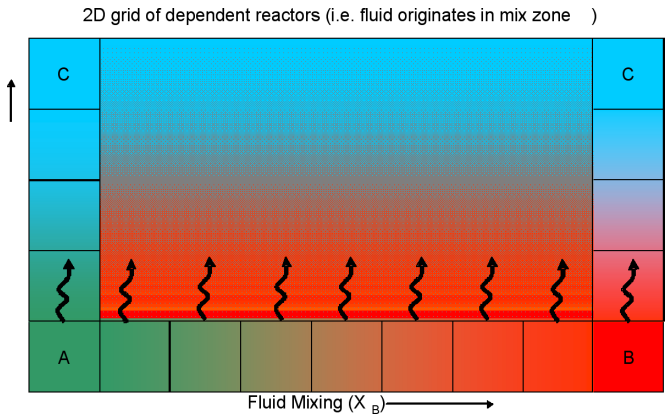

Figure 6. The principal of outflow modeling. Here, the concept model is that Cu-Au ore is produced by mixing of two fluids A (an HCOS fluid) and B (a brine). The squiggly arrows represent the effluent fluid leaving the ore deposition site and infiltrating into the adjacent wallrock. Ideally the simulations would pick up aspects of the zonation that reflects both the ore depositional process, and the zones in which Cu and Au are coprecipitated (e.g. in an IOCG deposit)

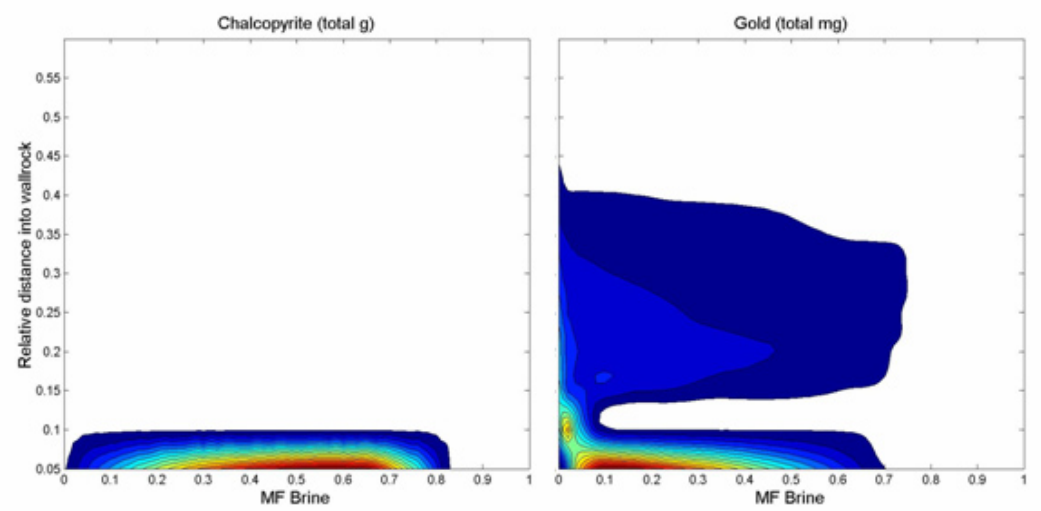

Figure 7. Modeled chalcopyrite and gold reveals a weak gold halo distal to the fluid mixing zone.

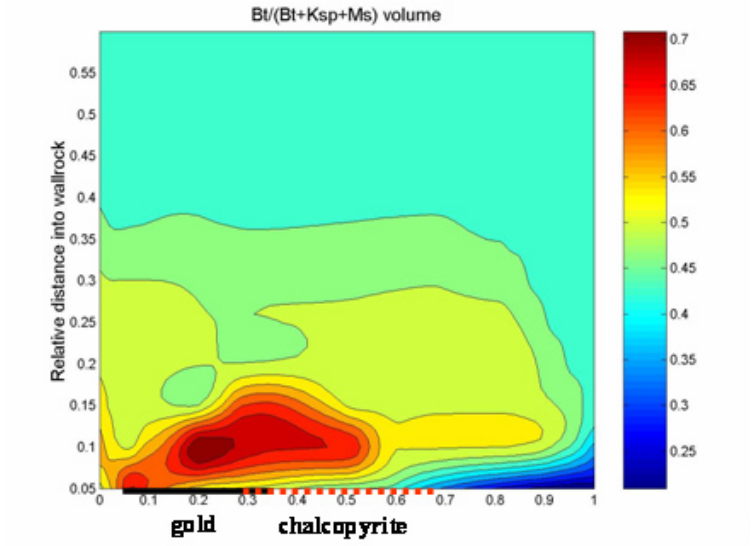

Figure 8. The outflow above the zone of richest Cu and Au is marked by a zone of biotite predominance over other K-bearing minerals.

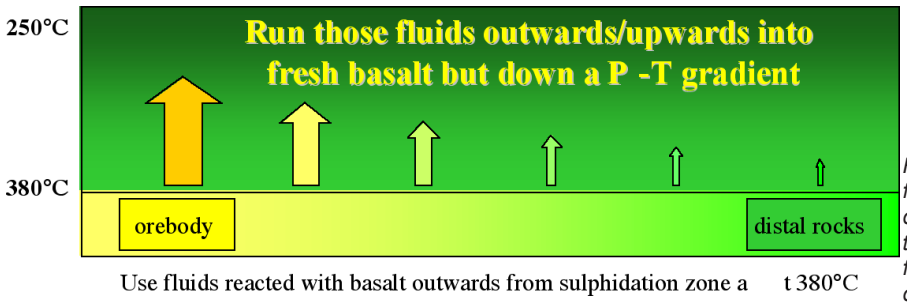

Figure 10: concept model for a) lateral flow away from a mineralization site at depth (produced by sulphidation from left to right), followed by allowing the spent fluid to infiltrate into the overlying rocks down a T gradient.

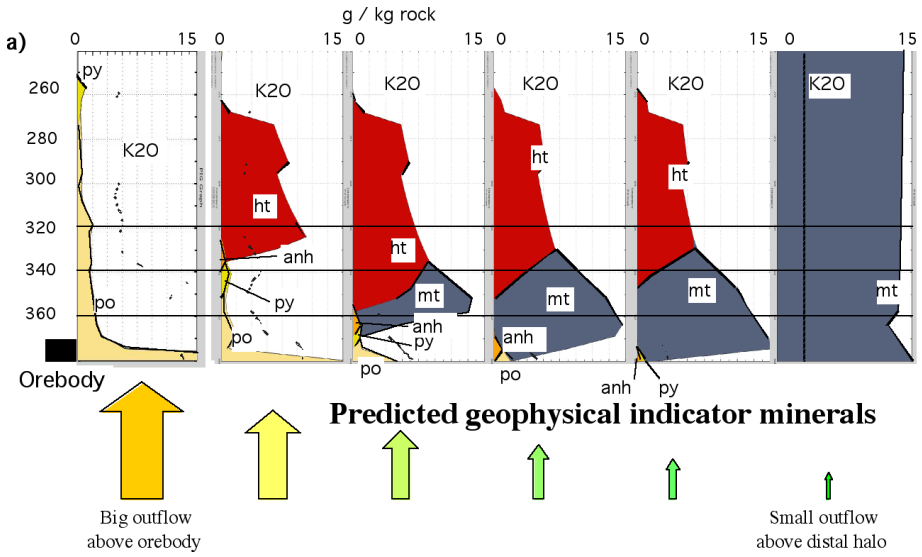

Figure 11: We then calculated the mineral assemblages and extracted out those minerals which may have a definable geophysical signal. The horizontal lines might represent the zoning one would observe at progressively higher crustal levels (T on left axis). Predicted geophysical signals could be calculated (see below).

Predictive geophysics

An exciting development has been in the area of predicted aeromagnetics, gravity, radiometrics, electrical response and PIMA response arising from geochemical simulations. There are some ongoing developments in Phase 2 of the ***pmd****CRC* that are considering the processes needed to be able to incorporate geochemical model results into predictive geophysical models and inversions.

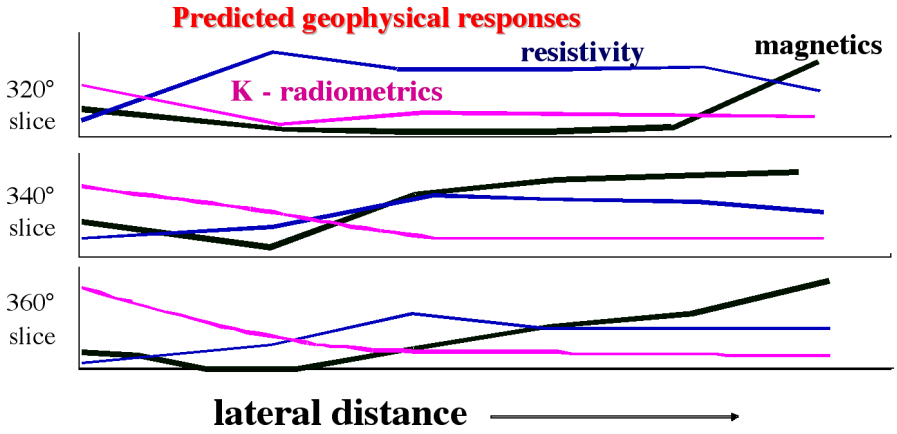

Figure 12: Following on from the model above, we have developed at least a conceptual modeling protocol whereby we can determine semi-quantitative or qualitative (as in this case) geophysical responses to the modeled outflow scenarios. The challenge now is to routinely incorporate such outputs into the model results and test them against real datasets.

Conclusions: Analysis of the strengths, weaknesses, opportunities and threats to using predictive geochemistry for exploration

Strengths: We now have a unified thermodynamic database, being used in several modeling packages (HCh, GWB, Fastflo), that will ensure stability and a high degree of communication and collaboration in the future. The software running these models has improved greatly in the life of the CRC, and, together with software modules developed by this team, means that the modeling techniques are now much more utilitarian and portable. We have demonstrated the power of the modeling in several ore deposit types, the best results being generated in modeling of greenschist-facies lode gold systems. The number of people using the software has improved throughout the life of the CRC.

Weaknesses: The software tools remain in the hands of expert academic users and some postgraduate students. This is likely to remain the pattern for the foreseeable future until the training exercises to demonstrate the software useage have substantial impact (i.e. new users of the software). The database

does not readily handle high salinity fluids, so shortcuts taken in modeling IOCGs (for example) could produce somewhat erroneous results that may be difficult to directly interpret in the context of known or targeted alteration or mineralization types. There are issues with some complex minerals particularly in the area of poor activity-composition models for solid solutions, including many amphiboles, garnet, and some chlorite and carbonates. The rate at which these thermodynamic/experimental issues can be solved is very slow relative to the software speed and growth of useage of the modeling techniques.

Opportunities: There is still immense opportunity for industry to use these techniques in routine and novel exploration programs. There is a great opportunity to further develop short courses around these models and train new users to expert or semi-expert levels. There are great opportunities remaining in attempting to fuse geochemical model outputs with predictive geophysical signals. There are opportunities, currently being explored, in the area of fusion of geochemical with geomechanical modeling.

Threats: The biggest threat lies in developing critical mass of expertise at several research and industry nodes that has the capacity to use and understand the models. This is essentially a communication and training issue. Threats are apparent in that the models to date have not publically been associated with a major exploration success, and unless such an association is made then the take-up by industry may wane after the CRC finishes. Other external threats relate to the health of the minerals and tertiary education sectors overall.

Chapter 1: Theoretical tools of exploration geochemistry

N.H.S. Oliver[1], J.S. Cleverley[1] and E. N. Bastrakov[2]

Predictive Mineral Discovery Cooperative Research Centre @
1. James Cook University School of Earth Sciences, Townsville, 4811, Australia; and
2. Geoscience Australia, PO Box 378, Canberra, 2601, Australia

This paper is modified from the following source:
Oliver, N.H.S., Cleverley, J.S., & Bastrakov, E.N., 2004. Modelling hydrothermal systems: a future for exploration geochemistry. In: Muhling, J. et al. (eds), Predictive Mineral Discovery Under Cover. Centre for Global Metallogeny, University of Western Australia, Publication No. 33, p.62-66.

Abstract

Recent advances in geochemical modelling may yet breathe life into mineral exploration. Empirically based exploration geochemistry has seen few improvements in the last decade and its use as a mainstream exploration tool is in decline. The inherent complexities of geochemical thermodynamics and geochemical modelling in general have also hindered progress in the educational and academic sectors. The Predictive Mineral Discovery CRC (***pmd****CRC*) has formed a core geochemical modelling group as the hub of a broader Australian collaboration, and significant progress has been made on many of the problem areas. Here we demonstrate some applications of this new technology to mineral exploration, with examples of fluid-rock reaction, the role of intrusions, outflow above buried deposits, dispersion haloes, and forward modelling of geophysical signatures, in greenstone terranes.

The core to the new models is a web-enabled thermodynamic database, FreeGs, consistent with the Geoscience Australia version of the UNITHERM database (Bastrakov et al. 2004b). The operating software is HCh (Shvarov 1999; Shvarov & Bastrakov 1999), presently the benchmark for geochemical modelling in the ***pmd****CRC*. HCh can be used across a temperature range of 0–1000°C and pressures up to 500 MPa. This broad range of possible P-T conditions provides one of the biggest advantages of HCh over conventional log K based codes that are either restricted to the vapor saturation curve of water, or to constant pressures. In this regard it extends the potential for such modelling into the P-T realm of lode gold and IOCG deposits, and into porphyry Cu-Au.

Setting up a model – the required inputs and philosophy

Commonly, the act of construction of the geochemical model provides greater insights than the model results! The modelling has the capacity to greatly influence and improve a rigorous approach to ranking various exploration criteria, but individual results only infrequently provide a unique solution to an exploration problem. Rather, a series of models can give insight into which aspects of an existing strategy are flawed, and which types of fluid-rock scenarios and pathways are likely to have led to mineralization. Typically, inputs to a model include whole rock geochemistry or estimates of the modal mineralogy of fresh and/or altered rocks. A knowledge of the range of P-T conditions of interest is highly desirable. Fluid compositions are usually the most difficult aspect to define, but can be derived through intuition or experience (with particular consideration of pH and f_{O2}), fluid inclusion analysis, and modelling of mineral stabilities using the software. Typically a combination of these three approaches provides the best solution. The simplest scenario of Fresh Rock A + Fluid = Altered Rock B can be used to broadly bracket fluid compositions if Rocks A and B are known. Alternately, if the altered rock has sufficient minerals to buffer most fluid species of interest, then an excess of Altered Rock B and a small amount of Simple Fluid 1 (e.g. H_2O-HCl) can produce, via mineral-fluid equilibriation, a Complex Fluid 2 in equilibrium with Altered Rock B. Once these fluid compositions have been established, an excess of these fluids can be used to populate other models.

Granites in greenstones – heat or fluid sources?

Many ore deposit models contain inherent uncertainties concerning the role of intrusions, irrespective of depth of ore formation. For example, some models for Archean lode gold deposits appeal mostly to derivation of gold and fluids from the metamorphic pile, with gold leached at depth and precipitated during retrogression, characteristically in brittle-ductile shear zones (Groves 1993). Other models expanded on this concept, proposing that pre- to syn-tectonic granitoids provided a thermal structure in which cooler, denser

fluid was drawn inwards towards hotter granite and/or granite gneiss cores during prograde metamorphism, and subsequently precipitated gold on a cooling path (Witt et al. 1997). Still other models have speculated that both heat and fluids were derived from granitoids, with reaction between oxidized granite-derived fluids and reduced rocks (or reduced fluids) causing gold precipitation (Neumayr et al. 2003; Walshe et al. 2003). These controversies remain at the forefront of research in this area, and impact significantly on exploration. We demonstrate here, for realistic greenstone assemblages, the effects of simple heating and cooling around intrusions, as well as the effects of both outwards and inwards fluid flow, building on some of the generic numerical models pertinent to metamorphic fluids and gold considered by Bastrakov et. al. (2004a).

Fluid and heat transfer away from and towards intrusions

We compare here the effects of simple conductive heat transfer away from an intrusion with outwards flux of fluid from an intrusion, and with inwards fluid flux towards an intrusion (Fig. 1-1). The conductive case could apply to both syn- or pre-mineralization intrusions; Otherwise, we consider the potential role of intrusions in adding fluid to potential ore systems via the exsolution of a water-dominant volatile phase during crystallization. Figure 1-1 shows the contrast between simple outwards conductive heating and both outwards and inwards fluid flow.

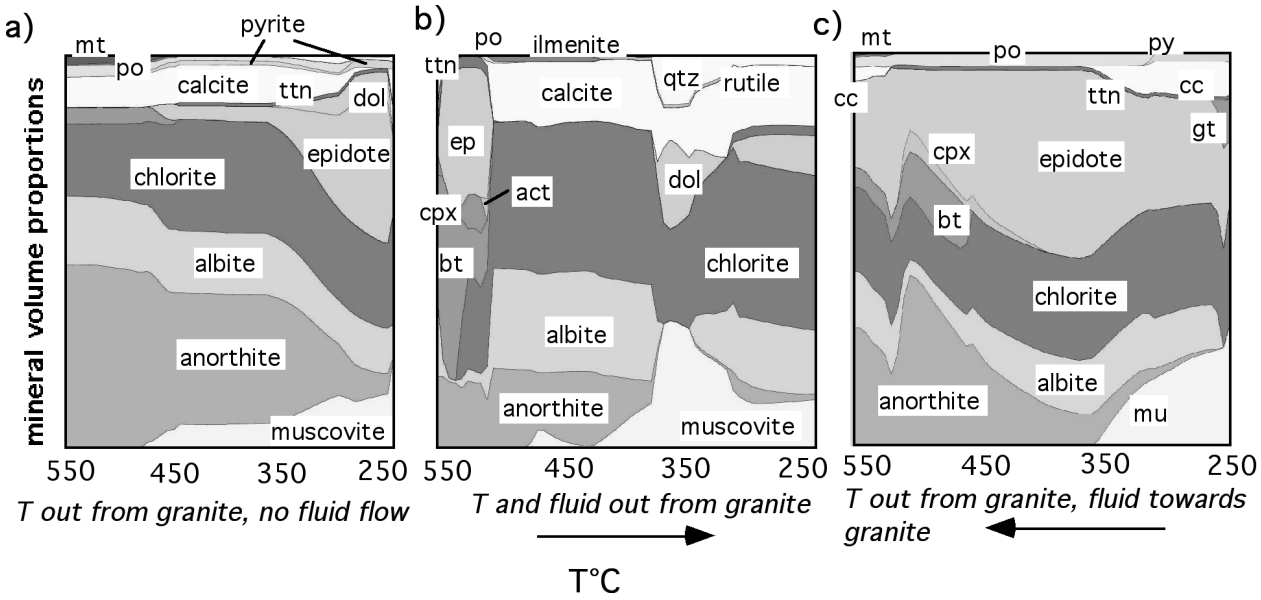

Figure 1-1. Comparison of HCh model results for a) closed system metamorphism of greenschist facies metaba-salt, b) open system metamorphsim with fluid emanating from a granite at high T and infiltrating into the green-schist down a T gradient, and c) open system metamorphism with fluid in equilibrium with greenschist at low T, moving up the T gradient towards the granite. Temperatures as indicated, all models run at 250 MPa.

These different patterns should be readily distinguished in the field. Up-temperature flow towards a pluton (e.g. Witt et al. 1997), would produce voluminous epidote zones, calcic plagioclase and little or no quartz; outflow from an intrusion would produce distinctive but relatively narrow calc-silicate alteration zones with fairly sodic plagioclase and quartz; and the thermal effects alone, with no fluid flow, would produce broadly changing zones with calcic plagioclase and no calc-silicate alteration.

Sulphidation and redox reactions in alteration haloes of gold systems

Fluid mixing, infiltration, and rock buffering of fluid all provide scenarios in which steep geochemical gradients can lead to gold precipitation. One of the main models for precipitation of gold in greenstone systems is the destabilization of bisulfide gold complexes upon precipitation of sulphides (e.g. Mikucki 1998). Here we have modelled sulfidation using a reactor-style infiltration algorithm in which fluid of a constant composition is fed into the left of the models, reacts in the first reactor and then is displaced to the right by the next aliquot of fluid (the “step-flow-through reactor”technique). Note the contrast between the two examined models that results as a consequence of the differing proportions of H_2S/SO_4 and CH_4/CO_2 in the initial fluid. In a strongly reduced fluid (Fig. 1-2a), interaction with Fe-oxide + Fe-silicate bearing rocks produces pyrrhotite zones in conjunction with the commonly observed silica-carbonate-white mica alteration, favouring broad gold deposition across the sulfidation zone. However, when the H_2S/SO_4 ratio is decreased, initial sulfidation of the wallrocks makes way for a narrow anhydrite zone (Fig. 1-2b), and when all the fluid sulfur is exhausted,

the relatively low CH_4/CO_2 ratio results in oxidation of the host metabasalt. Thus, a change from reduced to oxidized mineral assemblages in time and space may not reflect the operation of two separate fluids, nor even a temperature gradient, rather it may reflect a balance between differing buffers during progressive infiltration of one fluid.

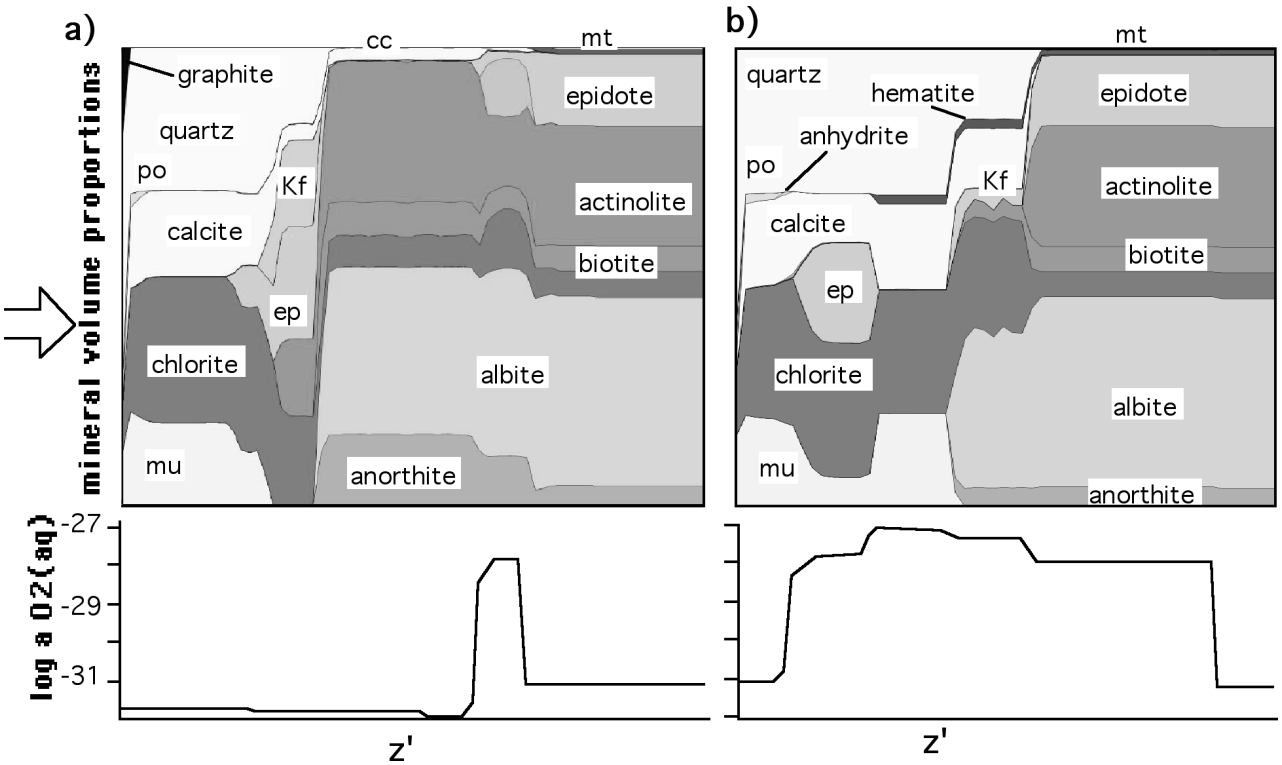

Figure 1-2. HCh model results for infiltration of fluid (from left to right) with NaCl molality 0.2, KCl 0.5, $CaCl_2$ 0.4, $FeCl_2$ 0.03, H_4SiO_4 0.035 (and other varying redox and sulphur parameters as below) into metabasalt with mineralogy shown on the right of the diagrams (buffering log a_{O2} –31). The models were run under isothermal, isobaric conditions at 380°C and 250 MPa. The x-axis is the nominal distance the front has travelled for a fixed time, fluid velocity and permeability. Alternately it can be regarded as the time taken for a reaction front to reach a certain distance for a given fluid flow rate. The last step shown on the log a_{O2} diagrams represents the limit of infiltration of the exotic fluid. a) Reduced fluid with initial molality of CO_2 2.0, CH_4 0.1, H_2S 0.1 and SO_2 10^{-10}, pH of 3.5 and log a_{O2} –32.0 showing sulfidation assemblages characteristic of proximal zones of many ore deposits; b) Moderately reduced fluid with initial CO_2 molality 4.0, CH_4 0.01, H_2S 0.1 and SO_2 10^{-7}, pH of 3.25 and log a_{O2} –31.1, in which exhaustion of the fluid's sulfidation capacity leads to formation of oxidized assemblages ahead of the front, including the anhydrite- and hematite-bearing assemblages found in several large deposits in the Yilgarn.

Outflow above orebodies – prediction of hangingwall geochemical and geophysical haloes

Change in the predicted magnetic susceptibility within an ore body due to water-rock interaction was modelled for Fe-oxide Cu-Au systems by Bastrakov et. al (2004c). We take this approach further into the realm of other geophysical signatures and exploration scenarios. The passage of ore fluids through and beyond depositional sites can be considered to involve depletion of key ore-forming ingredients from the fluid, but also the transport of some tracer and major elements into hangingwall rocks, assuming that the general fluid flow vector is upwards. Here, our particular outflow model utilizes the different results across the x-axis of Figure 1-2a, passing effluent from the different reactor steps into fresh rock, but down a P-T gradient.

Figure 1-3 shows the main geophysically detectable minerals produced by outflow upwards from an orebody formed at 380°C and 250 MPa. Figure 3a is essentially a cross section. The distal (right) parts of the diagram display the effects of fluid, initially in equilibrium with little altered basalt (at 380°), rising upwards down a P-T gradient into fresh basalt. The proximal (left) parts of the diagram correspond to the main effluent fluid from the sulphidized ore-deposition site, passing upwards down the same P-T gradient, albeit with a greater fluid flux than for the distal sections. Magnetite is preserved during fluid upflow from the distal parts of the system, whereas it is destroyed as the hangingwall to the orebody is approached. Figure 1-3b shows some approximated geophysical signatures which would arise if erosion had cut to the indicated exhumation level (corresponding to decreased paleotemperatures above the orebody level). For surface or sub-surface exposures tilted relative to metamorphic grade, other sections through this space would be useful. We

could also calculate density, and we also note that detectable gold contents in the model (above 10ppb) correspond very closely to the distribution of pyrrhotite + pyrite, and that K from radiometrics (in exposed or little weathered rocks) is a moderately good proxy for sulfides. Similarly, we have the capacity to run the outflow through rocks other than the orebody host rocks, for example, granitoids, BIFs or clastic rocks;

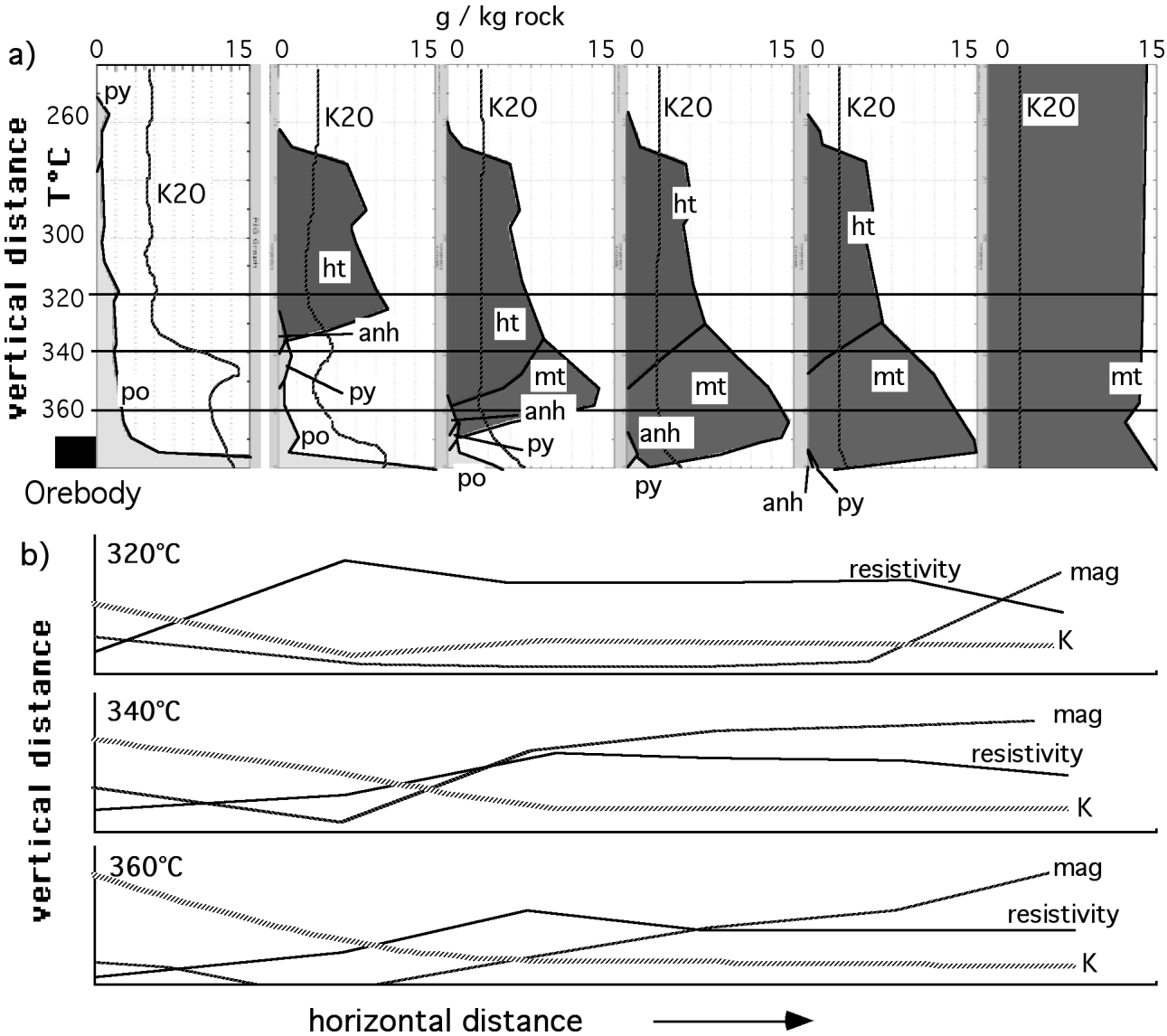

Figure 1-3. a) Schematic cross sections (around an orebody as depicted) of predicted oxide-sulfide-sulfate assemblages, and total K_2O, for outflow of fluid extracted from Figure 1-2a, passed upwards into fresh basalt down the T gradient indicated, also with corresponding P decrease of 6 MPa/10°C. For the individual mineral graphs and K_2O, the x-axis is the weight (g/kg) as indicated; for the overall x-axis, see Figure 1-2. b) Schematic profiles of geophysical response, at different erosion levels corresponding to different temperature slices, as indicated.

indeed it is possible to run the outflow fluid through a designated rock package of considerable geochemical complexity.

Acknowledgments

This paper is published with permission of the CEO, Predictive Mineral Discovery CRC. We thank Nick Fox, Greg Hall, Scott Halley, Peter Neumayr, Roger Skirrow, John Walshe and Lesley Wyborn for discussions. ***Pmd*CRC*** projects F1 and G9 (AngloGold Brazil) have supported the research.

References

Bastrakov, E., Mernagh, T., Cassidy, K., Wyborn, L., and Shvarov, Y., 2004a, Evaluating mineral systems processes in a geological province: The potential of lode gold deposits: AUSGEO News, 74 (in press).

Bastrakov, E., Shvarov, Y., Girvan, S., Cleverley, J., and Wyborn, L., 2004b, FreeGs: web-enabled thermodynamic database for modelling of geochemical processes, Geol. Soc. Australia Abstracts, 73, 52.

Bastrakov, E. N., Skirrow, R. G., Direen, N. G., Mernagh, T. P., and Wyborn, L. A. I., 2004c, Coupling geochemical and geophysical modelling to detect mineral systems undercover: an example from the Gawler Craton, Geol. Soc. Australia Abstracts, 73, 52.

Groves, D. I., 1993, The crustal continuum model for late-Archaean lode-gold deposits of the Yilgarn block, Western Australia, Mineral. Deposit., 28, 366-374.

Mikucki, E. J., 1998, Hydrothermal transport and depositional processes in Archean lode-gold systems: A review, Ore Geol. Rev. 13, 307-321.

Neumayr, P., Hageman, S. G., Walshe, J. L. & Morrison, R., 2003, Camp- to deposit-scale zonation of hydrothermal alteration in the St Ives gold camp, Yilgarn Craton, Western Australia: evidence for two fluid systems?, in, Mineral exploration and sustainable development, Eliopoulos, D.G. et. al., eds., 799-802, Millpress.

Walshe, J. L., Halley, S. W., Hall, G. A. & Kitto, P. (2003). Contrasting fluid systems, chemical gradients and controls on large-tonnage, high-grade Au deposits, Eastern Goldfields Province, Yilgarn Craton, Western Australia, in, Mineral exploration and sustainable development, Eliopoulos, D.G. et. al., eds., 827-830, Millpress. 827-830

Witt, W. K., Knight, J. T. & Mikucki, E. M., 1997, A synmetamorphic lateral fluid flow model for gold mineralization in the Archaean southern Kalgoorlie and Norseman terranes, Western Australia, Econ. Geol., 92, 407-437.

Chapter 2: Comparing Closed System, Flow-through and Fluid Infiltration Geochemical Modelling: Examples from K-alteration in the Ernest Henry Fe-oxide Cu-Au system.

James S. Cleverley & Nicholas H.S. Oliver

This paper has been published as follows:
Cleverley, J.S. & Oliver, N.H.S. 2005. Comparing closed system, flow-through and fluid infiltration geochemical modelling: examples from K-alteration in the Ernest Henry Fe-oxideCuAu system. Geofluids, 5, 289-307

Abstract
Potassic alteration of rocks adjacent to, and within the Ernest Henry Fe-oxide Cu-Au deposit is used here as a test case to investigate fluid-rock interactions using various equilibrium dynamic geochemical modelling approaches available in the HCh code. Reaction of a simple K-Fe-(Na,Ca) brine (constrained by published fluid inclusion analysis) with an albite-bearing felsic volcanic rock, resulted in predicted assemblages defined by a) k-feldspar-muscovite-magnetite, b) biotite-k-feldspar-magnetite, c) biotite-quartz-albite and d) albite-biotite-actinolite-pyroxene with increasing rock buffering (decreasing log w/r). Models for isothermal-isobaric conditions (450oC and 2500 bars) were compared with models run over a PT gradient (450 to 200oC and 2500 to 500 bars). Three principal equilibrium dynamic simulation methods have been used; 1) static closed system, where individual steps are independent of all others, 2) flow-through and flush, where a part of the result is passed as input further along the flow line and, 3) fluid infiltration models that simulate fluid moving though a rock column. Each type is best suited to a specific geological fluid-rock scenario, with increasing complexity, computation requirements and approximation to different parts of the natural system. Static closed system models can be used to quickly ascertain the broad alteration assemblages related to changes in the water/rock ratio, while flow-though models are better suited to simulating outflow of reacted fluid into fresh rock. The fluid infiltration model can be used to simulate spatially controlled fluid metasomatism of rock, and we show that given assumptions of porosity relationships and spatial dimensions that this model is a first order approximation to full reactive transport, without requiring significant computational time. This work presents an overview of the current state of equilibrium dynamic modelling technology using the HCh code with a view to applying these techniques to predictive modelling in exploration for mineral deposits. Application to the Ernest Henry Fe-oxide-Cu-Au deposit demonstrates that isothermal fluid-rock reaction was responsible for some of the alteration zonation around the deposit.

Introduction
Geochemical modelling of fluid-rock interactions during ore-deposit genesis and alteration is a potentially important tool for exploration because such modelling can be predictive in locating future ore deposits. In their review of chemical mass transfer modelling, Heinrich et al. (1996) stated that, aside from the assumption of local fluid-rock equilibrium, there were two significant problems with simulating geochemical processes in natural fluid-rock systems: a) Difficulties in understanding how to apply geochemical models to real world geological problems and, b) the quality and availability of much of the thermodynamic data at elevated pressure and temperatures. The limited uptake of geochemical modelling by the wider community, especially the exploration industry is probably also related to: a) the complexity of the modelling process and the required geochemical literacy and, b) the lack of published applied exploration ‘success stories’. While the quality and quantity of thermodynamic data is being addressed by institutes around the world, the conceptualization of fluid-rock interactions within the context of a geochemical modelling package can be equally difficult. Shvarov (1999) highlighted this by stating that “the choice of model is often determined not by the properties of the object studied and the personal wishes of the researcher, but by the programs available”. It is often the step between geological conceptualization of a fluid-rock system and the ability of the user to model this using the available software that precludes attempts to simulate natural fluid-rock systems.

There are two major approaches to simulating fluid-rock interactions in natural systems (Grichuk & Shvarov, 2002). Firstly, the macro kinetic approach accounts for the dynamics of mass transfer and kinetics (e.g. Balashov & Yardley, 1998), although this application is not widely applied due to limitations in the available kinetic data. Secondly the equilibrium dynamic approach combines the dynamics of mass transfer and

progress of chemical reactions through a series of equilibrium states of the system. The latter approach is most widely used in predicting fluid-rock interactions in geochemical systems and is the focus of this work.

For geochemical equilibrium dynamic modelling there are three principal modelling conceptualisation schemes: a) static closed system, b) flow-through and c) fluid infiltration models (Heinrich et al., 1996; Reed, 1997, 1998). Each scheme uses a different methodology to interact the fluid and rock components over the course of the model. Shvarov (1999) presented a series of HCh control algorithms for different fluid-rock interaction processes (chemical changes by reaction progress, sequential flow reactors and inhomogeneous starting conditions) illustrating with examples the conceptualization of these processes by equilibrium dynamic modelling codes. The application of equilibrium dynamic modelling to predicted metasomatic zoning was reviewed and discussed by Grichuk & Shvarov (2002), and they show that 1D fluid infiltration models best approximate the Korzhinskii (1970) metasomatic zoning principles.

One of the key relationships effecting the result of fluid rock interaction modelling is the ratio of total fluid to total rock in each calculation. The fluid/rock ratio (referred to here as water/rock or w/r for consistency with Reed, 1997) is used to define many equilibrium dynamic models. The relationship between equilibrium dynamic modelling, reactive transport (a coupling between fluid-flow and chemical solver codes), and the usage of fluid-rock ratios were subjects of extensive debate (Blattner & Lassey, 1989; Bickle & Baker, 1990; Ferry & Dipple, 1991; Dipple & Ferry, 1996). For theoretical fluid infiltration through a saturated rock column, models using equilibrium steps should converge on reactive transport models only when the equilibrium steps are infinitesimally small and kinetic effects are ignored. However, as demonstrated previously (Shvarov, 1999; Grichuk & Shvarov, 2002) and in this work, HCh is capable of approximating reactive transport. Furthermore, there are a range of geological processes for which step-like changes and instantaneous equilibration provide realistic scenarios that reactive transport simulations cannot (see below). Reactive transport codes also require information on kinetic rates for which data are commonly lacking. Finally, even with recent advances in computer speed, reactive transport codes require long solution times even for relatively simple input configurations. For these reasons, equilibrium dynamic modelling codes will continue to play an important role in simulating fluid-rock interaction for the foreseeable future. This paper builds on and expands these models of conceptual fluid-rock interaction by using the HCh modelling package (Shvarov & Bastrakov, 1999). This work aims to apply and compare the merits of each of the major fluid-rock interaction modelling methodologies to a single geological problem that of K-alteration at the Ernest Henry Cu-Au deposit. We aim to demonstrate the role of equilibrium dynamic modelling codes in predicting mineral zonation during fluid-rock interaction processes related to alteration and ore genesis.

Introduction to HCh

The HCh software (Shvarov, 1999; Shvarov & Bastrakov, 1999) is a geochemical modelling code capable of describing local equilibrium dynamic models (Shvarov, 1999). At each calculation step the equilibrium compositions of multi-phase chemical systems are found using the Gibbs free-energy minimization technique (Shvarov, 1978, 1981, 1987). The up-to-date specifications of the package can be found at the Geoscience Australia website:

http://www.ga.gov.au/rural/projects/geofluids.jsp

The software includes a fully interactive database system (UNITHERM) that allows the user to maintain a readily customized database containing key basic thermodynamic parameters for solids, aqueous species, gases and non-aqueous liquids. HCh can be used rigorously within the limitations of the modified Helgeson-Flowers-Kirkham model from 0 to 1000oC, 1 to 5000 bars (Helgeson et al., 1981), and water densities greater than 0.35 g /cm3 and for fluid salinities limited by extended versions of the Debye-Hückel equation (ionic strengths between 3-5, Oelkers & Helgeson, 1990). This makes the software ideal for simulating a broad range of hydrogeochemical processes and is especially useful in modelling fluid-rock reaction processes at elevated pressure and temperatures.

The Gibbs solver uses the bulk composition of the system to calculate the equilibrium configuration, however input to HCh can be defined in variety of different ways depending on the users own preferences, including bulk oxide compositions, modal minerals, ionic components and element abundances. The Gibbs free energy (G) is calculated for any temperature-pressure (T-P) as a function of the standard molal entropy (S), volume (V), Gibbs free energy of formation (Gf) and the molal isobaric heat capacity (Cp(t)) (Shvarov & Bastrakov, 1999). This thermodynamic data is stored in the UNITHERM database and used by the Gibbs solver to calculate each GT-P as the model requires it, making HCh well-placed in its ability to model

changing T-P conditions. Changes in T-P and the interaction of different input components are controlled in the software by a set of customisable algorithms, and the details of these algorithms and their relationship to hydrogeological processes have been described in detail elsewhere (Shvarov, 1999; Shvarov & Bastrakov, 1999; Grichuk & Shvarov, 2002).

Thermodynamic Data

The thermodynamic data used by the HCh package in this work are based on the Geoscience Australia version of the UNITHERM database (Bastrakov, 2003), and is now available publically through the 'FreeGs' project (Bastrakov et al., 2004). For aluminosilicates and carbonates, most of the thermodynamic data for minerals were taken from the self-consistent datasets of Berman (1988) for aluminosilicates, with corrections for K and Na as suggested by Sverjensky et al. (1991), and a minor correction for Fe to keep consistency with oxides and sulfides from the IVANTERMO database. The remaining mineral data were sourced predominantly from the ETH version of SUPCRT (Pokrovskii et al., 1998). Aqueous species are derived from the ETH version of SUPCRT (Pokrovskii et al., 1998), with additional data from Shock et al. (1997) and Sverjensky et al. (1997) for Fe and Cu complexes. Aqueous chloride data where possible was kept consistent with data for $HCl_{(aq)}$ from Pokrovskii & Helgeson (1995).

HCh has the option to define mineral solid solutions using the ideal mixing-on-site model (e.g. Powell, 1977), or local-charge-balance model when ions have different charges (e.g. plagioclase). In the work presented here mineral solid solutions were calculated for the following phases: plagioclase (albite-anorthite), biotite (phlogopite-annite), epidote (epidote-clinozoisite), chlorite (chamosite-clinochlore) and actinolite (tremolite-ferrotremolite) and, where plotted, the end-members are combined, with the exception of albite-anorthite. The mineral abbreviations and solid-solution end-member chemistry is given in Table 2-1.

Although there are a range of activity coefficient models that can be used within HCh, activity coefficients for charged aqueous species are calculated here using the extended Debye-Hückel equation with the KCl-dominated solution modification scheme of Oelkers & Helgeson (1990). The neutral species are calculated using the common Setchenow coefficient calculated as a function of T-P according to an empirical fit for $H_2S_{(aq)}$ based on Ding & Seyfried (1990) and Suleimenov & Krupp (1994) (see Shvarov & Bastrakov, 1999, pages 52-53).

Mineral	Symbol	Solid-Solution?
Albite	ab	NaSi-CaAl
Anorthite	an	
Actinolite	act	Fe-Mg
Biotite	bt	Fe-Mg
Chalcocite	cc	-
Chlorite	chl	Fe-Mg
Epidote	ep	Fe-Al
Graphite	grph	-
Garnet	gt	MgAl-FeAl-CaAl-CaFe
Hematite	hm	-
K-feldspar	kfs	-
Muscovite	ms	K-Na (limited)
Magnetite	mt	-
Quartz	qtz	-
Talc	tlc	Fe-Mg

Table 2-1: List of mineral abbreviations (based on recommendations of Kretz, 1983) used in plotting model results. Minerals that form a solid-solution series are shown as the combined name with the associated ideal cation exchange, only albite-anorthite are plotted as the calculated mole fraction of the end-member phase

Calculation Terminology

The terminology employed by HCh has been primarily used for “step-flow-through-reactor” style modelling and we closely follow the terminology here. A single equilibrium calculation is called a step and a series of steps related by a common rule are termed a step series (see Fig. 2-1) (the HCh manual and previous literature calls the step series a wave, although we opted for the former for clarity). The step series is a synonym for solution batch as described by Heinrich et al., (1996) and noted by Grichuk & Shvarov (2002). Figure 1 shows a typical concept for a multi-step series HCh model, where the step-series relates individual reaction steps at different w/r (x-axis) performed over variable temperatures (y-axis). Results can be visualised as variable w/r at constant temperature, variable temperature for a constant w/r and as a grid of data showing the assemblage distribution (2D). All these features will be explored in this paper.

The Ernest Henry Copper-Gold Deposit

We have chosen a system well known to us, that of the Fe-oxide copper-gold deposits and the related alteration of the Cloncurry District in northern Australia (see review by Williams, 1998). The largest deposit in this district is the c. 1530 Ma Ernest Henry Deposit, with a resource of 167 Mt @ 1.1% Cu and 0.5 g/t Au. The deposit is hosted in variably Na-Ca altered felsic volcanic rocks of the 1760-1730 Ma Mary Kathleen Group (Mark et al., 2000).

K-Metasomatism at Ernest Henry

The Ernest Henry ore zone contains and is surrounded by a halo of potassic alteration (K-alteration) that cuts and post-dates, regional Na±Ca alteration (Mark et al., 2000; Oliver et al., 2004; Mark et al., 2005). The Na±Ca alteration is dominated by albite with infill of actinolite and calcite ± clinopyroxene ± magnetite ± apatite. Near the orebody the Na-Ca assemblage is destructively overprinted by the K-feldspar and coeval biotite and magnetite veins. K-alteration forms a km-scale envelope around the ore body but is most intense where ore grades are highest (Mark et al., 2000). Typically, K-feldspar altered rock comprises breccia clasts floating in a matrix of ore minerals (chalcopyrite, pyrite and magnetite). Thus, although K-alteration precedes ore minerals in the detailed ore paragenesis (Mark et al., in revision), the K-alteration appears to form during the passage of the ore-forming brine (Fig. 1-2). Mixing of this brine with another fluid containing sulphur was the likely mechanism of ore deposition (Mark et al., 2000; Oliver et al., 2004), but this mixing is not considered further here. HCh has been used to test the formation of destructive K-alteration of the previously Na±Ca altered rocks using the Cu-bearing brine fluid as constrained by PIXE analysis of fluid inclusions (Mark et al., 2000) and geochemical knowledge of the system, and the bulk composition of a typical Na±Ca altered volcanic rock.

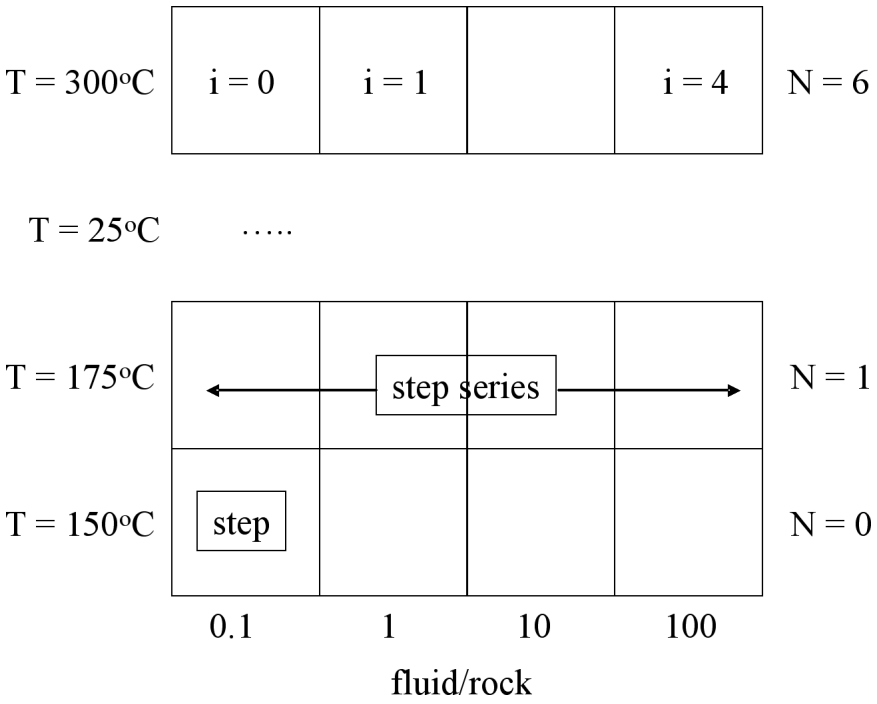

Figure 2-1: Example of the use of steps and step series in constructing an HCh model. In this example a fluid-rock titration model contains a different w/r at each step. The step series can also be combined with other step series to explore the effect of changing temperature. The output from this model can be viewed as a 1D slice at constant temperature or as a 2D grid of outputs showing the change in mineral assemblages.

Predictive Geochemical Modelling

By understanding and modelling the fluid-rock reactions, fluid chemistry and hydrological pathways of ore deposit genesis, we can increase the success rate for locating undiscovered deposits and help to decrease exploration costs. Figure 2-2 is a schematic of the Ernest Henry ore system as used to illustrate the potential predictive modelling scenarios and those presented in this work (the following refer to Fig. 2-2):

A. Fluid and metal source region. The development of an 'ore-fluid' by fluid-rock interactions with rocks containing the component of interest, including predicting metal solubility, transport and speciation.

B. Pre-deposit fluid-rock interactions ('inflow zone'). The simulation of metal-enriched fluid interacting with rock prior to precipitation. Separate models would exist for every separate fluid involved in deposit formation.

C. Ore deposit formation. Simulating the processes leading to the efficient precipitation of ore components of interest (e.g. fluid-rock reactions, changes in T-P or fluid-mixing).

D. Deposit proximal alteration. Simulating the outflow of fluid after ore-component precipitation (i.e. spent fluid) and its interaction with the host rock to the deposit. Model D would typically be at the T-P conditions of the deposit or models with T gradients only.

E. Deposit distal alteration ('outflow zone'). This simulation is the same as model D except the spent fluid is interacting with different rock units than the deposit host typically at different T-P conditions or over a T-P gradient.

F. Outflow alteration of fluids not responsible for ore deposition (the 'red-herring' fluid). This is important in predictive geochemical modelling to distinguish prospective from non-prospective alteration pathways.

Input Model Compositions

For this case study the HCh input file includes a fluid (component 1, Table 2-2) and a rock (component 2, Table 2-2). The model fluid is constrained by conventional and PIXE fluid inclusion analysis of pertinent pre-ore stage fluid inclusions (as recalculated from Mark et al. (2000) by Oliver et al. (2004) and reproduced in Table 2-2), as well as analysis of regional fluid inclusion types and modelling of effluent fluid from Na-Ca alteration simulations (Fu et al., 2003; Oliver et al., 2004). The molar Na/(Na+K) ratio of the analysed fluid (0.84) is not able to produce k-feldspar (the key potasic mineral in the alteration sequence), and this fluid may represent an outflow or spent fluid. For the examples discussed in this paper the Na/(Na+K) of the model fluid was changed to 0.16 to allow the precipitation of k-feldspar. The redox state of the model fluid was varied using the ratio of Fe^{2+}/Fe^{3+} as balanced chloride species in the input. A value was chosen based on the best representation of the range of alteration sequences reported for the Ernest Henry K-alteration stage. The calculated log $f_{O2(g)}$ of the model fluid (see Table 2-1) is above the SO_2/H_2S, and close to the hematite-pyrite buffer. The rock is defined by an XRF bulk composition from G. Mark (unpublished data, analysis G2L), mineral percentages could also be used. This bulk composition was hydrated with 0.005 kg of water (not reported in the original analysis) which is the minimum required to stabilise hydrous minerals in this example.

Two different T-P conditions are used in the following examples. Isothermal-isobaric conditions for fluid-rock interaction paths at 450°C and 2500 bars are based on the average of conditions estimated for the Ernest Henry ore stage (Twyerould, 1997; Mark et al., 2000). Polythermal-polybaric conditions for the passage of fluids along a defined T-P gradient from 450 to 250°C and 2500 to 500 bars were used to simulate possible retrograde outflow paths and compare with other (lower T-P) Fe-oxide-Cu-Au districts. The pressure is constrained to vary linearly as a function of temperature (P (bars) = 8T – 1100), however this T-P path is arbitrarily defined and needs to be constrained by observations and/or fluid-flow and deformation modelling.

	Brine Fluid 450°C/2500b	G2L fine grain volcanic	G2L Gt stage brine fluid (ref 1)
Component	1	2	3
H2O (kg)	1.0	0.005	1.0
NaCl (mol)	0.7		3.62
KCl (mol)	3.6		0.69
CaCl2 (mol)	0.5		0.45
FeCl2 (mol)	1.05		1.2
FeCl3 (mol)	0.05		
H2S (mol)	1.0x10-4		
SO4 (mol)	7.0x10-4		
Cu (mol)	0.035		
SiO2 (g)		558.0	
TiO2 (g)		14.0	
Al2O3 (g)		163.0	
Fe2O3 (g)		46.6	
FeO (g)		21.0	
MgO (g)		57.8	
CaO (g)		38.3	
Na2O (g)		69.0	
K2O (g)		57.0	
log fO2(g)	-18.2	-	
pH	2.9	-	
I (true)	2.7	-	
XH2O	0.87	-	

Table 2-2: Input used in HCh models presented in this work, 1) Na-K-(Fe-Ca) brine, 2) Na-Ca altered felsic volcanic rock, 3) Na end-member brine and, 3) K end-member brine. Last 4 rows are calculated values based on 450oC and 2500 bars. Abbreviations as for Table 2-1.

Fluid-Rock Interaction Models

The theoretical approaches used by many geochemical modelling codes are a compromise between simple equilibrium relationships presented through activity diagram analysis, and fully coupled modelling codes that consider infiltration, diffusion, and kinetics in spatially and temporally defined systems (Reed, 1997). Following on from the terminology of Reed (1997; 1998), there are three principle geochemical model types (i.e. for non-coupled models): a) Static closed system (includes rock titration without fractionation), b) Flow-through, and, d) 1-D Fluid Infiltration, and these approaches will be described further in this section. The most familiar type of fluid-rock interaction modelling in the literature is the rock titration (static closed system) method (e.g. Helgeson, 1968; Wolery, 1983; Bethke, 1996; Reed, 1997, 1998) whereby a rock (defined by its mineral assemblage) is added in discrete aliquots into a fixed mass of fluid. The total mass of rock titrated increases with reaction progress so that there is a stepwise change in water/rock (w/r) ratio over the course of the model. The 1D fluid infiltration models are less common than the titration approach, but are possible with the HCh code, and their comparison to titration models for Ernest Henry K-alteration form a focus of discussion in this work.

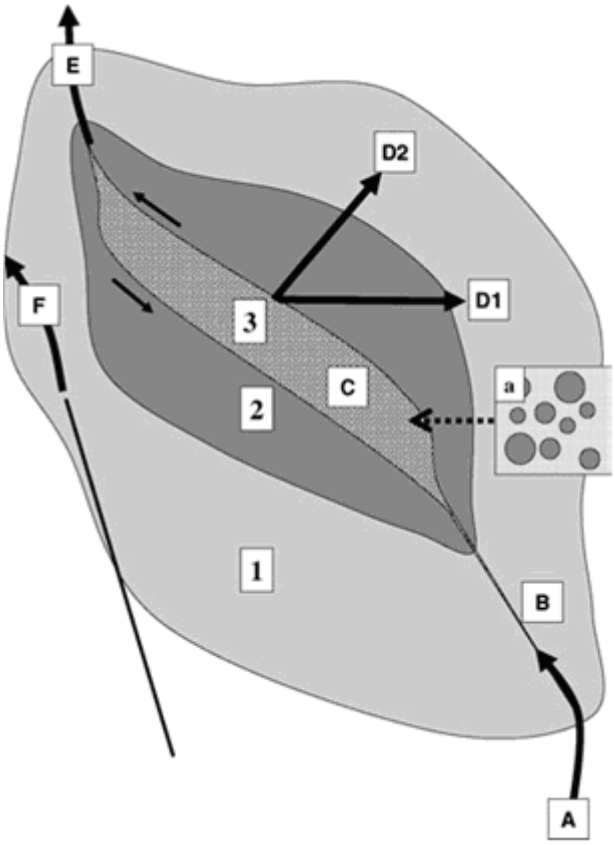

Figure 2-2: Schamatic diagram for the Ernest Henry Ore-system illustrating the different fluid-rock interaction scenarios that are important in modelling mineral deposit formation and related alteration. In this diagram ore deposition takes place during brecciation of K-altered volcanic rocks within a dilatent shear zone jog (3). The K-altered clasts are typically rounded set in a matrix of infill magnetite-chaclopyrite-pyrite±calcite-k-feldspar (inset box a). A broad area of Na-Ca altered felsic volcanic rocks (1) are overprinted by pre- to syn-ore K-alteration (2) during the passage of oxidised K-Fe brine. Large letters in stars are broad areas where geochemical models can be used (see text), A) Metal sourcing and transport, B) Pre-deposition fluid-rock interactions, C) Ore deposition, D) Proximal outflow and alteration modelling (the focus of case studies presented here) and, E) Outflow of fluids postdating ore deposition (or alteration). If geochemical modelling is to be truly predictive for exploration it must also be used to distinguish 'red-herring' outflow signatures (F). The alteration and outflow models can be isothermal-isobaric (D1) or polythermal-polybaric (D2).

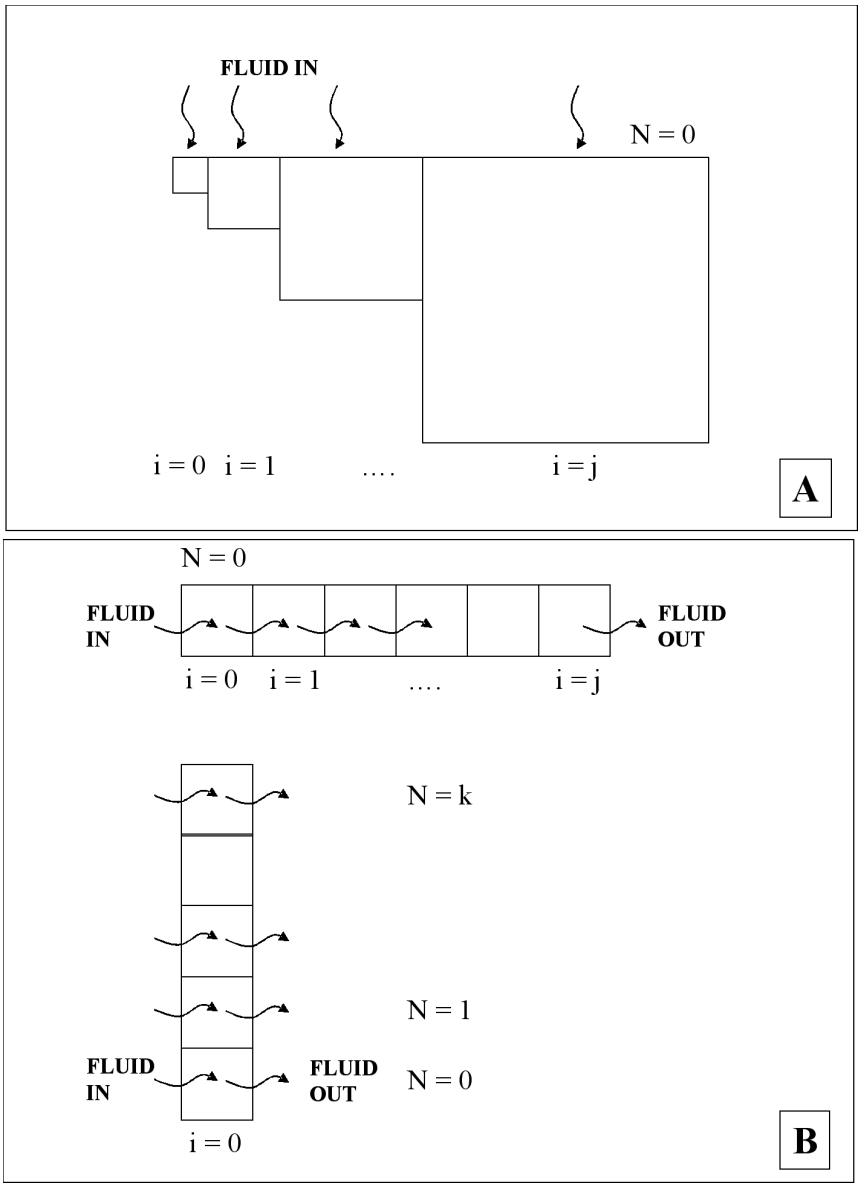

Figure 2-3: Box diagrams for the different modelling methodologies presented in this work: A) Static closed system model with a single fluid aliquot reacted with increasing amount of rock with no mass transfer between steps (i). This is a single step-series model (N=0). B) Flow-through (top) and flush (bottom) models depending on the focus of the model (rock or fluid) and C) Fluid infiltration model showing the advancing fluid front for each incremental step series (N). In this example the step with the limit of infiltration is always equivalent to the current step series.

Static Closed System Models

The static closed system models have no mass transfer between steps and hence the fluid is assumed to be static. There are many variations and most commonly this is the rock titration without fractionation models as described by Reed (1997), however this terminology was not used here because these models can equally encompass changing T-P conditions for fixed w/r ratio and composition.

The rock titration model simulates the equilibrium composition for a series of closed system steps, with a fixed mass of fluid and variable rock (Fig. 2-3A) and was proposed and executed by Helgeson (1968) and illustrated in terms of HCh notation by Shvarov (1999) for 1D investigations of chemical interactions by the method of reaction progress.

The geological scenario for each step of the static closed system model requires that unreacted fluid and rock equilibrate at a single w/r ratio. A 1- or 2-D model can be used to understand the change in predicted mineral assemblages (and other chemical parameters) with different w/r ratios (Fig. 2-2, changes in mass of rock in location C) or for constant w/r ratio over a T-P gradient (Fig. 2-2, changes through-out depth of ore deposition at location C). These models are best suited to answering the question: What is the predicted

mineral assemblage if the fluid reacts with a known mass of rock, and what is the change in the predicted mineral assemblage as the system changes from fluid dominated to rock dominated?

Flow-Through Models

The flow-through model differs from the static closed system in that a portion of the chemical system (fluid or rock) is passed on as input to the next step along the reaction path. Commonly the fluid is passed through, in which case the model is equivalent to the titration with mineral fractionation type equilibrium models discussed in the literature (Reed, 1997, 1998).

Flow-through models can be used to simulate the passage of a single fluid pulse from a site of fluid-rock reaction outwards through increasing amounts of fresh wall rock (Fig. 2-2, pathways D1 and D2). This is a reasonable proxy for outflow of small amounts of fluid away from a site of rock reaction or ore deposition. The w/r ratio of each step is constant but as the fluid is passed though several steps the integrated or through put w/r (Reed, 1998) decreases. Because the fluid is allowed to become modified by the rock, in isothermal-isobaric simulations the fluid will eventually become rock buffered and lose its capacity to change the rock chemically. Flow-through models can be formulated to track the evolution of the fluid by titrating rock or a special type tracks the evolution of a single rock packet by titrating fluid (Flash models, Bethke, 1996; Reed, 1998). The visualisation of the HCh formulation of flow-through and flush models is shown in Fig. 3B. Flow-through models can be used to answer questions, for instance: What is the assemblage related to outflow pulses from a complex ore forming scenario? As well as many other examples (e.g. Reed, 1997).

In the most extreme flow-through, down T-P simulation, the fluid leaving the site of fluid-rock reaction is isolated from further wall rock reaction and is allowed to precipitate minerals in each step along the T-P gradient, corresponding to the “open system without wallrock reaction” of Oliver (1996). Minerals are precipitated directly from the fluid only as a consequence of changing T-P solubilities and the model best approaches the simulation of a veining processes.

1D Fluid Infiltration

The fluid infiltration model is the most complicated of the three fluid-rock interaction models presented here. The infiltration model simulates the passage of a fluid through a column of rock, such that fresh fluid is always added to one side of the rock column and a fluid front moves through the rock column during reaction progress (Fig. 2-3C). The fluid and the rock are allowed to become modified as the fluid front passes though the rock and the model can be seen to contain a temporal dependency (i.e. the rate of fluid infiltration, the step series axis in Fig. 2-1) as well as a spatial dependency to the results (the step axis). The limit of infiltration (the position of the first step containing the reacting fluid) increments 1 step for each step series of the model (Fig. 2-3C); beyond this the rock is not infiltrated. The infiltration model has a defined w/r ratio at the start in which a fixed mass of fluid and rock are reacted. The rock mass is initially fixed in each step, however during infiltration and progressive reaction the mass of rock can change in response to dissolution and precipitation processes. The infiltration fluid mass can also change through processes such as rock hydration. In the most extreme case the fluid at the infiltration front can ‘dry up’ (see discussion in Reed, 1997), this is especially true for models with anhydrous rocks not containing a pre-existing water-bearing phase. While HCh is able to calculate fluid absent equilibria, the ‘drying up’ process can cause very large ionic strengths in infiltration front fluids which in turn causes numerical problems (exceeding the limit for the Debye-Hückel criteria), and this parameter needs to be monitored during infiltration modelling.

Because fresh fluid is continuously added to the model the w/r ratio of a single step (a fixed location) increases over the course of the model, however the w/r of the fluid packet passing though the model decreases as it reacts with more rock at each step. A single 1D infiltration model combines the results of a flush and flow-through models, depending on how the results are visualised (see Fig 2-3C). The model presented here is a slight modification of that proposed by Shvarov (1999) for sequential flow reactors (see Appendix).

This model of chemically changing fluid moving through chemically changing rock is the closest to simulating fluid infiltration and metasomatic zoning of rocks, such as confined aquifer flow or flow in and out of a heat source (e.g. flow around plutons). It is also possible to fix a temperature and pressure gradient across the rock column to simulate flow driven by hydraulic and/or thermal gradients if these can be calculated externally to HCh. The direct geological question is: What is the predicted spatial zonation of metasomatic alteration produced by brine infiltrating the volcanic host sequence at Ernest Henry?

Model Results

This section presents the results of running the different geochemical model types discussed above with a specific fluid-rock interaction scenario, i.e. the interaction of oxidised-acidic K-Fe brine with Na-Ca altered volcanic rocks.

Static Closed System Model

The initial model is a static closed system model with increasing mass of rock from 10-4 to 104 kg, in 100.5 kg increments, equilibrated with 1 kg of fluid at each step. Because this is a closed system model there is no mass transfer between steps. The calculated log w/r changes from 2 to -4 and the change in mineralogy over this range is shown in Fig. 2-4.

There are three dominant mineral assemblages represented in Fig. 2-4, a) fluid dominated muscovite – magnetite - k-feldspar – hematite – rutile, b) intensely altered k-feldspar – biotite – muscovite – magnetite and, c) rock buffered assemblage albite – chlorite – biotite – clinopyroxene – actinolite – magnetite. There is also a transitional assemblage between the k-feldspar- and albite-dominant assemblages that contains quartz. As the model progresses from fluid- to rock-dominant, the fluid evolves from K- to Na-rich (Fig. 2-5A), with Na-Ca altered volcanic rock buffering the fluid to a Na/(Na+K) ratio of 0.98, compared to 0.16 in the starting fluid. Most of the change in Na/K ratio in the fluid takes place over only a few steps between log w/r of 1 to -1. The fluid pH changes gradually from 3.9 to 4.8 over the initial steps (< log w/r -2) changing from 6.2 to 7.4 (> log w/r -2) in the rock-dominant part of the model (Fig. 2-5B). The pH of the most fluid-dominant step (log w/r 2) is higher (3.9) than the starting condition (2.9) so that even a small amount of rock reaction causes a shift in the pH. The log $f_{O2(g)}$ stays between -26 and -28 (Fig. 2-5B), although as with the pH in the initial high w/r step the log $f_{O2(g)}$ is shifted dramatically from the starting value of -18.2, despite the small mass of rock (0.01 kg). The change in the bulk fluid chemistry from model 1 is given in Figure 2-6. The fluid changes character from an initial multi-cation fluid to a rock buffered fluid (>log w/r -1) dominated (>95%) by Na.

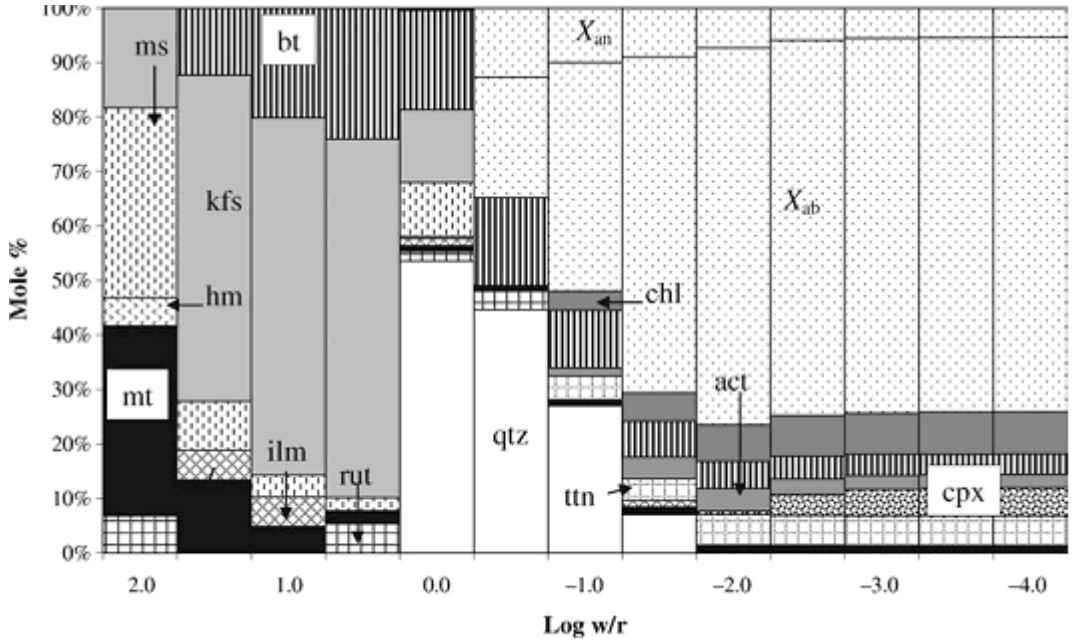

Figure 2-4. Predicted mineral assemblages (mole% of rock) for static closed system model with K-Fe brine reacting with Na-Ca altered rock. There is variable rock for a fixed content of fluid (1kg) and the calculated log w/r is by mass basis. The left hand side is fluid dominated and the right hand side is rock dominated. Mineral abbreviations are based on recommendations of Kretz (1983) and are listed in Table 2-1. Model geofa03.

The static closed system technique can also be used to model the predicted mineral distribution of fluid rock interactions at a variety of T-P conditions. Figure 2-7A to D is the predicted distribution across T-P for k-feldspar, muscovite, biotite and magnetite for a closed system model at log w/r = 1.0 (see Fig. 2-4). This 'assemblage diagram' can be usefully employed to investigate the sensitivity of T-P estimates and the changes in mineralogy expected for fluid-rock interactions under different conditions. By comparing Figure 2-7A to D we can see that k-feldspar-biotite-magnetite assemblage gives way to biotite-magnetite-muscovite at 400°C. The latter assemblage matches best with some of the dark-rock alteration (biotite-magnetite) described in the halo of the Ernest Henry deposit, in turn suggesting that there was a zoned temperature

distribution around the core of the deposit.

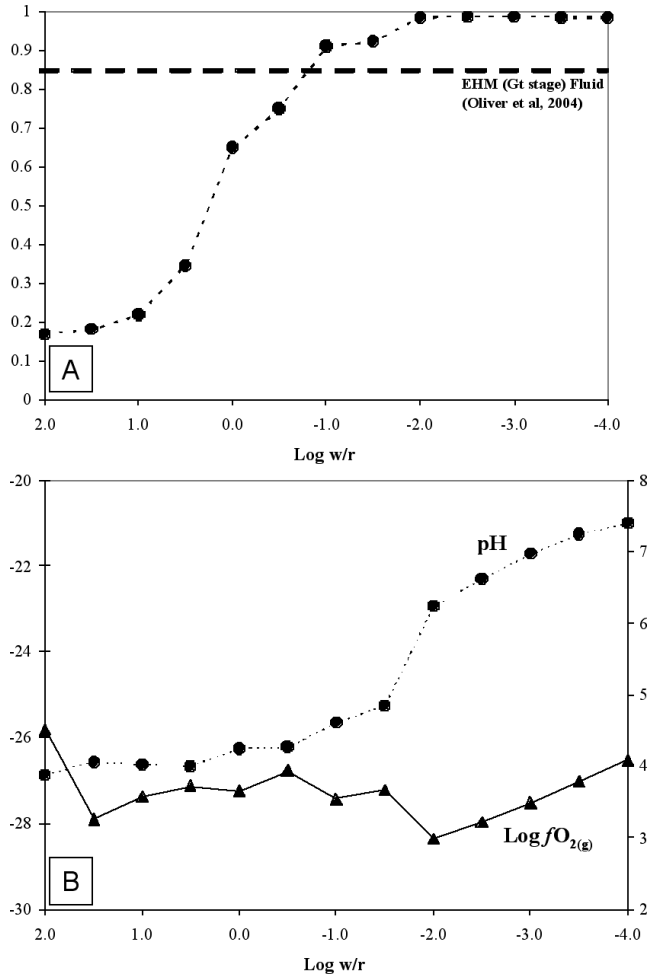

Figure 2-5. Changes in molar Na/Na+K ratio (A) and pH – log $f_{O2(g)}$- (B) predicted for the fluid from model 1 (Fig. 2-4), each data point is a single step.

Flush and Flow-through Models

The flush model is a special case of the flow-through model types, where 1 kg of rock is reacted with 0.6 kg of fresh fluid in each step. Reaction progress is measured using the through-put fluid mass (Reed, 1998), which is the total mass of fluid that has reacted with the rock. In model 2 the maximum through-put fluid mass is 120 kg and this represents a through-put log w/r of 2.08, where step 1 (0.6 kg fluid) is equivalent to log w/r of -0.22. The model evolves between two dominant mineral assemblages: k-feldspar – biotite – magnetite – muscovite, and hematite – muscovite – k-feldspar (Fig. 2-8). This approximates the assemblages in Fig. 2-4 for similar w/r but in this model mass is allowed to be removed from the rock by the fluid and so the bulk assemblage being reacted at each step is slightly different. The rock dominant assemblages from Fig. 2-4 are not apparent in Fig. 2-8 because they are lost in the first few steps, but by reducing the increment size of the reactant fluid it is possible to simulate the detail of high or low fluid flux systems.

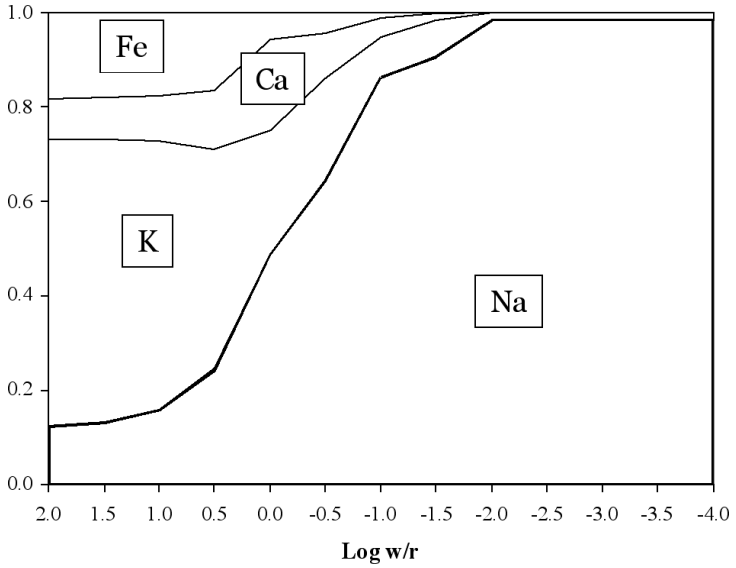

Figure 2-6: Change in the normalised major cation chemistry of fluid from model 1 (Fig. 2-4) showing the transition from K-Fe to Na dominated fluid with increasing rock buffering.

It is often useful to predict alteration assemblages where fluid interacts with rock across a T-P gradient. For example, a particular application is the simulation of outflow of cooling fluids above an orebody as a predictive exploration tool (Fig. 2-2, pathways E and F), as has recently been applied to the Ernest Henry ore forming fluid using Geochemists Workbench (Mark et al., 2005). The flow-through model can be applied to this scenario by stipulating a fixed T-P gradient along the reaction path. Figure 2-9 is an example of two distinct outflow models for spent fluid after k-alteration at Ernest Henry. In figure 2-9A the spent fluid from initial rock interaction at log w/r of 1.0 (at 450°C, 2500 bars in step 0) is reacted progressively with 0.1kg of rock while linearly changing T-P to 200°C and 500 bars (P = 8T – 1100). Although the change in mineral assemblage over the reaction path is similar to those in Fig. 2-4 with decreasing w/r, there are subtle differences. In the region from 450 to 390°C there is a transition from biotite – k-feldspar to biotite – muscovite - k-feldspar to biotite – k-feldspar – quartz that is not seen in the simple static closed system model (Fig. 2-4), and biotite is replaced by chlorite in the rock buffered zones below 330°C. Figure 2-9B is an extreme case of the influence of changes in T-P on the spent fluid where the reaction path contains no rock and the mineral precipitation is driven by the changes in T-P only. This scenario can be used with care in modelling the processes that lead to vein formation. Figure 2-9B shows that the fluid is capable of precipitating k-feldspar for the first couple of increments after fluid-rock interaction and is then dominated by the quartz precipitation. Some Cu-S minerals (chalcocite and bornite) precipitate at the coolest end of the model in response to un-buffered changes in pH and redox of the fluid.

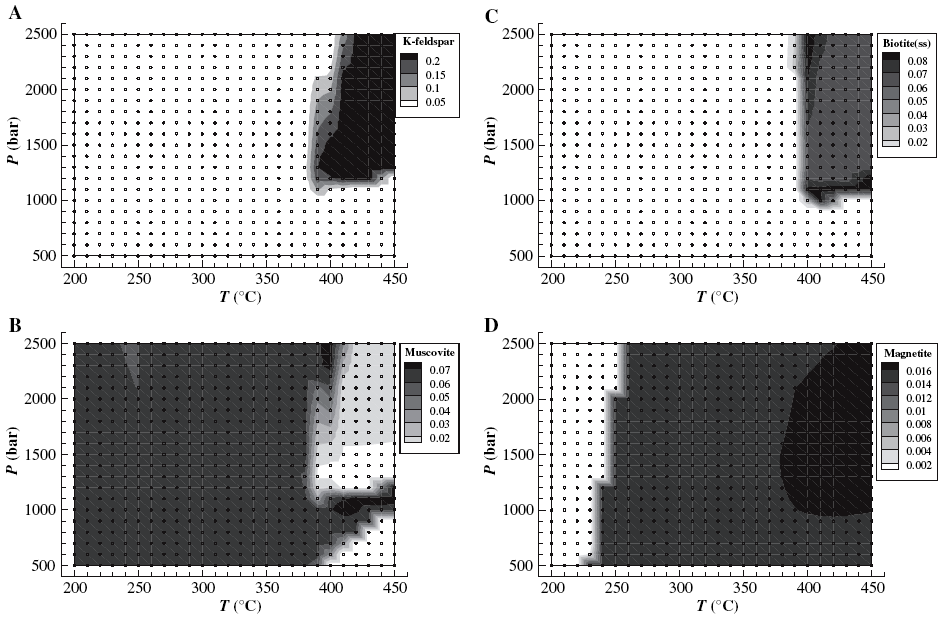

Figure 2-7: Distribution of (A) k-feldspar, (B) muscovite, (C) biotite and (D) magnetite over T-P for a fixed log w/r of 1.0. Mineral abundances are total moles with the reaction steps highlighted as clear dots on the graphs. Note that the grey shading levels are different for each phase and no shading indicates phase absence at that point. Model geofc03.

One of the key problems with running T-P outflow models in a non-coupled modelling code is the need to fix a T-P trajectory. The result will depend on the rate at which both T-P change relative to the interaction of and proportions of fluid and fresh rock. The T-P trajectory needs to be defined though geological observations or coupled flow-flow and/or deformation modelling, although with the speed of the equilibrium dynamic modelling many different case examples could be run to build up a picture of which trajectories fit the observed mineral paragenesis.

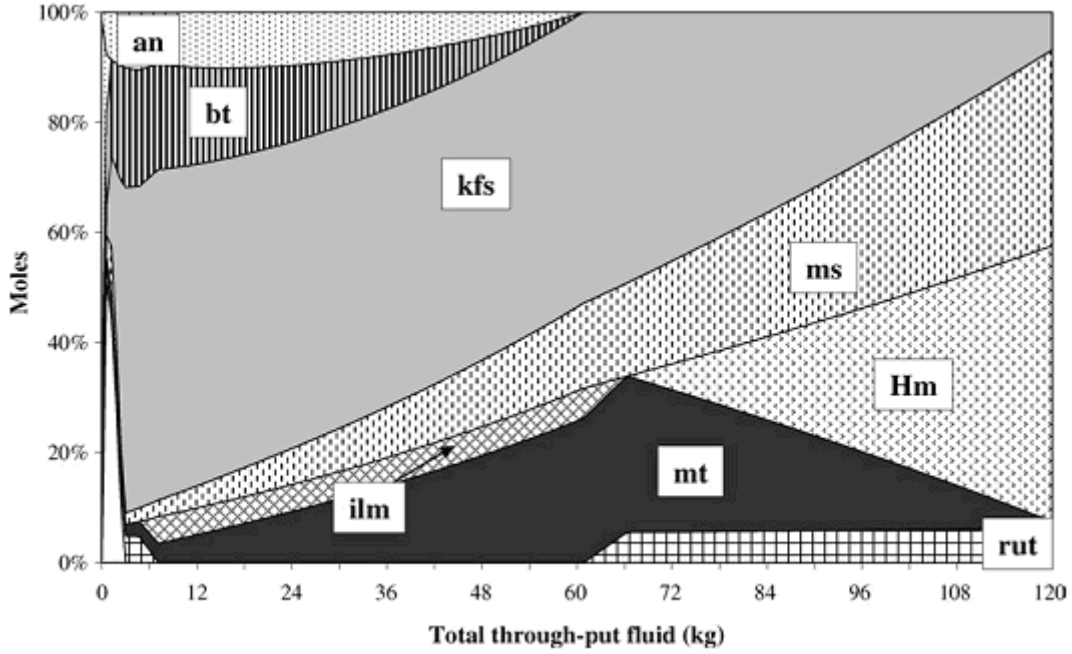

Figure 2-8: Predicted mineral assemblage from flush model with the total through-put mass of fluid per fixed 1kg of rock on the x-axis. Greater integrated fluid fluxes produce mineral assemblages more akin to the deposit core (k-feldspar-muscovite-hematite) that the alteration assemblage (k-feldspar-biotite-magnetite, left side). The maximum integrated log w/r is 2.1. Model geofa02.

Fluid Infiltration Model

The final model type is the fluid infiltration model, where a fluid front infiltrates a column of rock through the model, behind which a series of geochemical/mineralogical fronts develop. Figure 2-10A and B are fluid infiltration models with 100 steps and 100 step-series; the fluid front moves through the model at 1 step per new step series. Figure 2-10A is relatively rock dominant with an initial log w/r of -1 compared to log w/r of 1 in Fig. 2-10B. The mineral assemblages are plotted for step series 90, so that in both cases the limit of infiltration is at step 90, beyond which the rock is un-infiltrated.

The results in Figures 2-10A and B show the same general assemblage changes as those presented in Figure 2-4 except that there is now a spatial aspect to the results (distance of the fluid front through rock). Consistent with the metasomatic theory of Korzhinskii (1970) there are sharp geochemical fronts that mark both the appearance and disappearance of phases, and the mineralogical zones expand during infiltration (i.e. for each step-series). There are also different geochemical fronts observed within the fluid chemistry and between different fluid components (i.e. pH and redox, Fig. 2-11A and B) related to changes in the different buffering assemblages. Comparison of infiltration with different initial w/r values (Fig. 2-10A & B and Fig. 2-11A & B) shows major changes in the dominance, and subtle changes in the mineralogy of different alteration zones. In the case of low initial log w/r (-1, Fig. 2-10A) despite the infiltration of fluid to step 90, significant mineralogical alteration is only observed to step 50 (although the fluid chemistry is still being modified, see pH in Fig. 2-11A), and the k-feldspar – biotite zone is only present in the first few steps (proximal to the fluid source). In Fig. 2-10B (high initial log w/r = 1) the assemblage zones ahead of k-feldspar have been compressed to fewer steps and the k-feldspar – biotite (also additional epidote) now dominates much of the reacted rock. A new assemblage zone appears in the first few steps (hematite – quartz – muscovite) with corundum in the most proximal source zone. The presence of corundum here is a function of the fluid having stripped most of the silica and alkalis from the rock in these steps, leaving relatively immobile Al behind.

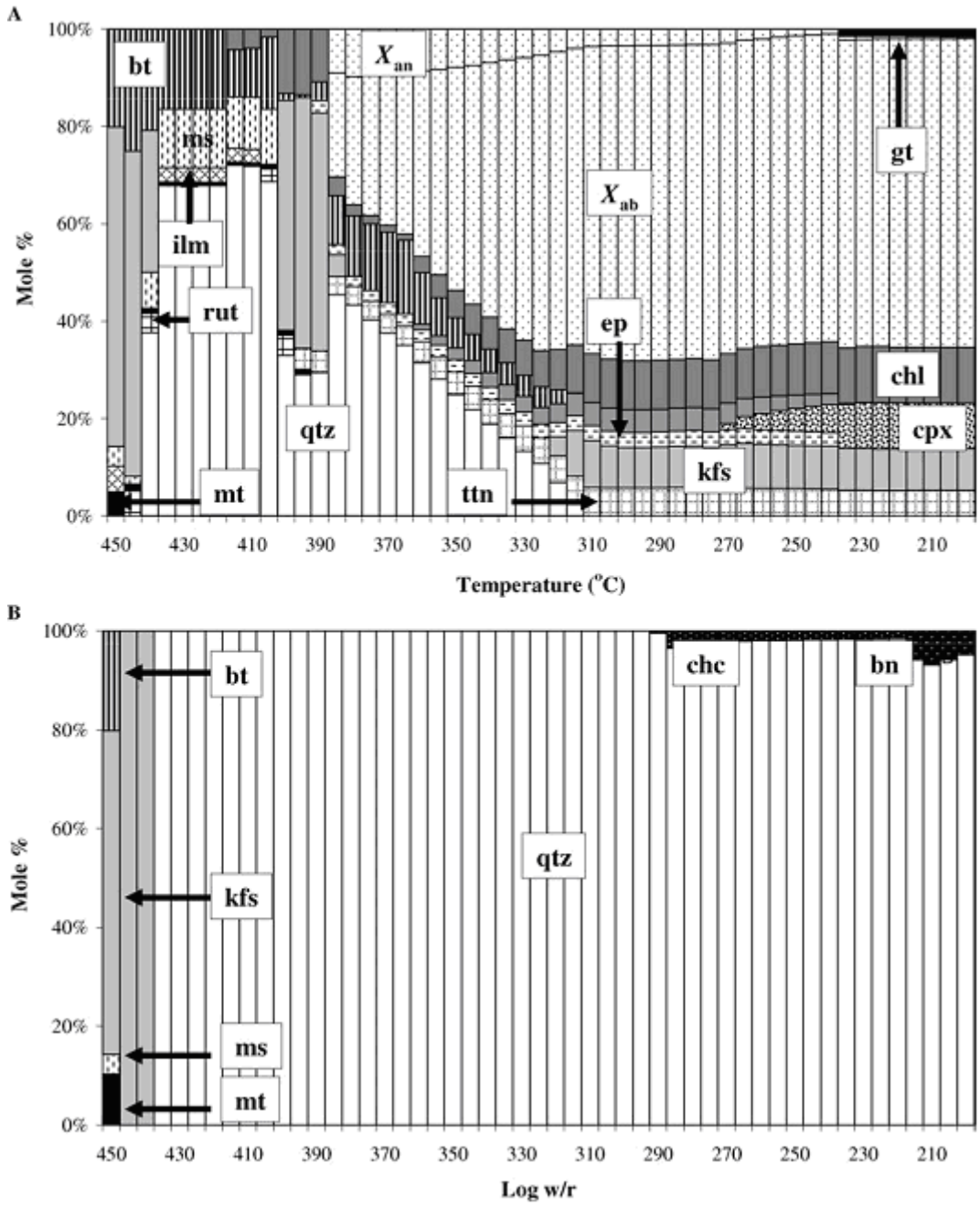

Figure 2-9: Predicted mineral assemblages for flow-through models across a T-P gradient (P (bars) = 8T - 1100), where the fluid is reacting with rock (A) and is isolated from rock reaction (B). In both models the initial step contains the result from reacting fluid with rock at log w/r = 1.0. Non-standard mineral abbreviations include: chc – chalcocite and bn – bornite. Model A) geof and B) geofc02.

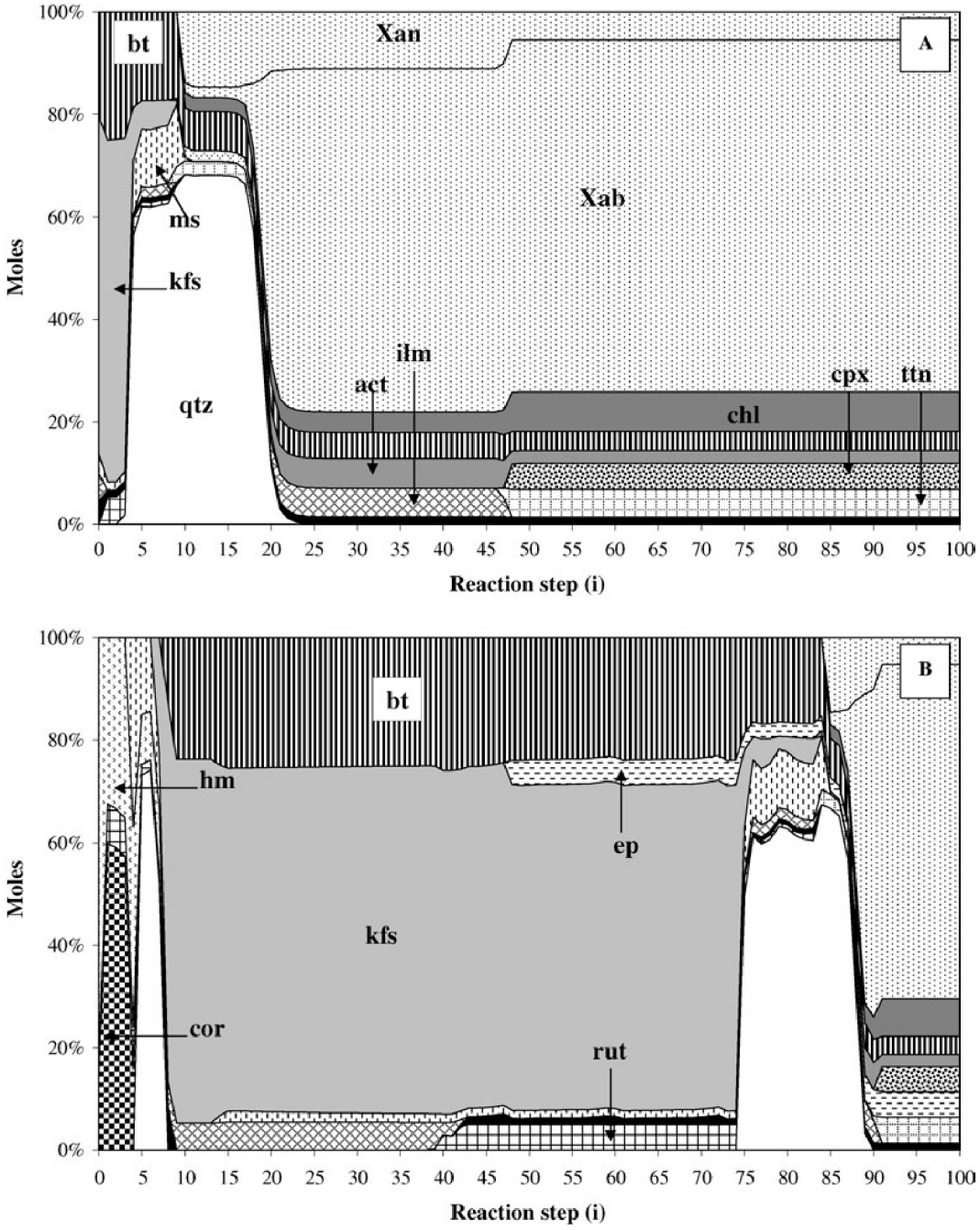

Figure 2-10: Mineral assemblages for fluid infiltration models plotted for a snap-shot at step series 90 (limit of infiltration is at step 90) for two different intial log w/r (A) -1 and (B) 1. The plot shows the mineralogical fronts forming behind the limit of infiltration. Model A) geofa05 and B) geof05c.

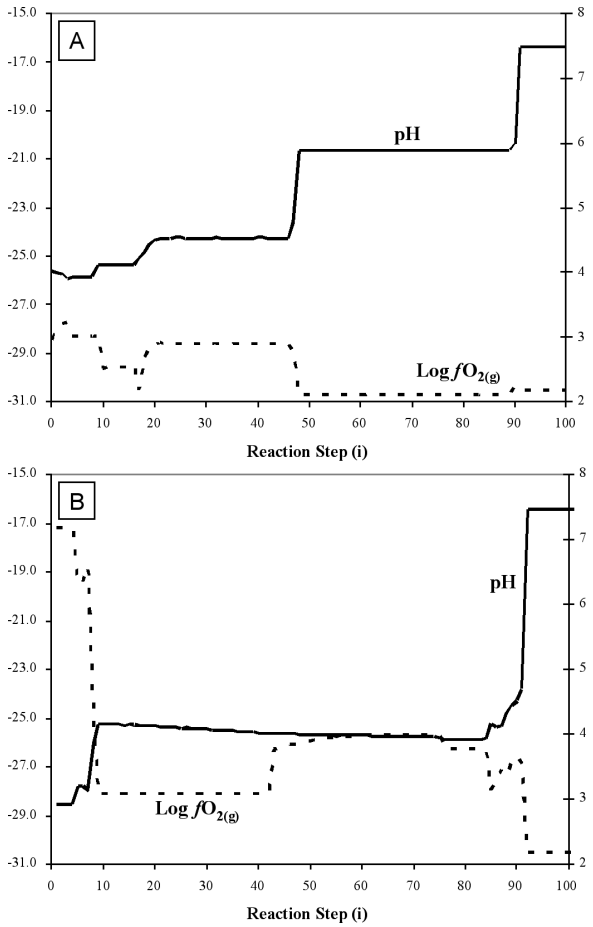

Figure 2-11: pH and log $f_{O2(g)}$ trends for fluid in the models from (A) Fig. 2-10A and (B) Fig. 2-10B. Conditions between step 90 and 100 represent the background rock buffered values with a small amount of coexisting water. The geochemical fronts behind the limit of infiltration are related to the different buffering assemblages and lateral changes in the chemistry of the infiltrating fluid.

Discussion

The flexibility of the input algorithms for modelling with HCh enable the simulation of a wide range of fluid-rock interaction processes. The examples explored above show that for K-alteration of Na-Ca-altered felsic volcanic rocks there are a number of different conceptual models that can be generated, each with subtle differences in the method used to react the rock and fluid. Comparison of the different conceptual models is a powerful tool allowing consideration of a very wide range of potential contributors to the real hydrothermal system development, and here we discuss how these models impact on our reasoning about genesis of ore-related alteration at Ernest Henry. The type of modelling presented here can be useful not only in elucidating the chemical and physical processes that lead to alteration and ore formation, but by modelling different aspects of an ore-forming system (Fig. 2-2, A-E) it may be possible to make predictions that aid decision making in exploration for mineral deposits.

The potassic alteration at Ernest Henry consists of an inner K-feldspar-rich zone (± biotite, magnetite, hematite, minor quartz, chlorite and muscovite) and an outer zone containing biotite with magnetite or hematite overprinting the earlier Na-Ca-altered felsic volcanic rocks (Mark et al., 2000). The static closed system models can be quickly used to explore the range of possible assemblages that would be predicted for interaction of fluid and rock or fluid mixing, in particular assemblage distributions across grids of results (e.g. T-P, Fig. 2-7). The models that best simulate the Ernest Henry spatial zonation are the isothermal, isobaric fluid infiltration models with K-rich fluid being continuously injected into progressively altered rock (Fig. 2-10). In the paragenetic sequence of Mark et al. (2000), minor amounts of chlorite and muscovite overprint biotite and K-feldspar in the core of the deposit, and are regarded as representing lower temperature conditions than the main K-feldspar rich assemblages. Chlorite-muscovite-dominant assemblages are lacking at Ernest Henry, and there is no indication of a major retrograde overprint, so we infer the present assemblages developed predominantly at high T-P (> 400°C). However, there is some indication that subtle temperature differences (450 to 400°C) may have existed between the core of the deposit and the margins, as shown by the assemblage maps derived from the static closed system models. Because the margins of the deposit were also likely to have had smaller total fluid fluxes than the core, this apparent lateral temperature variation

may be a consequence of heat advection by the fluids, focussed through the deposit core. However, this temperature variation, if real, did not result in any silica addition to the lower temperature domains, as might be expected from consideration of silica solubility in metamorphic fluid-rock systems (e.g. Ferry & Dipple, 1991).

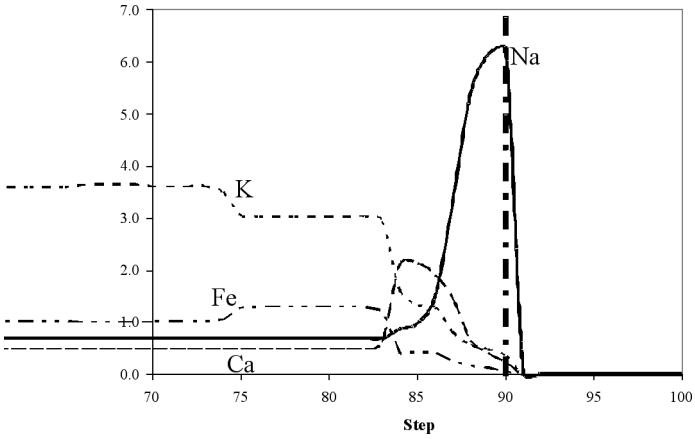

Figure 2-12: Total element concentrations in fluid for fluid in steps 70-100 of infiltration model shown in Fig. 10B. Na is stripped from the rock and transported in the fluid front (steps 90-85), while fluid behind the infiltration front is similar in composition to the incoming fluid (refer Fig. 2-6).

In all the models quartz is present in the assemblage at the transitions from k-feldspar to plagioclase (albite-anorthite solid-solution), which makes sense considering the reaction between k-feldspar and the anorthite component in plagioclase. In the deposit, however, obvious alteration-related quartz is not obvious at this interface, but Mark et al. (2000) describe quartz-phyric meta-volcanic rocks as one of the varieties of precursor rocks in the Ernest Henry envelope. It is thus possible that some of the quartz in these rocks is alteration related rather than primary, possibly having grown around earlier igneous quartz during conversion of plagioclase to K-feldspar. However, the quartz-rich transition assemblage could also relate to weaknesses in the solid-solution models for plagioclase and other minerals. It is possible that the model is overstepping a phase that should be stable under these conditions. The absence of corundum (or aluminosilicates) in the deposit requires that the fluid fluxes were insufficient to completely strip all but the immobile elements from the rocks, and/or that large fluid fluxes were not moving along an up-temperature pathway, which would also have the capacity to deplete silica (e.g. Dipple & Ferry, 1992).

Finally, the simulations of veining, with fluid moving from the high T-P initial alteration site to a lower T-P point without further wallrock interaction, do not match closely the vein assemblages found at Ernest Henry. Although K-feldspar-dominant veining is present (and also predicted at high T in Fig. 2-9), there is no indication of the predicted quartz veins. We infer from this that the veining at Ernest Henry was either exclusively high temperature, or involved a mixture of other components (e.g. fluid mixing) not addressed by our present models.

Infiltration Models and Fluid Chemistry

The input fluid chemistry in the work was constrained by analysis of K-alteration related fluid inclusions. The calculated Na/K of the fluid was not capable of generating the K-alteration assemblages described around Ernest Henry and has to be adjusted accordingly (see earlier). When analysing fluid inclusions, even well constrained petrographically there is a chance that the inflow and modified outflow chemistry could be measured. Figure 2-12 shows a plot of the total element concentrations at the active infiltration fluid front. Despite there being a constant inflow chemistry and reacting rock it can be seen that should fluid inclusions be trapped at the fluid infiltration front (Na>>Ca,K,Fe), immediately behind the fluid infiltration front (Ca>K>Na,Fe) or well inbored of the fluid front (K>>Fe,Na,Ca) the chemistry would be very different. It is also true that these chemical fronts migrate with progressive infiltration so that fluid inclusions of subtly different paragenesis could contain different chemistry, yet they are all related to a single event of K-alteration.

Length Scales During Infiltration

The fluid infiltration model, where fluid migrates through a rock column, can be considered to contain a temporal-spatial dimension despite there being no explicit definition of time and distance parameters. In the design of the model the step direction is equivalent to distance while the wave direction is equivalent to time (Fig. 2-3C), and the fluid front moves forward one step for each wave. While the results of this model

generate a spatial zonation of mineral assemblages (Fig. 2-10), the distance between the assemblage changes is not considered. Can the pseudo-spatial dimension of an equilibrium dynamic infiltration model be quantified?

The time and distance relationships for a fluid front moving through rock can be related to the rock and fluid properties and chemistry using the general transport equation of Dipple and Ferry (1996),

$$\frac{\partial(\phi C_i)}{\partial t} = -\frac{\partial(v C_i)}{\partial z} + . \qquad (1),$$

where is the porosity, Ci is the concentration of component i in the fluid, t is time, v is the Darcy flux, z is the distance along the flow path, and Ri is a reaction rate term for component i. This equation ignores the effects of diffusion and dispersion acting on the component being transported. Eq. 1 illustrates that given the chemical force to drive the reactions involving component i (in the Ri term), the time (t) and distance (z) terms are related to changing porosity and fluid flux (v, m/s). Dipple and Ferry (1996) simplify the relationship for a given fluid flux and the passage of the physical flow front as,

$$v_j^n = \frac{\Delta z}{\Delta t}\beta_j^n \quad (2),$$

where j is the cell reference and n is the time reference for the model. Here we see that for the infiltration of the fluid front (independent of the chemistry and mass transfer) the time-distance terms are co-dependent on fluid flux rate and porosity. For both reactive transport and our equilibrium dynamic infiltration transport models, flux rate needs to be specified to determine time or vice versa, in order to quantify the other variables. The porosity term can be estimated from HCh results by assuming that the mass ratio of fluid/rock is a directly proportional to the porosity after correction for the volumes of the components, and this then represents a close approximation to true reactive transport. Combining equations of Bickle and McKenzie (1987), Oliver et al. (1994) present a relationship for time integrated fluid flux which accounts for the relationships described above,

$$q = zK_i \frac{\partial_S}{\partial_F} = w_0 \phi t \quad (3),$$

where q is the time integrated fluid flux (m3/m2), z is distance (m), K_i is the mass fraction ratio of component i in the rock/fluid, and ∂_S/∂_F is the density ratio between rock and fluid, w_0 is the fluid velocity (m3/m2/s), Ø is the porosity and t is time (s). Using this relationship the HCh fluid infiltration model results can be used to estimate the total time integrated fluid flux (where K_i becomes fluid/rock mass ratio) based on a defined distance (length-scale of the reactor of interest) per reactor, alternatively with a fixed time integrated fluid flux it is possible to calculate the distance between the phase changes and the scale of the spatial zonation of the models. Because the fluid/rock ratio will change across any model as a function of the chemical reactions taking place in each reactor, the K_i in equation 3 will also change. This means that for a fixed time integrated fluid flux (q) the calculated distance between successive reactors (z) will change slightly, the inverse is also true, if the length scale of the reactors is fixed then the time integrated flux must change.

Using the model from Fig. 2-10B as an example the length-scale of each reactor had been estimated for a fixed integrated fluid-flux using the relationships in equation 3. The rock density and fluid/rock mass ratio (K_i) is calculated from the model results at each step, fluid density is estimated from the bulk chemical properties using the formulations of (Batzle & Wang, 1992) at 450˚C and 2500 bars (= 1.2105 g/cm^3) and is kept constant. The integrated fluid flux is kept constant at q = 2000 which is similar to values calculated for hydrothermal systems from isotope studies (i.e. q = 1680, Teagle et al., 2000). Figure 2-13 is a plot of the model from Fig. 2-10B showing the calculated length-scales of each step. It can be seen that for a fixed value of q the calculated length of each step varies, with the largest zones proximal to fluid input and no length associated with un-infiltrated rocks (> step 90). The total length of alteration in Fig. 2-10B calculated from Fig. 2-13 is 1200m, compared to the mapped distribution of 500-1000m in Mark (2005). By inverting the problem the total length of alteration from Fig. 2-10B is 600m when q = 1000.

Genesis of Ernest Henry

The Ernest Henry ore zone is dominated by infill between K-altered clasts by combinations of magnetite – calcite – k-feldspar – biotite – quartz and pyrite – chalcopyrite – bornite (Mark et al., 2005), over printed by a later stage of muscovite – hematite. In an attempt to model the K-alteration at Ernest Henry it can be

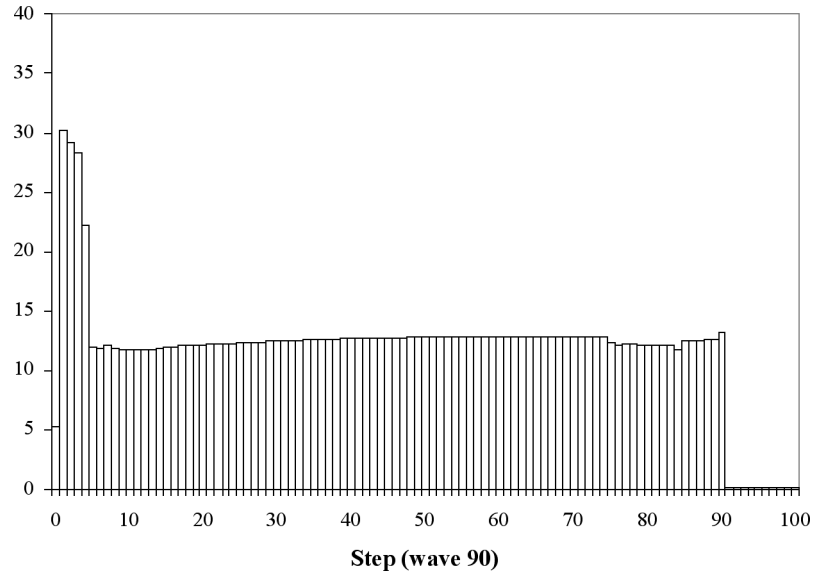

Figure 2-13: Calculated length-scale (meters) for the infiltration results from Fig. 2-10B assuming a fixed time integrated fluid flux (q) of 2000 m^3/m^2. The total distance of alteration in this example is approximately 1200 meters. See text for numerical assumptions and calculation procedures.

shown that high fluid flux (flush) assemblages from Fig. 2-8 (k-feldspar – magnetite – biotite to k-feldspar – hematite – muscovite) and the k-feldspar vein precipitation matches closely some of the ore zone assemblages. However the voluminous calcite – magnetite and sulphides (pyrite – chalcopyrite) observed in the natural system are not present in the model results. This leads us to suggest that while at least some of the ore zone alteration can be produced with a single fluid following interaction with the local wall rock other components require the presence of a second fluid, in agreement with the fluid mixing models proposed by other authors (Oliver et al., 2004; Mark et al., 2005). It is interesting to note however that many of the alteration assemblages do require at least some rock interaction, and that the flush model predicts the evolution of the system to muscovite – hematite assemblage by continued fluxing of fluid through a single rock package.

Application to Exploration

The distal assemblages predicted here, including ones for both down-T-P and isobaric, isothermal conditions, theoretically provide clear vector tools for explorationists if the construction of the inputs and model scenarios is geologically valid. For near constant T-P conditions, the infiltration model predicts biotite alteration outboard of K-feldspar alteration, matching the known zonation around the Ernest Henry deposit. Elsewhere, such a zonation could reasonably be inferred to indicate potential geographical proximity to ore, assuming that the ore system isotherms were fairly shallow. Also, our specific example here is for a rock type that is particular to Ernest Henry (felsic volcanics), so different lateral zonations might be expected for different rock types. Despite the variation in host rock types for other iron oxide-Cu-Au deposits in the district (Williams, 1998), distal biotite alteration is a common feature of the deposits. This suggests a common origin for at least one of the fluids regionally involved in ore genesis, and also that this fluid was capable of dominating the fluid-rock budget sufficiently to stabilize biotite as a dominant alteration phase in a variety of host rocks.

The lack of widespread low temperature retrograde assemblages in the deposits at the present level of exposure suggests that cooling fluids either had exhausted their capacity to alter the rocks further, or were effectively removed from the ore environment into overlying rocks. As for the previous discussion on K-feldspar – biotite zoning, the predicted low temperature assemblages (e.g. muscovite-chlorite) and model veins (e.g. quartz – K-feldspar) generated here would theoretically only apply to retrogression in altered meta-volcanic rocks, unless the fluid fluxes were sufficiently high that different rocks converged to similar retrograde alteration or vein assemblages. Ongoing work is considering the down-T-P outflow of Ernest Henry fluids into rocks other than the immediate metavolcanic hosts (e.g. pelitic and calc-silicate rocks, mafic amphibolites). However, if we assume that 1 kilometre is the maximum depth to which an exploration company would wish to consider drilling to find ore, then a 30°C /km paleogeothermal gradient would only give rise to a 30°C variation in possible assemblage variation along an outflow path, unless the paleo-geothermal gradient were tilted or telescoped in some way. Calculation of outflow above an orebody down to temperatures of 250 to 300°C, then, is not of direct use here, but serves to illustrate the types

of assemblages that might be present in the far hangingwall of deposits above which steep geothermal gradients were prevalent. Mark et al. (2005) used such a deduction to draw the interesting conclusion that the modeled low-temperature outflow signal of Ernest Henry ore genesis produces alteration assemblages similar to those in the proximity of the giant Olympic Dam deposit in South Australia.

This work has applied a number of conceptual models (closed system, flush and infiltration) to understand the effects of different fluid-rock interactions for a single geochemical problem. While the fluid infiltration model is best for describing lateral zonation in assemblages, the static closed system and flush/flow-through models are useful in understanding different aspects of the system (breccia infill and veining) or for rapid examination of a range of possible outcomes. In the application of geochemical modelling to exploration and ore system studies a combination of all these model types can be utilised to best understand the evolution of different areas of a single natural system and it is equally important to understand what process a model is conceptualising as to understand the model itself.

Acknowledgments

The authors would like to thank Evgeniy Bastrakov for providing his customised version of the UNITHERM database and for his constructive comments on the initial draft of this manuscript. Discussions over a protracted period with Geordie Mark, Pat Williams and Ernest Henry staff helped improve the model inputs, and Mark Reed and an anonymous reviewer are thanked for useful comments in their formal reviews. Work reported here was conducted as part of the Predictive Mineral Discovery Cooperative Research Centre and this work is published with the permission of the CEO.

References

Balashov VN, Yardley BWD (1998) Modeling metamorphic fluid flow with reaction-compaction-permeability feedbacks. American Journal of Science, 298, 441-470.

Bastrakov EN (2003) Geoscience Australia version of UNITHERM database for the HCh package for geochemical modelling, v. unpublished computer file.

Bastrakov EN, Shvarov YV, Girvan S, Cleverley JS, Wyborn L (2004) FreeGs: web-enabled thermodynamic database for modelling of geochemical processes. In: Dynamic Earth: Past, present and future. Abstracts of the 17th Australian Geological Convention, Hobart, Tasmania, Australia, Feburary 8-13th (eds J. McPhie & P. McGoldrick), pp. 52.

Batzle M, Wang Z (1992) Seismic properties of pore fluids. Geophysics, 57, 1396-1408.

Berman RG (1988) Internally-consistent thermodynamic data for minerals in the system Na2O-K2O-CaO-MgO-FeO-Fe2O3-Al2O3-SiO2-TiO2-H2O-CO2. Journal of Petrology, 29, 445-522.

Bethke CM (1996) Geochemical Reaction Path Modeling: Concepts and applications. Oxford University Press, New York.

Bickle M, Baker J (1990) Migration of reaction and isotope fronts in infiltration zones: assessments of fluid flux in metamorphic terrains. Earth and Planetary Science Letters, 98, 1-13.

Bickle MJ, McKenzie D (1987) The transport of heat and matter by fluids during metamorphism. Contributions to Mineralogy and Petrology, 95(384-392).

Blattner P, Lassey KR (1989) Stable-isotope exchange fronts, Damkohler numbers, and fluid to rock ratios. Chemical Geology, 78, 381-392.

Ding K, Seyfried WE (1990) Activity coefficients of H2 and H2S in NaCl solutions at 300-400oC, 300-500 bars with application to ridge crest hydrothermal systems. EOS, 71(43), 1680.

Dipple GM, Ferry JM (1996) The effect of thermal history on the development of mineral assemblages during infiltration-driven contact metamorphism. Contributions to Mineralogy and Petrology, 124, 334-345.

Ferry JM, Dipple GM (1991) Fluid flow, mineral reactions, and metasomatism. Geology, 19, 211-214.

Fu B, Williams PJ, Oliver NHS, Dong G, Pollard PJ, Mark G (2003) Fluid mixing versus unmixing as an ore-forming process in the Cloncurry Fe-oxide-Cu-Au District, NW Queensland, Australia: evidence from fluid inclusions. Journal of Geochemical Exploration, 78-79, 617-622.

Grichuk DV, Shvarov YV (2002) Comparative analysis of techniques used in the equilibrium-dynamic simulations of infiltration metasomatic zoning. Petrology, 10(6), 580-592.

Heinrich CA, Walshe JL, Harrold BP (1996) Chemical mass transfer modelling of ore-forming hydrothermal systems: current practise and problems. Ore Geology Reviews, 10, 319-338.

Helgeson HC (1968) Evaluation of irreversible reactions in geochemical processes involving minerals and aqeuous solutions I. Thermodynamic relations. Geochimica Et Cosmochimica Acta, 32(8), 853-877.

Helgeson HC, Kirkham DH, Flowers GC (1981) Theoretical prediction of the thermodynamic behaviour of aqueous electrolytes at high pressures and temperatures: Calculation of activity coefficients, osmotic coefficients, and apparent molal and standard and relative partial molal properties to 600oC and 5 kb. American Journal of Science, 281(10), 1249-1516.

Korzhinskii DS (1970) The theory of metasomatic zoning. Clarendon Press, Oxford.

Kretz R (1983) Symbols for rock-forming minerals. American Mineralogist, 68, 277-279.

Mark G, Oliver NHS, Williams PJ (in revision) Mineralogical and chemical evolution of the Ernest Henry Fe oxide-Cu-Au ore system, Cloncurry district, northwest Queensland, Australia. Mineralium Deposita.

Mark G, Oliver NHS, Williams PJ, Valenta RK, Crookes RA (2000) The evolution of the Ernest Henry hydrothermal system. In: Hydrothermal Iron-Oxide Copper-Gold and related deposits: A global perspective (ed T. M. Porter), pp. 132-136, Australian Mineral Foundation, Adelaide.

Mark G, Wilde A, Oliver NHS, Williams PJ, Ryan CG (2005) Modeling outflow from the Ernest Henry Fe oxide Cu-Au deposit: implicaitons for ore genesis and exploration. Journal of Geochemical Exploration, 85, 31-46.

Oelkers EH, Helgeson HC (1990) Triple-ion anions and polynuclear complexing in supercritical electrolyte solutions. Geochimica et Cosmochmica Acta, 54(3), 727-738.

Oliver NHS (1996) Review and classification of structural controls on fluid flow during regional metamorphism. Journal of Metamorphic Petrology, 14, 477-492.

Oliver NHS, Cartwright I, Rawling TR, Pearson PJ (1994) High temperature fluid-rock interaction and scapolitization in an extension-related hydrothermal system, Mary Kathleen, Australia. Journal of Petrology, 35, 1455-1493.

Oliver NHS, Cleverley JS, Mark G, Pollard PJ, Fu B, Marshall LJ, Rubenach MJ, Williams PJ, Baker T (2004) Modelling the role of sodic alteration in the genesis of iron oxide-copper-gold deposits; eastern Mt Isa Block, Australia. Economic Geology, 99, 1145-1176.

Pokrovskii VA, Harrold BP, Heinrich CA, Liu X (1998) Release notes for THERMODATA AGSO/ANU/ETH (version 5.2), v. Australian Geological Survey Organisation.

Pokrovskii VA, Helgeson HC (1995) Thermodynamic properties of aqueous species and the solubilities of minerals at high pressures and temperatures: the system Al2O3-H2O-NaCl. American Journal of Science, 295(10), 1255-1342.

Powell R (1977) Activity-composition relation for crystalline solutions. In: Thermodynamics in geology (ed D. G. Fraser), pp. 57-65, D. Reidel Publishing Company, Dordrecht.

Reed MH (1997) Hydrothermal alteration and its relationship to ore fluid composition. In: Geochemistry of hydrothermal ore deposits (ed H. L. Barnes), pp. 303-365, John Wiley & Sons, Inc, New York.

Reed MH (1998) Calculation of simultaneous chemical equilibrium in aqueous-mineral-gas systems and it sapplication to modeling hydrothermal processes. In: Techniques in hydrothermal ore deposits geology (eds J. P. Richards & P. B. Larson), pp. 109-123, Society of Economic Geologists.

Shock EL, Sassani DC, Willis M, Sverjensky DA (1997) Inorganic species in geological fluids: Correlations among standard molal thermodynamic properties of aqueous ions and hydroxide complexes. Geochimica et Cosmochmica Acta, 61, 907-950.

Shvarov YV (1978) Minimization of the thermodynamic potential of an open chemical system. Geochemistry International, 15(6), 200-203.

Shvarov YV (1981) A general equilibrium criterion for an isobaric-isothermal model of a chemical system. Geochemistry International, 18(4), 38-45.

Shvarov YV (1987) Use of electrical neutrality equation in calculations on the equilibrium compositions of geochemical systems. Geochemistry International, 24(2), 131-135.

Shvarov YV (1999) Algorithmization of the numeric equilibrium modeling of dynamic geochemical processes. Geochemistry International, 37(6), 571-576.

Shvarov YV, Bastrakov EN (1999) HCh: a software package for geochemical equilibrium modelling. User's Guide. Australian Geological Survey Organisation, Canberra.

Suleimenov OM, Krupp RE (1994) Solubility of hydrogen sulfide in pure water and in NaCl solutions, from 20 to 320oC and at saturation pressures. Geochimica et Cosmochmica Acta, 58(11), 2433-2444.

Sverjensky DA, Hemley JJ, D'Angelo WM (1991) Thermodynamic assessment of hydrothermal alkali feldspar-mica-aluminosilicate equilibria. Geochimica et Cosmochmica Acta, 55, 981-1104.

Sverjensky DA, Shock EL, Helgeson HC (1997) Prediction of the thermodynamic properties of aqueous metal complexes to 1000oC amd 5kb. Geochimica et Cosmochmica Acta, 61, 1359-1412.

Teagle DH, Bickle MJ, Alt J (2000) High temperature Mid-ocean ridge hydrothermal flux estimates from Sr-transport modeling of fluid-rock exchange in hole 504b. Journal of Conference Abstracts (Goldschmidt 2000), 5(2), 987.

Twyerould SC (1997) The geology and genesis of the Ernest Henry Fe-Cu-Au deposit, Northwest Queensland, Australia. Unpub. PhD Thesis, University of Oregon.

Williams PJ (1998) An introduction to the metallogeny of the McArthur River Mount Isa Cloncurry Minerals Province. Economic Geology and the Bulletin of the Society of Economic Geologists, 93(8), 1120-1131.

Wolery T (1983) EQ3NR, a computer program for geochemical aqueous speciation solubility calculations: User's guide and documentation. Lawrence Livermore National Laboratories. UCRL-53414.

Appendix

This appendix contains the numerical algorithms for each of the case example models presented in the text as they should be entered into the HCh control file. This is not intended to give readers a full instruction on the use of HCh control files as this can be found in Shvarov and Bastrakov (1999) and Shvarov (1999). A brief overview of control file symbols can be found in Table A1. In the following examples the boxed numbers refer to the input components as defined in Table 2 (e.g. [1] is component 1). Unless otherwise specified all models are isothermal and isobaric at 450°C and 2500 bars.

Symbol	Variable
T	Current temperature (°C).
P	Current Pressure (bars).
i	Current step number.
N	Current wave number.
[1]	Input composition (1 = 1st, 2 = 2nd etc).
[A]	Bulk composition of aqueous phase in system from current wave, previous step.
[S]	Bulk composition of solid phase in system from current wave, previous step.
[*]	Current total system bulk composition (all phases).
{A}	Bulk composition of aqueous phase in system from previous wave, current step.
{S}	Bulk composition of solid phase in the system from the previous wave, current step.
{A(i-1)}	Bulk composition of aqueous phase in the system from the previous wave, step number i-1.

Appendix Table 1: Important symbols and their meanings used in the construction of an HCh control file algorithm and used in the appendix of example control files. See Shvarov & Bastrakov (1999) for a complete list.

Static Closed System

Initial Step:

[*] = [1]

General Step:

[*] = [1]+([2]*10^((i*0.5)-6))

STATIC CLOSED SYSTEM T-P GRID

Initial Step:

T = 450

P = 2500

[*] = [1]+(0.1*[2])

General Step:

T = T-10

P = P-20

[*] = [1]+(0.1*[2])

OUTFLOW

Initial Step:

T = 450

P = 2500

[*] = [1]+(0.1*[2])

General Step:

T = T-10

P = P-20

[*] = [A]+(0.1*[2])

VEINING

Initial Step:

T = 450

P = 2500

[*] = [1]+(0.1*[2])

General Step:

T = T-10

P = P-20

[*] = [A]

FLOW-THROUGH

Initial Step:

[*] = [1]

General Step:

[*] = [A] + ([2]*(0.015*i))

FLOW-THROUGH

Initial Step:

[*] = [1]+([2]*10^-1)

General Step:

[*] = [1] + [S]

FLUID INFILTRATION

Step Series 0, Initial Step:

[*] = ([1]*10)+[2]

Step Series 0, General Step:

[*] = [2]

Step Series N, Initial Step:

[*] = ([1]*10)+{S}

Step Series N, General Step:

[*] = ({A}-1)+{S}

Chapter 3: Hydrothermal geochemistry and modelling of sodic alteration around iron oxide–copper–gold deposits, eastern Mt. Isa Block, Australia

Nicholas H. S. Oliver, James S. Cleverley, Geordie Mark‡, Peter J. Pollard, Bin Fu, Lucas J. Marshall, Michael J. Rubenach, Patrick J. Williams, and Timothy Baker

Economic Geology Research Unit, School of Earth Sciences, James Cook University, Townsville, Australia 4811, and the Predictive Mineral Discovery Cooperative Research Centre

‡Present address: School of Geosciences, Monash University, Clayton, Australia 3168

This report is modified from Oliver, N.H.S., Cleverley, J.S., Mark, G., Pollard, P.J., Fu, B., Marshall, L.J., Rubenach, M.J., Williams, P.J. & Baker, T., 2004. Modeling the role of sodic alteration in the genesis of iron oxide-copper-gold deposits, Eastern Mount Isa Block, Australia. Economic Geology, Vol. 99, pp. 1145–1176

Abstract

Liberation of iron and potassium by widespread albitization of country rocks was one of the contributing processes in the formation of (magnetite + biotite ± hematite) metasomatic ironstones that host Proterozoic Cu-Au mineralization in the Cloncurry District of the Proterozoic Mt Isa Block. Using a reference frame defined by isocons with near constant volume change and effectively immobile Al, Ga ± Ti, Zr, whole rock geochemical data for transformation of a variety of initial rocks towards albitite indicates that Na addition to the rock from an initial NaCl-rich hypersaline brine accompanied the loss of Fe, K, Ba, Rb ± Ca, Si, Sr, Co, V, Mn from altered rocks to the brine. Conversely, the formation of metasomatic ironstones, the immediate hosts to Cu-Au ores, from a similarly broad range of host rock varieties, involves addition of most of the same elements that were lost during albitization. This type of chemical pathway has been modelled using the HCh hydrothermal geochemistry package for conditions appropriate to albitization (450 to 550°C, 3 kb), in which fluid-rock titrations using input fluids that are initially in equilibrium with albite and quartz result in production of alteration assemblages at different fluid fluxes that closely match those observed in the field. With increasing amounts of fluid-rock interaction in the models, the fluids were enriched in K, Fe and Ca, approaching compositions observed in fluid inclusions in the ore deposits. These fluids, reacted with pelitic rocks (which are common ore hosts), would produce magnetite-clinopyroxene± biotite-actinolite alteration at high temperature, similar to the proximal alteration around ore deposits. The extraordinary extent of albitic alteration precludes up-temperature fluid flow as the mechanism for Na–K-(Fe) exchange, instead requiring that fluids evolving from 2-feldspar intrusions were initially albite-stable, a circumstance best explained by reduced aH_2O due to the presence of high CO_2 contents of the magmas and fluids. Previously reported fluid inclusion data (PIXE and LA-ICPMS) from some ironstones hosted in c. 1515 Ma intrusions of the Williams Batholith, along with our geochemical results, confirm that copper (and likely gold) were sourced from the magmas rather than from the albitization process, and were transported predominantly as chlorides within the brine. We infer that precipitation of sulfides in the Cu-Au deposits was the result of mixing of Cu-bearing brine, of ultimately magmatic origin but modified extensively via albitization, with sulphur-bearing fluids, or reaction of the brine with sulphur-bearing rocks. When Cu was absent from the initial magmatic fluid, barren ironstones may have been the result.

Introduction

The association of sodic (± calcic) alteration with deposits of the mesothermal Fe-oxide–Cu–Au category has been recognized for some time (Hitzman et al., 1992; Williams, 1994, 1998; deJong and Williams, 1995; Barton and Johnson, 1996; Frietsch et al., 1997; Haynes, 2000; Marschik et al., 2003). However, the role of the sodic alteration in orebody formation remains uncertain. Albitization may occur as a consequence of hydrothermal fluid circulation around seafloor hydrothermal cells (Ito et al., 1983; Bird et al., 1984; Rose et al., 1992), and is thought to occur in the up-temperature portions of such flow systems as a consequence of the thermal dependence of the stability of albite relative to potassic minerals. Albite-rich rocks in continental rifts have also been interpreted as the products of syngenetic, diagenetic or metamorphic recycling of evaporite components (Cook and Ashley, 1992; Oliver et al., 1994), and Barton and Johnson (1996)

proposed that circulation of saline, evaporite derived brines was instrumental in production of mineralized ironstones in Nevada, stripping iron and base metals from wall rocks during sodic-calcic alteration. Alternative models, particularly in post-metamorphic environments where basin-derived fluid sources are not readily apparent, appeal to fluid release from igneous crystallization to provide ore-forming constituents in Fe-oxide-Cu-Au deposits (Hitzman et al., 1992; Oreskes and Einaudi, 1992). Highly saline fluids may exsolve from crystallizing intermediate or felsic magma and move along down-temperature flow paths (e.g., Cline and Bodnar, 1991), and this has been proposed as the source of metal and brine for La Candelaria (Marschik and Fontboté, 2001; Marschik et al., 2003) and other Andean (Sillitoe, 2003) Fe-oxide–Cu–Au, and for the post-metamorphic Proterozoic Fe-oxide–Cu–Au deposits of the Cloncurry District (Rotherham et al., 1998; Williams, 1998; Mark et al., 2000; Perring et al., 2000; Baker et al., 2001; Pollard, 2001). However, some Fe-oxide–Cu–Au districts, particularly in the lower temperature spectrum, are not associated with regional sodic alteration even when a magmatic source is suggested for some of the ore forming components (e.g., Skirrow and Walshe, 2002). Important questions for research and exploration for Fe-oxide–Cu–Au deposits are:

1. Were albitizing brines derived from evaporite dissolution or release of fluid from crystallizing magmas or both?
2. If magmatic-hydrothermal fluids were responsible for albitization, how are the high Na/K ratios attained in fluids released by crystallizing two-feldspar granitoids;?
3. If evaporite dissolution was responsible for albitization, were evaporites and solvents available, and can a mechanism of interaction with granitoids be found that explains the magmatic stable isotope signatures?
4. Is albitization a necessary precursor to Fe-oxide–Cu–Au mineralization, or is it unrelated;? And
5. Where were the ore forming metals and sulphur derived?

Here, we attempt to answer some of these questions for regional sodic alteration and mesothermal Fe-oxide–Cu–Au deposits of the Eastern Succession of the Mt. Isa Block (Fig. 3-1), building on previous deposit studies, our regional alteration mapping, fluid inclusion data, and geochemical modeling. In particular, we test the hypothesis of Williams (1994) that at least some ironstones of the Cloncurry District were the products of saline brines whose chemistry was modified through fluid-rock reaction (albitization), and the resulting liberation of Fe, K and related elements to the fluid. For copper, our geochemical analyses provide some insights as to the likely source(s), and whether or not albitization was crucial for copper enrichment in metasomatic fluids. We simulate possible reaction paths and mass transfer for fluid-rock interaction using the geochemical modeling package HCh (HydroChemistry) of Shvarov and Bastrakov (1999), which is a Gibbs free energy minimization program particularly suited to high P-T fluid-rock interaction simulations.

Regional Geology

The Eastern Succession refers to the eastern part of the Mt. Isa Block, including the Mary Kathleen Fold Belt (MKFB) in the centre, and the Cloncurry District in the east (Fig. 3-1). Hosts of the alteration and mineralization across the whole Eastern Succession are dominated by calc-silicate rocks, marbles and minor pelitic and volcanic rocks of the 1760-1730 Ma Mary Kathleen Group (particularly the Corella Fm.), and siliciclastic metasedimentary and mafic metavolcanic rocks of the 1670 – 1620 Ma Soldiers Cap Group. Other rocks include intrusions of various ages, mostly from two main cycles comprising the premetamorphic Wonga Granite and related gabbros (1750 – 1730 Ma), and the post-metamorphic Williams and Naraku Granites and related gabbros and intermediate intrusions (1550 – 1500 Ma) referred to here as the Williams Suite. The chronology of deformation, metamorphism, alteration and mineralization in the Eastern Succession has been explored elsewhere in some depth and is summarized in Oliver et al. (2004). Recently, it has been recognized that the peak metamorphic event, previously inferred to be at ca. 1550 Ma, lies in the range 1600 – 1580 Ma (Giles and Nutman, 2002; Hand and Rubatto, 2002). The greenschist to upper amphibolite facies “Isan” metamorphism accompanied localized early thrusts and folds (D1) and widespread upright (D2) folds. From 1555 to 1500 Ma, there was another major thermal event, associated with intrusion of the Williams Suite, simultaneously with several deformation phases involving ductile shear zones, brittle-ductile fault zones, and brecciation (D3 and later). Several phases of syn- or post-tectonic intrusions of the Williams Suite can be recognized, including a spatially restricted one at ~ 1545 Ma (exposed in the southeast) and less well defined but more voluminous phases in the range 1530 to 1500 Ma (Page and Sun, 1998; Pollard et al., 1998). Widespread albitization (Pollard et al., 1998; Pollard, 2001) and Cu-Au mineralization (e.g., Perkins and Wyborn, 1998; Williams, 1998; Baker et al., 2001) occurred during this

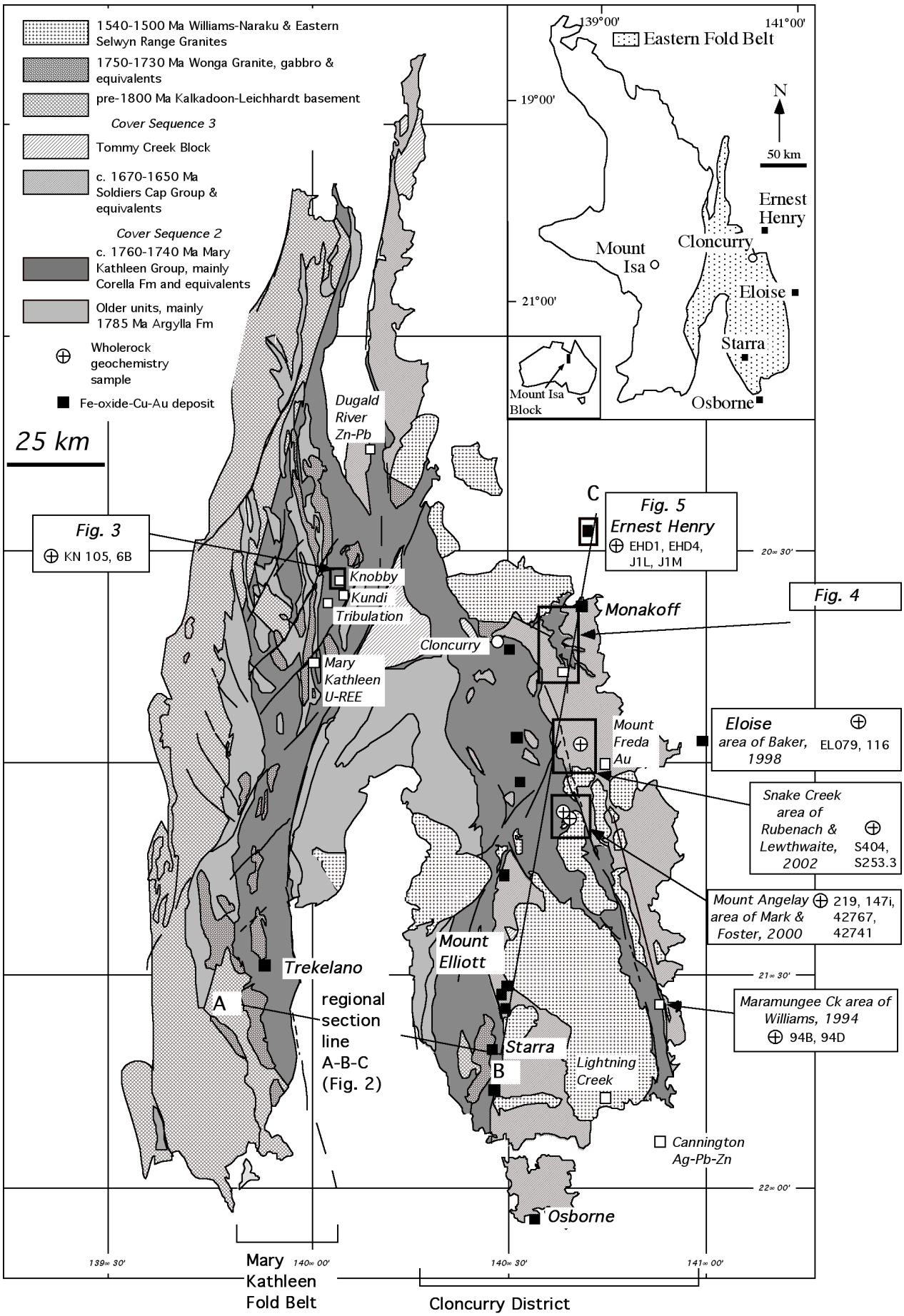

Figure 3-1. Map of the Eastern Succession of the Proterozoic Mt. Isa Block, showing the location of more detailed maps and cross sections in this paper and locations of study areas from previous papers, the major Fe-oxide–Cu-Au deposits, other localities mentioned in the text, and whole-rock geochemistry locations. Inset shows the location of the Eastern Succession of the Mount Isa Block in northern Australia. Modified from Williams (1998).

period. Notably, however, the Osborne Cu-Au deposit and associated albite alteration record the earlier Isan peak metamorphic cycle, as do several regional albitites in the Snake Creek area (see below). Thermal events and alteration postdating 1500 Ma are not discussed here (see Oliver, 1995).

The Cu-Au deposits have been described in detail elsewhere. They generally comprise an association of magnetite, chalcopyrite, pyrite ± pyrrhotite or hematite, surrounded by a proximal (50 to 200 m-scale) halo of magnetite ± hematite ± biotite and combinations (at different deposits) of calcite, garnet, chlorite, epidote, diopside, actinolite, orthoamphiboles, K-feldspar, scapolite, titanite, apatite, uraninite, fluorite and a host of complex phases containing Mn, U, Co, REE, P, and Cl. At the largest deposit, Ernest Henry, conversion of host rocks to magnetite-biotite gangue involved addition of Fe, K and a range of other elements (Mark et al., 2000). Almost all deposits are surrounded by a distal 100 m- to km-scale halo of Na±Ca alteration, although distinctions between distal and more regional albite alteration are commonly unclear because of the widespread extent of the latter (see below). Fluid inclusions, mostly from quartz veins in the deposits, reveal highly complex brines and CO2-rich compositions (Oliver et al., 2004), and most of the brines have highly elevated Rb, Ba, K, Ca, Fe, Mn, Cu, Pb and Zn concentrations (Williams et al., 1999; 2001; Mark et al., 2000; Perring et al., 2000). Stable isotope data for carbonates and sulfides are dominated by apparent igneous signatures, with local influences of host rock carbon and sulphur (Davidson and Dixon, 1992; Mark et al., 2000; Marshall and Oliver, 2005; Marshall et al., 2006). Marshall and Oliver (2005) and Marshall et al. (2006) demonstrate that fluids involved in both albite alteration and in IOCG mineralization shared characteristics of the infiltration of an isotopically homogeneous, medium- to high-temperature fluid derived from or equilibrated with intrusive rocks. However, the deposits are mostly distal to intrusions, with only the Mt. Elliott deposit lying within 1 km of an exposed km-scale intrusion (Fig. 1). Ore deposition is thought to have occurred by two main mechanisms: (1) reaction of Cu-bearing brines with previous ironstones and/or sulfide-bearing rocks such as black shales (Davidson and Dixon, 1992; Williams, 1998; Baker et al., 2001), or (2) reaction of two (or more) fluids, including one or more Cu–bearing brines, and a S-bearing fluid of varying oxidation state (e.g., Mark et al., 2000; Williams et al., 2001).

Characteristics of albite alteration

Oliver et al. (1994) recognized synextensional (ca. 1740 Ma) sodic-calcic alteration in the Mary Kathleen Fold Belt (MKFB) in the westernmost part of the Eastern Succession (Table 3-1). This alteration is dominated by scapolite, is relatively restricted in extent, predates deposition of the Soldiers Cap Group which elsewhere is mineralized, and is not discussed further here.

Event	Mineral associations	Extent, host rock	P-T	General references	Fluid source, references
Wongan extension & intrusions, 1750-1730 Ma					
Skarns	cpx-gt-sc skarns	km-scale in calc-silicate rocks	500-700°C, 150 –200 MPa	Oliver et al., 1994; Oliver, 1995	Metamorphic, evaporitic, magmatic (Oliver et al., 1994)
Shear zones	sc-ab shear zones	1m-100m scales in granite	500-700°C, 150 –200 MPa		
Dolerite alteration	sc-am alteration in mafic rocks	100m-km scales in dolerites			
Regional metamorphism, 1600-1580 Ma (Isan Orogeny)					
Regional metamorphism of calc-silicate and pelitic rocks	sc-qz-cc-kf±bt-am-cpx-ttn-ap-mt-ilm in calc-silicate rocks, bt-mu-qz±and-crd-ky-st-gt-ilm in pelites	District scale, variably preserved at mm- to km-scales in metasediments	500-670°C, 300-450MPa	Oliver et al., 1991; 2001; Laing, 1998; Giles and Nutman, 2002; Hand and Rubatto, 2002	Metamorphic-evaporitic (locally derived, Oliver et al., 1992)
Albite shear zones and patches	ab-ru±qz-bt-kf-crd-st-ged in pelites	100m- to km-scale in pelites, mostly Snake Ck and Osborne Mine surrounds	500-690°C, 300-450MPa	Rubenach and Barker, 1998	Magmatic/ metamorphic? + evaporite (Rubenach and Lewthwaite, 2002)

Osborne Cu-Au deposit	mt-bt-qz-ab-cpy-py-po±am-cc-mu-ht	100m scale in BIF?, feldspathic metapelites and arenites	500-650°C, 300-400MPa	Gauthier et al., 2001; Rubenach et al., 2001	Magmatic? + evaporite (R. Mustard, personal communication, 2003)
Thermal metamorphism, 1550-1500 Ma (Williams Batholith)					
Early Williams Batholith 1550 – 1520 Ma	Zoned pegmatite-ab-qz-am-ap veins, UST	Plutons and roof pendants, e.g., Mt. Angelay Granite	500-650°C, 300-400 MPa	Page and Sun, 1998; Pollard et al., 1998; Mark et al., 1999; Davis et al., 2001	Magmatic (Mark et al, 1999; Mark and Foster, 2000; Pollard, 2001)
Later Williams Batholith 1530 – 1500 Ma	Mairolitic cavities with qz-cc, qz-ab±am-mt-py breccia	Plutons and widespread stocks and polymictic breccia cutting pelitic and calc-silicate rocks	500-700°C, 200 to 300 MPa	Page and Sun, 1998; Pollard et al., 1998; Mark et al., 1999; Davis et al., 2001	Magmatic (Mark et al, 1999; Mark and Foster, 2000; Pollard, 2001)
Lightning Ck prospect	mt-ap-ttn ironstones	100m scale, intrusion hosted	500-700°C, 200 to 400 MPa	Perring et al., 2000	Magmatic (Perring et al., 2000; Pollard, 2001)
Albitites	ab-am-ttn±cpx-ep-ap-cc in calc-silicate rocks; ab-ru-bt±act-ged-crd in pelites; ab-am-ttn±cpx-sc and am±cc veins in mafic rocks	Regional, abundant in all rock types, shear zones, veins and alteration, breccias	450-600°C, 200 to 400 MPa	Oliver et al., 1990; 2001; Oliver, 1995; deJong and Williams, 1995; Baker and Laing, 1998; Laing, 1998; Mark, 1998a	Modified magmatic? (Oliver et al., 1993; this study)
Barren ironstones	BIF?, metasomatic replacement, veins	Local to abundant in pelitic, calc-silicate- and mafic rocks	No constraints	Williams, 1998	Modified magmatic? (this study)
Fe-oxide–Cu-Au deposits	mt-cpy-py-ap-ttn-bt-Au±cc-po-ht-sc-am-gt-flu-bar	Felsic volcanic, pelitic and mafic rock hosts	370-470°C, 150 to 400 MPa	Summary in Williams, 1998; Baker, 1998; Rotherham et al., 1998; Mark et al., 2000; Baker et al., 2001; Williams et al., 2001	Modified magmatic? (Mark et al. 2000; Baker et al., 2001)

Table 3-1. Characteristics and Interpreted Fluid Sources of Regional Alteration (1750 – 1500 Ma) in the Eastern Mt. Isa Block. Abbreviations: ab = albite, ap = apatite, am = actinolitic to complex calcic amphibole, and = andalusite, bar = barite, bt = biotite, cc = calcite, cpx = clinopyroxene, cpy = chalcopyrite, crd = cordierite, ep = epidote, flu = fluorite, ged = gedrite, gt = garnet (grossular-andradite in skarns, almandine-spessartine in pelites), ht = hematite, ilm = ilmenite, ky = kyanite, mt = magnetite, mu = muscovite, po = pyrrhotite, py = pyrite, qz = quartz, sc = scapolite (mostly sodic), st = staurolite, ttn = titanite, UST = Unidirectional Solidification Texture.

During the 1600–1580 Ma Isan orogeny, some foliated rocks developed abundant albite, particularly in Soldiers Cap Group pelites at the Osborne Mine and in the Snake Creek area (Adshead et al., 1998; Rubenach and Barker, 1998; Rubenach et al., 2001; Rubenach and Lewthwaite, 2002). No major intrusions appear to have been temporally associated with this alteration, although pegmatites are abundant at Osborne. The rocks reached maximum P and T of 450 MPa and ≥ 650°C, determined by pelite mineral equilibria and thermobarometry (Rubenach and Lewthwaite, 2002). Albitization occurred relatively early in this cycle, at approximately 500 to 550°C and ≤ 400 MPa; the specific timing and P-T conditions of the albitization are tightly constrained by relationships between biotite, albite and orthoamphiboles in and around andalusite porphyroblasts and by the absence of paragonite (Rubenach and Lewthwaite, 2002). These rocks are distributed in broad, foliation parallel alteration zones surrounding cm- to m-scale zones of intense albitization and are transgressive to bedding at m- to 100 m- scales (Table 3-2). At mm- to cm-scales, the transition into albitized rocks is marked by replacement of matrix quartz and muscovite by albite and rutile, with localised development of orthoamphibole and cordierite; biotite is also consumed in the most altered rocks. These rocks, described in detail by Rubenach and Lewthwaite (2002), are used for some of the

modeling presented below.

Association	Timing, P-T conditions, references	Hostrocks	Pre-alteration (or primary) assemblages	Alteration/vein assemblages, (% of area affected)	Fluid chemistry
Isan Orogeny (1600 – 1580 Ma)					
100 m- to km-scale high strain zones parallel to major D2 fold axial zones	1600-1580 Ma, 500 to 650°C, 300 to 450 MPa (Foster and Rubenach, 2000; Gauthier et al., 2001; Rubenach and Lewthwaite, 2002)	Pelitic rocks of Soldiers Cap Gp., Snake Creek and Osborne	Mu, bt, qz, ilm ± and, gt, sill, kf, ky, st	Ab, ru ± oam, crd, mt, bt, qtz, chl; rare act, mt, cpx (5%)	No F.I., chemical modelling, this study
Williams thermal event (1550 – 1500 Ma)					
(1) 10 m- to 100 m-scale D3 high strain zones along rock contacts	1555 – 1540? Ma, 400-600°C, 300-400 MPa (Oliver, 1995; Mark et al., 2000, 2001)	Calc-silicate rocks of Mary Kathleen Gp., amphibolitic metadolerites,metatonalites	Sc-bt-qz-cc±am-cpx-ep-kf-ttn-ap in calc-silicate rocks, am-pl-ttn-ilm±sc-cpx-to in metadolerites	Ab-ttn±am-cpx-bt-ap-ep-mt-ht-py (5%)	F.I. from associated veins (see below); _ 34Spy = –1 to 1‰ at Ernest Henry; C, O isotopes see Fig. 12
(2) cm- to 100 m-scale veins	1555 – 1500 Ma, 475 to 600°C, 300 to 450 MPa (Oliver et al., 1993; Oliver, 1995; Mark, 1998a)	Calc-silicate rocks of Mary Kathleen Gp., amphibolitic metadolerites,metatonalites	Sc-bt-qz-cc±am-cpx-ep-kf-ttn-ap in calc-silicate rocks, am-pl-ttn-ilm±sc-cpx-to in metadolerites	(6) cc-qz-am-cpx±ab-dol-py-cpy-ap-bt (7) am±cpx-mt-py-ab-cc (5%)	C, O isotopes see Fig. 12. F.I. (Fu et al., 2003) 1. variable density CO2, 200-400 MPa, 2. L+V±halite, Ca-bearing, 3. multisolid hypersaline halite-sylvite±cc-mt
(3) Layer-transgressive alteration around (2) veins	1555 – 1500 Ma, 475 to 600°C, 300 to 450 MPa (Oliver et al., 1993; deJong and Williams, 1995; Oliver, 1995; Mark et al., 2001)	Calc-silicate rocks of Mary Kathleen Gp., amphibolitic metadolerites,metatonalites	Sc-bt-qz-cc±am-cpx-ep-kf-ttn-ap in calc-silicate rocks, am-pl-ttn-ilm±sc-cpx-to in metadolerites	Ab-ttn±am-cpx-bt-ap-ep-mt-ht (10%)	Association with (2) veins; C, O isotopes see Fig. 12
(4) 10 m – km-scale breccias along faults and around granite stocks	1535 – 1500 Ma based on intrusion ages & titanites; 475 to 600°C, 300 to 450 MPa (Mark, 1998b; Mark and Foster, 2000; Mark et al., 2001; this study)	Calc-silicate rocks, pelites, dolerites, gabbros, diorites	As for rock descriptions above	As for (3) in calc-silicate and mafic rocks. Ab-ru±bt-ttn-act-oam-qtz-crd-mt. (10 to 20% in MKFB;, up to 50% in Cloncurry)	C, O isotopes see Fig. 12; F.I. (Fu et al., 2003; this study) 1. Rare high density CO2, 2. multisolid hypersaline halite-sylvite±cc-mt-cpx, 3. halite-H2O-CaCl2

Table 3-2. Associations of albitites during the Isan Orogeny and Williams thermal event.
Abbreviations as for Table 3-1 but also oam = orthoamphibole, pl = intermediate to calcic plagioclase, ru = rutile, to = tourmaline.

The third type of alteration and the focus of this report includes widespread and layer-transgressive albite (Table 3-2).The clearest evidence for the relative timing of most of the albitization comes from an association of albite-rich alteration zones with shear zones, veins and breccia that cut the regional ductile structural fabrics (see also Oliver et al. 1990; Williams, 1994; deJong and Williams, 1995; Oliver, 1995; Baker and Laing, 1998; Laing, 1998; Mark, 1998a, b). Albitization during this stage reached temperatures of 450

to 600°C, determined from concurrently developed calc-silicate mineral equilibria and calcite-dolomite geothermometry on related veins (Oliver et al., 1993; Oliver, 1995), and oxygen isotope geothermometry on quartz, magnetite, albite and amphibole (Mark, 1998a; Mark and Foster, 2000; Marshall and Oliver, 2005). Pressures are not well constrained by mineral geobarometers, but conventional microthermobarometry on high density CO2-rich fluid inclusions in quartz vein material associated with albitites indicate entrapment at 200 to 450 MPa at assumed temperatures of 400 to 600°C (Mark et al., 2000). Oliver et al. (2004) used titanite U-Pb geochronology on metasomatic titanites, produced during albitization, to confirm an association between intrusion of the Williams Batholith and this stage of albitization.

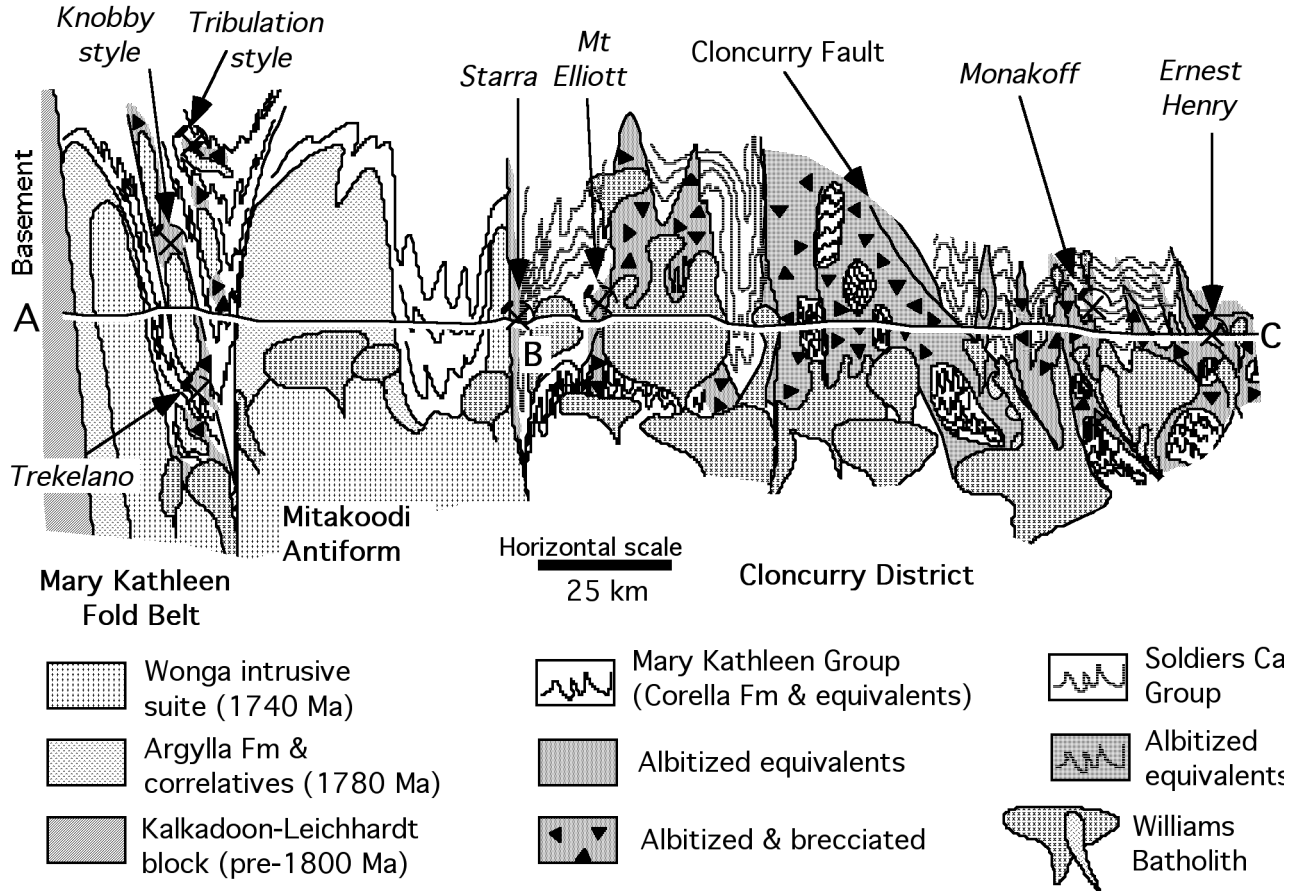

Figure 3-2. Schematic cross section of the Eastern Succession of the Mt. Isa Block showing the general distribution of major rock units, alteration, brecciation, faults and Cu-Au mineral deposits, corresponding to the section line A-B-C on Figure 3-1. Williams-age intrusions below the Mary Kathleen Fold Belt are inferred; the positions of the other intrusions are extrapolated from the map but depths and detailed shapes are uncertain. The vertical scale is exaggerated, approximately 10:1 to 20:1.

At 100 m- to km-scales, albite alteration is distributed along broader zones of contrasting rheology in the MKFB (Oliver et al., 1990; Figs. 3-2 and 3-*3) and in isolated km-scale breccia bodies (e.g., Mt. Philp Breccia). In the MKFB, approximately 20% of the exposed rocks are affected by intense zones of veining and related albitization (Fig. 3-3 and Table 3-2). In the Cloncurry District, albite alteration and brecciation is very widespread in the Corella Fm. and other Mary Kathleen Group equivalents but is moderately restricted in the pelitic rocks. At least some of the localization at this scale appears to be dependent on an association with small stocks and roof zones of the Williams Batholith and with Faults (Figs. 3-2 and 3-4).

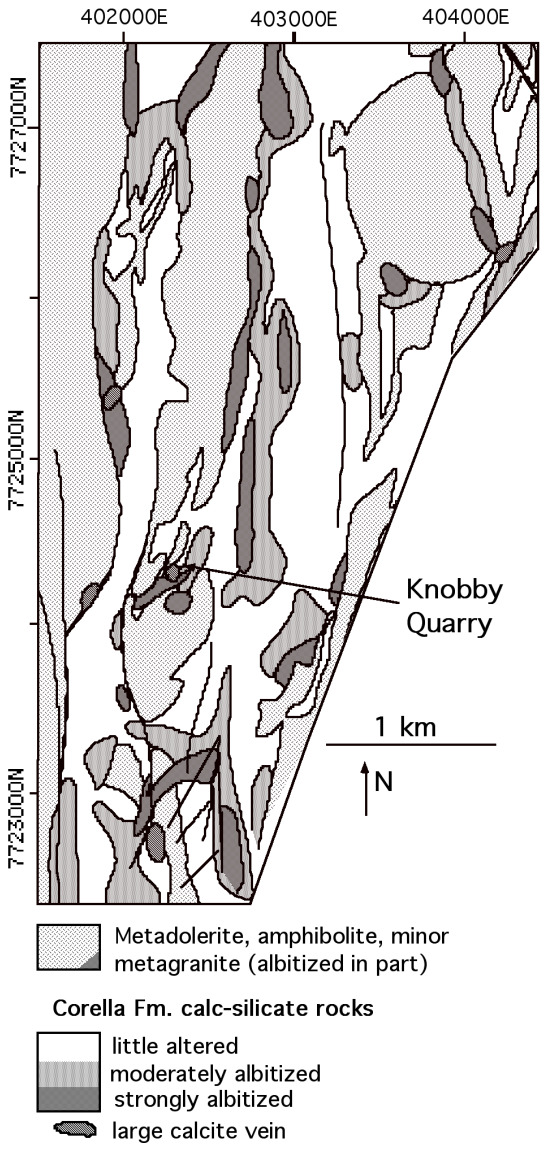

Fig. 3. Details of mapped albite alteration and calcite veins in part of the Mary Kathleen Fold Belt (MKFB), adapted from Oliver et al. (1990). Australian Map Grid coordinates are indicated. For location see Figure 1. Little altered = < 5% of m- to 10 m-scale outcrops contain any albite or related calcite veins, moderately albitized = 20 to 80% of m- to 10 m-scale outcrops contain ca. 30 to 90% albite (including related calcite veins and other calc-silicate alteration minerals), strongly albitized = 70 to 100% of m- to 10 m-scale outcrops contain 70 to 100% albite (including related calcite veins and other calc-silicate alteration minerals). Note that alteration occurs mainly on rock contacts, as a consequence of stress and strain heterogeneities developed during deformation (Oliver et al., 1990). The remainder of the MKFB shows similar patterns.

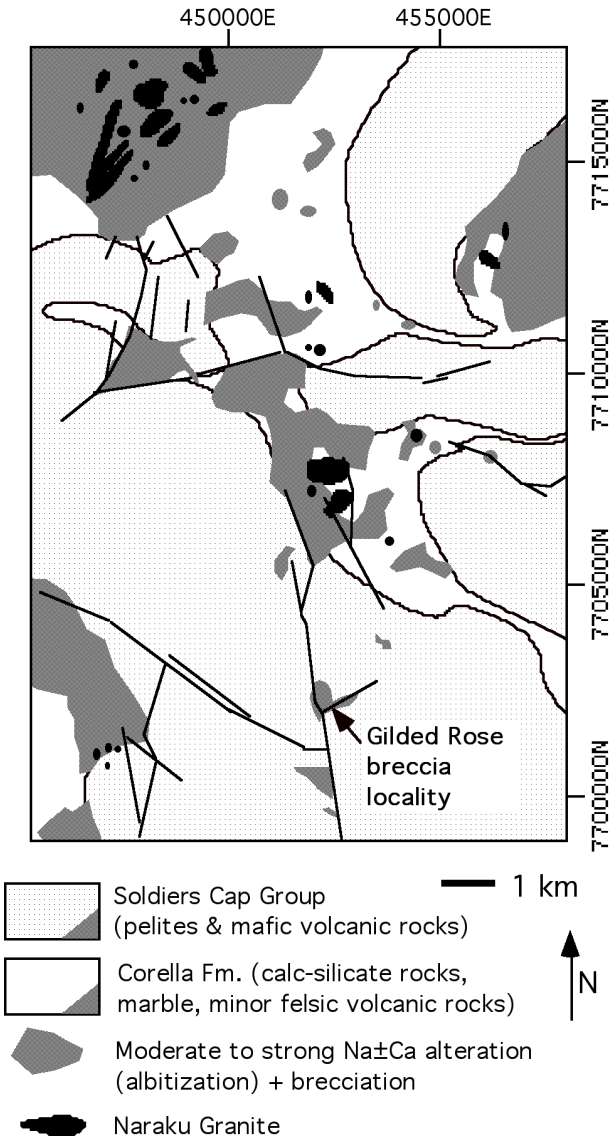

FIG. 4. Map of the broad distribution of albite alteration and brecciation in the northern Cloncurry District, adapted from Marshall (2003). For the altered zones, at m- to 10 m-scales, 20 to 100% of the rocks contain in excess of 10% albite, and details of the intensities of alteration are similar to those depicted for altered zones in Fig. 3. For location see Fig. 1. Australian Map Grid coordinates are iindicated. The remainder of the Cloncurry District shows a similar or greater extent of albitization. Note the widespread alteration in the Corella Fm. but restriction of alteration to the vicinity of faults in the overlying Soldiers Cap Group. Abundant minor intrusions of the Naraku Batholith occur at the core of many of the altered zones.

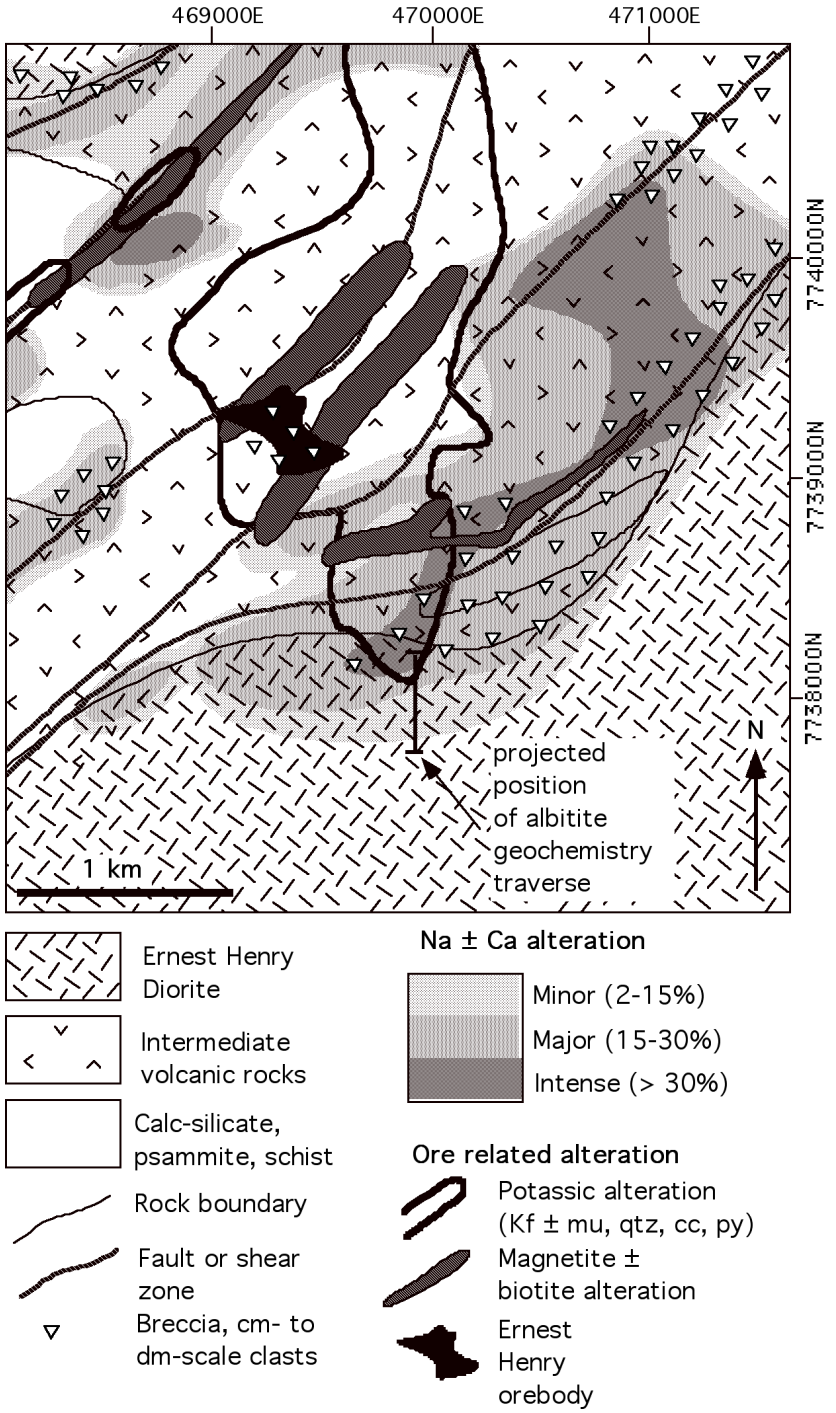

FIG. 5. Map of the detailed distribution of two of the major phases of alteration and mineralization around the Ernest Henry Cu-Au deposit, based on logging of 110 diamond drill holes (Mark et al., 2000), the resource model for the deposit, and the location of major aeromagnetic highs (aeromagnetic data courtesy Ernest Henry Mining). Drill-hole data are projected to the 1947 Relative Level but aeromagnetic highs are projected to surface. Location shown on Fig. 1. Australian Map Grid coordinates are indicated. Minor Na ± Ca alteration = 5 to 15 % of m-scale drill core intervals contain rocks with ca. 80 to 100% albite, major = 15 to 30% of m-scale drill-core intervals contain rocks with ca. 80 to 100% albite, intense = 30 to 100% of m-scale drill core intervals contain rocks with ca. 80 to 100% albite. Altered zones contain additional alteration minerals and veinlets, so these descriptions of major and intense alteration are similar to the moderately and strongly albitized zones depicted on Fig. 3. Potassic and magnetite-biotite alteration zones are not subdivided due to their complexity, but typically contain >50% total of the indicated minerals in m-scale drill core intervals. The Ernest Henry orebody is dominated by magnetite, pyrite, chalcopyrite and calcite. Na-Ca alteration is mostly distributed along rock boundaries and shear zones; the orebody and proximal ironstones also lie in brecciated zones between shear zones but the ore-related K-Fe alteration is somewhat discordant.

At m- to 100 m-scales, albite-altered rocks of the same timing are found in every rock type within the Easterm Succession (Figs. 3-4, 3-5 and Table 3-2), although to a lesser extent in the Williams Batholith granitoids (Mark, 1998a; Pollard, 2001). It occurs in m-scale shear zones (Fig. 3-6a), around veins dominated by calcite or actinolite (Figs. 3-6b, c), and in very widespread brecciated rocks (Figs. 3-4, 3-5 and 3-6d). Albite alteration is predominantly discordant to bedding in metasedimentary rocks, the most obvious controls at this scale being relationship to zones of dilation or shear developed during the D3 deformation event. These zones of dilation are best developed along the contacts between rocks of contrasting rheology, and along fault zones, as explored in depth by Oliver et al. (1990) and Marshall and Oliver (2002). Both the Fe-oxide-Cu-Au mineralization and the albite alteration share similar structural controls, commonly being best developed in brittle-ductile shear zones in which synshearing albitization predated or was synchronous with ore-related alteration. Around the Ernest Henry deposit, for example (Fig. 3-5), albite-rich Na±Ca alteration lies along lithologic contacts but also within the rock masses, particularly around faults and brittle-ductile shear zones. In detail, it has an almost antithetic relationship with the distribution of ore-related potassic alteration assemblages, but is also locally overprinted by the latter, as shown (Fig. 3-5).

Pegmatites occur locally within or cross-cutting some albite breccia bodies. At the Tribulation Quarry (Marshall, 2003; Fig. 3-1), pegmatite both cuts albite breccia and is contained as clasts within breccia, confirming that periods of intrusion and albitization overlapped. Post-brecciation pegmatite sheets, themselves albitized, are found at Knobby Quarry (Fig. 3-6b). In the Snake Creek and Gilded Rose regions near Cloncurry, albite breccias are commonly cored by m- to 10 m-scale pegmatites (Fig. 3-4). Mark (1998a, b), Pollard et al. (1998), Mark and Foster (2000), Perring et al. (2000), and Pollard (2001) have described direct relationships between roof pendants of the Williams Batholith intrusions and local albitization, and proposed that fluids released during magma crystallization were largely responsible for the albitization. At Mt. Angelay, Mark (1998a, b) described a complex magmatic-hydrothermal transition (e.g., Fig. 3-6d) with Unidirectional Solidification Textures in pegmatites grading laterally into hydrothermal infill, the latter including albite and actinolite. In the country rocks surrounding this pluton (and others in the district), calc-silicate rocks locally form proximal clinopyroxene-K-feldspar-albite± actinolite-garnet skarns up to 20 m from the contacts. More common, however, are broad zones of albitization extending away from the intrusion, in which albite and actinolite compositions are very similar to those developed in the quartz monzonite roof pendants (Mark, 1998a). Geochemical models relating to this situation are presented below.

At mm- to cm-scales, fine grained mosaics of albite replaced feldspars, scapolite and quartz (Fig. 3-6e, f). Locally, granoblastic, polygonal calcite and scapolite that formed in calc-silicate rocks during regional metamorphism (Fig. 3-7e) were replaced by albite and a second generation of coarser grained calcite. Clinopyroxene and titanite ± actinolite formed in calc-silicate and mafic rocks during albitization, replacing earlier biotite and pargasitic to hastingsitic amphiboles. In pelites, albite and rutile replaced micas and quartz, but actinolite formed rarely, particularly near contacts with granites and/or calc-silicate rocks.

Geochemistry of albitites

Table 3-3 and Figure 3-7 show results of geochemical analyses of calc-silicate rocks, psammopelitic rocks, and various intrusive rocks from the Eastern Succession, and their albitized equivalents. These data are based on systematic sampling and whole-rock XRF and INAA (neutron activation) analyses of 24 least altered rocks and 21 albitized rocks. Our sampling strategy was intended to cover the broadest possible range of starting compositions to see how different rocks responded to the albitization. Other analyses reported in Baker (1996) and Mark (1998b) show similar trends. In addition, we present results for metadiorite and a mineralization-related biotite-magnetite altered equivalent from the Ernest Henry Cu-Au deposit (Fig. 3-7g). The isocon method of Grant (1986) was employed for the paired samples, or pairs of averaged samples, whereby the concentration of a particular oxide or element is multiplied by a factor for both the unaltered and altered rock, in order to construct a line of best fit for the immobile elements (the isocon), on a dimensionless plot of unaltered versus altered rock. Once this line is established, a mass change can be determined, as well as the relative gains and losses of elements accompanying alteration. Errors and averaging methods are discussed for specific examples. Representative geochemical analyses are given in Table 3-3.

Metasedimentary rocks

The most widespread rocks in the exposed part of the Eastern Succession are the impure marbles, calc-silicate rocks and metasiltstones of the Corella Formation and equivalents in the Mary Kathleen Group. Away from the alteration zones, the unaltered precursor rocks contain scapolite, biotite, calcite, quartz, microcline, calcic amphibole, clinopyroxene and various accessory minerals, particularly titanite, apatite, allanite, and

tourmaline (Table 2, Oliver et al., 1992).

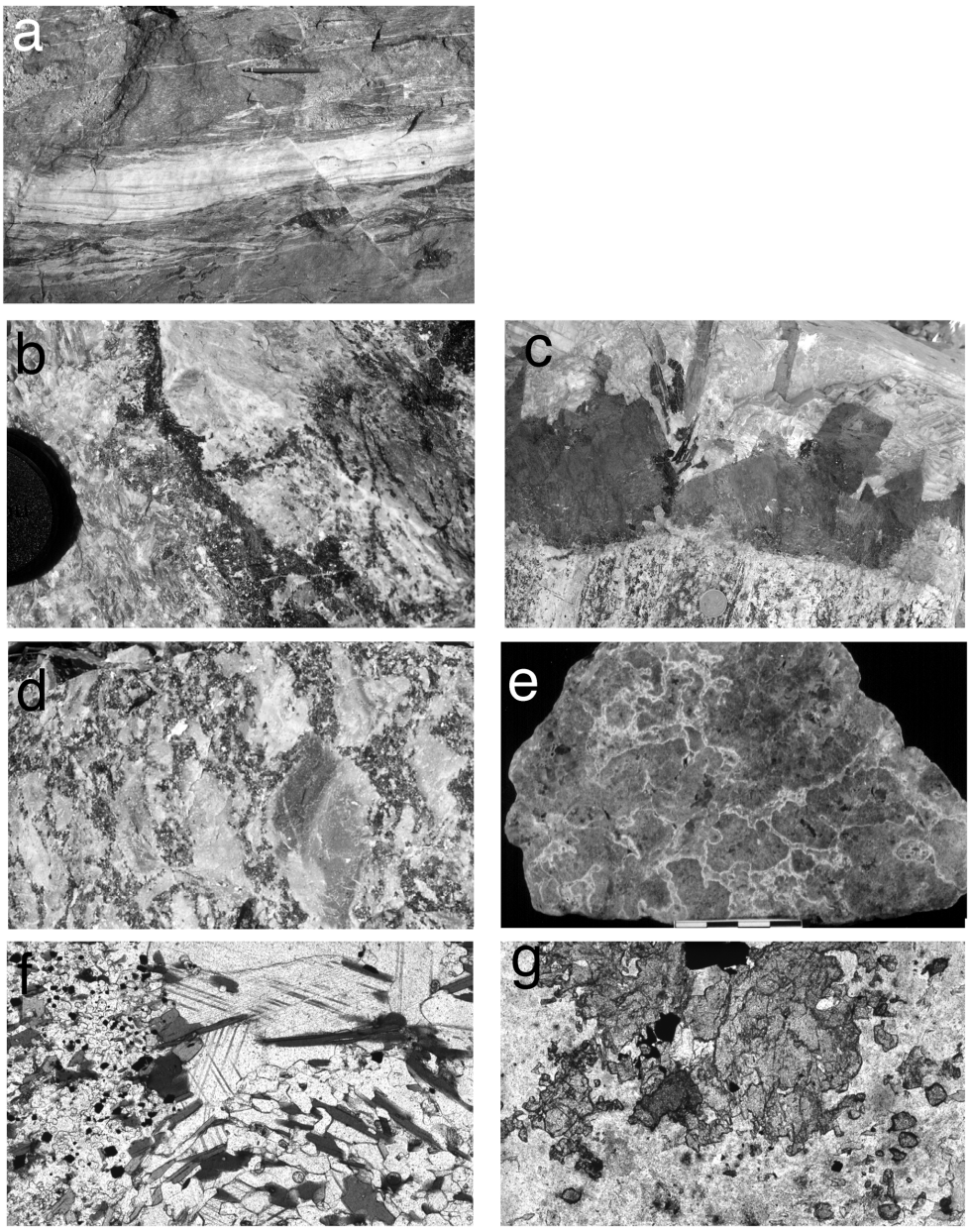

Figure 3-6. Outcrop photographs and photomicrographs of albitized rocks from the Mary Kathleen Fold Belt (MKFB) and Cloncurry District. (a) Albite shear zone from the MKFB, here cutting amphibolitic metadolerite, 2 km NW of Tribulation Quarry (location Fig. 3-1), pencil for scale. (b) Knobby Quarry vein-related albitite (KN6) from the MKFB (location Figs. 3-3 and 3-6b), showing calcite (cc) vein (left, lens cap for scale) with thin zone of clinopyroxene (cpx) and actinolitic amphibole (black) at the edge of the vein adjacent to intensely bleached albite (ab) alteration zone (with minor clinopyroxene, calcic amphibole and titanite). The albite alteration cuts weakly altered gray calc-silicate rock (right). (c) Calcite vein in Tribulation Quarry from the MKFB (Fig. 3-1) showing strongly altered bedded calc-silicate at bottom (2.5 cm coin for scale), large equant idiomorphic clinopyroxene (cpx) crystals on the vein margin, with minor elongate actinolite (act) and platy (black) biotite crystals adjacent to very coarse grained calcite (up to 1m^3 crystals) in the vein core. (d) Typical Corella Breccia from the Cloncurry District (Mt. Avarice Quarry in Cloncurry township, Fig. 3-1), showing partially to completely albitized clasts in an actinolite-calcite±quartz matrix. (e) Complexly textured albite-actinolite rocks in the granite/hydrothermal transition zone in the carapace of the Mt. Angelay plutonic complex, Cloncurry District (see Mark and Foster, 2000, for details). (f) Photomicrograph of unaltered impure marble (KN 105, Table 3-4) from the MKFB sampled from the traverse shown on Fig. 3-6b, showing poikiloblastic intermediate scapolite (sc) with calcite and ilmenite(?) inclusions. Calcite (cc), biotite (bt) and calcic pargasitic amphibole (am) and additional quartz and K-feldspar are also present. This rock represents a likely precursor to albitization shown in Fig. 3-7g. (g) Albitized calc-silicate (KN 6B, Table 3-4) also from the traverse shown on Fig. 3-6b, showing total replacement of scapolite, K-feldspar, biotite and most of the calcite by albite, clinopyroxene, titanite and magnetite. The titanite produced by such albitization yielded an age of 1527 Ma from this sample (Oliver et al., 2004).

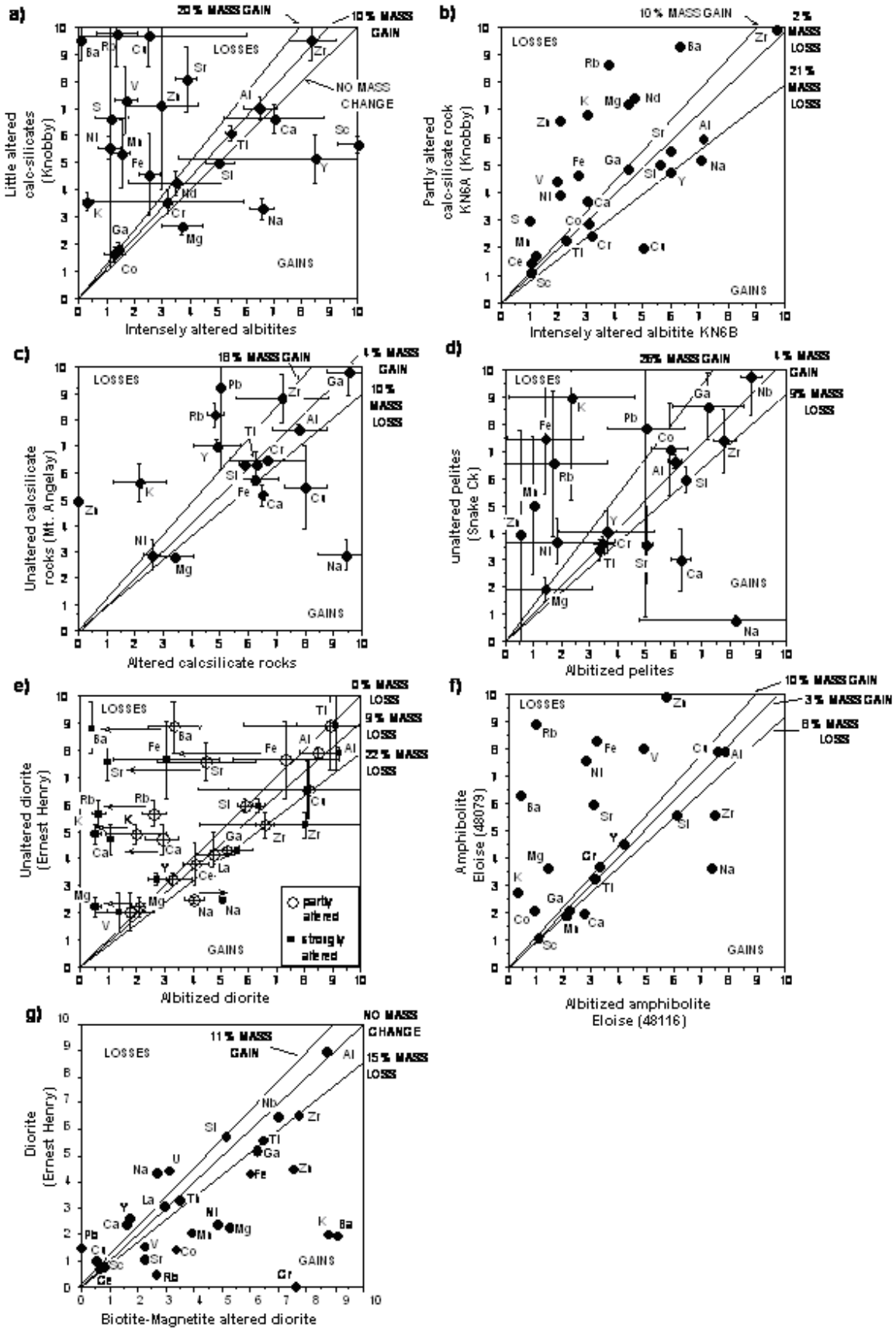

FIG. 7. Isocon plots (after Grant, 1986) constructed for individual pairs or averaged sets of rocks, comparing little altered precursors with albitized equivalents (a – f), and comparing weakly altered diorite with its magnetite-biotite altered equivalent in the Ernest Henry deposit (g). For sample locations see Figures 1 and 5; the raw data is presented in Table 3. In each case the main isocon (heaviest line) was determined by a visual best fit to constant Al and Ti ± Ga, Zr and Si. The lighter lines show a range of possible isocons for which other elements could also have been immobile. Fm (the mass factor) is the ratio of the total mass of the altered rock to that of the less altered equivalent, determined solely from the slope of the isocon, giving some idea of whether dilation (Fm > 1) or dissolution (Fm < 1) accompanied the alteration.

Sample No.	94b	94d	S404	S253.3	219	147i	KN105	KN6B	EHD1	EHD4	42767	42741	EL079	EL116	J1L	J1M
Rock type	pelite	alb-pelite	pelite	alb-pelite	calc-sil	alb-calc-sil	calc-sil	alb-calc-sil	diorite	alb-diorite	qtz monz.	alb-qtz monz.	Amph-ib	Alb-amph-ib	Diorite	Bt- alb-diorite
Location	Marra	Marra	SnkCk	SnkCk	MA	MA	Knobby	Knobby	EHM	EHM	MA	MA	Eloise	Eloise	EHM	EHM
SiO_2	75.57	73.51	56.10	65.30	63.21	59.53	46.91	55.90	62.18	58.80	66.50	68.41	55.71	60.79	57.50	51.30
TiO_2	0.51	0.40	0.64	0.70	0.57	0.62	0.39	0.46	0.90	0.85	0.57	0.63	1.08	1.04	1.12	1.28
Al_2O_3	11.91	11.36	21.70	19.50	15.37	14.25	11.50	14.24	15.78	18.37	14.96	15.69	15.9	15.72	18.0	17.4
Fe_2O_3 (t)	4.36	2.40	8.29	0.47	5.85	5.66	6.11	2.74	6.18	6.25	3.81	1.99	11.85	4.5	8.69	11.93
MnO	0.05	0.02	0.05	0.01	0.06	0.07	0.23	0.12	0.03	0.07	0.02	0.03	0.19	0.21	0.03	0.06
MgO	1.01	2.47	2.22	0.28	2.90	3.87	2.05	4.48	1.83	1.79	0.95	0.77	3.67	1.46	2.28	5.26
CaO	0.42	2.24	0.35	0.65	5.58	6.55	15.50	10.13	4.08	2.65	2.02	2.47	3.97	5.47	1.19	0.78
Na_2O	1.40	6.55	0.53	10.69	1.21	4.38	5.00	7.07	5.24	8.93	4.83	8.94	3.63	7.37	8.72	5.30
K_2O	3.20	0.11	6.52	0.38	5.11	2.84	1.18	0.51	2.64	0.59	4.79	0.17	2.77	0.31	1.01	4.38
P_2O_5	0.11	0.20	0.21	0.19	0.14	0.22	0.12	0.20	0.19	0.25	0.17	0.17	0.13	0.14	0.00	0.00
Cl	na	na	na	na	0.02	0.01	0.08	0.15	0.29	0.05	0.06	0.05	na	na	0.03	0.06
LOI	2.10	0.63	2.72	0.28	2.51	0.16	10.18	4.01	0.96	1.12	0.88	b.d.	0.90	3.45	1.23	2.03
Total	**100.64**	**99.89**	**99.50**	**98.50**	**102.53**	**98.17**	**99.37**	**100.07**	**100.30**	**99.72**	**99.60**	**99.27**	**99.86**	**100.45**	**99.80**	**99.80**
Ba	na	na	875	44	na	na	320	63	489	139	1375	233	632	43	193	909
Rb	156	4	327	13	192	116	58	38	54	21	323	4	127	14	49	266
Sr	36	20	33	52	80	80	79	60	136	130	139	132	99	51	104	224
Pb	na	na	6	6	3	2	na	na	4	4	17	17	bd	bd	3	bd
Zr	211	212	131	162	200	209	106	97	174	207	343	550	139	186	163	192
Nb	na	na	21	18	na	na	na	na	16	12	31	39	10	13	13	14
Y	26	24	24	16	29	22	20	60	34	26	31	57	30	28	26	17
La	na	na	na	na	na	na	na	na	41	53	104	99	na	na	31	29.6
Ce	na	na	na	na	na	na	92	103	88	82	261	195	na	na	65.8	62.6
Sc	na	na	20	9	na	na	17	21	13	18	6	5	22	22	4	4
V	na	na	106	32	na	na	62	20	66	62	47	27	268	162	157	225
Cr	na	na	101	92	65	57	26	64	8	12	156	12	46	41	bd	19
Co	na	na	17	21	28	9	20	31	13	10	7	27	42	18	7.31	16.7
Ni	na	na	34	4	24	24	23	7	5	11	8	6	38	14	24	48
Cu	na	na	7	8	10	15	5	5	20	23	13	10	79	76	10	5
Zn	na	na	49	5	7	0	5	7	58	26	20	24	33	19	15	25
Ga	na	na	34	21	19	18	16	15	21	27	9	13	21	22	26	31
100Na/ (Na+K)	30.4	98.3	7.5	96.6	19.1	60.7	80.9	93.3	66.5	93.8	50.2	98.1	56.7	96.0	89.6	54.8
100(Na+Ca)/ (Na+Ca+K)	36.3	98.8	11.9	96.8	57.0	79.4	94.6	97.1	77.9	95.2	58.9	98.5	73.3	97.6	90.8	58.1
100Na/ (Na+Fe)	24.3	73.2	6.0	95.8	17.1	43.6	45.0	72.1	45.9	58.8	55.9	81.8	23.4	62.1	50.1	30.8

Table 3-3. Whole Rock Analyses of Pairs of Less Altered Rocks and Equivalent Albitites from the Eastern Succession, along with Select Alteration Indices.

Major element oxides in weight %, minor elements in ppm. Other analyses available from the authors upon request. Abbreviations: alb = albitized, calc-sil = calc-silicate rock, monz. = monzonite, amphib = mafic meta-igneous amphibolite, Marra = Marramungee Creek, SnkCk = Snake Creek, EHM = Ernest Henry Mine, MA = Mt. Angelay, locations on Figure 3-; LOI = loss on ignition, b.d. = below detection limit, na = not analysed. The two samples in italics represent the transition from amphibolite (already partly albitized) to the biotite-magnetite altered equivalent in the proximal alteration halo of the Ernest Henry orebody (Fig. 3-5), for which most trends are opposite to those determined for albitization (see text).

Rocks from around the Knobby Quarry in the MKFB were sampled in a 20 m transect, with one 15 cm-wide calc-silicate dominant layer tracked from unaltered, well bedded rock into its albitized equivalent. At the transition to the most intensely albitized rocks, it was no longer possible to discern this particular layer, and results for this part of the transect are averaged (Fig. 3-7a). Confidence that the transition was appropriately sampled is based on the distinctive Ti/Zr and Ti/Al ratios in the altered and least-altered equivalent. Figure 3-7b shows results for a pair of closely spaced samples. Al, Zr, Ti, Ga, Si, and Co all show immobile behaviour in the altered examples (Fig. 3-7a, b). The best fit isocon for the averaged dataset (Fig. 3-7a) suggests that albitization occurred at near constant mass or with a slight mass increase (Fm > 1, where Fm = mass final rock / mass initial rock), whereas there was a slight mass decrease in the transition in Figure 3-7b. It is clear that the altered rocks have gained Na, and lost Fe, Mg, K, Mn, Ni, V, Zn, Nd, S, Rb and Ba. The patterns for total mass change and for Cu and Ca are inconsistent between Figure 3-7a and 3-7b. These two elements are apparently recording differential mobility across a range of scales (from metres in Fig. 3-7a to cm in Fig. 3-7b). The variations are not surprising given the abundance of calcite veinlets accompanying albitization, which locally contain minor chalcopyrite (see below).

A second set of albitized calc-silicate rocks was sampled in the Mt. Angelay area where the rocks could be readily separated into unaltered and altered types, but could not be readily tracked from one to the other due to synalbitization brecciation. For these 5 samples, we averaged the 3 unaltered rocks and compared them with the average of the two albitized equivalents in Figure 3-7c, with the variability in precursor compositions represented by the standard deviation between the samples (error bars). The isocon plot shows that Al, Si, Ti, and Ga were immobile, generally consistent with the observations from the MKFB. Na, Ca ± Cu and Mg were gained during albitization, and K, Zn, Y, Rb and Pb were lost. Other trace elements not shown on this plot had very large standard deviations. One of the least altered samples (sample 219, with an assemblage of scapolite, biotite, quartz, K-feldspar, clinopyroxene, titanite and minor epidote, magnetite and actinolite), characteristic of the majority of least-altered calc-silicate rocks in the Cloncurry District, was used as a calc-silicate reference material for the geochemical modeling presented below.

Albitized pelites from the Snake Creek Anticline (Rubenach and Lewthwaite, 2002) are present in shear zones, in alteration veins surrounding the shear zones and related quartz veins, and in more broadly distributed zones along the contacts with mafic amphibolites. Average albitized pelites sampled at five locations spaced over several kilometres (Rubenach and Lewthwaite, 2002), compared with their least altered equivalents (Fig. 7d), show constant Al, Si, Ti, Ga, Zr, Y, Cr and Nb, and a mass increase of approximately 4%. Na and Ca are enriched, and K, Fe, Rb and Mn are clearly depleted. The Ca enrichment is similar to that observed by Williams (1994), and, as there is no local source for the Ca, must reflect transport of this component from outside the sequence via the infiltrating fluid.

Igneous rocks

Pristine and albitized diorites were sampled near Ernest Henry (Fig. 3-5), and the 9 samples were separated into 3 least altered, 3 moderately altered and 3 intensely altered. Ga, Si, Al, Ce and La remain immobile even in the intensely altered rocks. Ti, Cu and Zn have large standard deviations, although Ti was most likely immobile based on the other samples. Na was added, particularly in the intensely altered rocks. Fe, Mg, V and Y were nearly immobile in the moderately altered rocks but were significantly depleted in the intensely altered rocks, and there is a suggestion also that Al may have been slightly depleted in the most altered rocks. K, Ba, Ca, Sr and Rb were all lost from the moderately altered rocks and are extremely depleted in the most altered rocks. Similar trends (but with large standard deviations for several trace elements) are shown by the albitized quartz monzonite and syenogranite samples from Mt. Angelay (Fig. 3-1 and Table 3-3). The most mafic rocks analyzed were a pair of samples from the Eloise Cu-Au deposit (Baker, 1996), a little-altered amphibolite and a strongly albitized equivalent (Fig. 3-7f). A very well constrained isochron is defined on the basis of immobile Al, Ti, Y, Cu, Ga and Sc, with near immobile Si, Cr and Mn, and little total mass change between the precursor and albitized equivalent (ca. 3% mass increase). K, Rb and Ba are extremely depleted, Fe, Ni, V, Sr, Mg and Co are moderately depleted, and Na, Ca and Zr are enriched. We interpret the apparent Zr enrichment either as an artifact of incomplete dissolution during preparation of one sample, or as a “spike” effect due to irregular distribution of Zr in accessory minerals spaced further apart than the sampling distance.

Ore related alteration

Magnetite-biotite alteration is a common feature of the proximal alteration halo of the Cu-Au orebodies. In order to compare the albitization with the ore-forming process, we compared one example of the Ernest Henry Diorite to its magnetite-biotite altered equivalent (Fig. 3-5 and 3-7g). Because our sample pair involves

an intrusive igneous rock with a well studied paragenetic history (Mark et al., 2000) we are confident that the changes measured do not relate to primary iron enrichments. Comparison of Figures 7e and 7g shows that the effects of ore-related potassic alteration are dramatically different from albitization of the same rock, with trends for individual elements mostly being the opposite between the two alteration types. Ca is the only obvious anomalous element, being lost from both albitized and biotite-magnetite-altered diorite. Calcite is found in abundance, however, as vein infill to crackle-brecciated diorite on the edge of the ore deposit some 10s of metres from these samples.

Summary

Aluminium, Ga, Ti and Zr are consistently immobile, and Si is also mostly immobile. The very local presence of titanite in some veins suggests local mobility of Ti. Consistent gains in Na are matched by depletions in K, alkali earth elements, Zn, and Fe, that latter being very mobile (depleted) in intensely altered rocks. Uranium and Pb are generally low in abundance but are depleted in the most altered rocks, as are Cr, Mn, V and Ni. Variable gains and losses are indicated for Ca, Cu, and Mg. The sample suites with 3 to 12% mass gains all show increases in Ca and Mg, and samples with 2 to 10% mass loss (and inferred volume decrease) are correspondingly depleted in Ca and Mg. This suggests that Ca- and Mg-bearing minerals in microveinlets and microbreccia matrix are at least partly responsible for the variation in Fm. Cu may have been mobile during albitization, but the variability may reflect the role of several Cu-bearing minerals, and the albitization is not considered to have been responsible for significant mass transfer of Cu. Finally, excepting Cu and Ca, elements gained during albitization were apparently lost during ore-related potassic alteration, and vice-versa (Fig. 3-7e, g).

Geochemical Modeling

Hydrothermal geochemical modeling of fluid-rock reaction is a powerful way to test hypotheses concerning the source and reaction paths of metasomatic fluids. It has the capacity to reveal aspects of progressive fluid-rock reaction, the effects of differing P and T, variations in initial starting fluid composition and the composition of different fluids equilibrated with different rocks. The results of the modeling can also be compared with fluid inclusion studies. Principles of this style of analysis in mineralised systems have been demonstrated by Reed and Spycher (1985), Heinrich et al. (1995, 1996), Borisov and Shvarov (1998) and Cooke and McPhail (2001), among others. Here we have simulated the albitization process using the software HCh (Shvarov, 1999; Shvarov and Bastrakov, 1999). The HCh package permits equilibrium-dynamic modeling of hydrothermal systems and processes using the free-energy minimization technique (Shvarov, 1978, 1999), rather than the log K method. HCh can be used across a temperature range of 0–1000°C and pressures up to 500 MPa, within the limitations of the Helgeson-Flowers-Kirkham model, and for fluid salinities limited by the extended Debye-Hückel equations. The package can be obtained from Geoscience Australia (http://www.ga.gov.au/rural/projects/ 1007080747_28318.jsp). The model calculations were completed using the Geoscience Australia version of the UNITHERM database, which is included with the software, and the description of the software and database are detailed in Shvarov and Bastrakov (1999). In the UNITHERM database, mineral thermodynamic data were adopted from self-consistent datasets compiled by Berman (1988) for aluminosilicates, with corrections for K and Na minerals suggested by Sverjensky et al. (1991), and the rest of the mineral data sourced mostly from the ETH version of SUPCRT (Pokrovskii et al., 1998). Most of the aqueous species were adopted from the ETH version of SUPCRT (Pokrovskii et al., 1998), complemented by data of Shock et al. (1997) and Sverjensky et al. (1997) for Fe and Cu complexes. Mineral solid solutions were derived using an ideal mixing-on-sites model (e.g., Powell, 1977). In the output plots in this paper, except for plagioclase, we have combined the minerals of solid-solution series without specifying the specific mineral compositions.

The types of modelling possible using HCh are described by Cleverley and Oliver (2005; see this report). The simplest equilibrium calculations to model albitization were completed in a single mixing mode, an approach similar to one used by Heinrich et al. (1995, 1996). Rock is “dropped” into fluid (Fig. 3-8a) in order to avoid problems associated with initial low fluid/rock ratios for which ionic strengths can be too high for the valid range of available thermodynamic data. After an aliquot of rock has been added to the fluid, the equilibrium state is calculated by adjusting the proportions and compositions of mineral phases and by concomitantly adjusting the fluid composition to minimize the Gibbs free energy. There is not a great physical significance to the “zonation” produced in such models; rather they are simply tests of possible alteration assemblages that might pertain to a range of fluid fluxes. However, there is some geological basis for choosing such simple models – the distribution of alteration around veins, with the largest veins showing the largest ^{18}O and ^{13}C depletions relative to the wall rocks (Oliver et al., 1993; Marshall et al., 2006), suggests that the fluid was rapidly introduced to the system via these fractures and attempted to equilibrate with the wall rocks

via diffusion and infiltration of components between the wall rocks and the fluid-filled cracks. The size of the fracture and the flow rate of fluid in that fracture would have dictated the degree of reaction. Simulated alteration zones are very similar to those observed in the field (see below). This simplistic modeling approach is enhanced by knowing the starting composition of the unaltered rock and by being able to compare the output to the known compositions of the altered rocks. Similarly, data from fluid inclusions may be used to populate parts of the models, or for comparison with model results.

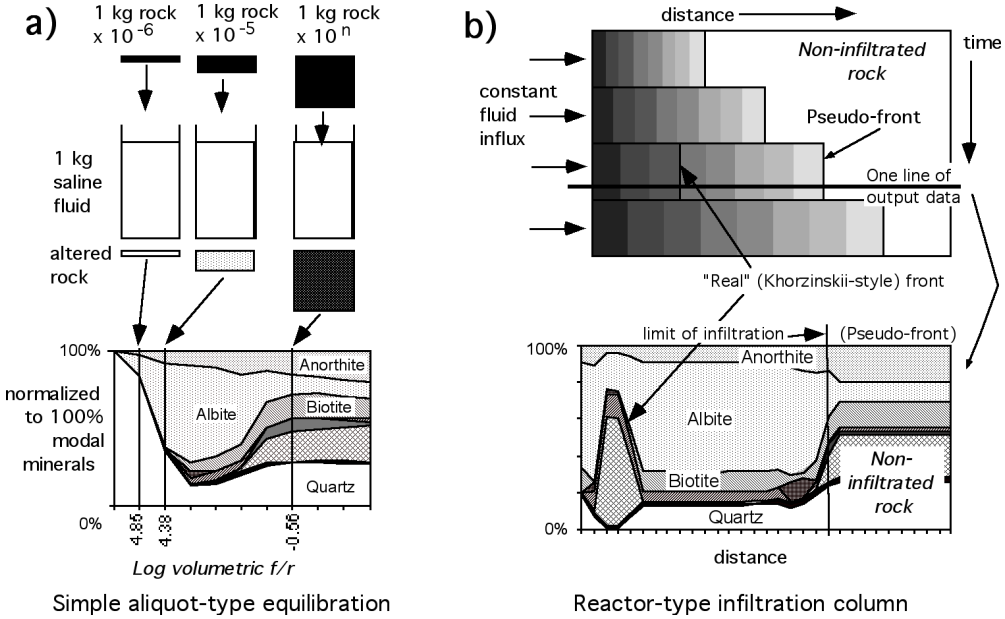

Figure3-8. Conceptual models showing the techniques used in the geochemical simulations of fluid-rock interaction using HCh (Shvarov and Bastrakov, 1999; Cleverley and Oliver, 2005). (a) Simple aliquot-type mixing of different masses of rock with a set mass of fluid, equilibrated to produce individual outputs of altered rock assemblages, which are recalculated from moles to volumes using mineral molar volume data and plotted as a function of volumetric fluid/rock ratio (f/r). (b) A flow-through model which is a closer approach to reactive transport models (cf. Heinrich et al., 1996). Khorzinskii-type fronts correspond to specific solubility limits of different minerals in the moving fluid column, whereby position is a function of the fluid flux and the specific fluid-rock partitioning for the minerals of interest. Also shown is a "pseudo-front", which is a realistic simulation of the boundary between infiltrated and non-infiltrated rock. Such a front is dependent on the total fluid flux, which defines the distance of the front from the inlet position, but is also dependent on the assumption that beyond the front, there is no reaction and therefore no capacity for metasomatic reactions to create or destroy any permeability. Assemblages beyond the pseudo-front would be considered rock-buffered or least altered. This corresponds to the concept of reaction-enhanced permeability and coincident isotopic and geochemical fronts developed by Cartwright (1997). One horizontal line of output data from the computations (as depicted in Figs. 3-11 and 3-12) corresponds to a spatial array of alteration zones at a particular time that can be compared to alteration maps; output derived from vertical lines would correspond to the temporal sequence at one point in space that could be compared to a paragenesis.

The second type of model may be termed a "reactor", in which an algorithm is constructed that approximates a proper flow-through simulation, where fresh fluid is continually added to one end of an infiltration column (Fig. 3-8b). "Stale" fluid leaving a reactor site infiltrates the next reactor where it is modified further. Influx of fresh fluid "pushes" the previously modified fluid ahead so that it can react with fresh rock. Two types of reaction fronts are apparent in our models: 1) a pseudo-front beyond which the infiltrating fluid has not physically passed, and 2) fronts in the true Korzhinskii (1970) geochemical sense which occur along the flow path as a consequence of one or major minerals reaching or exceeding their solubility limit. A horizontal section through the output matrix is then a snapshot of the system at a moment in time. This reactor-type approach (Heinrich et al., 1996) is an approximation to reactive transport modeling (e.g., Ferry and Dipple, 1991; Dipple and Ferry, 1992) in terms of the zonation of mineral assemblages, with the limitation that real dimensions and the effects of kinetics cannot be adequately included. In theory, reactor-type models converge upon true reactive transport only when the aliquot size or reaction step is infinitesimally small (cf. Blattner and Lassey, 1990). However, the infiltration of fluid into rock that was not previously fluid saturated does not readily lend itself to a conventional Korzhinskii-type interpretation of reaction fronts, nor to conventional reactive transport models. The algorithm we used approximates a reaction-enhanced permeability in which isotopic and geochemical pseudo-fronts would be coincident, as noted in detail by Cartwright (1997). Such calculations can then provide good approximations of realistic physical situations around veins in which the previous rock was essentially impermeable.

Model inputs

Model input rocks (calc-silicate Mount Angelay 219 and pelite Snake Creek S404, Table 3-4) were selected from those presented in Table 3-3. We also include an analysis of the Mount Angelay quartz monzonite (42767) in order to determine one possible input fluid composition (see below). We obtained poor model results, not presented here, from albitization of intermediate to mafic rocks (Ernest Henry diorite, Eloise amphibolite) containing abundant complex amphiboles (hornblende, hastingsite, pargasite), because inadequate activity-composition models resulted in artificial partitioning of alumina and silica into other phases. Inputs are specified as whole-rock oxides in the compositional space Si-Al-Ti-Fe-Mg-Ca-Na-K-C-H-O-S. Ti in this context acts as a completely immobile element by default as there are no soluble Ti species in the fluid database, nor have we included any solid solution models pertaining to Ti (such as Ti in biotite).

The composition of the best possible model input fluids was based on associated mineral assemblages, fluid inclusion data and iterative modeling. One possible approach could be to take fluid inclusion data from the top of an intrusion believed to have caused albitization, such as the Mt. Angelay quartz monzonite (Mark and Foster, 2000). However, the difficulties associated with using fluid inclusion data directly are: (i) uncertainty about whether the analyzed fluid inclusion represents the bulk composition of the infiltrating fluid initially out of equilibrium with the rocks or the product of local rock-fluid equilibration; (ii) the common occurrence of CO_2-rich inclusions, locally in the same trails as primary hypersaline fluids, raising the possibility that the hypersaline fluid chemistry was derived, at least in part, by fluid immiscibility; and (iii) the complexity of the fluid inclusion populations in any one sample, requiring an assumption as to which fluid could possibly relate to a given alteration assemblage. Despite the uncertainties, we have compared conventional and microanalytical (PIXE) fluid inclusion results (Mark et al., 2000; Williams et al., 2001; Oliver et al., 2004) with the geochemical models, and have utilized some preliminary PIXE results from Mt Angelay quartz monzonite and pegmatite, and from regional albitites. In the albitites, complex NaCl-KCl-$CaCl_2$-H_2O-CO_2± hematite-gypsum fluids with two or more daughter minerals and estimated salinity > 50 wt % NaCl equivalent are found with relatively simple NaCl-H_2O-CO_2 inclusions of ca. 20-30 wt % NaCl equivalent containing only halite as a daughter mineral and with rare mixed CO_2-H_2O-NaCl±nahcolite inclusions at Knobby and Tribulation Quarries (deJong and Williams, 1995; Oliver, 1995; Fu et al., 2003). CO_2-rich inclusions are also prominent (Oliver et al., 2004). These inclusion types are generally similar to those observed in quartz grains, veins and pegmatites at the top of Williams Batholith intrusions (e.g., Perring et al., 2000). Complex fluid inclusion chemistry is also evident in iron-oxide–Cu–Au deposits of the district (Williams et al., 2001; Oliver et al., 2004). Three main inclusion types are found in the ores that correlate generally with those in the albitite-related veins (hypersaline brine, brine, and CO_2-rich fluid), although the hypersaline variety tends to be more chemically complex in the ore deposits than in the albitites.

	MA monzonite [1]	MA calc-silicate rock [4]	Snake Ck Pelite [5]
H_2O (g)	8.8	12	22
SiO_2 (g)	665	632.1	591
TiO_2 (g)	5.7	5.7	6.4
Fe_2O_3 (g)	20.6	22.3	-
FeO (g)	17.5	36.2	74
MgO (g)	9.5	29	22.2
Al_2O_3 (g)	149.6	153.7	217
CaO (g)	20.2	55.8	3.5
Na_2O (g)	48.3	12.1	5.3 §
K_2O (g)	47.9	51.1	65.2
C (mol)	-	-	0.4
CO_2 (mol)	-	0.32	-
Log Na/K(maq, tot)	0.48	-0.02	-1.90
pH	5.12	6.13	4.06
log f_{O2}	-19.9	-20.1	-24.4

Table 3-4. Compositions of Rocks Used in HCh Models.
Compositions were derived from data shown on Table 3-3 and are expressed as g/kg for the solid components and mineral-bound volatiles. Na/K, pH, f_{O2} were derived by equilibrating an excess of each rock with a 3m HCl solution according to the methods described by Shvarov and Bastrakov (1999). These parameters are representative of fluid in equilibrium with the rock, as confirmed by the correct positioning of the Mount Angelay monzonite fluid on the 2-feldspar line shown in Fig. 3-14. However, lack of a paragonite-muscovite solid solution model inhibits calculations of $m_{Na,aq}$ for rock [5] so the value shown is approximate. MA = Mt. Angelay.

The inferred (pressure corrected) entrapment temperatures of inclusions associated both with albitites and with the ores are 300 to 550°C and are comparable to the temperatures inferred from mineral assemblages (Table 3-2). Pressures estimated from CO_2 fluid inclusion densities range from 150 to 400 MPa for the deposits and the albitites (e.g., Mark et al., 2000; Fu et al., 2003). The highest homogenization temperatures and CO_2 densities for individual samples suggest primary fluid entrapment at 400 to 550 °C and 300 to 400 MPa, consistent with the alteration assemblages developed (Table 3-2). Using starting model conditions of 530 to 550°C and 350 MPa, consistent with the hottest and deepest parts of the system (e.g., Fig. 3-2 and Table 3-2), we chose three possible starting fluid compositions (Table 3-5): (1) in equilibrium with Mount Angelay 2 feldspar quartz monzonite; (2) a somewhat arbitrary composition similar to (1) but having a slightly elevated Na/K ratio just inside the albite-stable field; and (3) with its starting Na/K ratio increased to match the calculated Na/K ratio determined from fluid inclusions within quartz grains in the quartz monzonite.

Model fluid in equilibrium with the two-feldspar quartz monzonite at the top of the Mount Angelay pluton was calculated by titrating an excess of that rock into a simple 3mHCl fluid (similar calculations were performed on the calc-silicate and pelitic rocks to determine the background composition of fluids buffered by these rock types; Table 3-4). The calculation then partitions the chlorine into molecular and dissociated species in fluid in equilibrium with a subsolidus granitoid. A realistic pH (5.1), a mineral assemblage that remains the same as in the input (i.e., the system is rock buffered), and a calculated Na/K ratio that is consistent with previously published studies of albite–K-feldspar equilibrium (Table 3-5 and Fig. 3-9) are positive encouragement that the calculations are valid. The relatively high Na/K ratio observed in the actual fluid inclusions could reflect a number of different processes (see below). Our three chosen model fluids have Na/K ratios that range between this theoretically determined fluid (in equilibrium with two feldspars) and the Na/K ratio determined from the fluid inclusion analysis. This range of model fluid inputs then provides some permissive tests of whether granite-derived fluids could have caused bulk albitization of the wall rocks, notwithstanding the many uncertainties associated with the assumption of simple activity-composition relationships in hypersaline brines. We also needed to make the model fluids more dilute than the fluid inclusions to avoid problems of uncertainty in extrapolation of the extended Debye-Hückel equations to high salinity at high T and P. Finally, we added some sulphur species (0.001 m each of H_2S and SO_4) to approximate conditions near hematite-magnetite-pyrite even though these sulphur species were not readily detectable in the fluid inclusions.

Results

Figure 3-10 shows the results of the simple isothermal fluid/rock mixing models for calc-silicate rocks from Mount Angelay, and for the Snake Creek pelites, the two rocks most representative of metasedimentary precursors to albitization. When we used the model fluid initially in equilibrium with 2-feldspar quartz monzonite (fluid [1]), alteration assemblages in the pelites generally did not match those observed in the field. Reacting the same fluid with Mt. Angelay calc-silicate rocks, quartz-rich alteration at the highest fluid/rock ratios precedes an albite-rich assemblage with lesser quartz, biotite, actinolite, clinopyroxene, epidote and magnetite, followed at low fluid/rock ratios by assemblages similar to those of the least altered rocks observed in the field (biotite-K feldspar-quartz-clinopyroxene and plagioclase). Plagioclase of An60 is an approximation to mizzonitic (calcic) scapolite found in the actual rock, for which no thermodynamic data are available in the version of UNITHERM we used. The albite-rich alteration assemblage is not entirely unrealistic; however, the anorthite content of the model plagioclase is high relative to that observed in the field (An10 to An20 instead of An1 to An11), and biotite is still preserved in the model rocks whereas it is usually absent in strongly albitized calc-silicate rocks in the field. Nevertheless, because the fluid Na/K ratio of a two-feldspar granitoid is initially higher than that in equilibrium with a K-feldspar + biotite bearing scapolitic calc-silicate rock (Fig. 3-9), the albite alteration predicted in this model is consistent with the field data.

	Calculated Compositions using HCh				*PIXE Data from Fluid Inclusions*						
	[1] Mt Angelay 2-fspar fluid #1	[2] Mt Angelay adjusted fluid #2	[3] Mt Angelay adjusted fluid #3	Output fluid after alteration of calc-silicates	Mt. Angelay monzonite Mean (3)	Mt. Angelay pegmatite Mean (12)	Regional albitite Mean (7)	Starra ironstone Mean (6)	Starra ore Mean (8)	Eloise ore Mean (2)	Ernest Henry Gt stage 3444
Log Na/K (tot)	0.48	0.64	1.43	0.88	1.43	0.95	0.66	0.69	0.72	0.60	0.72
Log Na/Fe	2.63	2.66	2.74	1.75	1.68	1.36	1.34	0.48	0.82	0.73	0.48
Log Ca/Fe	0.29	0.29	0.29	-0.20	1.01	0.40	0.61	-0.42	0.51	0.52	-0.39
Log Na^+/K^+	0.33	0.50	1.32	0.73							
H^+	1.90E-05	2.40E-05	2.01E-05	4.87E-05							
K^+	4.63E-01	3.45E-01	6.26E-02	2.10E-01							
Na^+	9.92E-01	1.09E+00	1.31E+00	1.17E+00							
log K^+/H^+	4.39	4.16	3.49	3.64							
log Na^+/H^+	4.72	4.66	4.81	4.38							
pH	5.23	5.13	5.20	4.83							
log f_{O2}	-19.9	-19.8	-18.9	-20.0							
H_2O (g)	1000	1000	1000	1000							
Ca (mol)	1.01E-02	1.01E-02	1.01E-02	2.81E-02	1.30E+00	5.95E-01	1.12E+00	5.49E-01	1.55E+00	1.64E+00	4.94E-01
Cl (mol)	2.96E+00	2.96E+00	2.96E+00	2.90E+00	9.38E+00	8.11E+00	1.04E+01	9.62E+00	9.33E+00	8.53E+00	1.08E+01
Fe (mol)	5.17E-03	5.17E-03	5.17E-03	4.47E-02	1.27E-01	2.39E-01	2.76E-01	1.43E+00	4.84E-01	5.01E-01	1.20E+00
K (mol)	7.35E-01	5.44E-01	9.77E-02	3.26E-01	2.26E-01	6.14E-01	1.31E+00	8.83E-01	6.04E-01	6.89E-01	6.86E-01
Na (mol)	2.20E+00	2.39E+00	2.84E+00	2.49E+00	6.08E+00	5.50E+00	6.00E+00	4.30E+00	3.17E+00	2.72E+00	3.62E+00
Mg (mol)	1.07E-04	1.07E-04	1.07E-04	8.30E-04							
Al (mol)	3.09E-04	2.94E-04	3.09E-04	2.52E-04							
Si (mol)	1.29E-01	1.28E-01	1.29E-01	1.28E-01							
H (mol)	5.16E-01	5.18E-01	5.16E-01	5.72E-01							
O (mol)	5.16E-01	5.16E-01	5.16E-01	5.19E-01							
CH_4 (mol)	-	-	-	6.86E-12							
CO_2 (mol)	-	-	-	3.20E-03							
H_2S (mol)	1.00E-04	1.00E-04	1.00E-04	1.81E-04							
SO_4 (mol)	1.00E-04	1.00E-04	1.00E-04	1.18E-05							

Table 3-5. Compositions of Calculated Input Fluids and Comparison with PIXE Data from Fluid Inclusions
Fluids in the first three columns were calculated using the methods described in the text and figures. Data is reported as molal or molal ratios for the calculated data, and as moles determined by direct recalculation for the PIXE data (see also Fig. 3-17). Locations are shown on Figure 1. The fourth column is model "effluent" fluid from reaction of fluid [3] with Mt. Angelay calc-silicate rock during albitization (Figs. 3-15 and 3-16). PIXE data was gathered according to the methods outlined by Ryan et al. (1995); PIXE data is from Williams et al. (1999, 2001), Mark et al. (2000), Fu et al. (2003), and the Mt. Angelay data are from G. Mark (unpublished data).

In the simple fluid/rock mixing models, use of fluids [2] and [3] with Na/K set to values higher than for fluids in equilibrium with 2-feldspar granite, produces more realistic alteration assemblages. Using the slightly modified fluid [2] interacting with the pelite, albite-rich alteration with accessory biotite is the outcome of high fluid/rock ratio models, and at moderate fluid/rock ratio an albite-biotite-rutile-muscovite assemblage is produced. These assemblages are observed in the field, although it is rare for muscovite to be stable together with albite, and biotite is normally destroyed in the most albitized rocks, with rutile stable instead (Rubenach & Lewthwaite, 2002). Using fluid [3], with Na/K set to that of the Mt. Angelay fluid inclusions produces an albite-actinolite-titanite assemblage at high fluid/rock ratio, and interesting albite-talc-chlorite-paragonite-rutile assemblages at moderate fluid/rock ratio. Talc is not observed in the field, however cordierite and orthoamphiboles are locally found together with chlorite in albite alteration zones. The version of UNITHERM we used in the calculations does not contain cordierite because of incompatibilities with some of the modified data for iron (Shock et al., 1997). We regard the albite-talc-chlorite assemblage as equivalent to the albite-chlorite-orthoamphibole-cordierite assemblage observed in the field. Actinolite and titanite are found in some extremely albitized pelitic rocks. Both fluids [2] and [3] interacting with Mt. Angelay calc-silicate rock produce very realistic alteration assemblages, but these do not differ greatly from that produced by fluid in equilibrium with 2-feldspar granite [1]. The main difference is the more realistic destruction of biotite during Na-Ca alteration (albite-actinolite-clinopyroxene-titanite). Running any of these models at lower temperatures for pelites produces much more paragonite, and its absence in the field suggests that, at least in the Snake Creek location, alteration occurred at high temperature.

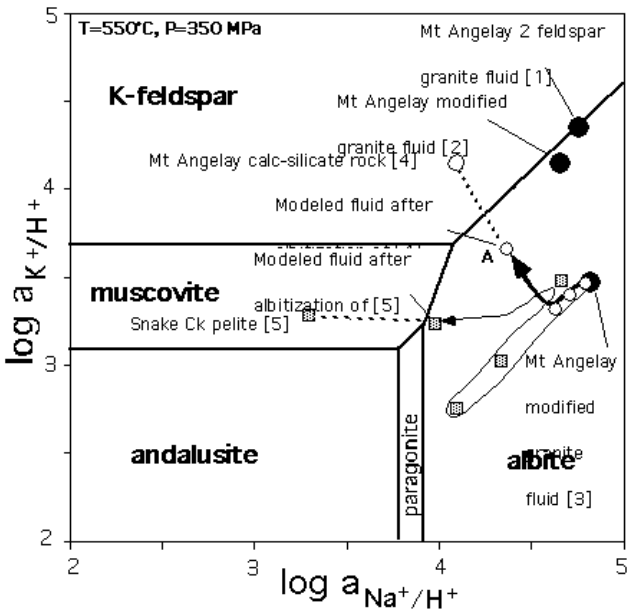

Figure 3-9. Na-K activity-activity diagram, constructed for the P-T conditions indicated using the ACT2 module of The Geochemists Workbench (version 4.0.2, Bethke, 2002) and a revised thermodynamic dataset derived from the UNITHERM database of HCh using the UT2K and K2GWB utilities of Cleverley and Bastrakov (unpublished data). The three starting fluids are shown as heavy dots ([1], [2] and [3]). The compositions of fluid in initial equilibrium with Mt. Angelay 2-feldpsar quartz monzonite [1], Snake Creek pelite [4] and Mt. Angelay calc-silicate rock [5] were calculated by model equilibration of a small amount of dilute HCl solution with an excess of rock as described in the text. Modified initial fluid [3] was calculated by adjusting the Na/K ratio of fluid [1] to match the fluid inclusion data, and fluid [2] is an arbitrary mixture of 10% of fluid [3] with fluid [1]. The paths indicated represent the shift in the Na^+/K^+ ratio of the modified Mt. Angelay fluid [3] during albitization of Mt. Angelay calc-silicate (heavy arrow, open circles) and Snake Creek pelite (light arrow, shaded squares) corresponding to the fluid outputs shown in Fig. 11 e and f. Molality ratios from HCh output are equated to activity ratios on this diagram with the assumption that the activity coefficients cancel out. However, the diagram is constructed for a_{H2O} = 1.0, which is the main reason why the andalusite-bearing Snake Creek pelite plots in the muscovite field instead of on the muscovite-andalusite boundary. The condition of a_{H2O} = 1.0 is not sustained during the model runs due in part to fluid interaction with rocks containing volatile-bearing phases.

In the more realistic reactor-type models (Fig. 8b), isothermal infiltration of fluid equilibrated with 2-feldspar granite [1] into pelites produces broad albite–K-feldspar alteration zones in which biotite remains stable, and muscovite also remains stable closer to the pseudo-front (Fig. 11a). This alteration is not observed in the field. Reaction of the same fluid with the calc-silicate rock, however, produces very interesting assemblages (Fig. 11b). Closest to the pseudo-front a realistic assemblage of albite-actinolite-quartz-magnetite is produced, with biotite remaining stable but less abundant than in the unaltered rock ahead of the pseudo-front. A reaction front is observed in the proximal part of the system in which K-feldspar and clinopyroxene dominate over albite and actinolite. In the field, K-feldspar–clinopyroxene skarns are common in close proximity to the granitoids, so overall, this model, using granite-equilibrated fluids, produces quite realistic results.

If the modified input fluids [2] and [3] are used, albite-rich alteration is prominent in the pelites. Biotite is preserved over larger distances if the only slightly modified fluid [2] is used (Fig. 3-11c), whereas albite-talc-rutile assemblages are prominent if the Na-rich fluid [3] is used, approximating the cordierite-bearing field assemblages discussed above (Fig. 3-11e). Paragonite is produced, although it is not observed in the field. The same fluids infiltrating calc-silicate rock produce very realistic alteration assemblages (Fig. 3-11d, f) in which the restricted distribution of biotite in the albite altered rocks, together with zoning from albite-actinolite to albite-clinopyroxene, are reminiscent of some of the detailed zonation observed in the field (Table 3-2). However, these models do not reproduce the K-feldspar-clinopyroxene skarns observed close to the granitoids.

To see what effect temperature gradients away from the fluid source may have had, we ran polythermal, polybaric models for reaction with the calc-silicate rock across a range of P-T such that the influx point was still at 550°C and 350 MPa but the limit of infiltration was at 450°C and 250 MPa (Figs. 3-11g-i). The fluid equilibrated with the 2-feldspar granite [1] produced a broad zone of quartz-bearing biotite–K-feldspar alteration with minor magnetite, reminiscent of one of the main alteration stages at Ernest Henry (Fig. 3-5), but also typical for cooling fluids emanating from granites (e.g., in porphyry systems, Ulrich and Heinrich, 2001). If the starting fluid composition is shifted just into the albite field (fluid [2], Fig. 3-9), cooling produces voluminous albite with additional actinolite, then biotite and magnetite with increasing distance from the source. Using the most Na-rich starting fluid composition [3], quartz-destructive albite-clinopyroxene alteration is followed at lower temperature (and further from the starting point) by albite-actinolite-quartz and eventually biotite- and chlorite-bearing albite rocks.

Aspects of the fluid evolution through these reactor-type models are also presented (Fig. 3-11). Notably, in the reaction zones just behind the pseudo-front, where albitization is most intense, the locally equilibrated fluid attains high concentrations of components initially absent from the fluid but present in the rock. For

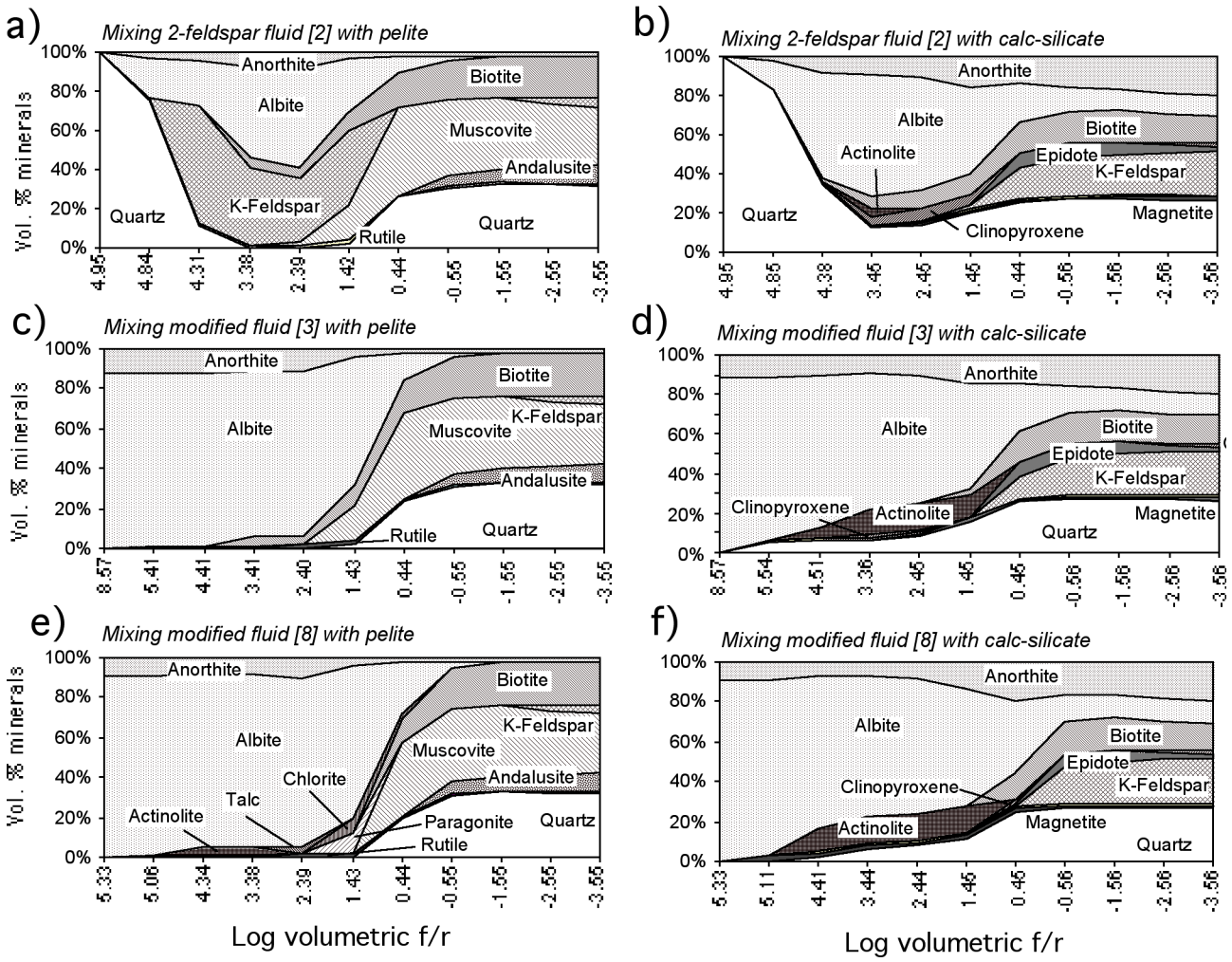

Figure 3-10. Simple aliquot-type HCh models of fluid-rock interaction, calculated using the methods described in the text and in Fig. 3-8a. Input rocks and fluids are shown in Tables 3-4 and 3-5. (a), (b) and (c) show results from reaction of pelite with the three fluids with different starting Na/K ratios, [1], [2] and [3] on Fig. 9. (d), (e) and (f) show results from reaction of calc-silicate rock with the same three fluids. Outputs are in normalized volume % of minerals; the fluid/rock ratio (f/r) in the individual equilibrations are shown on the bottom axes. Slight variations in these ratios from diagram to diagram are a function of the specific fluid composition chosen and also the loss or gain of volatile-bearing phases in the rock. Predicted assemblages corresponding to each fluid/rock ratio are independent of adjacent calculations, so the bottom axes do not correspond to progressive reaction zones. However, they give some indication of the types of assemblages that may occur from the distal to proximal parts of the hydrothermal system.

the isothermal models, the granite-equilibrated fluid [1] leaches Fe from the pelite, and Ca and Fe from the calc-silicate rock, but its Na/K ratio remains nearly constant. The more sodic fluids [2] and [3] strip Fe and K from the pelite, and Fe, K, and Ca from the calc-silicate rock. The latter trends are more consistent with the bulk geochemical changes observed for albitization (Fig. 3-7). The preliminary PIXE work shows that fluid inclusions in albitized calc-silicate rocks are Ca-rich relative to those hosted by pelites (B. Fu et al., unpublished data), suggesting at least some of the chemistry of the fluids was a consequence of partial equilibration with the wall rocks. For reaction with altered calc-silicate rock in a thermal gradient (Figs. 3-11g-i), both fluids [1] and [2] fail to leach Fe from the rocks, rather they lose iron to the rock via biotite formation and gain substantial Ca. These trends do not match the geochemical patterns for albitization (Fig. 3-7), although they are interesting in the context of ore-proximal alteration (see below). In contrast, the initially high Na/K fluid [3] leaches a large amount of iron during albitization in the thermal gradient, and shows a good match with the alteration geochemistry (Fig. 3-7) and mineral assemblages developed.

The results of the isothermal models are compared with the compositions of the model input and output fluids in Figure 3-9. The diagram shows the different starting fluid compositions from equilibrium with the granite ([1]) through to fluids ([2] and [3]) initially in the albite field. For fluid [3], with the Na/K ratio adjusted to that of the Mt. Angelay fluid inclusions, the initial path during albitization of calc-silicate rock is along a line of near constant Na+/K+ ratio but within the albite field, followed by a shift towards more potassic fluid compositions as the effect of the host rock impacts on the fluid chemistry at the head of the infiltration column. For infiltration of this same fluid into the pelites, the fluid follows a convoluted path partly controlled by the stability of the talc and chlorite-bearing assemblages, with fluid just behind the head of the infiltration

column being close to the muscovite field (Fig. 3-11).

Most of the Fe-oxide Cu-Au deposits occur in the Soldiers Cap Group, and those that are hosted in the Mary Kathleen Group are predominantly in siliciclastic or volcanic rocks rather than calc-silicate rocks (e.g., Fig. 3-2). To test this scenario, we took the effluent fluid from albitized calc-silicate rocks (labelled A on Fig. 3-9), and reacted that fluid with fresh pelitic rocks at 550°C (Fig. 3-12). Possible alteration assemblages contain abundant magnetite, clinopyroxene, biotite and titanite, as well as albite, mimicking many of the alteration styles seen in the near vicinity of the deposits (Table 2). Calcite veins or breccia matrix are common in some of the deposits – if the Ca content of this effluent fluid is lowered to simulate loss of Ca to calcite veins (Fig. 3-12b), actinolite becomes predominant in the alteration rather than clinopyroxene. Particularly noteworthy in this context are the clinopyroxene-magnetite gangue at Mt Elliott (Little, 1997), some albite-magnetite rocks in the Snake Creek area, the transition from hornblende-magnetite to biotite-chlorite alteration at Eloise (Baker, 1998), and early Na-Ca-Fe alteration (actinolite, clinopyroxene, magnetite) followed by biotite-magnetite-K-feldspar at Ernest Henry (Mark et al., 2000).

Figure 3-11. (overleaf) Reactor-type HCh models portraying progressive infiltration of the same fluids used in Fig. 3-10 (Table 3-5) through a rock column (rocks in Table 3-4), according to the methods described in Fig. 3-8b and the text. Fluid of the same composition is added to the input point (left), and, upon completion of each reaction step (ticks on x-axis), is then displaced into the next block of rock by a fresh batch of fluid added to the left (cf. Heinrich et al., 1996). Models (a), (c) and (e) show isothermal infiltration of pelites with the three fluids of different Na/K ratio, as indicated. Models (b), (d) and (f) show isothermal infiltration of calc-silicate rocks with the same three fluids. The real starting rocks contain scapolite, but our version of UNITHERM contained no scapolite data. However, the predicted plagioclase composition (An60) is similar to the equivalent anorthite content in the actual scapolites (Mark, 1998b). Models (g), (h) and (i) show retrograde (down P-T) infiltration of calc-silicate rocks from 550°C and 350 MPa to 400°C and 200 MPa, also with the same three starting fluids. The down-T variation in assemblages ahead of the limit of infiltration is not relevant to the field situation as the rocks had already been metamorphosed to at least 450°C prior to the alteration depicted behind the fronts. The bottom half of each part of the diagram shows the calculated molalities of the indicated fluid species. Although no dimensions are shown on the x-axis of each plot, they are interpreted to correspond to the distances indicated for altered versus non-altered rocks shown in Figs. 3-3 and 3-4, i.e., km- to 10 km-scales. However, because we have demonstrated that complex fracture systems hosted the infiltrating fluid (e.g. Oliver et al., 1990; Marshall, 2003), the x-axes could also represent m-scale variations in alteration assemblage dependent on proximity to fractures, in which case multiple fracturing and wall rock alteration overlapping in time and space could have produced the 100 m-scale patterns shown on Fig. 3-5, and ultimately the km-scale patterns shown on Figs. 3-1, 2 and 3. Figures (e) and (f) correspond to the paths shown on Fig. 3-9. The indicated point immediately behind the limit of infiltration in (f) was used as an input fluid to simulate ore-proximal alteration in Fig. 3-12.

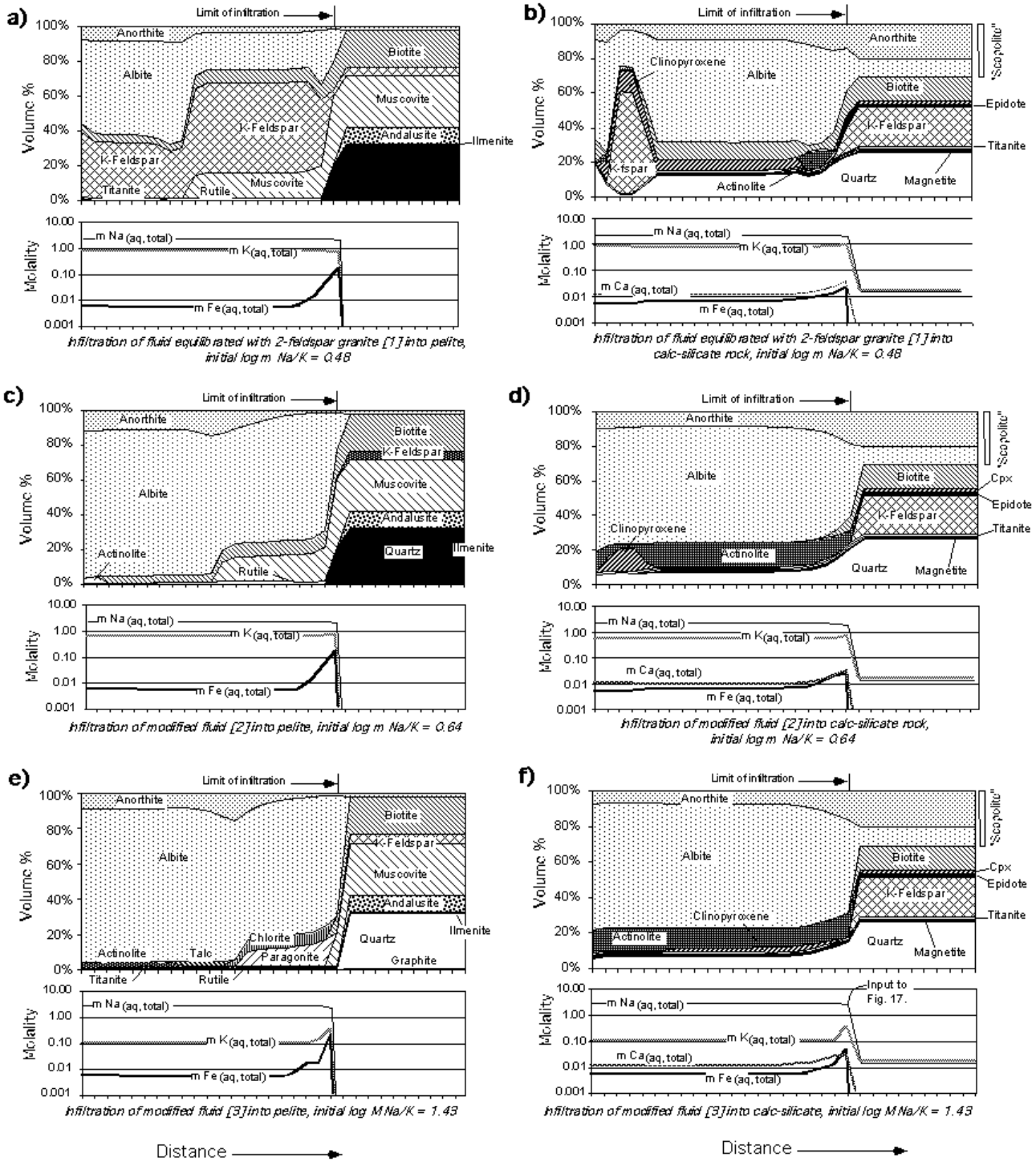
a)
Limit of infiltration
Anorthite
Albite
Biotite
Muscovite
K-Feldspar
Andalusite
Ilmenite
K-Feldspar
Titanite
Rutile
Muscovite
Volume %
100%
80%
60%
40%
20%
0%
Molality
10.00
1.00
0.10
0.01
0.001
m Na (aq, total)
m K (aq, total)
m Fe (aq, total)
Infiltration of fluid equilibrated with 2-feldspar granite [1] into pelite, initial log m Na/K = 0.48
b)
Limit of infiltration
Anorthite
"Scapolite"
Clinopyroxene
Albite
Biotite
Epidote
K-Feldspar
Titanite
K-fspar
Actinolite
Quartz
Magnetite
m Na (aq, total)
m K (aq, total)
m Ca (aq, total)
m Fe (aq, total)
Infiltration of fluid equilibrated with 2-feldspar granite [1] into calc-silicate rock, initial log m Na/K = 0.48
c)
Limit of infiltration
Anorthite
Biotite
K-Feldspar
Albite
Muscovite
Andalusite
Actinolite
Quartz
Ilmenite
Rutile
m Na (aq, total)
m K (aq, total)
m Fe (aq, total)
Infiltration of modified fluid [2] into pelite, initial log m Na/K = 0.64
d)
Limit of infiltration
Anorthite
"Scapolite"
Albite
Biotite
Cpx
Epidote
K-Feldspar
Clinopyroxene
Titanite
Actinolite
Quartz
Magnetite
m Na (aq, total)
m K (aq, total)
m Ca (aq, total)
m Fe (aq, total)
Infiltration of modified fluid [2] into calc-silicate rock, initial log m Na/K = 0.64
e)
Limit of infiltration
Anorthite
Biotite
Albite
K-Feldspar
Muscovite
Andalusite
Chlorite
Quartz
Ilmenite
Actinolite
Talc
Paragonite
Graphite
Titanite
Rutile
m Na (aq, total)
m K (aq, total)
m Fe (aq, total)
Infiltration of modified fluid [3] into pelite, initial log M Na/K = 1.43
Distance
f)
Limit of infiltration
Anorthite
"Scapolite"
Albite
Biotite
Cpx
Epidote
K-Feldspar
Clinopyroxene
Titanite
Actinolite
Quartz
Magnetite
Input to Fig. 17.
m Na (aq, total)
m K (aq, total)
m Ca (aq, total)
m Fe (aq, total)
Infiltration of modified fluid [3] into calc-silicate, initial log M Na/K = 1.43
Distance

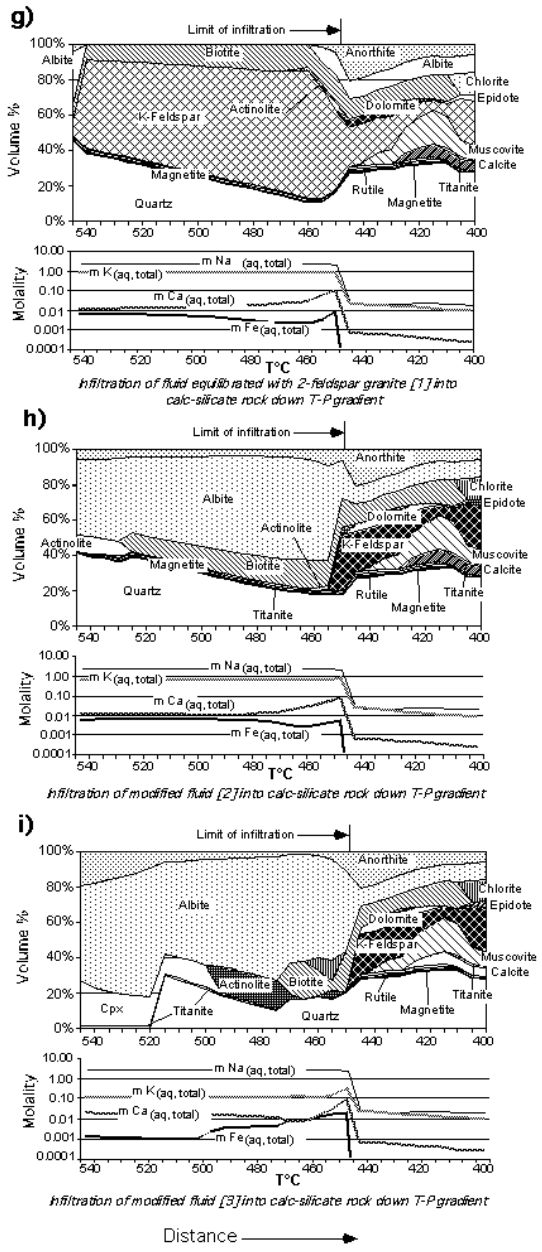

Figure 3-11 (cont) above.

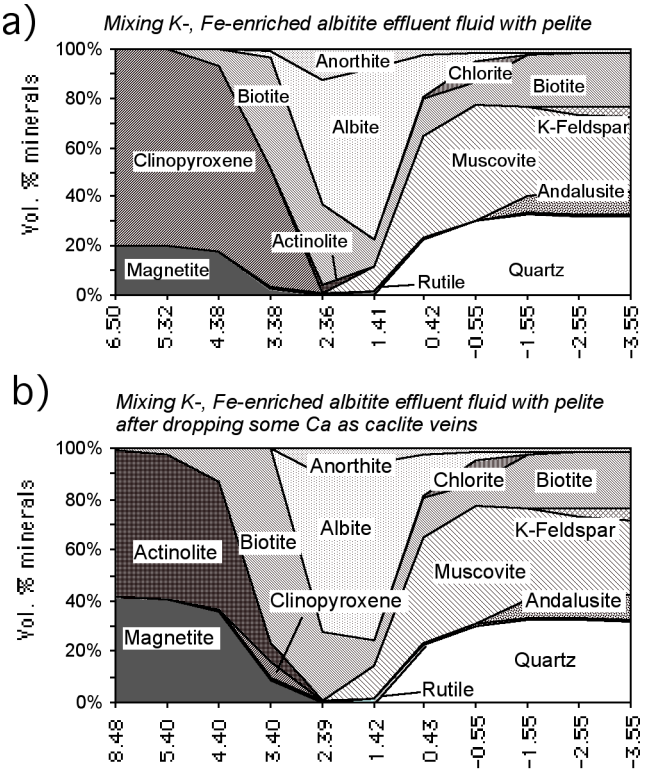

Figure 3-12. Aliquot-type HCh models (see Fig. 3-8a) for reaction of fluid modified by albitization of calc-silicate rocks (see indicated arrow in bottom of Fig. 3-11f and column 4 of data in Table 3-5) with pelites (Table 3-4). The models attempt to test the envisaged reaction path of fluids shown in Fig. 3-13 in which albitization of calc-silicate rocks in the lower sequences above the granites and the associated increase in K, Fe and Ca concentrations in the fluid is a likely precursor to formation of ironstones in the overlying sequence. (a) Model based on the output from Fig. 13-1f. (b) Model generated by decreasing the $m_{Ca(aq, total)}$ artifically from 0.028 to 0.018 with the assumption of Ca loss due to calcite veining. The outputs, particularly on the left side of the diagrams (high f/r), are similar to proximal alteration surrounding several of the deposits, as discussed in the text.

Discussion and Conclusions

Source of NaCl

Oliver et al. (1993), in their discussion of the calcite veins in the MKFB, concluded that the externally-derived fluid was of igneous or “average metamorphic” (but non-carbonate) derivation. However, they noted that the intense albitization required highly saline fluids, for which a salt source was not clearly evident in that belt. They appealed to selective dissolution of pure halite layers from the meta-evaporite sequence to explain the high salinities but drew particular attention to the paradox of highly saline fluids and apparently magmatic stable isotope values grossly out of equilibrium with the host meta-carbonate-evaporite sequence. After deposition of the Corella Fm (ca. 1750 Ma) and up to and including the Isan Orogeny at 1600 Ma, it is possible that production of saline fluids occurred at moderate temperatures by evaporite dissolution (Oliver et al., 1994). This may be an explanation for the high fluid salinities associated with albitites in the ca. 1600 Ma Osborne deposit. However, during the later intrusion of the Williams Batholith, saline fluids could no longer have been derived én masse from Corella Fm meta-evaporites because most of the evaporite “salt” should have been sequestered into scapolite by the earlier thermal events. Saline pore fluid contained within scapolitic metamorphic rocks (Oliver et al., 1992) may have been liberated during albitization (e.g., by destruction of fluid inclusions and release of other grain boundary fluids). A small amount of NaCl may have been all that was needed to shift the fluids into the albite-stable field (Fig. 3-9), but the amount of Na actually transferred into the albitized rocks is still extraordinary, and the stable isotope data also require that the bulk of the oxygen and carbon in calcite, at least, were derived from outside the Corella Formation and most likely had an igneous source (Marshall and Oliver, 2005; Marshall et al., 2006). An evaporite would have had to be situated in an overlying, unmetamorphosed sequence, which would have required either (i) exhumation of the sequence immediately after the 1600 Ma metamorphism, or (ii) the downward penetration of surface evaporite-derived fluids into the belt during exhumation. Penetration of near surface fluids deep into mountain ranges such as the Isan orogenic belt has been proposed elsewhere (Wickham and Taylor, 1987; Koons and Craw, 1991; Jenkin et al., 1994), but typically such topographically or mechanically driven fluid flow is incapable of penetrating more than 5 or 8 km. Some of the fluid inclusion data would permit low pressure exhumation interpretations (130 to 150 MPa), but CO_2 density data for fluid inclusions in the ore deposits gives pressures in excess of 300 MPa, making it less likely that surface-derived evaporite fluids could have been involved.

A more likely source for most of the salt that caused post-peak metamorphic albitization was from the crystallization of the Williams Suite intrusions (Fig. 3-13). Pollard (2001) proposed a model whereby immiscible separation of a complex NaCl-H_2O-CO_2±$CaCl_2$ fluid into a hypersaline brine and CO_2-rich gas resulted in a hydrothermal fluid that would have been in equilibrium with albite at high temperatures above the pluton. He also estimated that the total Na budget accompanying albitization could be achieved by release of magmatic fluids given the wide extent of the Williams Suite (Fig. 3-2). Albitization by magmatic fluids has been observed for some 2-feldspar granites and pegmatites elsewhere (e.g., Charoy and Pollard, 1989). Relative to H_2O-NaCl fluids, albite is preferentially stabilized over K-feldspar in the presence of elevated CO_2 (Liyama, 1965), and this is the basis for shifting our preferred model albitizing fluid to a higher Na/K ratio than fluid in equilibrium with 2-feldspar granite. The widespread abundance of albite in the Eastern Succession alteration systems, predominant over K-feldspar, is interpreted to reflect periodic replenishment of NaCl but also the contribution of CO_2 released by both magma crystallization and by wall rock alteration of carbonates.

Relationship to mineralization

Geochemical data indicate that the albitization process added Na to the rocks and released Fe, K, Ba, Rb ± Ca, Sr, Co, V, Mn, Pb and Zn to the fluid. The leached elements are those that are specifically enriched in the proximal biotite-magnetite alteration zones of the Cu-Au ore deposits (Fig. 3-6g), although Fe and K are also found in barren ironstones and biotite-rich alteration in Snake Creek rocks (Rubenach and Lewthwaite, 2002). In the case of Pb and Zn (which we have not modeled), the loss of these components is apparently matched by their enrichment in ore-related fluid inclusions (e.g., Williams et al., 2001). The geochemical modeling (i) is consistent with the progressive enrichment of Fe and K in the fluid during albitization, (ii) demonstrates that the Fe and K concentrations are close to that observed in equilibrium with magnetite and biotite in some of the Cu-Au deposits, and (iii) adequately predicts the mineralogy of ore-proximal alteration zones formed in pelites from fluids that had previously albitized calc-silicate rocks (Table 3-4, Fig. 3-12).

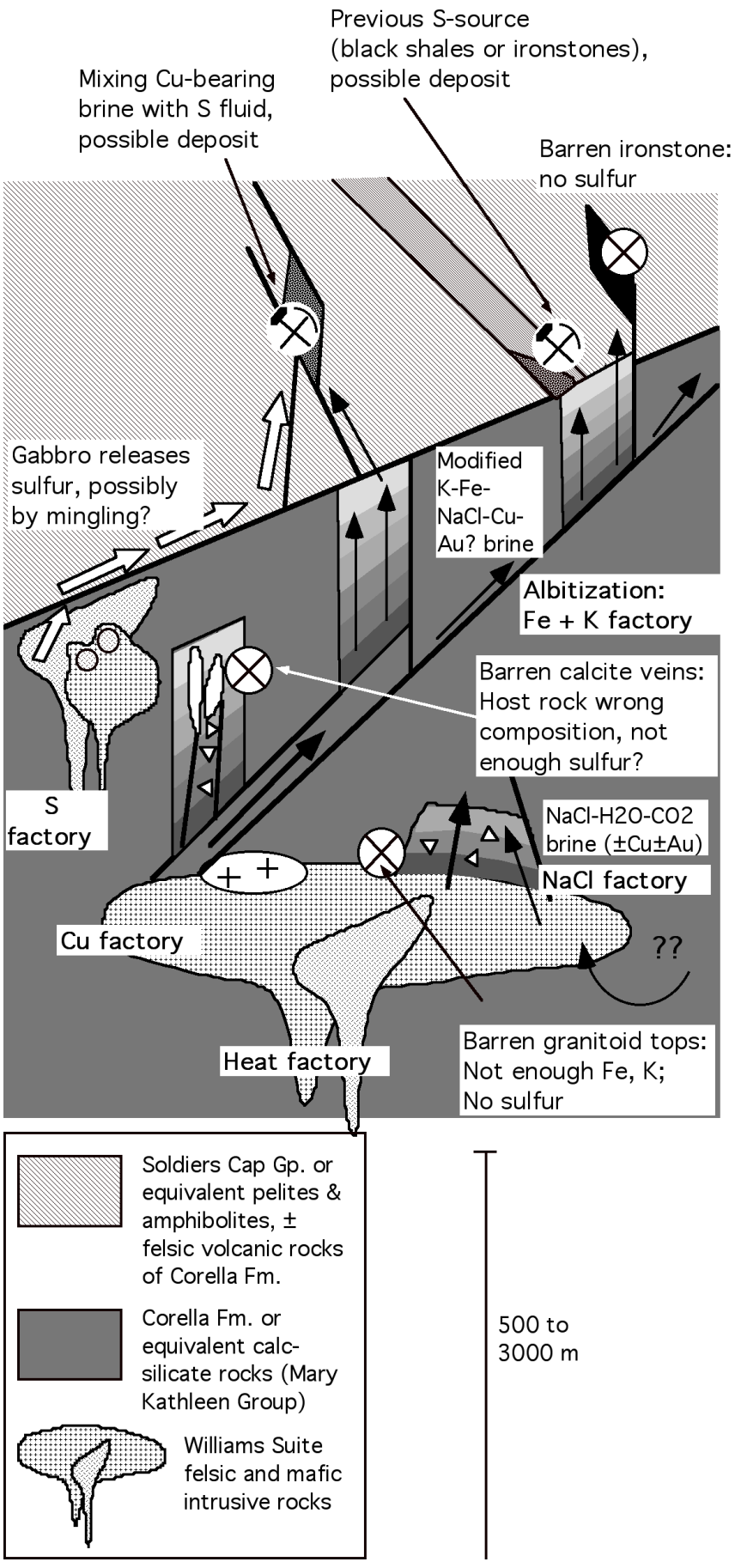

Figure 3-13. Cartoon cross section explaining the distribution and generation of albitites and the likely chemical reaction paths between source rocks, albitites and ore deposits of the Eastern Succession. Black arrows are inferred pathways of brines, white arrows are speculated sulphur-bearing fluids. Optimal conditions for ore genesis require a previous history of fluid modification via albitization (variable gray shading), a structural trap, a reactive host rock in overlying schists (or non–calc-silicate rocks of the Mary Kathleen Group), and a sulphur source, as indicated. Barren ironstones may be produced via the modelled albitization path but lack sulphur. All pyrite-magnetite ironstones contain chalcopyrite, so the availability of Cu is not a limiting factor. For at least some of the deposits a likely origin for sulphur from crystallizing or leached gabbros (or possibly even mantle-derived fluids) is constrained by $\partial^{34}S$ values of sulfides from the deposits near 0 ‰ (Mark et al., 2000; Baker et al., 2001). Also, although our data strongly support a major magmatic component to the alteration and mineralization (including Cu), we have not completely excluded possibilities of exotic NaCl replenishment (see also Williams et al., 2001).

Our model of fluid infiltration through calc-silicate rock in a thermal gradient using fluids equilibrated with 2-feldspar granite produces biotite–K-feldspar alteration similar to that seen around some of the deposits. However, the small amount of magnetite precipitated during such model alteration, and the observation that the deposits are not generally hosted in calc-silicate rocks, precludes a simple conclusion that down-temperature infiltration can produce the ore-proximal alteration.

The pattern for Cu during albitization remains unclear, and our geochemical data for albitization show no consistent patterns for Cu mobility, despite consistent transfer of Pb and Zn from the rock to the fluid. This could mean that the source of the copper for the deposits may have been from outside the metasedimentary sequence, possibly the Williams Suite for at least the young albitites and ore deposits (Fig. 13). Barren ironstones may have been produced when albitizing fluids were initially poor in Cu, or S, or both. Given the alteration path suggested here for albitization, it is possible that the chalcopyrite only became saturated in the albitizing fluids upon mixing with S-bearing wall rocks or fluids. Mixing of Cu-bearing fluids with a more juvenile magmatic fluid containing sulphur, or fluid equilibrated with sulphide-bearing mafic rocks, may be required to explain the large tonnage magnetite-chalcopyrite deposits of the district, particularly Ernest Henry. Similarly, strong Ba depletion during albitization requires low sulfate concentrations in the fluid, and mixing to produce barite has apparently occurred only at the sites of known Cu-Au mineralization (Table 1). Some mineralized ironstones in the Cloncurry District may have depended on S-rich fluids reacting with earlier ironstone rocks (e.g., Rotherham et al., 1998). However, we propose that ore formation mostly occurred by mixing between (i) primitive magmatic S-bearing fluids and (ii) saline brines, probably initially of igneous derivation, that were extensively modified by wall-rock interaction which caused the albitization described here.

Acknowledgments

Evgeniy Bastrakov (Geoscience Australia) is thanked for some training, the Geoscience Australia version of the UNITHERM database, and his working files for initial setting of the modeling problem. This research has been conducted through the support of the Australian Research Council (1998 – 2002), the Australian Minerals Industry Research Association (1993 – 1997), and the Predictive Minerals Discovery Cooperative Research Centre (2001 – 2002). Mount Isa Mines Exploration (now XStrata) and James Cook University also provided research support, particularly through the contribution of MIM and Ernest Henry Mines through an ARC-SPIRT project to Williams and Oliver at Ernest Henry. We acknowledge fruitful discussions with Mark Barton, Mick Carew, Ian Cartwright, Dave Cooke, Richard Crookes, Garry Davidson, Paul Gow, Caroline Perring, Neil Phillips, Chris Salt, Roger Skirrow, Max Tuesley, Rick Valenta, Vic Wall, John Walshe, Steve Walters, Andy Wilde, Dugi Wilson, and Bruce Yardley.

References

Adshead, N.D., Voulgaris, P., and Muscio, V.N., 1998, Osborne copper-gold deposit: in Berkman, D.A. and MacKenzie, D.H., eds., Geology of Australian and Papua New Guinean mineral deposits: Australasian Institute of Mining and Metallurgy, v. 22, p. 793-799.

Baker, T., 1996, The geology and genesis of the Eloise Cu-Au deposit, Cloncurry district, NW Queensland, Australia: Unpublished PhD thesis, Townsville, James Cook University. 303 p.

Baker, T., 1998, Alteration, mineralization and fluid evolution at the Eloise Cu-Au deposit, Cloncurry district, NW Queensland: ECONOMIC GEOLOGY, v. 93, p. 1213-1236.

Baker, T., and Laing, W.P., 1998, Eloise Cu-Au deposit, east Mt. Isa Block: structural environment and structural controls on ore: Australian Journal of Earth Sciences, 45: 429-444.

Baker, T., Perkins, C., Blake, K.L., and Williams, P.J., 2001, Radiogenic and stable isotope constraints on the genesis of the Eloise Cu-Au deposit, Cloncurry District, northwest Queensland: ECONOMIC GEOLOGY, v. 96, p. 723-742.

Barton, M.D. and Johnson, D.A., 1996, Evaporitic source model for igneous-related Fe oxide-(REE-Cu-Au-U) mineralization: Geology, v. 24, p. 259-262.

Berman, R.G., 1988, Internally-consistent thermodynamic data for minerals in the system Na2O-K2O-CaO-MgO-FeO-Fe2O3-Al2O3-SiO2-TiO2-H2O-CO2: Journal of Petrology, v. 29, p. 445-522.

Bethke, C.M., 2002. The Geochemists Workbench, Version 4.0.2: A Users Guide., University of Illinois, 224 pp.

Bird, D.K., Schiffman, P., Elders, W.A., Williams, A.E. and McDowell, S.D., 1984, Calc-silicate mineralization in active geothermal systems: ECONOMIC GEOLOGY, v. 79, p. 671-695.

Blattner, P. and Lassey, K.R. 1990, Transport of stable isotopes, kinetics, dispersive advection and the 'isotopic fronts' of Baumgartner and Rumble (1988): Contributions to Mineralogy and Petrology, v. 105, p. 486-490.

Borisov, M.V. and Shvarov, Yu.V., 1998, Mobilization of ore components during the formation of Pb-Zn hydrothermal lodes: Geochemistry International, v. 36, 134-149.

Cartwright, I., 1997. Permeability generation and resetting of tracers during metamorphic fluid flow: implications for advection-dispersion models: Contributions to Mineralogy and Petrology, v. 129, p. 198-208.

Charoy, B. and Pollard, P.J., 1989, Albite-rich, silica-depleted metasomatic rocks at Emuford, northeast Queensland: mineralogical, geochemical and fluid inclusion constraints on hydrothermal evolution and tin mineralization: ECONOMIC GEOLOGY, v. 84, p. 1850-1874.

Cleverley, J.S. and Oliver, N.H.S., 2005, Comparing closed system, flow-through and fluid infiltration geochemical modelling: examples from K-alteration in the Ernest Henry Fe-oxide-Cu-Au system: Geofluids, v. 5, p. 289-307.

Cline, J.S. and Bodnar, R.J., 1991, Can economic porphyry copper mineralization be generated by a typical calc-alkaline melt?: Journal of Geophysical Research, v. 96, p. 8113-8126.

Cook, N.D.J. and Ashley, P.M., 1992, Meta-evaporite sequence, exhalative chemical sediments and associated rocks in the Proterozoic Willyama Supergroup, South Australia: implications for metallogenesis: Precambrian Research, v. 56, p. 211-226.

Cooke, D.R., and McPhail, D.C., 2001. Epithermal Au-Ag-Te mineralization, Acupan, Baguio District, Phillipines; numerical simulations of mineral deposition: ECONOMIC GEOLOGY, v.96, p. 109-132.

Davidson, G.J. and Dixon, G.H., 1992, Two sulphur isotope provinces deduced from ores in the Mount Isa eastern succession, Australia: Mineralium Deposita, v. 27, p. 30-41.

Davis, B.K., Pollard, P.J., Lally, J.H., McNaughton, N.J., Blake,K., and Williams, P.J., 2001, Deformation history of the Naraku Batholith, Mt. Isa Inlier, Australia: implications for pluton ages and geometries from structural studies of the Dipvale Granodiorite and Levian Granite: Australian Journal of Earth Sciences, v. 48, p. 131-150.

deJong, G. and Williams, P.J., 1995. Giant metasomatic system formed during exhumation of mid-crustal Proterozoic rocks in the vicinity of the Cloncurry Fault, northwest Queensland. Australian Journal of Earth Sciences, v. 42, p. 281-290.

Dipple, G.M. and Ferry, J.M., 1992, Metasomatism and fluid flow in ductile fault zones, Contributions to Mineralogy and Petrology: v. 112, p. 149-164.

Dixon, G. and Davidson, G.J. 1996, Stable isotope evidence for thermochemical sulfate reduction in the Dugald River (Australia) strata-bound shale-hosted zinc-lead deposit: Chemical Geology, v.129, p.227-246.

Ferry, J.M. and Dipple, G.M. 1991, Fluid flow, mineral reactions, and metasomatism, Geology: v. 19, p. 211-214.

Foster, D.R.W. and Rubenach, M.J., 2000, Comment: high radiogenic heat-producing granites and metamorphism – an example from the western Mount Isa Inlier, Australia: Geology, v. 28, p. 671.

Frietsch, R., Tuisku, P., Martinsson, O.L., and Perdahl, J.–A., 1997, Early Proterozoic Cu-(Au) and Fe ore deposits associated with regional Na-Cl metasomatism in northern Fennoscandia: Ore Geology Reviews,v. 12,p. 1-34.

Fu, B., Williams, P.J., Oliver, N.H.S., Dong, G., Pollard, P.J., and Mark, G., 2003. Fluid mixing versus unmixing as an ore-forming process in the Cloncurry Fe-oxide-Cu-Au District, NW Queensland, Australia: evidence from fluid inclusions: Journal of Geochemical Exploration, v, 78-79, p. 617-622.

Gauthier, L., Hall, G., Stein, H. and Schaltegger, U., 2001, The Osborne Deposit, Cloncurry District: a 1595 Ma Cu-Au skarn deposit, in Williams, P. J., ed., 2001: A Hydrothermal Odyssey: Extended Conference Abstracts, Economic Geology Research Unit Contribution v. 59, p. 58-59.

Giles, D. and Nutman, A.P., 2002, SHRIMP U-Pb monazite dating of 1600-1580 Ma amphibolite facies metamorphism in the southeastern Mt. Isa Block, Australia: Australian Journal of Earth Sciences, v. 49, p. 455-466.

Grant, J.A. 1986, The isocon diagram - a simple solution to Gresens equation for metasomatic alteration, ECONOMIC GEOLOGY: v. 81, p. 1976-1982.

Hand, M. and Rubatto, D., 2002, The scale of the thermal problem in the Mt. Isa Inlier [abs]: Geological Society of Australia Abstracts, v. 67, p. 173.

Haynes, D. W., 2000. Iron oxide copper (-gold) deposits: their position in the ore deposit spectrum, in Porter, T.M., ed., Hydrothermal iron oxide copper-gold and related deposits: a global perspective: Australian Mineral Foundation, Adelaide, p. 71-90.

Heinrich, C.A., Bain, J.H.C., Mernagh, T.P., Wyborn, L.A.I., Andrew, A.S. and Waring, C.L. 1995, Fluid and mass transfer during metabasalt alteration and copper mineralization at Mount Isa, Australia, ECONOMIC GEOLOGY: v. 90, p. 705-730.

Heinrich, C.A., Walshe, J.L., and Harrold, B.P., 1996, Chemical mass transfer of ore-forming hydrothermal systems: current practise and problems: Ore Geology Reviews, v10, p. 319-338.

Hitzman, M.W., Oreskes, N., and Einaudi, M.T., 1992, Geological characteristics and tectonic setting of Proterozoic iron oxide (Cu-U-Au-REE) deposits: Precambrian Research, v. 58, p 241-287.

Iiyama, J.T., 1965, Influence des anions sur les équilibres d'échange d'ions Na-K dans les feldspaths alcalins à 600°C sous une pression de 1000 bars: Bulletin de Societe françois Minéralogie et Cristallographie, v. 88, p. 618-622.

Ito, E., Harris, D.M. and Anderson, A.T.J., 1983, Alteration of oceanic crust and geologic cycling of chlorine and water: Geochimica et Cosmochimica Acta, v. 47, p. 1613-1624.

Jenkin, G.R.T., Craw, D. and Fallick, A.E. 1994, Stable isotopic and fluid inclusion evidence for meteoric fluid penetration into an active mountain belt; Alpine Schist, New Zealand: Journal of Metamorphic Geology, v. 12, p. 429-444.

Koons, P.O. and Craw, D. 1991, Evolution of fluid driving forces and composition within collisional orogens: Geophysical Research Letters:, v. 18, p. 935-938.

Korzhinskii, D.S. 1970, Theory of metasomatic zoning: London, Oxford University Press, 162 pp.

Laing, W.P., 1998, Structural-metasomatic environment of the East Mt. Isa Block base-metal-gold province: Australian Journal of Earth Sciences, v. 45, p. 413-428.

Little, G.A., 1997. Structural evolution and paragenesis of alteration and mineralization at Mount Elliott Cu-Au mine, northwest Queensland: Unpublished B.Sc. (Hons.) thesis, James Cook University, 98 pp.

Mark, G., 1998a, Albitite formation by selective pervasive sodic alteration of tonalite plutons in the Cloncurry district, NW Queensland: Australian Journal of Earth Sciences, v. 45, p. 765-774.

Mark, G. 1998b, Granites and regional alteration in the Cloncurry district, northwest Queensland, Australia: Unpublished PhD thesis, James Cook University of North Queensland, 354 p.

Mark, G., and Foster, D.R.W., 2000, Magmatic-hydrothermal albite-actinolite-apatite-rich rocks from the Cloncurry district, NW Queensland, Australia: Lithos, v. 51, p. 223-245.

Mark, G., Darvall, M., Tolman, J., Foster, D.R.W., Williams, P.J. and Pollard, P.J., 1999, Magmas and regional Na-Ca alteration, Cloncurry district, Australia, in Stanley, C.J. et al., eds., Mineral Deposits: Processes to Processing: Proceedings of the 5th Biennial SGA meeting and the 10th Quadrennial IAGOD Symposium, London, 22-25 August, 1999. Balkema, Rotterdam, p. 385-388.

Mark, G., Oliver, N.H.S., Williams, P.J., Valenta, R.K. and Crookes, R.A., 2000, The evolution of the Ernest Henry hydrothermal system, in Porter, T.M., ed., Hydrothermal iron oxide copper-gold and related deposits: a global perspective: Australian Mineral Foundation, Adelaide,p. 132-136.

Marschik, R., Chiaradia, M. and Fontboté, L., 2003, Implications of Pb isotope signatures or rocks and iron oxide Cu-Au ores in the Candelaria-Punta del Cobre district, Chile: Mineralium Deposita, v. 38, p. 900-912.

Marschik, R. and Fontboté, L., 2001, The Candelaria-Punta del Cobre iron oxide Cu-Au(-Zn-Ag) deposits, Chile: ECONOMIC GEOLOGY, v. 96, p. 1799-1826.

Marshall, L.J. and Oliver, N.H.S. 2002, From source to sink: evolving fluid characteristics in Mt. Isa Inlier Fe-oxide-Cu-Au mineralization [abs]: Geological Society of Australia Abstracts, v. 67, p. 292.

Marshall, L.J., 2003. Brecciation within the Mary Kathleen Group of the Eastern Succession, Mt. Isa Block, Australia: implications for Fe-oxide-Cu-Au mineralization. Unpublished PhD thesis, James Cook University of North Queensland, 325 p.

Marshall, L.J. and Oliver, N.H.S., 2005, Monitoring fluid chemistry in iron-oxide-copper-gold-related metasomatic processes, Eastern Mt. Isa Block, Australia. Geofluids, v. 5, p. 1-22.

Marshall, L.J., Oliver, N.H.S., and Davidson, G.J. 2006. Fluid sources and fluid-wallrock interaction in regional alteration and iron-oxide-copper-gold mineralisation, East Mt Isa Block: insight from C and O stable isotopes. Mineralium Deposita, in press.

Oliver, N.H.S., 1995, The hydrothermal history of the Mary Kathleen Fold Belt, Mount Isa Block, Queensland, Australia: Australian Journal of Earth Sciences, v. 42, p. 267-280.

Oliver, N.H.S., Cartwright, I., Wall, V.J. and Golding, S.D., 1993, The stable isotopic signature of large-scale fracture-hosted metamorphic fluid pathways, Mary Kathleen, Australia: Journal of Metamorphic Geology, v. 11, p. 705-720.

Oliver, N.H.S., Cleverley, J.S., Mark, G., Pollard, P.J., Fu, B., Marshall, L.J., Rubenach, M.J., Williams, P.J. & Baker, T., 2004. Modeling the role of sodic alteration in the genesis of iron oxide-copper-gold deposits, Eastern Mount Isa Block, Australia. Economic Geology, Vol. 99, p. 1145–1176.

Oliver, N.H.S., Holcombe, R.J., Hill, E.J., and Pearson, P.J. 1991. Tectono-metamorphic evolution of the Mary Kathleen Fold Belt, northwest Queensland: a reflection of mantle plume processes ?: Australian Journal of Earth Sciences, v. 38, p. 425-455.

Oliver, N.H.S., Rawling, T.R., Cartwright, I. and Pearson, P.J., 1994, High temperature fluid-rock interaction and scapolitization in a large extension-related hydrothermal system, Mary Kathleen, Australia: Journal of Petrology, v. 35, p. 1455-1491.

Oliver, N.H.S., Valenta, R.K. and Wall, V.J., 1990, The effect of heterogeneous stress and strain on

metamorphic fluid flow, Mary Kathleen, Australia, and a model for large-scale fluid circulation. Journal of Metamorphic Geology, v. 8, p. 311-331.

Oliver, N.H.S., Wall, V.J. and Cartwright, I., 1992, Internal control of fluid compositions in amphibolite-facies scapolitic calc-silicates, Mary Kathleen, Australia: Contributions to Mineralogy and Petrology, v. 111, p. 94-112.

Oreskes, N., and Einaudi, M. T., 1992, Origin of hydrothermal fluids at Olympic Dam: preliminary results from fluid inclusions and stable isotopes: ECONOMIC GEOLOGY, v. 87, p. 64-90.

Page, R. W. and Sun, S-S., 1998, Aspects of geochronology and crustal evolution in the Eastern Fold Belt, Mt. Isa Inlier: Australian Journal of Earth Sciences, v. 45, p. 343-362.

Perkins, C. and Wyborn, L.A.I., 1998, Age of Cu-Au mineralization, Cloncurry district, Mount Isa Inlier, as determined by 40Ar/39Ar dating: Australian Journal of Earth Sciences, v. 45, p. 233-246.

Perring, C.S., Pollard, P.J., Dong, G., Nunn, A.J. and Blake, K.L., 2000, The Lightning Creek sill complex, Cloncurry District, northwest Queensland: a source of fluids for Fe-oxide-Cu-Au mineralization and sodic-calcic alteration: ECONOMIC GEOLOGY, v.95, p. 1067-1089.

Pokrovskii, V.A., Harrold, B.P., Heinrich, C.A., and Liu, X., 1998, Release notes for THERMODATA AGSO/ANU/ETHZ (version 5.2). Computer file, ETH (for availability contact Prof. C. Heinrich, Department Erdwissenschaften NO, ETH Zentrum, CH-8092 Zurich, Switzerland).

Pollard, P.J., 2001, Sodic(-calcic) alteration associated with Fe-oxide-Cu-Au deposits: an origin via unmixing of magmatic-derived H2O-CO2-salt fluids: Mineralium Deposita,v. 36, p. 93-100.

Pollard, P.J., Mark, G. and Mitchell, L.C., 1998, Geochemistry of post-1540 Ma granites in the Cloncurry District, northwest Queensland: ECONOMIC GEOLOGY, v.93, p. 1330-1344.

Powell, R., 1977, Activity-composition relation for crystalline solutions, in Fraser, D. G., ed., Thermodynamics in Geology: Dordrecht, D. Reidel Publishing Company, p. 57-65.

Reed, M.H., and Spycher, N.F., 1985, Boiling, cooling, and oxidation in epithermal systems: a numerical approach: REVIEWS IN ECONOMIC GEOLOGY, v. 2, p. 249-272.

Rose, N.M., Bird, D.K., and Liou, J.G., 1992, Experimental investigation of mass transfer - albite, Ca Al silicates and aqueous solutions: American Journal of Science, v. 292, p. 21-57.

Rotherham, J.F., Blake, K.L., Cartwright, I. and Williams, P.J., 1998, Stable isotope evidence for the origin of the Starra Au-Cu deposit, Cloncurry district: ECONOMIC GEOLOGY, v. 93, p. 1435-1449.

Rubenach, M.J. and Barker, A.J., 1998, Metamorphic and metasomatic evolution of the Snake Creek Anticline, Eastern Succession, Mount Isa Inlier: Australian Journal of Earth Sciences, v. 45, p. 363-372.

Rubenach, M.J. and Lewthwaite, K.J., 2002, Metasomatic albitites and related biotite-rich schists from a low-pressure polymetamorphic terrane, Snake Creek Anticline, Mount Isa Inlier, northeastern Australia: microstructures and P-T-d paths: Journal of Metamorphic Geology, v. 20, p. 191-202

Rubenach, M.J., Adshead, N.D., Oliver, N.H.S., Tullemans, F., Esser, D. and Stein, H., 2001, The Osborne Ca-Au deposit: geochronology and genesis of mineralization in relation to host albitites and ironstones, in Williams, P.J., ed., 2001: A Hydrothermal Odyssey: Extended Conference Abstracts, Economic Geology Research Unit Contribution v. 59, p. 172-173.

Shock E.L., Sassani D.C., Willis M., and Sverjensky D.A., 1997, Inorganic species in geologic fluids: Correlations among standard molal thermodynamic properties of aqueous ions and hydroxide complexes: Geochimica et Cosmochimica Acta, v. 61, p. 907-950.

Shvarov, Y.V., 1999, Algorithmization of the numerical equilibrium modeling of dynamic geochemical processes: Geochemistry International, v. 37, p. 571-576.

Shvarov, Y.V. and Bastrakov, E.N., 1999, HCh: a software package for geochemical equilibrium modeling, User's Guide: Australian Geological Survey Organisation, Record 1999/25, 60pp.

Shvarov, Y.V., 1978, Minimization of the thermodynamic potential of an open chemical system: Geochemistry International, v. 15, p. 38-45.

Sillitoe, R.H., 2003, Iron oxide-copper-gold deposits: an Andean view: Mineralium Deposita, v. 38, p. 787-812.

Skirrow, R.G., and Walshe, J.L., 2002. Reduced and oxidized Au-Cu-Bi iron oxide deposits of the Tennant Creek Inlier, Australia: an intregrated geologic and chemical model: ECONOMIC GEOLOGY, v. 97, p. 1167-1202.

Sverjensky D.A., Hemley J.J., and D'Angelo W.M.D., 1991, Thermodynamic assessment of hydrothermal alkali feldspar-mica-aluminosilicate equilibria: Geochimica et Cosmochimica Acta, v. 55, p. 989-1004.

Sverjensky D.A., Shock E.L., and Helgeson H.C., 1997, Prediction of the thermodynamic properties of aqueous metal complexes to 1000°C and 5kb: Geochimica et Cosmochimica Acta, v. 61, p. 1359-1412.

Twyerould, S.C. 1997, The geology and genesis of the Ernest Henry Fe-Cu-Au deposit, Northwest Queensland, Australia: Unpublished PhD thesis, University of Oregon.

Ulrich, T., and Heinrich, C.A., 2001. Geology and alteration geochemistry of the porphyry Cu-Au deposit at Bajo de la Alumbrera, Argentina: ECONOMIC GEOLOGY, v. 96, p. 1719-1742.

Wickham, S.M. and Taylor, H.P. Jr., 1987, Stable isotope constraints on the origin and depth of penetration of hydrothermal fluids associated with Hercynian regional metamorphism and crustal anatexis in the Pyrenees, Contributions to Mineralogy and Petrology: v. 95, p. 255-268.

Williams, P.J., 1994, Iron mobility during synmetamorphic alteration in the Selwyn Range area, NW Queensland: implications for the origin of ironstone-hosted Au-Cu deposits: Mineralium Deposita, v. 29, p. 250-260.

Williams, P.J., 1998, Metalliferous economic geology of the Mt. Isa Eastern Succession, Queensland. Australian Journal of Earth Sciences, v. 45, p. 329-341.

Williams, P.J., Dong, G., Pollard, P.J., Perring, C.S., Ryan, C.G., and Mernagh, T.P., 1999, Fluid inclusion geochemistry of Cloncurry (Fe)-Cu-Au deposits, in, Stanley, C.J., ed., Mineral Deposits: Processes to Processing: Proceedings of the 5th Biennial SGA meeting and the 10th Quadrennial IAGOD Symposium, London, 22-25 August, 1999. Balkema, Rotterdam, p. 111-114.

Williams, P.J., Dong, G., Ryan, C.G., Pollard, P.J., Rotherham, J.F., Mernagh, T.P. and Chapman, L.H., 2001, Geochemistry of hypersaline fluid inclusions from the Starra (Fe oxide)-Au-Cu deposit, Cloncurry District, Queensland: ECONOMIC GEOLOGY, v. 96, p. 875-884.

Chapter 4: From source to sink: protracted metal, sulphur and fluid evolution in the Mount Isa Eastern Succession IOCG district

Oliver, N.H.S., Butera, K., Collins, W.J., Cleverley, J.S., Fu, B., Marshall, L.J. & Rubenach, M.J.

Predictive Mineral Discovery Cooperative Research Centre @ Economic Geology Research Unit, JCU School of Earth Sciences, Townsville, Qld, Australia 4811.

*This paper was produced as part of the Mt Isa **pmd***CRC delivery workshop held in Mt Isa, March 2005. Geordie Mark is acknowledged for comments on magma genesis in the Williams Batholith in companion papers to this original report.*

Abstract

Protracted metal and sulphur contributions to the Eastern Succession iron-oxide-Cu-Au province occurred primarily as a consequence of long-lived fluid and melt fluxes from the base of the crust, stimulated by back-arc emplacement of voluminous mafic magmas. The concentration of iron, copper and gold into the presently observed mineral deposits mostly involved remobilisation and reworking of early initial enrichments (pre- to syn-Isan Orogeny) by later fluids (syn- to post-Isan and syn-Williams/Naraku Batholith). Osborne (eastern domain) and Eloise-type ores formed or were strongly remobilized at c. 1600 Ma by reduced, mafic-derived fluids, whereas oxidised brines released by the Williams/Naraku granitoids overprinted magnetite ± sulphides at Osborne (western domain) and Starra to produce hematite-chalcopyrite associations. Direct, potentially carbonatite-related mantle fluid may have periodically pulsed through the system, manifest now as pyrrhotite-stable carbonate veins and pods. Ernest Henry remains the best candidate for a true syn-Williams orebody, with reduced mantle- or mafic-derived HCOS fluid mixing with saline, oxidised brine derived from the Williams/Naraku Batholith. Exploration for Ernest Henry and Starra style deposits should focus on recognition of oxidised corridors in relation to structurally-defined targets, but recognition of truly large deposits (Ernest Henry and larger) will require recognition in the 3D model of both oxidised and reduced corridors.

Introduction

Ore genesis models developed in recent years for iron-oxide-Cu-Au deposits of the Cloncurry District have focussed attention mostly on the role of volatile phase separation from the Williams-Naraku Batholiths as the most likely source of metals. This paradigm has not particularly helped explorers because of the apparent distal relationship between the intrusions and known ore deposits, even though an appreciation of the development of upwards fluid flow and brecciation relative to some ore deposits has recently been gained (see below). Our recent work (Butera et al., 2005, I 2-3 final report) has identified a more protracted history of contribution of metals and sulphur, and a spatial distribution implicating, in particular, faults and mafic rocks (see also Mustard et al., McLellan et al., this report). We develop these themes here, including also an appraisal of the tectonic evolution that contributed to the protracted metals contribution, and we also attempt to develop a more holistic model that incorporates previous work on the Williams-Naraku as well as the recent data.

Williams-Naraku Batholith issues

One of the obvious features of the Eastern Succession is the huge volume of metasomatic rocks, even more so than in the west. Decades of research have failed to explain the volume of fluid, with circular arguments about the roles of metamorphism, evaporites and the Williams Batholith, which have not resolved the following issues:

The lack of Williams-age intrusions in the Mary Kathleen Fold Belt, despite comparable styles, if not extent, of albite alteration to the Cloncurry District, supposedly mostly related to the Williams-Naraku batholiths (Williams 1998; Oliver et al. 2004)

The convergence of stable isotopic signature of alteration systems of all ages (from 1740 to 1500 Ma) upon mantle-like values, with outliers clearly related to admixture with Corella marine carbonates, or Soldiers Cap black shales (Oliver et al. 1993; 1994; 2004; Oliver 1995; deJong &Williams 1995; Rotherham et al. 1998;

Mark et al. 2000; 2005b; Baker et al. 2001; Marshall 2003). The convergence cannot be related only to the influence of Williams-age magmatic fluids because it includes pre-1530 Ma veins (Fig. 4-1).

The apparent metallogenic similarity of IOCG deposits apparently formed at different times, i.e. Osborne at 1600-1590 Ma and Ernest Henry and Mt Elliott at 1530 Ma, with only the latter being coeval with Williams-Naraku Batholiths (Williams, 1998; Rubenach et al., 2001; Mark et al., 2005a)

The high salinity of fluid inclusion populations throughout the protracted hydrothermal history, implying that the Williams-Naraku system was not the only contributor to the unusual salinities, and that recycling of evaporite (Corella Fm) salt may have occurred several times (Fig. 4-2)

Another feature noted by Williams (1998) for many of the deposits is a strong mafic minor element association for many of the ores and alteration systems, including enriched Ni, Co, V and Mn. Mingling and mixing of mafic magmas with the Williams-Naraku suite prior to or synchronous with fluid exsolution may explain the contribution of some of these elements to the IOCGs, but the same enrichments are apparent at deposits which have a pre-Williams age (i.e. Osborne).

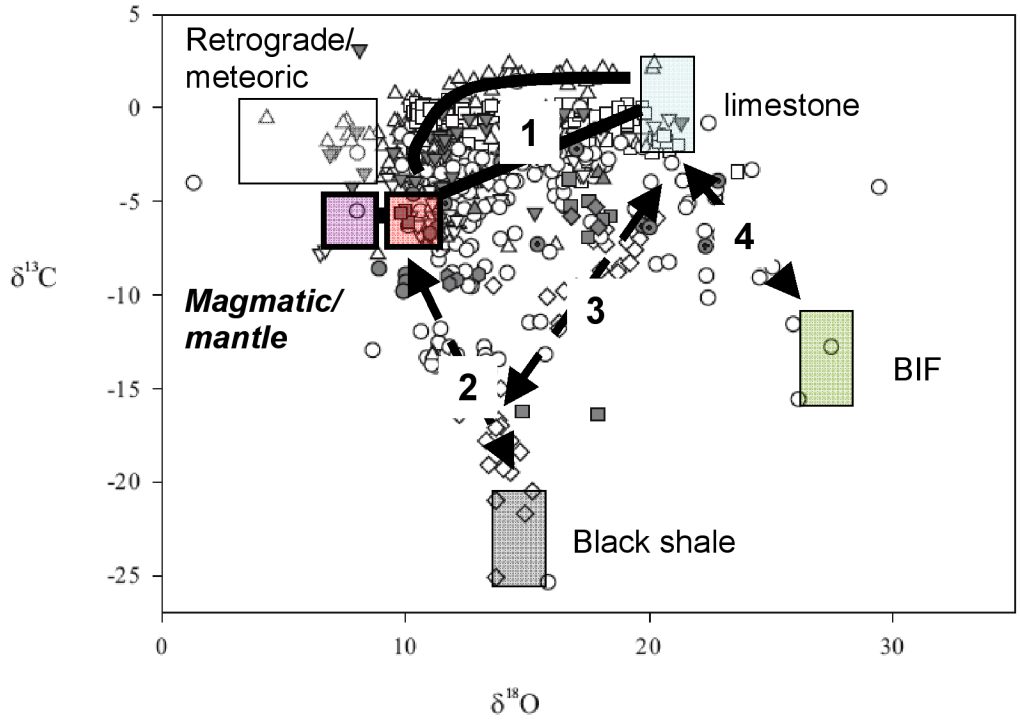

Figure 4-1: C and O isotope data for calcite and dolomite from IOCG deposits, veins and alteration systems in the Eastern Succession, from Oliver et al. (1993), Marshall (2003) and Marshall et al. (submitted). The red box shows the inferred magmatic or mantle derived signal, the adjacent purple box to the left is the calculated fluid composition for fluid with modest CO_2 content at 450 to 500°C. This box has values closer to mafic or mantle fluids than felsic-derived fluids. The other boxes are the end-member isotope reservoirs as indicated, trends 1 and 2 represent admixture of Corella marine carbonates and Soldiers Cap black shales (respectively) with the mantle-like fluid, trend 3 is observed only at Dugald River(Zn-Pb-Mn) prospect and reflects an absence of the mantle signal and admixture of carbonate and black shale signals, and trend 4 is found only at Starra and Osborne in carbonates associated with the earliest iron oxides, which we therefore infer are true BIFs rather than metasomatic products. Data between trends 1 and 3 reflect likely passage of mantle or magmatic fluids through Corella carbonates before interacting with Soldiers Cap schists (Marshall, 2003).

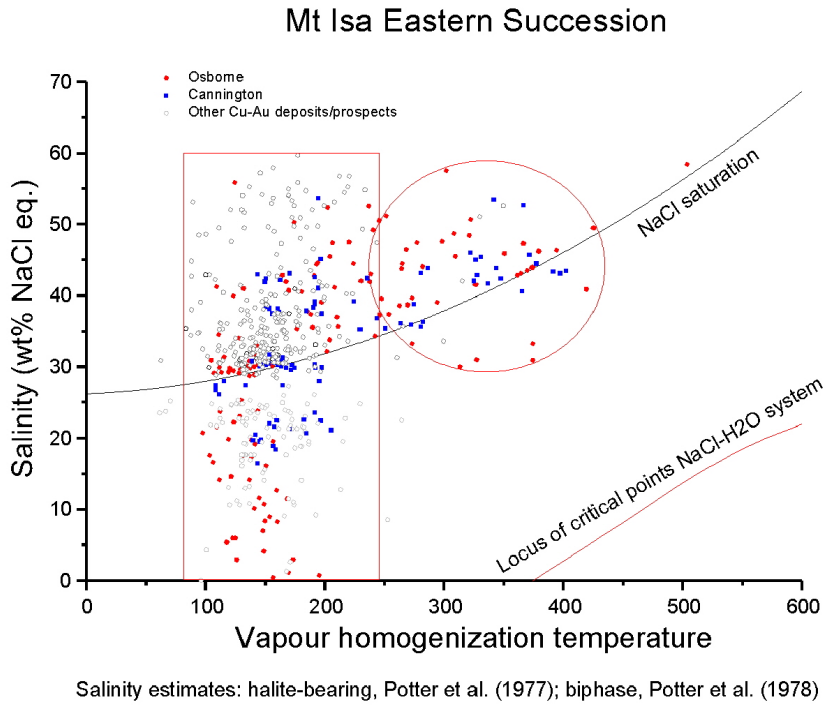

Salinity estimates: halite-bearing, Potter et al. (1977); biphase, Potter et al. (1978)

Figure 4-2: Fluid inclusion data from IOCG deposits and regional alteration systems of the Cloncurry District, from Fu et al. (2004). Note both Osborne and Cannington have a distinctive population of high T, high salinity inclusions (see also (Williams et al. 1999). These are probably early, pre-Williams age brines, distinctive from likely Williams-age fluids (rectangle).

Orebody paragenesis

Despite a proliferation of Ar-Ar ages in the range 1540 to 1490 Ma for Eastern Succession IOCGs and abundant evidence for late sulphides and related alteration, U-Pb and Re-Os ages of many of these deposits point to inherited components. The original understanding of the age of peak metamorphism at the time of these studies was focussed around the 1550 Ma age inferred from the Western Succession and Mary Kathleen orebody, such that the Williams Batholith was regarded as immediately post-peak metamorphic and evolving metamorphic-magmatic fluid systems were seen as viable. More recent recognition of earlier metamorphism, peaking at 1600-1590 Ma with D2 deformation, and earlier events at 1640 Ma (Rubenach et al., I 2-3 final report), requires a reinterpretation of earlier workers' paragenetic stages.

The protracted history of mineralisation and remobilisation is well displayed by Mary Kathleen, which has a clear history of initial U-REE enrichment at km-scales associated with emplacement of the c. 1740 Ma Wonga-Burstall granites (providing a notable prospector's target at 1:100 000 scales), and yet the orebody in its present guise was assembled at 1550 to 1500 Ma (Page 1983a; Maas et al. 1988; Oliver et al. 1999). The timing of these events implies initial enrichment followed by repeated recycling and remobilization, leaving behind the ultimate question as to whether the 1550-1500 Ma event involved regional scouring of disseminated U-REE, or remobilization of an already formed orebody or protore. Similar issues are now quite pertinent to the IOCG deposits. Silica alteration forming the envelope to Osborne is locally marked by a banded, gneissic foliation, and this foliation is folded by folds which are correlated with regional D2 – i.e. this silica alteration is pre-D2 in timing. The earliest iron oxides in this deposit are clearly pre-D2 (Fig. 3), being overprinted by coarse magnetite and chalcopyrite that was apparently introduced (or remobilized) during and after D2. Similar observations can be made at Eloise, where at least one of the orebodies contains abundant folded and foliated sulphides and durchbewegung texture (Fig. 3). Baker (1998) originally inferred a progression from peak metamorphism to ore genesis at Eloise, with significant alteration and potential mineralization occurring during the metamorphic stage. By this reasoning, with the recent geochronology, these stages would be separated now by 70 m.y. or more.

Despite the bulk of the ore at Starra being dominated by coarse chalcopyrite and hematite which transgresses foliations, we have observed rocks in the open cuts containing magnetite and chalcopyrite in which the chalcopyrite forms irregularly spaced bands that look like bedding, and all are folded by D2 folds (i.e. similar to Fig. 3b). Some or even all of the later paragenesis of hematite-chalcopyrite may have overprinted or remobilized earlier magnetite that already contained chalcopyrite. The original premise of Davidson & Large (1994) concluding that some ironstones and possibly some sulphides pre-date peak metamorphism is also supported by our stable isotope data which support a clear, non-magmatic origin for early magnetite at both Osborne and Starra (Figs. 1, 3).

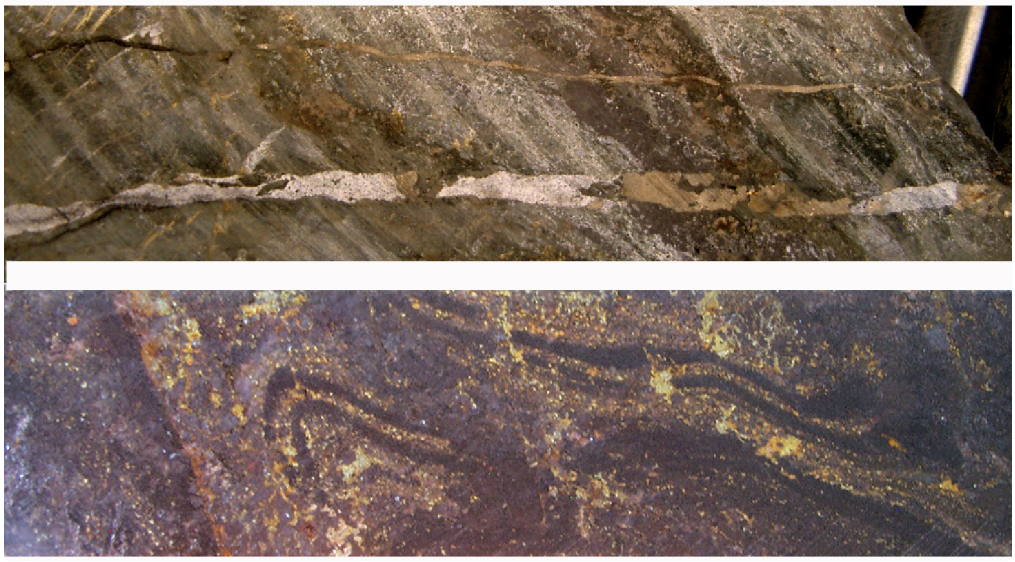

Figure 4-3: Textural evidence for protracted mineralisation at Eloise and Osborne. Top, strongly foliated bands of pyrrhotite and amphibole (brown, and calcite (pale) lie within the S_2 foliation at Eloise, suggesting pre- or syn S_2 growth. Two veins cut this banding at high angles – the bottom one in particular shows convincing evidence for short distance (diffusive) remobilization because of the mimicry of the host rock banding by the vein mineralogy. These veins may be post-S_2 in timing, correlating with the Williams-age Ar-Ar ages for biotite (Baker et al. 2001). Bottom, bands of magnetite, probably primary in origin, are folded by F_2 and cut by coarse grained magnetite lying in S_2 parallel bands. The two varieties of chalcopyrite in this view have apparent pre- (disseminated) and post- (patchy) D_2 timing, consistent with the 1600 – 1590 Ma Re-Os and U-Pb ages for initial mineralisation followed by post-D_2 reworking to give abundant 1570 to 1540 Ma Ar-Ar mica ages.

Although old ages persist in some of the recent geochronological data for Ernest Henry (Mark et al., unpubl. data; Butera et al., I 2-3 final report), Ernest Henry does not show any apparent physical or paragenetic inheritance within the orebody. The ore is defined by a fairly sharp-edged breccia in which magnetite-chalcopyrite-pyrite-calcite ore is clearly related to the brecciation, and titanite and molybdenite within ore have precise 1530 Ma ages (Mark et al., 2005a), similar to the nearby Mt. Margaret Granite. The orebody is also notable for significant enrichment in fluorine (in biotite and fluorite), and F is also enriched in breccias emanating directly off the Mt Angelay intrusion (Rubenach, unpubl. data; Cleverley & Oliver, 2005a), and in the skarn-like Mt Elliott deposit (Wang & Williams 2001). In addition, the Ernest Henry breccia has very similar internal characteristics (clast spacing, roundness, roughness and particle size distribution) to the unmineralised but magnetite-enriched breccias near the Mt Angelay Granite (Fig. 4-4), and may share a common physical origin (comminution, chemical corrosion and abrasion in a fluidised breccia pipe or chamber).

Figure 4-4: Top – typical Ernest Henry ore breccia with hematite-Kfeldspar altered clasts in a magnetite- chalcopyrite-pyrite-Kfeldspar-calcite±barite-titanite matrix. Bottom – typical breccia from a breccia pipe emanating from the Mt Angelay Granite and crosscutting Soldiers Cap Group schists, from the western edge of the Snake Ck anticline, with albite-actinolite-magnetite±Kfeldspar-chlorite clasts set in a albite-magnetite-hematite-actinolite matrix Scale is similar in both photographs..

Tectonic setting – arcs, mantle and the carbonatite connection

On the basis of the major early phase of mapping by the GSQ and BMR in the Mt Isa Block, Wilson (1978) proposed, on the basis of the overall asymmetry of the sedimentary-volcanic packages, that the eastern edge of the Mt Isa Inlier was close to a plate boundary. Part of the evidence included an appreciation of the Soldiers Cap Group as relatively deep water, high energy turbidites in comparison to possible time equivalents in the centre and west of the Inlier. Subsequently, a continent-scale model for intra-cratonic rifting and limited thickening was developed (Etheridge et al. 1987), supported by concepts of bimodal igneous geochemistry, lack of andesites and blueschists, and recognition of apparent temporal similarity between packages of rocks in the Western and Eastern Successions. Both these models have some validity in our recent reinterpretation, because the mafic magma chemistry, and indeed the asymmetry of the metal endowments, can be interpreted in the context of a back-arc continental environment (Butera et al., I 2-3). Modern continental back-arcs are characterised by high heat flow and bimodal igneous activity and any possible blueschists typically lie closer to the trench, such as the relationship between the Basin-and-Range and the Franciscan blueschists in western USA. The global distribution of IOCGs is also certainly not restricted to rifted continental interiors, with several examples lying in arcs or back-arcs in the Cainozoic tectonic context, particularly in the Andes (Williams et al., 2005). Hypotheses of plate boundaries sitting within 200km of the eastern boundary of the exposed Mt Isa Block are well worth reconsidering.

Another feature of arc-related hydrothermal systems worldwide is the capacity of dewatering subducted oceanic slabs to act over a protracted period, to liberate fluids and incompatible elements directly by devolatilization, and to trigger mantle metasomatism, upper mantle partial melting and lower crustal melting, all of which subsequently can lead to further volatile release via emplacement of crustal magmas. The Eastern Succession is marked by c. 250 m.y. of metasomatic activity, not just by two major phases related to metamorphic devolatilization and granite emplacement. In modern convergent systems, porphyry copper deposits and island-arc related epithermal systems are a product of this type of process in fore-arcs, and such deposits are not apparently found at Mt Isa.. However, back-arc extension systems can produce both Cyprus-style (magnetite-chalcopyrite-dominant) and Kuroko-type (Cu-Pb-Zn) VHMS deposits, IOCGs, and a range of sediment-hosted deposits, right from the initial volcanism and rift-related sedimentation, through to basin reactivation and local shortening triggered by subduction of oceanic plateaus or continent scale shift in plate vectors.

This particular environment, in which early basin metal contributions may be rapidly overprinted by the effects of convergent metamorphism, may be the specific reason for the distinction between BHT Ag-Pb-Zn and the “SEDEX” shale-hosted orebodies in northern Australia, the latter having formed in the distal flanks of the rifting system whereas BHTs may have formed and been reworked in a more arc-proximal setting.

Carbonatites and kimberlites are a product of long-lived mantle contributions to progressively cratonized continental crust, and their localisation late in the overall tectonic evolution of the Kimberleys (Argyle) and in Archean remnants in eastern South Africa (Phalaborwa), reflects very low % partial melts of metasomatized mantle containing abundant CO_2.

Various authors have speculated on the carbonatite connection with IOCGs (e.g. Groves & Vielreicher, 2001), and our current work is aimed at testing this connection. Specifically, the calcite pods of the Mary Kathleen Fold Belt and correlatives in the Cloncurry District, share mineralogical character with the volatile-dominant top part of Phalaborwa carbonatites (Fig. 4-5). Several other mid-crustal carbonate-rich alteration and vein systems worldwide show definitive mantle signatures (Wickham et al. 1994).

Figure 4-5 (a, left): Calcite-magnetite±apatite-pyrrhotite veins from Phalaborwa carbonatite, South Africa, cutting actinolite-biotite-apatite altered host gneisses. (b, right) calcite-actinolite-apatite-titanite-biotite veins from Knobby quarry, MKFB, Eastern Succession, Mt Isa Block, cutting albite-altered calc-silicate rock. The Knobby Quarry rocks have distinctive mantle-like C and O isotope rations (Fig. 4-1).

History of fluid systems and sources pertinent to metallogenesis

1750 to 1730 Ma

Prior to Soldiers Cap deposition, the end of the rifting and sag cycle that produced the Corella Fm and equivalents culminated in extensional deformation and the development of upper-crustal hydrothermal systems in which granite-gabbro bodies triggered circulation of basinal and magmatic-hydrothermal fluids. U-REE and probably gold (Tick Hill) were added in subhorizontal shear zones and skarns, despite preponderance of younger geochronological results at both Mary Kathleen and Tick Hill. Widespread dolerites and gabbros were emplaced into the Corellas and probably reflect the first major injection of Cu into the Eastern Succession. With the possible exception of Ernest Henry (see below), however, no significant Cu concentrations to ore grade were likely at this stage. Constraints on the oxidation state and sulphur and metal content of fluids responsible for the U-REE and gold enrichments are scant; however, widespread scapolitization of dolerites at this time, and some granites, points to the circulation of salty, CO_2-bearing basinal brines probably derived by evaporate dissolution (Oliver et al. 1994).

1690 to 1620 Ma

The 1690 to 1650 Ma part of this time period involved extension, widespread mafic volcanism, intrusion, and sedimentation in the Eastern Succession, and inferred contribution of significant copper via exsolution of a CO_2-H_2O-S fluid late during fractional crystallisation (Butera et al., I 2-3 report). In the Mt Isa area, Rubenach et al. (unpubl. report) have recently identified a major extensional hydrothermal system associated with the emplacement of the Sybella Batholith at c. 1660 Ma. Similar to the earlier Wonga-Mary Kathleen system, the Sybella was emplaced into an extensional shear zone, causing widespread circulation of basinal fluids. This system may have been responsible for localisation of syn-sedimentary and diagenetic Pb-Zn and possibly Cu enrichments in the c. 1650 Ma Mt Isa Group. A major mantle or mafic connection to the bulk metal budget at this time is implied from our recent work (Butera et al., I 2-3 final report), and the mantle-like isotopic character of the Cannington Ag-Pb-Zn deposit.

Later in this time period, shortening and a phase of metamorphism commenced at c. 1640 Ma (Rubenach et al., I 2-3 final report), probably shutting down the prior extension-related events, but also developing the first of a long history of sodic alteration systems in Soldiers Cap Group rocks. This pre-peak Isan metamorphism activity may have involved circulation of evaporate-derived fluids from overthrust Corella Fm, into the Soldiers Cap Group, driven by deformation and/or topography into the core of the newly developing orogenic belt. The impact of this system on Cu-Au distribution is uncertain, but was probably similar, although more localised, than the effects of the main phase of the Isan Orogeny. It may have leached a large volume of copper previously disseminated or concentrated around Osborne.

1610 – 1580 Ma

The main phase of the Isan Orogeny liberated metamorphic CO_2 from the Corella Fm and equivalents, and H_2O from the Soldiers Cap Group, as well as significant quantities of salt probably from scapolite breakdown. However, stable isotope data from carbonate veins hosted in Soldiers Cap Group require a mixed CO_2-source, from both Corella Fm carbonates (by dissolution or devolatilisation), but also from a

magmatic or mantle source (Fig. 1). As felsic magmas were absent at this time except for pegmatites at Osborne (see below), mafic rocks or the mantle are clearly implicated in the metamorphic fluid budget.

Mafic dykes emplaced into the core of the Snake Creek Anticline at this time share characteristics with earlier mafic rocks emplaced during rifting, implying that although the depth of mafic magma generation had shifted, it was still active (Butera et al., I 2-3 report). In situ or proximal partial melting of near-granulite facies metasediments produced localised pegmatites at Osborne, probably triggered by fluid fluxing. The abundance of pyrrhotite preserved in the eastern domain at Osborne suggest that metamorphic or other fluids at this time were relatively reduced, as reflected in the local presence of methane and nitrogen in the fluid inclusions there (Fu et al. 2003; Mustard et al., 2003). Osborne methane-bearing brines contain elevated Cu concentrations, and this may reflect the capacity of reduced S-poor fluids to carry Cu as species other than sulphate, i.e. various Cu chlorides (Mustard et al., 2003). CO2-rich fluids at Osborne display elevated arsenic contents and relatively low chloride – if As acted as a proxy for Au, this may indicate that Au in these systems is carried in an HCOS vapour (F3 final report). This vapour may have exsolved from mafic rocks or come directly from the mantle, although it may have been derived by unmixing (Mustard et al., 2003) of a complex metamorphic fluid.

Elsewhere, metamorphic fluids leached sulphides from mafic rocks (Butera et al., I 2-3 final report). If we accept that 1600 to 1590 Ma Re-Os and U-Pb ages at Osborne represent the major time for metal accumulation, then a cycle of leaching by and reprecipitation from metamorphic fluids may explain this deposit (and potentially other enrichments elsewhere such as pre-ore shear zones at Ernest Henry). Alternately, if it was formed earlier during or soon after sedimentation (e.g. similar in timing to metal introduction at Cannington), then the metamorphic fluids both imparted the radiogenic isotope signal and redistributed sulphides (both chemically and mechanically) into favourable D2 structures. In any case, mantle and/or mafic derived fluids most likely provided the bulk of the metal and sulphur for this deposit, and similar ore types (e.g. Eloise, ?early magnetite-chalcopyrite at Starra). The key characteristic of fluids at this time (metamorphic-magmatic-mantle) was their reduced nature, unlike at least some fluids exsolved off the later Williams Batholith.

1550 – 1500 Ma

1) The oxidised brines

Examination of alteration systems in close proximity to the Williams-Naraku Batholith gives the best idea of how these intrusions may have contributed to the IOCG deposits. Mark (1998b) first documented the complexity of alteration around the top of intrusions at Mt Angelay, speculating on the exsolution of hypersaline, CO2-bearing brines as a cause of albite alteration that affected the granite carapace and surrounds. Perring et al. (2000) and Pollard (2001) documented the co-occurrence of sodic alteration and voluminous magnetite at Lightning Creek, inferring an origin for this alteration by unmixing of complex brines upon release from the crystallizing granite-gabbro sill complex. Oliver et al. (2004) built on this work to propose that granite-derived fluids moving through metasedimentary rocks attained elevated Fe- and K-contents by wallrock interaction, prior to their involvement in Ernest Henry-type IOCG genesis. Fluid inclusions at Lightning Creek are distinctive for their highly elevated Fe, Ba and Cu contents, implying at least one of the fluids present was sulphur-deficient (Perring et al., 2000). The apparent absence of sulphur in these granite-proximal systems, but the presence of sulphur with distinctive mantle- or magmatic _34S values in the deposits, requires derivation of deposit sulphur from sources other than the c. 1530 Williams Batholith.

In the Snake Creek area, breccia pipes emanating from contact aureoles of 1530 Ma granitoids are dominated by magnetite, hematite, and albite (Cleverley & Oliver, 2005a). Sulphides are found only in these pipes either within relict gabbro bodies (that themselves were probably emplaced syn-granite) or in distal locations where wallrocks or other fluids may have provided the sulphur. The implication of all of these lines of evidence is that the Williams Batholith released large volumes of oxidised, sulphur-poor fluids that locally carried copper and iron, and released some of this fluid via violent brecciation processes. This fluid may have oxidised earlier reduced iron oxide ± sulphide assemblages at Osborne and Starra, for example in the reaction of oxidised copper chloride brine with previous pyrrhotite – pyrite ± magnetite rocks to produce hematite and chalcopyrite. Without adding significant copper, such oxidised fluids may simply have remobilized earlier IOCGs and produced hematite-ore associations that reworked or possibly concentrated earlier copper produced during or before peak-metamorphism.

2) Reduced, mantle-derived fluids

Another important fluid source at this time was probably derived by mantle degassing (the “carbonatite connection”), as inferred from the association of calcite-actinolite-clinopyroxene-apatite with minor titanite-pyrrhotite-chalcopyrite at Knobby Quarry (MKFB) and similar high temperature calcite pods in the Eastern Succession (Fig. 4). These fluids contained reduced sulphur, abundant CO2, and Ca- and Na-chlorides (Fu et al., 2003). Although the surrounding albitic alteration was previously inferred to be related to salt dissolution or a felsic magmatic component in this fluid (e.g. Oliver et al., 1993), Manning (2004) has postulated that partial melting of seafloor-altered oceanic crust can carry alkalis into the crust during subduction. Given that there are no Williams-age felsic intrusions in the MKFB, then speculation of a mantle source to these fluids is warranted, although the specific carbonatite connection and proximity of a plate boundary remains enigmatic. Ongoing trace element geochemistry of apatite and carbonates will be used to determine the extent to which such fluids were directly mantle-derived.

3) Ernest Henry fluid mixing and sources

Unlike Osborne or Cannington, the Ernest Henry orebody shows little or no physical attributes that can clearly be related to pre-Williams-Naraku hydrothermal events: it appears to be a genuine 1530 Ma orebody (Mark et al., 2005a). Furthermore, despite the growing evidence for inheritance and protracted copper addition to the crust over 250 m.y., Ernest Henry still contains about half of all of the currently mineable or mined Cu ore yet discovered in the Eastern Succession, implying that this event was potentially the most important of all, at least in a targeting sense.

Although inherited source components are present at 1650 to 1600 Ma (Re-Os wholerock and Pb-Pb chalcopyrite, cf. Butera et al., I 2-3 final report), we remain uncertain as to the extent to which local (≤ 1km scales) pre-1530 Ma concentrations of Cu-Au ore, sulphides, or ironstones provided mass for the present orebody. The distinctive K-feldspar-hematite alteration of the host volcanic rocks associated with ore deposition (Mark et al., 2005a) was probably caused by reaction of initially granite-derived fluids, modified by albitization, with the host metavolcanic rock, as suggested by geochemical models (Oliver et al., 2004; Cleverley & Oliver, 2005b; this report). Barian K-feldspar associated with this ore-related alteration (Mark et al. 2005a) again reflects likely absence of sulphur in one of the fluids, whereas the presence of barite late in the ore paragenesis is a classic hallmark of fluid mixing. Using HCh, fluid mixing models for Ernest Henry work best with mixing an oxidised S-poor brine containing Cu as chlorides with a reduced HCOS fluid carrying Au (see Appendix). We now regard the key ore-forming fluid ingredients at Ernest Henry as:

- Oxidised Fe- and K-rich fluid derived by brine release from the Williams Batholith during violent brecciation events, modified by subsequent wallrock reaction along the transport and deposition sites, and potentially carrying copper derived from magma mingling with mafic bodies at 1530 Ma
- Reduced HCOS fluid derived either directly from the mantle, by leaching of pre-existing mafic rocks by mantle-derived fluids, or by release of fluids from crystallising Williams-age gabbros. This fluid may have contained the gold.

Rationalising the Williams/Naraku - mafic rocks issues, and exploration outcomes

Interaction between mantle-derived fluids, mantle-derived melts, and the lower crust which produced the Williams Batholith can explain the diversity of ages and associations in the district, but also the commonalities (Fig. 4-5). Highly abundant CO_2-rich fluid inclusions in the district are not primarily a consequence of devolatilisation of the Corella Fm carbonates, because the CO_2 is found in inclusions of most ages, and associated carbonates have C- and O-isotope signatures indicative of mantle or magmatic sources. This implies that mantle or magmatic CO_2 was available at almost every stage of the evolution of the belt, a situation most likely to evolve during protracted extension and crystallisation of mafic magmas. The interactions between mantle-derived melts, mantle fluids and generation and emplacement of felsic magmas (Fig. 4-5) involved:

1. Prior to 1550 Ma, significant concentrations of IOCGs had already occurred, by release of fluids directly off the top of crystallising mafic intrusions, potentially even by exhalation in mixed sedimentary-mafic rock packages, and probably by leaching and reprecipitation during regional metamorphism.
2. At c. 1550 Ma, a phase of extension or possibly volatile fluxes from deep in the mantle lithosphere triggered renewed generation of basaltic melt just below the Moho, and triggered anatexis of lower

crustal felsic melts with a distinctive mantle radiogenic isotope signature.

3. Some felsic intrusions, e.g. Lightning Creek, may have been contaminated with voluminous mafic melts at a relatively early stage of crystallisation, leading to widespread mingling, mixing, and transfer of metals in the melts. The net result may have been dispersion of metals throughout the mafic/felsic complex, retention of sulphur in the mafic rocks, rapid saturation of iron oxides in the mingled zones, and precipitation of magmatic-hydrothermal magnetite bodies.

4. Other felsic intrusions evolved to a much greater extent by protracted crystallisation (e.g. Mt Angelay, Mt Margaret), such that the remaining felsic liquid was near saturated with large volumes of oxidized, hematite-stable brine. Emplacement of CO_2- and possibly Cu-bearing mafic magmas into these rocks may have triggered release of Cu and CO_2 during quenching of the mafic rocks, which in turn forced exsolution of the brine from the granitoids. Consequently, explosive release of mixed volatiles at the granitoid carapaces produced violent breccia pipes which carried Fe, Mn, K, Na, Ca and possibly Cu to sites above the intrusions, potentially to make orebodies. The same fluid, where it interacted with pre-existing ironstones and/or IOCGs, oxidized these rocks and either redistributed or added copper as sulphide via redox reactions (e.g. Starra, Osborne western domain).

5. 5. Direct release of reduced CO_2- and S-bearing fluids from crystallising mantle melts (or gabbros emplaced at higher levels) produced carbonate-dominated vein systems in rocks away from the Williams Batholith. Because these fluids did not “collide” with crystallising felsic magmas (e.g. MKFB), they did not cross-fertilize with the alkali-laden and potentially Cu-carrying source.

6. Where the primitive mantle- or gabbro-derived HCOS fluids met with the brine-laden fluids evolved off highly fractionated Williams Batholith, Ernest Henry may have formed. Alternately, the S was derived from remobilised sources proximal to Ernest Henry. It is possible that orebodies such as Starra formed where oxidised Williams-derived fluids interacted with pre-existing sulphides until a point where the fluid became sufficiently reduced that sulphide saturation was imminent, with final ore precipitation occurring due to pressure changes and phase separation. However, this “single fluid” model does not explain the fluid inclusion complexity at Starra nor the presence of barite (see also (Williams et al. 2001)).

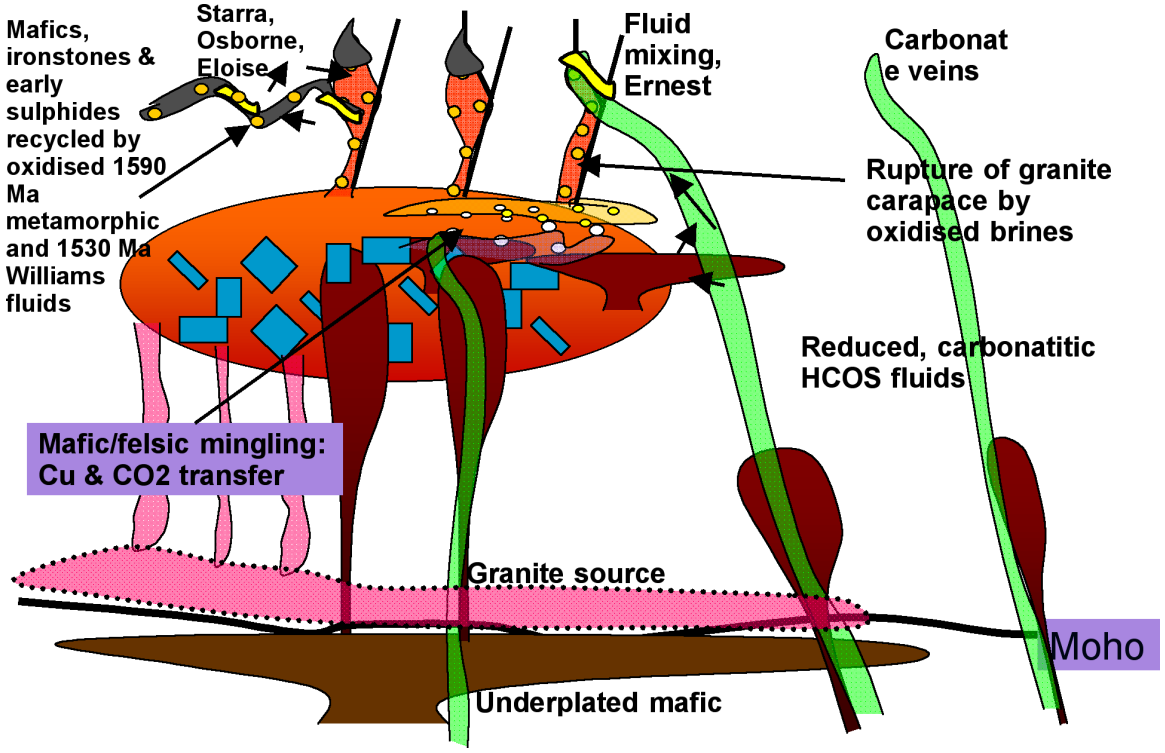

Figure 4-6: Cartoon showing the inferred relationships between mantle fluids and melts, granite crystallisation, fluid sources ,and recycling of early sulphides at the time of emplacement of the Williams Batholith. In some domains, sulphides were overprinted and reworked by Williams age oxidised fluids, leading to dissolution, remobilisation and reprecipitation (e.g. Starra); but in other domains the early reduced signal survived (Osborne eastern domain, Eloise). Release of oxidised brines at the top of the Williams/Naraku batholiths may have been triggered by mafic-felsic mingling and consequent CO2 contributions; mixing of this fluid with primitive, potentially carbonatitic HCOS fluids can explain fluid mixing attributes of Ernest Henry. In all cases, mantle derived CO2 and sulphur was added to the orebodies, by contamination of granites, release of fluid from mid crustal mafic rocks, recycling of earlier sulphides and carbonates by metamorphic and magmatic fluids, and direct mantle degassing.

Exploration implications

Recognition of Ernest Henry style deposits requires establishing whether corridors of oxidised rocks and recognisable sulphur sources are present at the current exposure levels. If the deposit was formed by reaction of Williams Batholith oxidised fluids with pre-existing mafic-proximal sulphide concentrations, then the prospectivity and geomechanical models developed by Butera et al., Ford et al., McLellan et al., and Mustard et al. (this report) provide a strong basis for identifying such oxidised corridors in the regional datasets, relative to the known areas of good prospectivity (e.g. Fig. 4-7?).

However, if the sulphur was truly primitive and juvenile (Fig. 4-6?), an understanding of how oxidised brines and reduced mantle-derived fluids could meet to make orebodies by fluid mixing will require close analysis of the 3D model and consideration of how mantle fluid pathways and oxidised Williams corridors could meet. Several clear strategies are apparent to advance this further:

1. Define zones of abundant hematite alteration that can be temporally linked with the Williams Batholith;
2. Attempt to identify which regional carbonate vein systems contain pyrrhotite±pyrite in preference to magnetite;
3. Determine where these two types of chemical indicators intersect with the favoured locations in the prospectivity analysis, and the geomechanical analysis; and
4. Determine to what extent the presence of dense mafic bodies could reflect a source of either sulphur

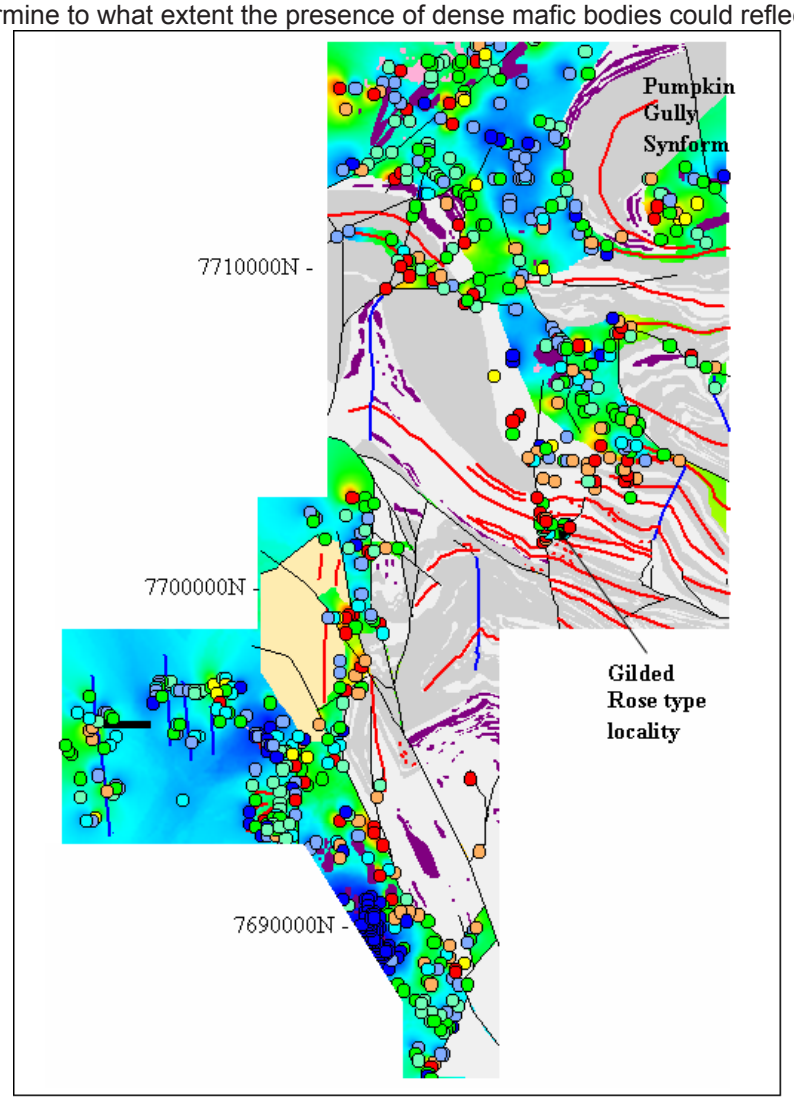

Figure 6 (from Marshall, 2003): East of Cloncurry, showing mapped distribution of intact, little altered Corella Fm rocks (blue dots and shading, albitized and in-situ brecciated equivalents (paler blues, greens), which can be separated from oxidized, hematite-K-feldspar altered breccias (red and orange dots) which cut across rock boundaries including penetrating into the Soldiers Cap Group. Greys – Soldiers Cap Gp. with red lines representing fold axes of the D1 and/or D2 stages of the Isan Orogeny; blues and green colours – Corella Fm calc-silicates; purple – felsic and mafic intrusions; black lines - faults. The intersection of the oxidised corridors with key structures, and the more difficult task of identifying reduced domains, is our recommended strategy for defining potential Ernest Henry-style targets.

(by leaching) or a juvenile HCOS fluid, by comparing the gravity data with the magnetics and results of petrographic studies that identify the fate of mafic-sourced sulphide.

Acknowledgments

We thank Tim Baker, Tom Blenkinsop, Mick Carew, Dave Cooke, Richard Crookes, Damien Foster, Michel Gauthier, Kathryn Lewthwaite, Geordie Mark, John McLellan, Roger Mustard, Peter Pollard, Rick Valenta, Pat Williams, Dugi Wilson and Bruce Yardley for discussions. Josh Bryant, Perry Collyer, Dan Johnson and Glen Little are thanked for collaboration and access at Ernest Henry, Frank Tullemans and Ian Hodkinson are thanked for their support at Osborne and Eloise respectively, Mustafa Cihan assisted with the recent breccia work, and Ian Cartwright and Garry Davidson provided stable isotope data at various stages. This report is a product of the collaboration between the F1-2 and I2-3 team members of the Predictive Mineral Discovery CRC, but includes concepts and data developed prior to that during the course of ARC- and MIMEX-sponsored research, particularly at Ernest Henry.

References

Baker, T. (1998). “Alteration, mineralization and fluid evolution at the Eloise Cu-Au deposit.” Econ. Geol. 93: 1213-1236.

Baker, T., Perkins, C., Blake, K. L. and Williams, P. J. (2001). “Radiogenic and stable isotope constraints on the genesis of the Eloise Cu-Au deposit, Cloncurry District, northwest Queensland.” Econ. Geol. 96: 723-742.

Cleverley, J.S. & Oliver, N.H.S. (2005a). Microscopic investigation of granite-related breccia pipes, Eastern Succession, Mt Isa Block.. EGRU News, March 2005 edition.

Cleverley, J.S. & Oliver, N.H.S. (2005b). Conceptualisation of fluid-rock reactions using the HCh modelling package: case studies from the Mt Isa Fe-oxide Cu-Au district. Geofluids, in press.

Davidson, G. J. and Large, R. R. (1994). “Gold metallogeny and the copper-gold association of the Australian Proterozoic.” Mineralium Deposita 29: 208-223.

deJong, G. and Williams, P. J. (1995). “Giant metasomatic system formed during exhumation of mid-crustal Proterozoic rocks in the vicinity of the Cloncurry Fault, northwest Queensland.” Austr. J. Eth. Sci. 42: 281-290.

Etheridge, M. A., Rutland, R. W. R. and Wyborn, L. A. I. (1987). “Orogenesis and tectonic processes in the Early to Middle Proterozoic of northern Australia.” Am. Geophys. Union, Geodyn. Ser. 17: 131-147.

Fu, B., Williams, P. J., Oliver, N. H. S., Dong, G., Pollard, P. J. and Mark, G. (2003). “Fluid mixing versus unmixing as an ore-forming process in the Cloncurry Fe-oxide-Cu-Au District, NW Queensland, Australia: evidence from fluid inclusions.” J. Geochem. Expl. 78-79: 617-622.

Fu, B., Oliver, N.H.S., Baker, T., Williams, P.J., Marshall, L.J., Rubenach, M.J., Ulrich, T., Mernagh, T.P., van Achterbergh, E., Ryan, C.G. & Yardley, B.W.D., 2004. Microanalysis of regional fluids from the Eastern Succession of the Mount Isa Block, NW Queensland. In: Muhling, J. et al. (eds), SEG 2004: Predictive Mineral Discovery Under Cover; Extended Abstracts. Centre for Global Metallogeny, the University of Western Australia, Publication No. 33, p. 378-382.

Groves, D. I., and Vielreicher, N. M., 2001, The Phalabowra (Palabora) carbonatite-hosted magnetite-copper sulfide deposit, South Africa; an end-member of the iron-oxide copper-gold-rare earth element deposit group: Mineralium Deposita, v. 36, p. 189-194.

Maas, R., McCulloch, M. T. and Campbell, I. H. (1988). “Sm-Nd isotope systematics in uranium rare-earth element mineralization at Mary Kathleen uranium mine, Queensland.” Econ. Geol. 82: 1805-1826.

Manning, C. E., 2004, The chemistry of subduction-zone fluids: Earth and Planetary Science Letters, v. 223, p. 1-16.

Mark, G. (1998b). “Albitite formation by selective pervasive sodic alteration of tonalite plutons in the Cloncurry district, NW Queensland.” Austr. J. Eth. Sci. 45: 765-774.

Mark, G., Oliver, N.H.S. and Williams, P.J. (2005a). Mineralogical and chemical evolution of the Ernest Henry Fe oxide-Cu-Au ore system, Cloncurry district, northwest Queensland, Australia. (Mineralium Deposita, in revision).

Mark, G., Oliver, N. H. S., Williams, P. J., Valenta, R. K. and Crookes, R. A. (2000). The evolution of the Ernest Henry hydrothermal system. Hydrothermal iron oxide copper-gold and related deposits: a global perspective. T. M. Porter. Adelaide, Australian Mineral Foundation: 132-136.

Mark, G., Williams, P.J. & Oliver, N.H.S. (2005b). Fluid Inclusion and Stable Isotope Geochemistry of the Ernest Henry Iron Oxide-Copper-Gold Deposit, Queensland, Australia. SGA Abstracts, Beijing, China, Aug. 2005.

Marshall, L. J. (2003). Brecciation within the Mary Kathleen Group of the Easterrn Succession, Mt Isa Block, Australia: implications of district-scale structural and metasoomatic processes for Fe-oxide-Cu-Au mineralisation. PhD thesis (unpubl.), School of Earth Sciences, James Cook University, Townsville, Australia: 323pp.

Mustard, R., Baker, T., Williams, P.J., Ulrich, T., Mernagh, T.P., Ryan, C.G., vanAchterbergh, E., Adshead, N. & Morrison, G. (2003). Cu-rich brines at the Osborne and Starra deposits: implications for immiscibility in Fe-oxide-Cu-Au systems. In: Baker, T. (ed.) Micrometallogeny of hydrothermal fluids. Annual ***pmd**CRC* report, July, 2003, unpubl. report.

Oliver, N. H. S. (1995). “The hydrothermal history of the Mary Kathleen Fold Belt, Mount Isa Block, Queensland, Australia.” Aust. J. Earth Sci. 42: 267-280.

Oliver, N.H.S. (2003). Project F1: fluid chemical paths in ore forming processes. Annual report, ***pmd**CRC*, unpublished.

Oliver, N. H. S., Cartwright, I., Wall, V. J. and Golding, S. D. (1993). “The stable isotopic signature of large-scale fracture-hosted metamorphic fluid pathways, Mary Kathleen, Australia.” J. Metamorphic Geol. 11: 705-720.

Oliver, N. H. S., Cleverley, J. S., Mark, G., Pollard, P. J., Fu, B., Marshall, L. J., Rubenach, M. J., Williams, P. J. and Baker, T. (2004). “Modeling the role of sodic alteration in the genesis of iron oxide–copper–gold deposits; eastern Mt. Isa Block, Australia.” Econ. Geol. 99: 1145-1176.

Oliver, N. H. S., Pearson, P. J., Holcombe, R. J. and Ord, A. (1999). “Mary Kathleen metamorphic-hydrothermal uranium-rare-earth deposit: ore genesis and a numerical model of coupled deformation and fluid flow.” Austr. J. Eth. Sci. 46: 467-484.

Oliver, N. H. S., Rawling, T. R., Cartwright, I. and Pearson, P. J. (1994). “High temperature fluid-rock interaction and scapolitization in a large extension-related hydrothermal system, Mary Kathleen, Australia.” J. Petrol. 35: 1455-1491.

Page, R. W. (1983). “Chronology of magmatism, skarn formation and uranium mineralisation, Mary Kathleen, Queensland, Australia.” Econ. Geol. 78: 838-853.

Perring, C. S., Pollard, P. J., Dong, G., Nunn, A. J. and Blake, K. L. (2000). “The Lightning Creek sill complex, Cloncurry District, northwest Queensland: a source of fluids for Fe oxide Cu-Au mineralization and sodic-calcic alteration.” Econ. Geol. 95: 1067-1089.

Pollard, P. J. (2001). “Sodic(-calcic) alteration associated with Fe-oxide-Cu-Au deposits: an origin via unmixing of magmatic-derived H2O-CO2-salt fluids.” Mineralium Deposita 36: 93-100.

Rotherham, J. F., Blake, K. L., Cartwright, I. and Williams, P. J. (1998). “Stable isotope evidence for the

origin of the Starra Au-Cu deposit, Cloncurry district." Econ. Geol. 93: 1435-1449.

Wang, S. and Williams, P. J. (2001). "Geochemistry and origin of Proterozoic skarns at the Mount Elliott Cu-Au(-Co-Ni) deposit, Cloncurry District, NW Queensland, Australia." Mineral. Deposita 36: 109-124.

Wickham, S. M., Janhardan, A. S. and Stern, R. J. (1994). "Regional carbonate alteration by mantle-derived magmatic fluids, Tamil Nadu, Southern India." J. Geol. 102: 379-398.

Williams, P. J. (1998). "Metalliferous economic geology of the Mt Isa Eastern Succession, Queensland." Austr. J. Eth. Sci. 45: 329-341.

Williams, P. J., Dong, G., Pollard, P. J., Perring, C. S., Ryan, C. G. and Mernagh, T. P. (1999). Fluid inclusion geochemistry of Cloncurry (Fe)-Cu-Au deposits. In Stanley, C. et al. (eds).Mineral deposits: Processes to processing. Rotterdam, Balkema: 111-114.

Williams, P. J., Dong, G., Ryan, C. G., Pollard, P. J., Rotherham, J. F., Mernagh, T. P. and Chapman, L. C. (2001). "Geochemistry of hypersaline fluid inclusions from the Starra (Fe-oxide)-Au-Cu deposit, Cloncurry District, Queensland." Econ. Geol. 96: 875-884.

Williams, P.J., Barton, M.D., Fontboté, L., deHaller, A., Johnson, D.A., Mark, G., Marschik, R., & Oliver, N.H.S., 2005. Iron oxide-copper-gold deposits: Geology, space-time distribution and possible modes of origin. Econ. Geol., in revision.

Chapter 5: Geochemical process modeling of the Century Zn deposit

A.R. Wilde

Predictive Mineral Discovery Cooperative Research Centre @ Monash University

This paper is duplicated from the following source:
*Wilde, A. R. (2004) Project F1: Geochemical process model for the Century Zn Deposit; data compilation and review. **pmd***CRC **Report,** December 2004, 22p.*

Executive Summary

This report presents a compilation of research data for the Century Zn deposit in order to guide further research under project F1 of the ***pmd****CRC*. Data have been compiled into an ACCESS database.

Key observations include:

- The bulk chemical composition and mineralogy of unaltered host-rocks around Century (particularly in stratigraphic units other than the Lawn Hill Formation) is poorly understood and few holes have been systematically logged and sampled with a view to defining alteration assemblages.
- Spatial plots of carbonate abundance and composition suggest that while the Proterozoic clastic sediments around Century are rich in siderite there is no evidence that siderite defines an hydrothermal alteration halo, nor does bulk carbonate composition change systematically with proximity to ore.
- An image of average vitirinite/alginite Ro by drillhole suggests a correlation between Pb-Zn and areas of moderate Ro (low maximum temperature) while Cu occurrences correlate to high Ro (high maximum temperature). This may be the basis of a useful exploration tool, but requires additional sampling to add confidence. Vitrinite may be more valuable than illite crystallinity as a means of documenting thermal gradients as the latter show extreme variation within individual drillholes.
- Existing K-Ar, Rb-Sr and Ar-Ar data are consistent with at least two thermal events in the Century area: peak metamorphism at >1565 ma and a second event at about 1200 ma, similar to that documented west of Mount Isa by Spikings et al. (2002). The absolute age framework of the Century region, however, needs to be confirmed using more reliable techniques such as Ar-Ar (taking into account recoil problems). This should be made a priority for the ***pmd****CRC* history projects.
- Sulphur isotope data are permissive of an origin for sulphur at Century by TSR of anhydrite deeper in the stratigraphic sequence. Thus, recognition of units containing anhydrite in the sub-surface could be a useful exploration tool.
- Carbonate isotope data (C and O) are widely scattered, an indication that bulk analysis is inappropriate for samples that contain multiple carbonate generations with differing chemical composition. A crude correlation between isotopic composition and depth within the Century pit is apparent but as yet unexplained.

Recommendations

- There is a clear need to sample several cored holes remote from the Century mine in order to better characterize the chemical and mineralogical character of the sediments (including stratigraphic units beyond those in the pit area) as a basis for exploration geochemistry and for geochemical modelling. I suggest that chemical analysis by means of portable XRF equipment and mineralogical analysis by PIMA or HYLOGGER be trialled. The advantages of these techniques are that they would allow near complete sampling of entire holes with obvious benefits.
- Key questions that need to be addressed are:
    - Should exploration target a particular stratigraphic level or levels?
    - Is a particular rock-type (chemically and mechanically) important for ore deposition or could oire be deposited in a variety of rock-types?

- What alteration assemblages should exploration geologists be looking for?

- The age of the Roper Group with respect to the MacNamara Group be carefully examined and the possibility that the Velkerri Formation is a possible base-metal host be evaluated. Furthermore the iron deposits of the Roper Group should be researched for possible links with Century and the insights that might bring with respect to regional hydrothermal processes.

Introduction

This report presents a compilation of research data for the Century Zn deposit in order to guide further research under project F1 of the ***pmd****CRC*. The data are critically evaluated and recommendations made for acquisition of new data, given that substantial gaps exist.

There is also a critical review of numerical modelling relevant to the Century Zn deposit.

The ACCESS database is included as a CD-ROM and a short summary presented as Appendix 1. I would like to thank Graeme Broadbent, Steve Andrews and Michael Whitbread for providing digital data from their respective PhD theses.

Temperature of Formation

Fluid Inclusion Homogenisation Behaviour

Knowledge of the temperature (and to a lesser extent pressure) is a key constraint on geochemical modelling of the Century ore system. Fluid inclusion data for sphalerite were presented by Polito et al. (2004;Table 1 - Table 5-1 in this report).

Paragenetic Stage	# Samples	# Measurements	Te ice (ºC)	Tm ice (ºC)	Calculated Salinity (wt% NaCl equiv.)	Homogenisation Temperature (ºC)
Main hydrothermal phase (Primary inclusions)	1	5	-59.9	-18.8	21	90
"Transgressive, crackle vein and breccia phase" (Primary inclusions)	4	32	-49.1	-16.3	20	99
(Post mineralization Secondary inclusions)	1	2	-48.3	-3.4	6	111

Table 5-1: Summary of fluid inclusion data for Century samples collected from the open pit (Polito et al. 2004; AMIRA P552). Te – eutectic temperature (ice/hydrohalite final disappearance). Tm – initial melt temperature of ice or hydrohalite. Salinity calculated assuming all cations present are Na+. Homogenisation is presumed to be by vapour disappearance.

The data suggest that sphalerite deposition occurred from a brine close to halite saturation. It should be noted, however, that it is assumed rather than demonstrated that the inclusions are primary or pseudosecondary and therefore sample fluid related to sphalerite formation (and are also unaffected by post-ore deformation). Homogenisation of fluid inclusions was observed at about 90 - 100ºC. If, the inclusions are indeed primary or pseudosecondary then this temperature range implies either extreme temperatures near the sediment-water interface (exhalative model) or formation at substantial depth (perhaps even > 3 km assuming a geothermal gradient of 35ºC/km).

Given that a substantial portion of the Century sphalerite is extremely fine-grained the inclusion data of Polito may relate to relatively late coarse sphalerite and hence may sample late hydrothermal fluids.

Vitrinite Reflectance

The reflectance of organic material, namely vitrinite, gives an indication of the maximum temperature experienced by the rock and is widely used in exploration for petroleum as a means of quantifying the thermal character of sedimentary basins.

Average vitrinite reflectance (R_o) measurements for drillholes in the Century area are plotted in Fig. 5-1. Plotting the average in this way smoothes some of the variation that is apparent with depth, but nevertheless gives an indication of regional thermal gradients. It can be seen that the data are concentrated around Century mine.

Given the possibility of three thermal events we need to be circumspect in relating the maximum temperatures as manifested in vitrinite data to the ore-forming process. Polito et al. (2004) suggested that the R_o temperature values from the vicinity of Century require a pressure correction of the order of 60-70ºC to the fluid inclusion data, implying sphalerite deposition at several kilometers depth. If the fluid inclusions represent exhalative brines, however, then the homogenisation temperatures reflect the entrapment temperatures (pressure correction is minimal).

Potentially of greater interest for exploration, is that the image of average vitirinite R_o by drillhole suggests a correlation between Pb-Zn and areas of moderate R_o while Cu occurrences correlate to high R_o. Additional sampling to add confidence is required. The “crystallinity” of fine-grained white-mica (‘‘illite’’) can be

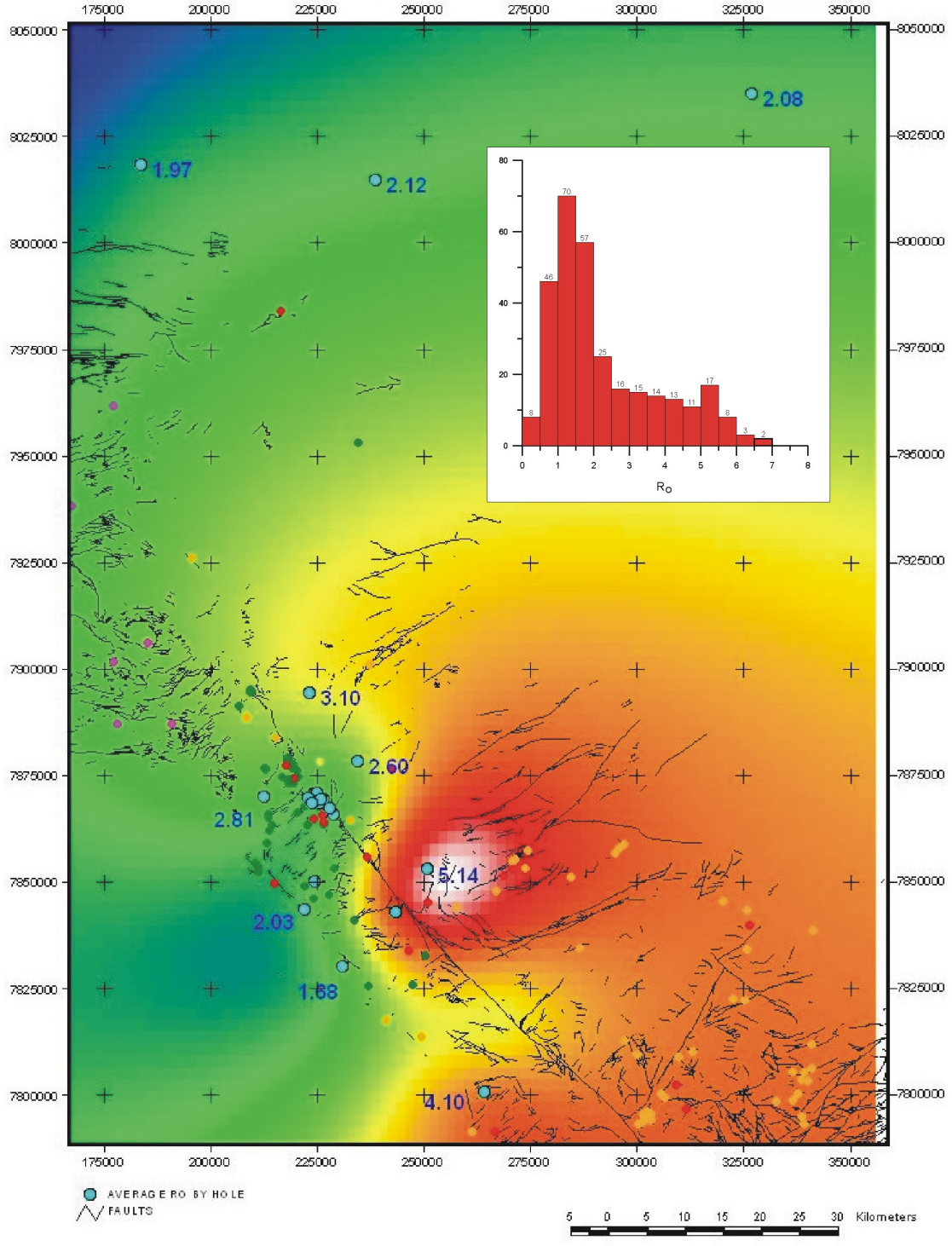

Figure 1: Image showing average Ro values for sampled drillholes (blue circles) in the Century area. These data suggest that Cu occurrences correlate with areas of higher Ro.

estimated from X-ray diffraction (or PIMA) and is related to temperature of equilibration.

Some 60 or more illite crystallinity determinations of material from the Century mine were completed by Stafford McKnight at the University of Ballarat (G. Broadbent, pers. comm., 2004). Unfortunately these data have been lost.

Additional data were collected by Sue Golding and co-workers as part of AMIRA project P552, mainly in petroleum exploration holes. These data are summarised in Fig. 5-2.

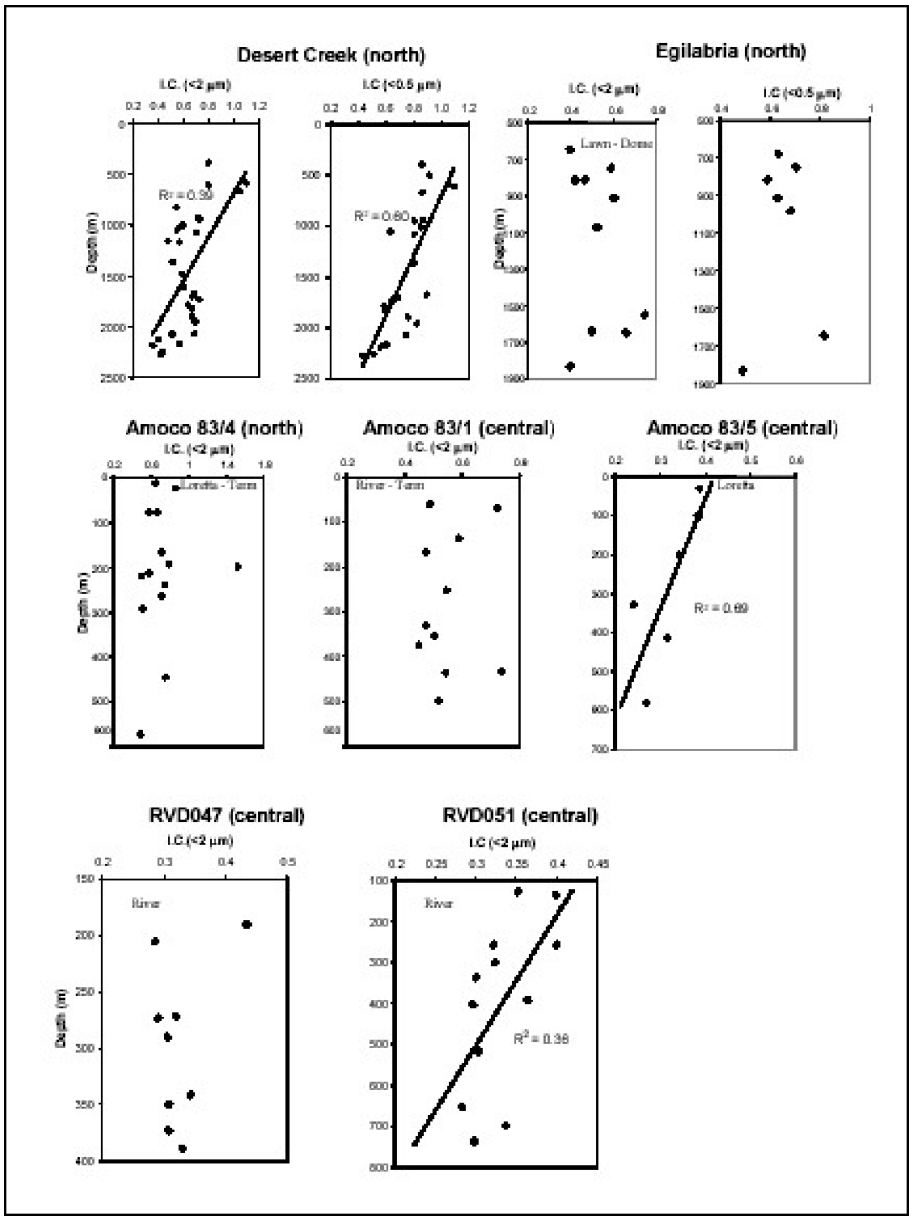

Figure 2: IC data for petroleum wells in the vicinity of Century (Golding unpub. data).

The extreme variation of crystallinity values within individual holes suggests that IC may not be reliable as an exploration tool. The possibility of multiple thermal events (see below) also mean that these data should be treated with caution.

Timing of Ore Formation

Inferences from Textures

The occurrence of base-metals in persistent sedimentary layers is one of the key observations in support of a syn-sedimentary origin, particularly when the host-rock (clay-rich rock) is likely to have been rendered more or less impermeable after burial to 2 km or more. Broadbent (1999) and Broadbent et al. (1998) have challenged the syn-sedimentary or syn-diagenetic hypotheses mainly on the basis of textural observations at thin section scale. The critical observation here is that sphalerite emplacement post-dated the development of stylolites in the host-rock. This would require a substantial degree of lithification prior to ore formation.

Figure 5-3 shows a sample used by Broadbent (1999) and Broadbent et al. (1998) to illustrate presence of stylolites. The so-called stylolites are the dark carbonaceous seams visible in various parts of the image. In my view the interpretation of these seams as stylolites is questionable, they could equally be sedimentary in origin.

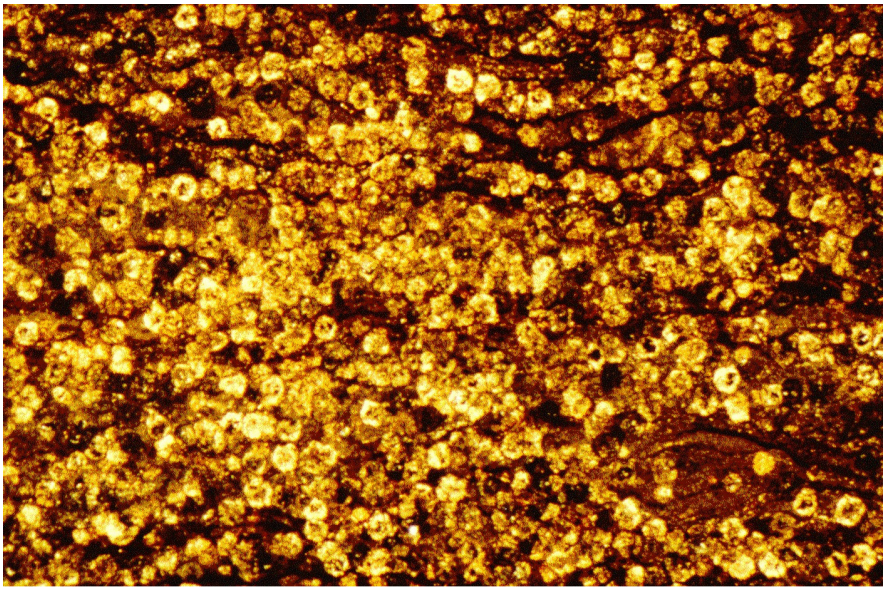

Figure 3: Photomicrograph illustrating "stylolite" formation. The so-called stylolites are the dark-coloured carbonaceous seams. The rounded grains are siderite.

Inferences from Radiogenic Isotopes

K-Ar and Rb-Sr data for the Century area have been obtained by McDougall et al., 1965, Kralik, 1982, Uysal et al., 2004 and Golding (unpub.; Fig. 4). Polito et al. (2004) obtained Ar-Ar analyses of two samples from the Flat Tyre deposit (Fig. 5).

Figure 5-4 illustrates why K-Ar is no longer regarded as a useful geochronometer in low grade meta-sediments, namely the extreme range of model ages equivalent to a large part of the Mid Proterozoic. Nevertheless, Uysal et al. (2004) have bravely interpreted these data to represent peak metamorphism at 1500 Ma with additional events at 1400 and 1220 Ma.

Rb-Sr data on glauconite and illite from the Roper Group have been published by MacDougall et al. (1965) and Kralik (1982). I have recalculated these data using ISOPLOT and obtained the following ages:

- 1436 ± 58 (MSWD 37). Data of Kralik (1982)
- 1428 ± 98 (MSWD 0.41). Data of Kralik (1982)
- 1293± 240 (MSWD 8.4). Data of MacDougall et al. 1965.

These data suggest post-Isan isotopic thermal event or events in the Roper Group, but precision is poor.

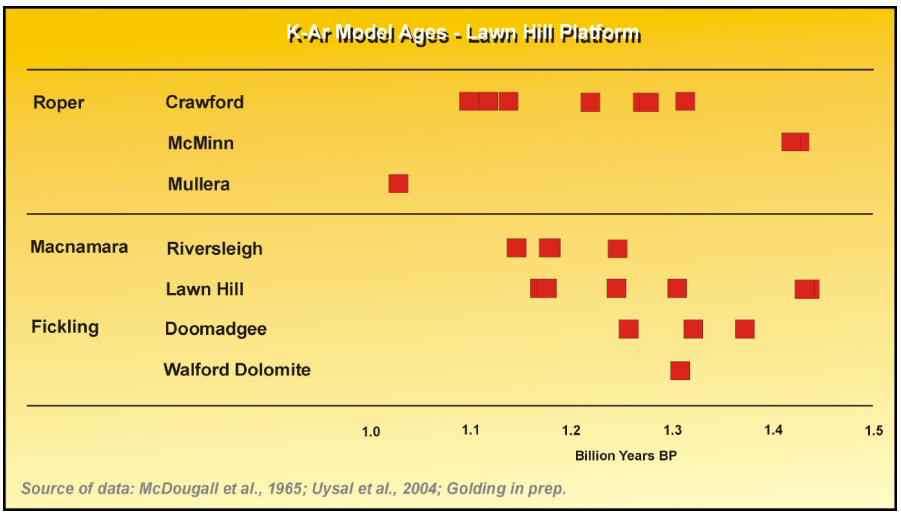

Figure 5-4: Compilation of K-Ar data for the Macnamara, Fickling & Roper Group sediments. Note the extreme spread in ages!

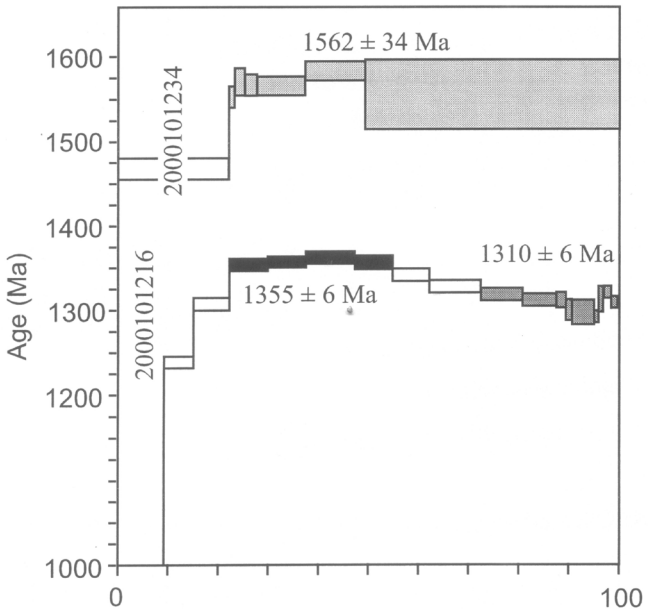

Figure 5-5: Ar-Ar spectra for two samples from the Flat Tyre deposit near Century (Polito et al, 2004). The two ages from the single spectrum of sample 2000191216 may not be meaningful.

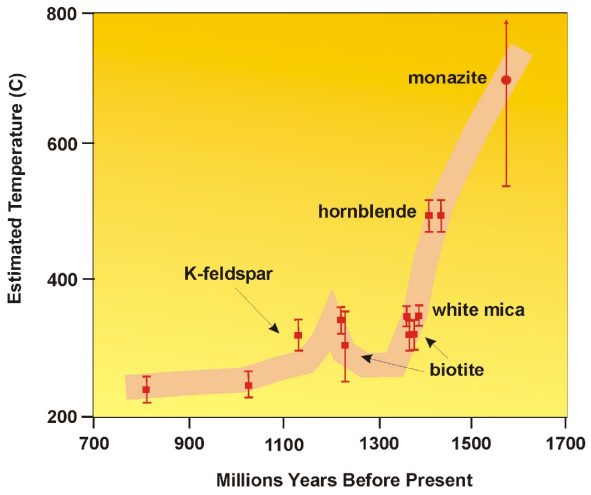

Figure 5-6: Interpreted cooling curve for samples west of the Mount Isa fault, near Mount Isa (Spikings et al., 2002).

It would be unwise to make too much of the Rb-Sr and K-Ar data. They are consistent within error, however, with the thermal history of the area west of Mount Isa as deduced by Spikings et al. (Fig. 6; 2002). Two thermal events could be preserved around Century. These are:

- Cooling from the peak of regional metamorphism at about 1580 Ma, as seen in the Ar-Ar age of 1562 ± 34 Ma
- A second thermal flow event (or inflection in the cooling trajectory) at 1200 ma as proposed by Uysal et al. (2004) and reflecting in partial resetting of K-Ar systems in illite.

There is, however, a clear need for high quality geochronological work to confirm this. Ar-Ar determinations are preferable to K-Ar and Rb-Sr and need to account for possible recoil in fine-grained minerals.

Hydrothermal Alteration and its Distribution

A major problem for geochemical modelling and indeed exploration is the fact that there is very little information on the nature of hydrothermal alteration beyond the Century pit area. Figure 5-7 shows the location of sampled drillholes and petroleum exploration holes (but excludes three drillholes outside the pit area sampled by Michael Whitbread).

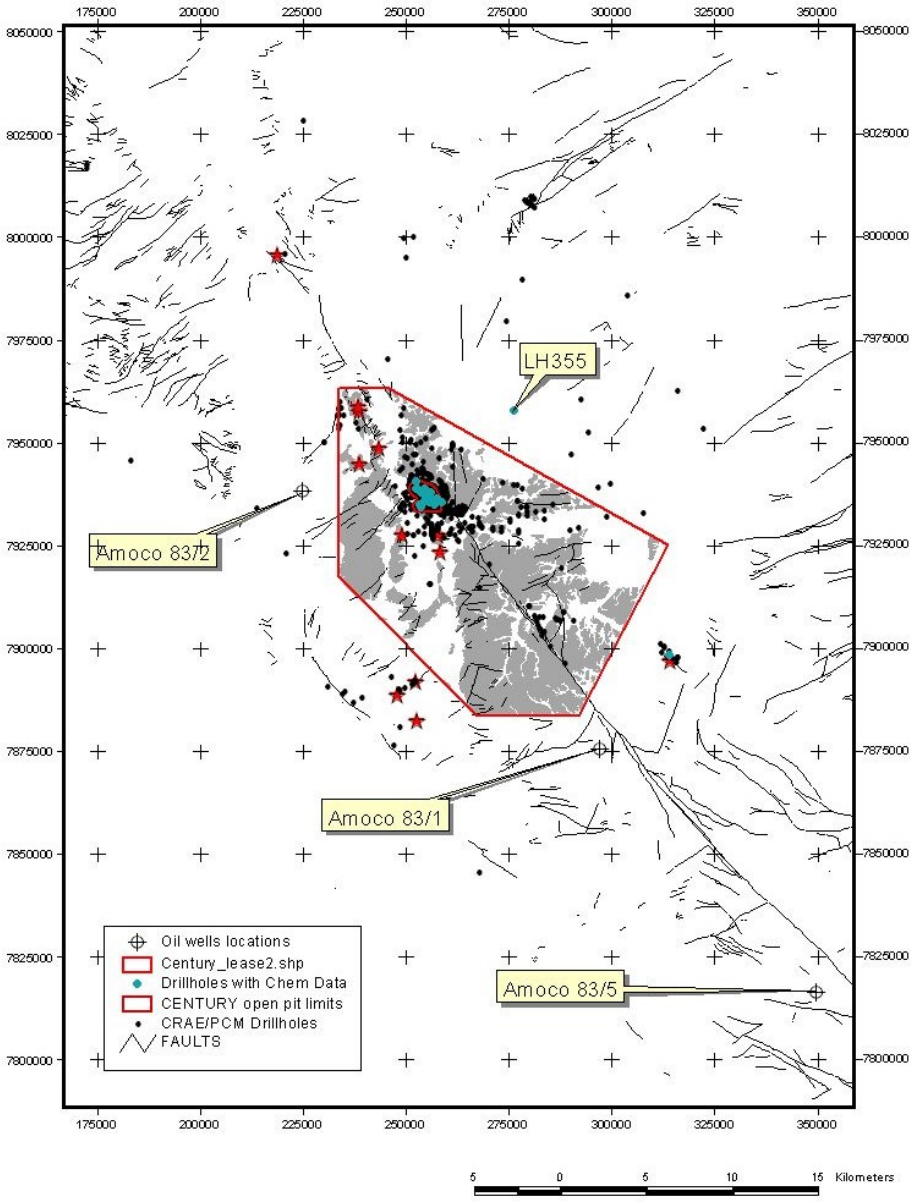

Figure 5-7: CRAE/PCM drillholes in black. Drillholes sampled for bulk chemistry during research work are shown in blue. Red stars are mineral occurrences. Oil wells "AMOCO 83"are also shown.

Mineral Composition as an Indicator of Proximity to Ore?

There are over 2,500 carbonate mineral analyses from the PhD research work of Andrews (1998) and Broadbent (1999). It has been suggested that the distribution of siderite defines an alteration halo about the deposit. To test this, the data of Broadbent and Andrews were combined and plotted by drillhole.

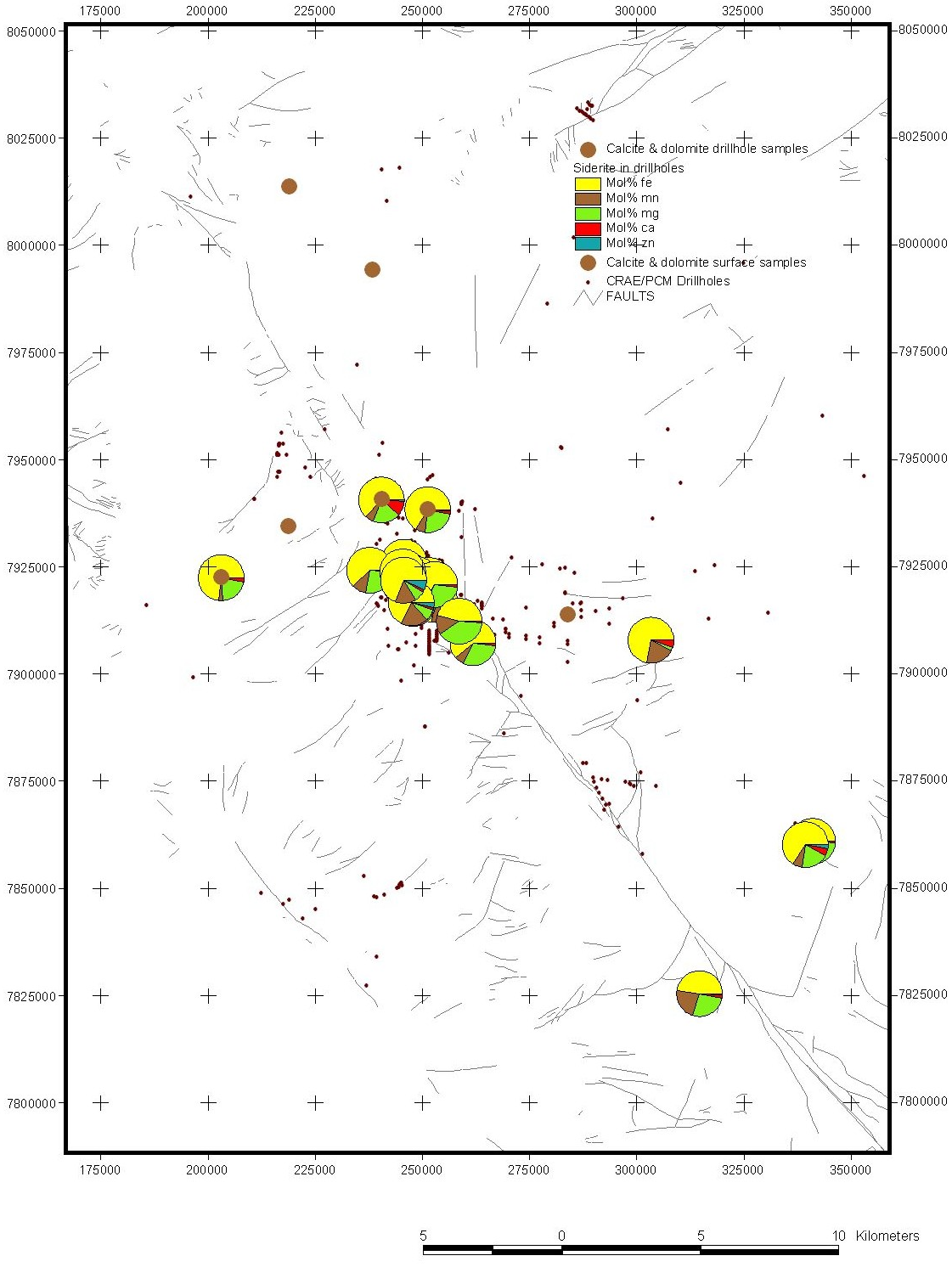

Figure 5-8: Pie charts show the composition of siderite in sampled drillholes. The brown circles are sampled holes containing dolomite and/or calcite instead of siderite. The small black dots are unsampled drillholes. This plot provides no compelling evidence for a sideritic halo around Century, nor for systematic chemical variation of siderite with proximity to ore.

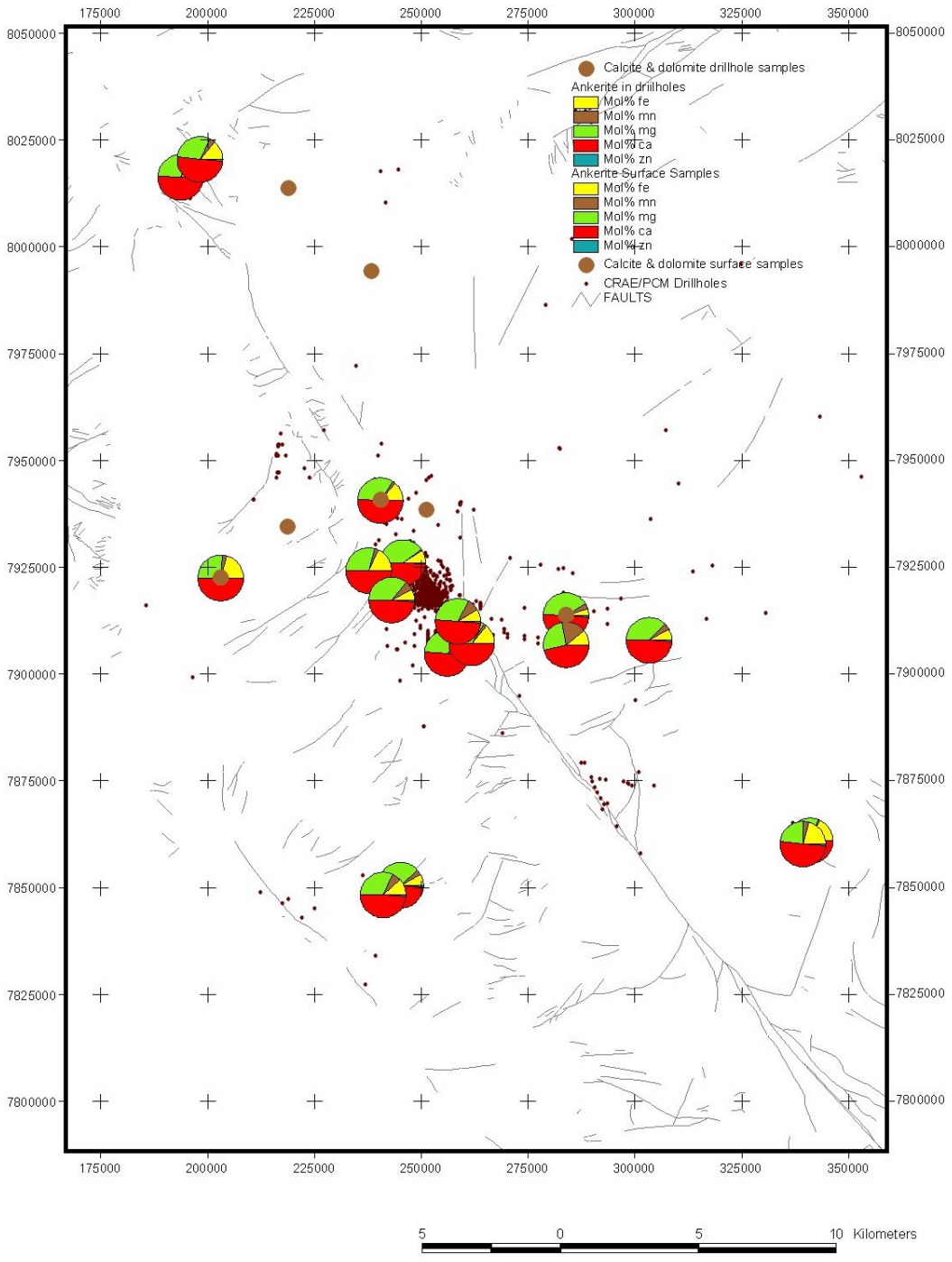

Figure 5-9: Pie charts show the composition of ankerite in sampled drillholes. The brown circles are sampled holes containing dolomite and/or calcite instead of ankerite. The small black dots are unsampled drillholes. This plot provides neither compelling evidence for a ankeritic halo around Century, nor of systematic chemical variation of ankerite with proximity to ore.

There is an apparent absence of siderite in several sample locations north of Century, but some of these samples are from the surface and may be affected by weathering. All sampled holes south of Century contain siderite. I conclude that the evidence of a sideritic halo is not compelling based on the data to hand. Neither is there evidence of systematic change in siderite composition with proximity to ore (Figs. 5-8 & 5-9). A plausible alternative explanation of the data is that siderite is a widespread diagenetic phase (as is common in the north sea oil fields for example).

Siderite is also abundant in Fe-rich rocks of the Roper Group where it is spatially associated with sub-economic volumes of hematite and minor pyrite (Harms, 1972). The Velkerri Formation of the Roper Group bears more than a passing resemblance to the Century host sequence, including extreme carbon enrichment and should be considered as a possible lateral equivalent and/or potential host rock.

Fluids involved in Ore Formation

Bulk Chemical Composition

The composition and source of fluids involved in metal transport and deposition is one of the main uncertainties in geochemical process modelling and in ore deposit studies generally. There are no analytical data on fluid composition at Century other than the salinity estimates based on fluid inclusion microthermometry (Polito et al., 2004) and these cannot be unambiguously related to the ore-forming event.

Cooke et al (2003) advocate the role of an oxidized brine as the metal carrier and assume a salinity of 25 wt% (Table 5-2). Oxidation state is a critical variable controlling metal solubility if the fluid is chloride rich and metals are complexed with chloride ions. The other fluid that has been implicated in ore formation is seawater, assuming that the process of ore deposition involves mixing of a hot brine with cool seawater. The main uncertainty here is the degree to which modern seawater resembles Proterozoic seawater.

	"McArthur Type" Brine (Cooke et al. 2003)	Contemporary Seawater (Turekian)
T	150	5
pH	4.5 (4.2*)	
log _O2	-43 (-43*)	
TDS (wt%)	25	3.5
ppm		
Na+	71919.2	10,800
Ca++	9051.1	411
Mg++	3709.7	1,290
K+	13138.9	392
Fe++	1467.5	0.00340
Mn++	302.1	0.00040
Al	0.00167	0.00100
SO42-	70.66	2740 (904 S)
Zn++	212.2	0.00500
Cu+	1.48	0.00090
Pb+	198.7	0.00003
Ag+	0.072	0.00028
Sr++	75.78	8.10000
Ba++	9.678	0.02100
H+	183.7	
SiO2aq	85.27	2.90000
Sb(OH)3	0.369	
Cl	152009.1	19,400
HCO3-	11493.2	152
HS-	85.27	nd
AuCl2-	0.0000008	0.00001
F-	0.106	13
	Saturated Minerals (GWB)	
	Dolomite (UT & LLNL)	
	Quartz (LLNL)	
	Chlorite (UT)	

Table 5-2: Composition of brine used in chemical modelling by Cooke et al. (2003) and contemporary seawater as well as parameters calculated in this study. NB the composition of Proterozoic seawater is likely to have been different to that of today.

**calculated using GWB.*
UT = UNITHERM database;
LLNL = Laurence Livermore

Stable Isotopes of C & O

Stable isotopic data for carbonate mineral have been used to constrain ore depositional models (Andrews, 1998; Broadbent et al. 1998; Polito et al., 2004; Figs. 10 to 12. The assumption that the analysed carbonate minerals are related to ore formation is, however, believed to be questionable. Furthermore, the analysed carbonates show an extraordinary range in major element composition within samples. This suggests that the isotopic composition may also vary and that bulk analyses of carbonates will average this variation (Fig. 5-10).

Fig. 5-11 however illustrates what is clearly a relationship between isotopic composition and depth of sampling. The reason for this has yet to be defined.

Fig. 5-12 illustrates that the shallow Century samples fall within the range of most carbonates from the Macnamara Group while the deeper samples show strong 13C enrichment.

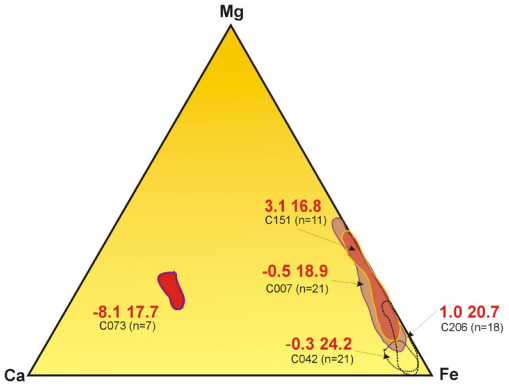

Figure 5-10: Range of carbonate composition (mol%) determined by EMP (Broadbent, 19xx). _34C and _18O are shown in bold red, with sample number and number of EMP analyses in black.

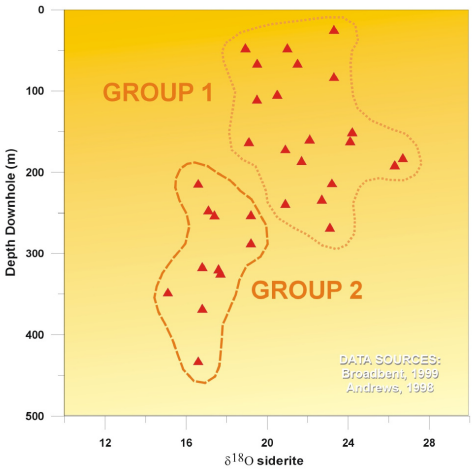

Figure 5-11: Stable isotopic data for carbonates from Century (Broadbent, 1999; Andrews, 1998) . Note the clear division into two populations at about 250m depth.

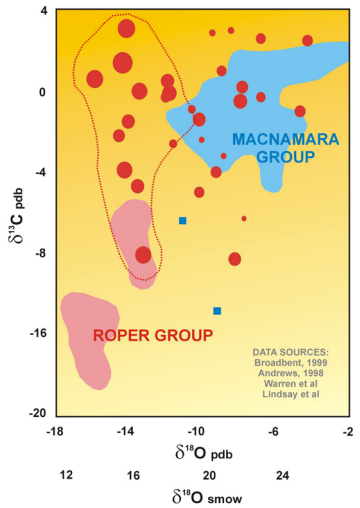

Figure 5-12: Century carbonates (red circles) plotted against siderites from the Roper Group (from Warren) and the Macnamara Group (Lindsay). The size of the circle corresponds to depth. Group 2 samples are enclosed within the red line.

Stable Isotopes of S

Sulphur isotope data show a huge range in 34S as shown below. Genetic models should take this into

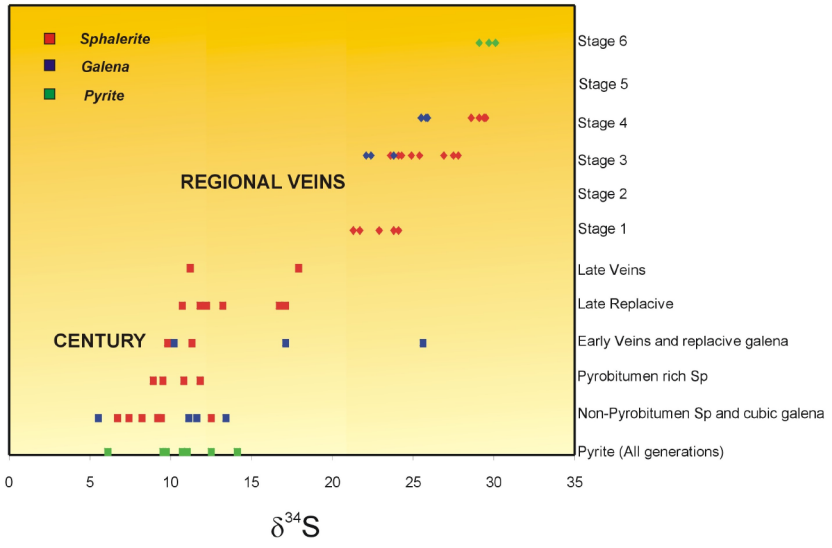

Figure 5-13: Compilation of sulphur isotope data for Century sulphides (from Bresser, 1993 & Broadbent, 1999).

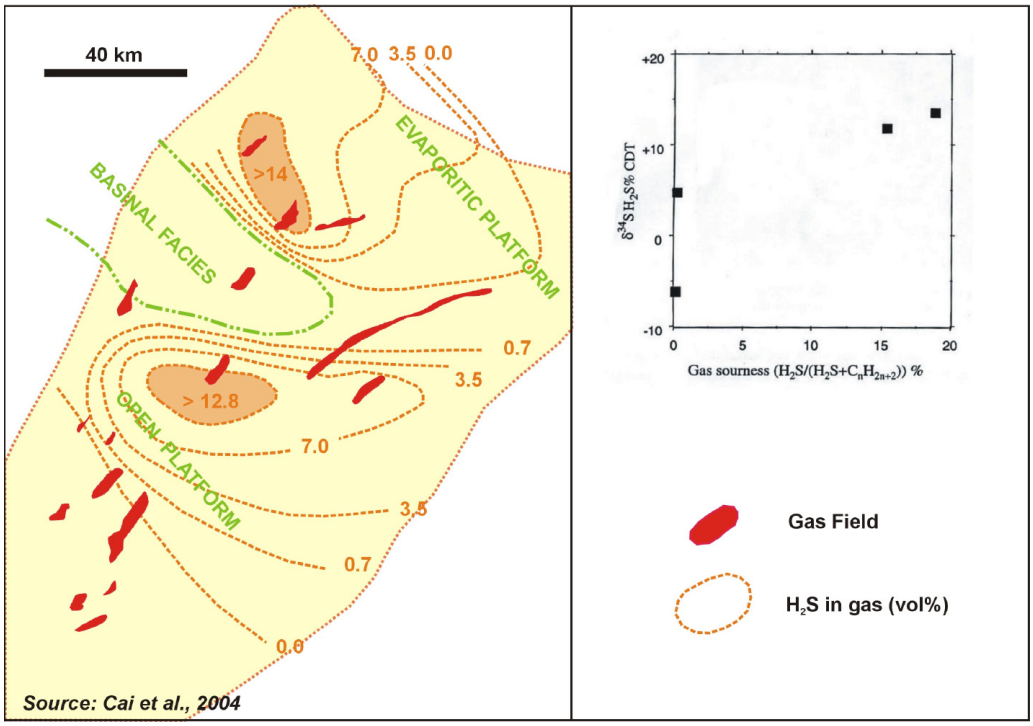

Figure 5-14: Distribution of gas fields and "sour"(H_2S-rich) gas in Sichuan, China. Note the extreme variation in ^{34}S of the sour gas. The gas is so potent that a gas blow-out lead to the deaths of over 200 people.

account. Possible sources of sulphur for the Century ore include:

- Pre-ore pyrite in the host-rocks
- Mantle-derived H2S introduced along major vertical structures such as the termite range fault
- H2S from another source (such as breakdown of anhydrite aka TSR)
- Seawater sulphate

The first option seems to be ruled out by the absence of any ore textures that would indicate consumption of pyrite during sphalerite formation. The second might be expected to generate a more limited range of _34S close to 0. Broadbent et al. (1998) appealed to in-situ thermochemical sulphate reduction, presumably of aqueous sulphate although the details of this process were not specified.

Sour gas is an interesting possibility, and if this process is relevant it would become valuable to map the occurrence of evaporites in the subsurface.

Published Depositional Models

Exhalative Mixing of "Crustal" Brine and Seawater

Exhalation has been proposed for other sediment-hosted Pb-Zn deposits of the North Australia Proterozoic and requires mixing of a hot oxidized brine flowing upwards from depth and reduced seawater on or about the sediment-water interface. This mechanism is attractive because it neatly explains how large masses of Pb and Zn can be emplaced into what is now impervious and impermeable rock, and the seemingly regularity and continuity of mineralized beds.

This "exhalative" scenario was modelled by Cooke et al. (2003). The model simulated exhalation of an oxidized brine onto the seafloor by titrating 10 grams of seawater into a kilogram of brine (Fig. 5-15).

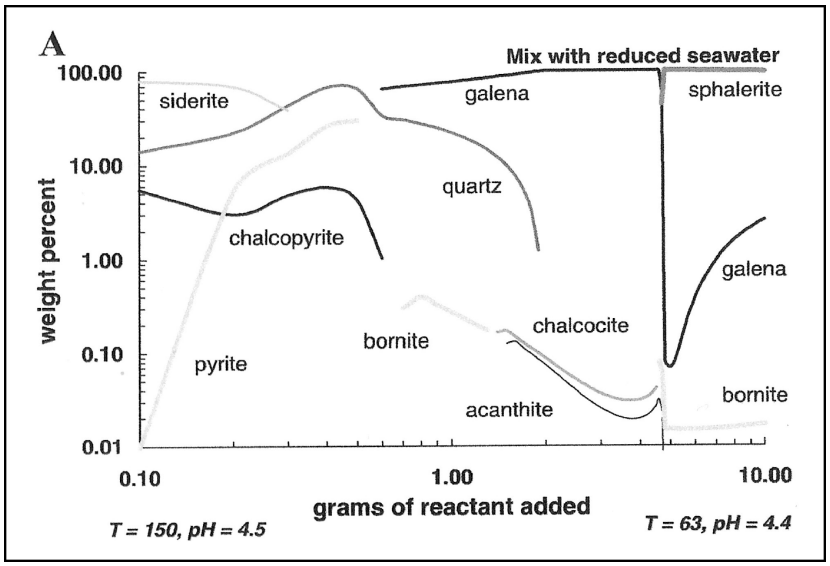

Figure 5-15: Simulation of exhalation of oxidized brine into seawater by Cooke et al. (2003) using the software Chiller. The model appears to have been set up as a titration, where small increments of one fluid are added to a "reservoir" of the other fluid. Note that both scales are logarithmic, suggesting that the assemblages shown in Fig. x are extremely sensitive to small masses of reduced seawater.

Cooke et al. (2003) concluded that this model demonstrated that exhalation is a viable mechanism for precipitating base-metal sulphides, although they conceded that this mechanism is not necessarily relevant to Century since the ore assemblage and spatial distribution of assemblages are not reproduced particularly well. The conclusion that exhalation is a viable mechanism for precipitating economic masses of base-metal sulphides is debatable however, because the masses of minerals precipitated was not considered!

Mixing generally results in precipitation of very small masses of metal and as can be seen from Fig. 15-5, the mass-ratio of end-member fluid is a critical parameter. Furthermore, the composition of Proterozoic seawater becomes an issue, and it is not clear that the assumptions of a temperature of 63ºC and pH of 4.4 are valid.

In-Situ Thermochemical Reduction of "Crustal Brine"

An alternative view to the exhalative model is that Zn and Pb were emplaced at depth and at elevated temperature. Broadbent et al. (1998) and Broadbent (1999) suggested that ore formation occurred as the result of interaction of a "crustal brine" and a transported hydrocarbon accumulation. In this model Zn, Pb, Fe and sulphate are transported to the site of deposition in the brine and precipitated by reduction involving gaseous CH_4 or heavier hydrocarbons (Broadbent et al., 1998). This process can be regarded as a mixing of hydrocarbon gas (or liquid) and brine and/or wall-rock reaction, although precise details of the process are not given.

No data are available on the composition of the brine or the reductant

No geochemical models of this process are available.

Mixing of "Deep Crustal" H_2S and CO_2 and "Crustal" Brine

In this model, proposed by Ord et al. (2002) an aqueous fluid containing H_2S and CO_2 flowed along the Termite Range fault (presumably its movement is predominantly upward in the vicinity of Century). Its source of H_2S is either from thermochemical reduction of the McNamara Group or "deep crustal devolatilization". On the other hand, Zn, Pb, Fe and sulphate are transported to the site of deposition in "circulating crustal

brines" introduced in a discrete aquifer. Ore deposition in this model is a consequence of mixing of an oxidized metalliferous brine and reduced H_2S-rich fluid. This would imply that a specific host-rock is NOT NECESSARY and appears to be contrary to the observations of Broadbent et al., (1998). The key aspect of this model is the hydrodynamic regime that allows mixing of the two end-member fluids in the requisite mass ratio for a protracted period of time.

Cooke et al. (2003) also modelled mixing of an oxidized brine and H_2S gas. The objective seems to have been to assess the likelihood that ore formation involved the scenario proposed by Ord et al. (2002). It is clear from Fig. 5-16 that mixing of the brine and H_2S gas in the absence of any rock would generate assemblages inappropriate to Century or indeed any sediment-hosted Pb-Zn deposit. The reason for this is that the H_2S gas condenses into the brine driving pH to extremely acidic values (a process similar to the condensation of hot sulphur-rich gases into cold groundwater above epithermal precious metal deposits). At such acidic conditions metals remain in solution and carbonate minerals are unstable.

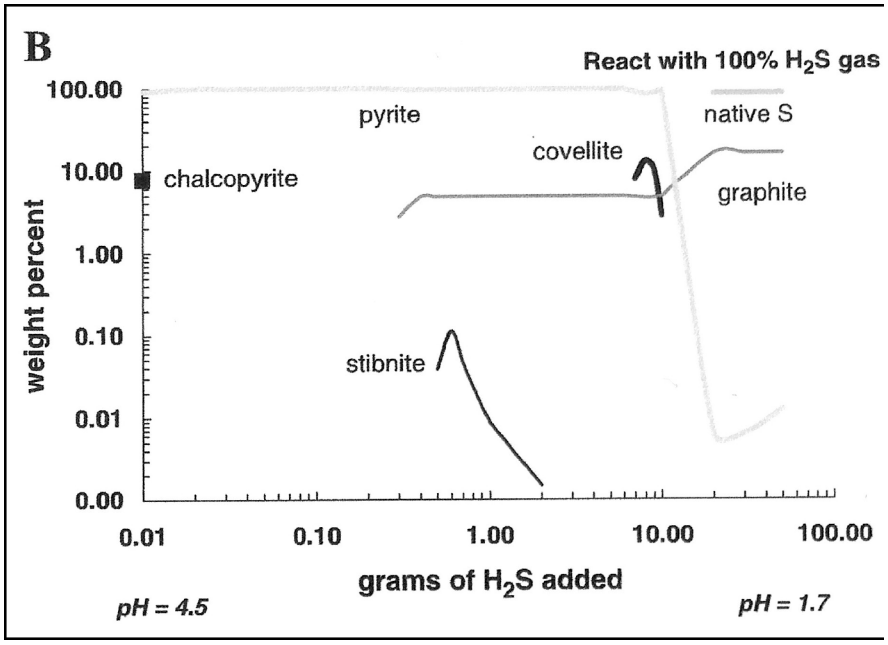

Figure 5-16: Simulation of mixing of oxidized brine and 100 grams of H_2S gas.

This model fails to account for the presence of rock and its buffering effect on the combined fluid composition and represents a geologically unrealistic scenario (i.e. no rock is present, mixing occurs in a cavity).

Mixing of Oxidised Brine & H_2S Gas in the Presence of Dolomite

In order to resolve the issue of extreme pH Cooke et al. (2003) added dolomite as a reactant (dolomite would dissolve and buffer pH at a more alkaline value). This generated more geologically realistic mineral assemblages (Fig. 5-17).

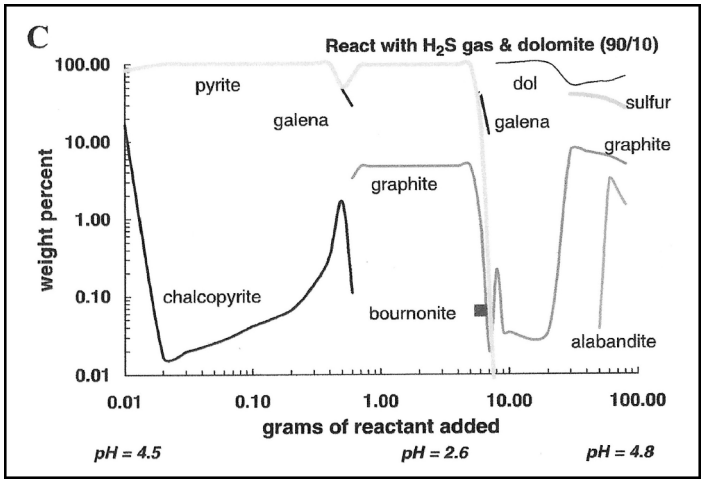

Figure 5-17: Simulation of mixing of oxidized brine and 100 grams of H_2S gas and dolomite (mass ratio 90:10)

Increasing the mass ratio of dolomite to H_2S (to 50:50) resulted in dolomite being present (saturated) throughout the reaction path (Fig. 5-18) and minor additional galena precipitating but otherwise the results of the two calculations are similar.

This model produces results that are closer to the observed assemblages at Century after 10 grams of reactant are added except that the abundant siderite is not replicated. At below 10 grams the assemblage is closer to the silica-dolomite at Mount Isa.

The fact that silicate phases are ignored in these calculations is also problematic since these could have controlled pH (or in the case of Fe-chlorite - redox).

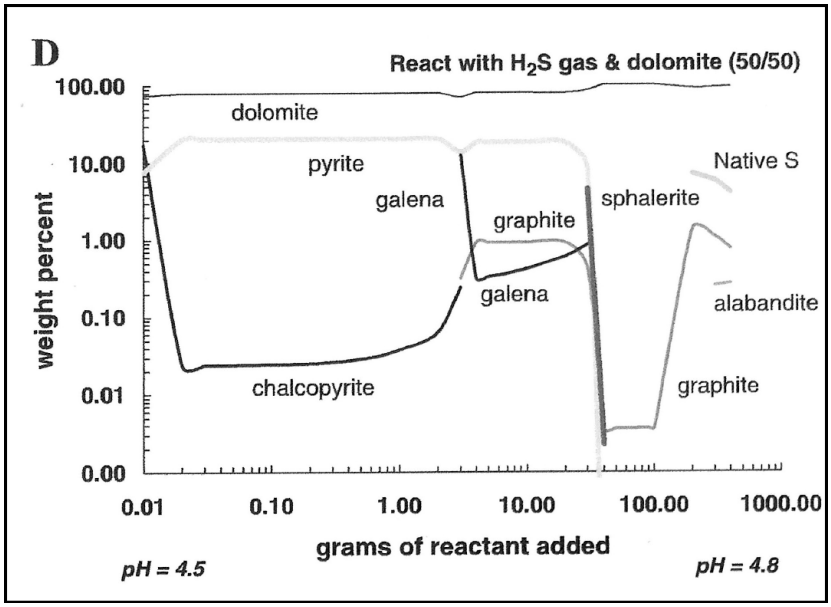

Figure 5-18: Simulation of mixing of oxidized brine and 1 kg of H2S gas and dolomite (mass ratio 50:50)

Mixing of Oxidised Brine & H_2S Gas with Fluid Flow

Ord et al. (2002) present reactive transport calculations using the software FIDAP. The results are shown in Fig. 5-19. Unfortunately there is so little explanation of the model and the fluid compositions used that these

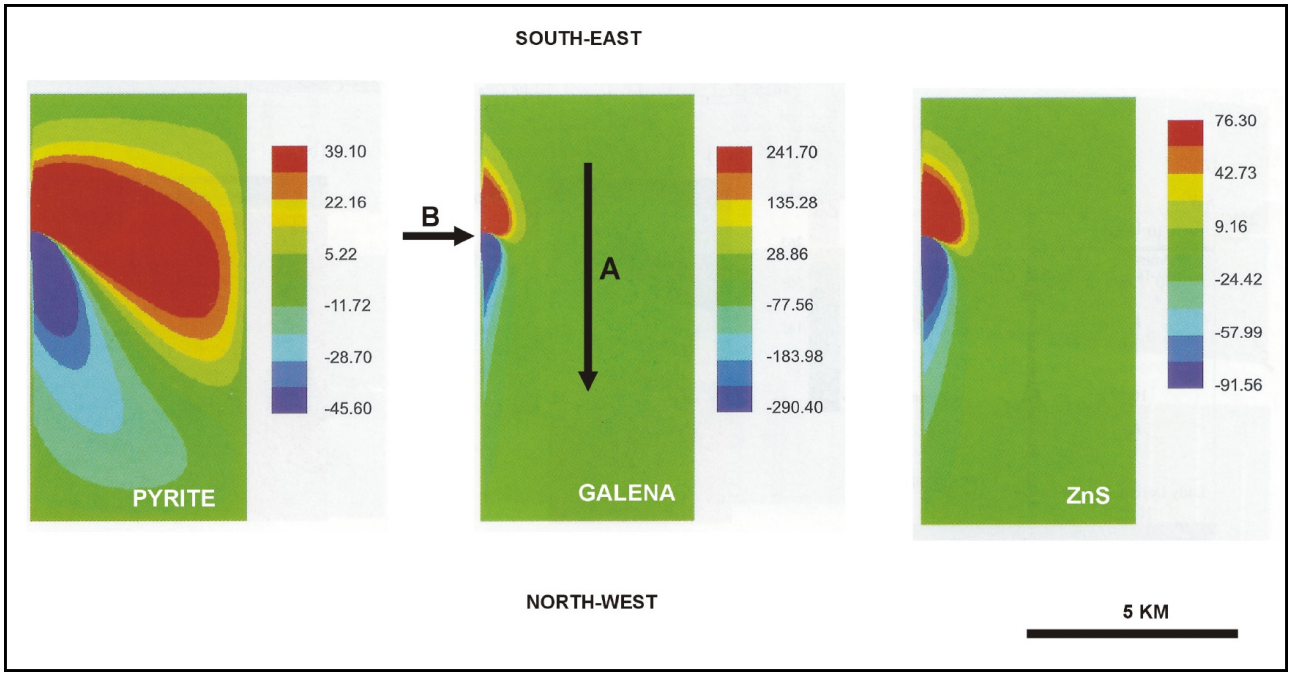

Figure 5-19: FIDAP reactive transport simulation of mixing. The images show predicted changes in mass of pyrite, galena and ZnS in a plan view of a 5 x 10km segment of crust, with the Termite Range Fault to the left side of each image.

results are largely meaningless.

Comments

The chemical models of Cooke et al. (2003) are flawed for a number of reasons:

- Titration (i.e. dropping bits of rock into an hypothetical bucket of fluid) is not a good way to simulate geological processes, where fluid flows through a more or less fixed mass of rock.
- Mixing calculations need to consider all possible mass ratios of fluid and account for the very small masses of metals that precipitate.
- Mixing calculations need to account for likelihood that mixing occurs in the presence of rock (except where exhalation occurs into seawater). HCh (hydrochemistry) is better software for this purpose. Even better is SHEMAT (or another reactive transport code) where the hydrologic aspects of mixing can also be explored.
- A key assumption (and one that is not explicitly stated) is that the sulphur source is extraneous to the Zn-rich hydrothermal solution. This requires the presence of sulphide (or sulphate) in the source rock or another fluid rich in sulphur. If the solution is Na-rich however, high sulphate concentrations can occur (limited by anhydrite and barite saturation). Thus sulphur could have been introduced with the Zn-rich brine. Another possibility is that the sulphur source is petroleum, which would be difficult to model, given the absence of thermodynamic data for appropriate compounds and the inability to effectively model brine-petroleum immiscibility.
- The effect of a migrating H_2S gas on the various lithologies around Century has been ignored, but would probably generate large volumes of pyrite-rich rocks (?Walford Creek).

Recommendations

A variety of depositional scenarios need to be chemically modelled. Key questions that need to be addressed are:

- How important is a particular stratigraphic level? Which level or levels should be targetted for further resources?
- How important is a particular rock-type (chemically and mechanically). Are particular host-rocks crucial?
- What alteration assemblages should exploration geologists be looking for?

There is a clear need to sample several cored holes remote from the Century mine in order to better characterize the chemical and mineralogical character of the sediments, as a basis for exploration geochemistry and for geochemical modelling. I suggest that chemical analysis by means of portable XRF equipment and mineralogical analysis by PIMA or HYLOGGER be trialled. The advantages of these techniques are that they would allow near complete sampling of entire holes with obvious benefits.

The availability of such data would make for more confident recognition of aquifer horizons, and provide better input for geochemical modelling.

The age of the Roper Group with respect to the MacNamara Group be carefully examined and the possibility that the Velkerri Formation is a possible base-metal host be evaluated. Furthermore the iron deposits of the Roper Group should be researched for possible links with Century and the insights that might bring with respect to regional hydrothermal processes. Sampling of old BHP exploration holes held by the GSQ is recommended.

The absolute age framework of the Century region needs to be established, using techniques such as Ar-Ar, recognizing the likelihood of recoil effects (loss of Ar in the irradiation process) in clay-sized phyllosilicates.

References

Andrews, S.J., 1998, Stratigraphy and depositional setting of the Upper McNamara Group, Lawn Hills region, northwest Queensland, Australia. Econ. Geol. 93, 1132– 1152.

Broadbent, G.C., 1999, Geology and Origin of Shale-Hosted Zn-Pb-Ag Mineralisation at the Century deposit, NW Queensland, Australia: PhD Thesis, James Cooke University (unpub.)

Broadbent, G.C., Myers, R.E., Wright, J.V., 1998, Geology and origin of shale-hosted Zn–Pb–Ag mineralisation at the Century deposit, Northwest Queensland. Economic Geology 93, 1264–1294.

Broadbent, G.C. and Waltho, A. E., 1998, Century zinc-lead-silver deposit. In: Geology of Australia and Papua New Guinean Mineral Deposits, Eds: D A Berkman and D H Mackenzie. Australasian Institute of Mining and Metallurgy, Melbourne:729-736.

Cai C., Xie Z., Worden, R., Hu, G., Wang, L., He, H., 2004, Methane-Dominated Thermochemical Sulphate Reduction in the Triassic Feixianguan Formation East Sichuan Basin, China: Towards Prediction of Fatal H2S Concentrations: Marine & Petroleum Geology, V21, pp. 1265-1279.

Cooke, D.R., Bull, S., Large, R.R, 2003, Processes of ore formation in the stratiform sediment-hosted Zn–Pb deposits of Northern Australia: testing the Century model: J. Geochem. Exploration, V78– 79, 519– 524

Cooke, D.R., Bull, S.W., Large, R.R., McGoldrick, P.J., 2000, The importance of oxidised brines for the formation of Australian Proterozoic stratiform sediment-hosted Pb–Zn deposits. Economic Geology 95, 1 – 17.

Large, R.R., Bull, S.W., Cooke, D.R., McGoldrick, P.J., 1998, Genetic models for the HYC deposit, McArthur Basin: constraints from sedimentological, alteration halo and chemical modeling studies. Economic Geology 93, 1345– 1368.

Lindsay J.F., Brasier, M.D., 2000, A Carbon Isotope Reference Curve for ca. 1700 - 1575 Ma, McArthur and Mount Isa Basins, Northern Australia: Precamb. Res., V.99, pp.271-308.

Ord A., Hobbs B.E., Zhang Y., Braodbent G., Brown, M., Willets, G., Sorjonen-Ward P., Walshe, J.L., Zhao, C., 2002, Geodynamic Modelling of the Century Deposit, Mt Isa Province, Queensland: AJES, V49, pp. 1011-1039.

Paul A. Polito, P.A., Kyser, T.K., Golding, S.D. and Southgate, P.N., 2004, The Century zinc deposit and related mineralization in the zinc-rich Burketown Mineral Field, northern Australia: fluid inclusion and stable isotopic evidence for a basin fluid source. Unpub. report, AMIRA P552.

Spikings R.A., Foster D.A., Kohn, B.P., Lister G.S, 2002, Post-Orogenic (<1500 Ma) thermal history of the Palaeo-MesoProterozoic , Mt Isa province, NE Australia: Tectonophysics, V349, pp. 327-365.

Uysal I.T., Glikson, M., Golding, S.D., Southgate P.N., 2004, Hydrothermal Control on Organic Matter Alteration and Illite Precipitation, Mt Isa Basin, Australia: Geofluids V4, 131-142.

Waltho, A.E. and Andrews, S.J., 1993, The Century zinc-lead deposit, in northwest Queensland. In: Proceedings AusIMM Centenary Conference. Australasian Institute of Mining and Metallurgy:41-61.

Warren J.K., George S.C., Hamilton, P.J., Tingate, P., 1998, Proterozoic Source Rocks: Sedimentology and Organic Characteristics of the Velkerri Formation, Northern Territory, Australia: AAPG Bull., V82, pp. 442-463.

APPENDIX 1: ACCESS DATABASE

Data Source	Type	Count
AMDEL	Not Specified	10
Andy Wilde, pmd*CRC Project F1	Drillcore	2
Andy Wilde, pmd*CRC Project F1	Open Pit	9
Donnelly & Crick, 1988	Drillcore	32
Graeme Broadbent, PhD Thesis	Drillcore	410
Graeme Broadbent, PhD Thesis	Not Specified	3
Graeme Broadbent, PhD Thesis	Surface Sample?	32
Graeme Broadbent, PhD Thesis	Underground (exploration shaft)	59
Helen Cutler, Honours Thesis	Drillcore	33
Kralik, 1982	Drillcore	11
Leita Johnson, Honours Thesis	Drillcore	442
Minenco 1990 (Report MRL90/001)	Drillcore	133
Miriam Glikson, AMIRA P552	Drillcore	226
OZCHEM (downloaded from web)		211
Paul Polito, AMIRA P552	Drillcore	38
Paul Polito, AMIRA P552	Mullock	32
Paul Polito, AMIRA P552	Open Pit	13
Paul Polito, AMIRA P552	Surface Sample?	3
PCM Database	Drillcore	53
Steve Andrews, PhD thesis	Drillcore	208
Steve Andrews, PhD thesis	Not Specified	4
Steve Andrews, PhD thesis	Surface Sample?	117

Table A5-1. Origin of samples listed in the database as at Nov 7th 2004. Note the 53 samples from the PCM database are quantitative determinations of mineralogy for various ore samples. The ultimate source of these data is not known.

Data pertinent to the geochemical evolution of the Century orebody were compiled into an ACCESS database in order to facilitate evaluation and identification of data gaps. Digital data were provided by Graeme Broadbent and Steve Andrews (Rio Tinto) and Michael Whitbread (IO Geochemistry). Other data were digitized by various individuals at Monash. Data sources are summarized in Table A5-1.

The database contains a number of data tables that are summarized in Fig. A5-1:

The key table is “sample details” which is linked to all others by a unique sample identifier (sample ID) or drillhole ID. I have used in most cases the sample numbers provided in the source, except where there were no sample numbers provided, and sample identifiers of Kralik (1982) have been renamed to avoid duplicating other sample numbers.

Drillhole details were imported from the PCM drilling database supplied by Leo Feltrin. This required some modification of the drillhole notation from the original sources in order to conform with the naming convention in the PCM database. For example some holes appear as DD99LH263 in the data sources, whereas this hole would be recorded in the PCM database as LH263.

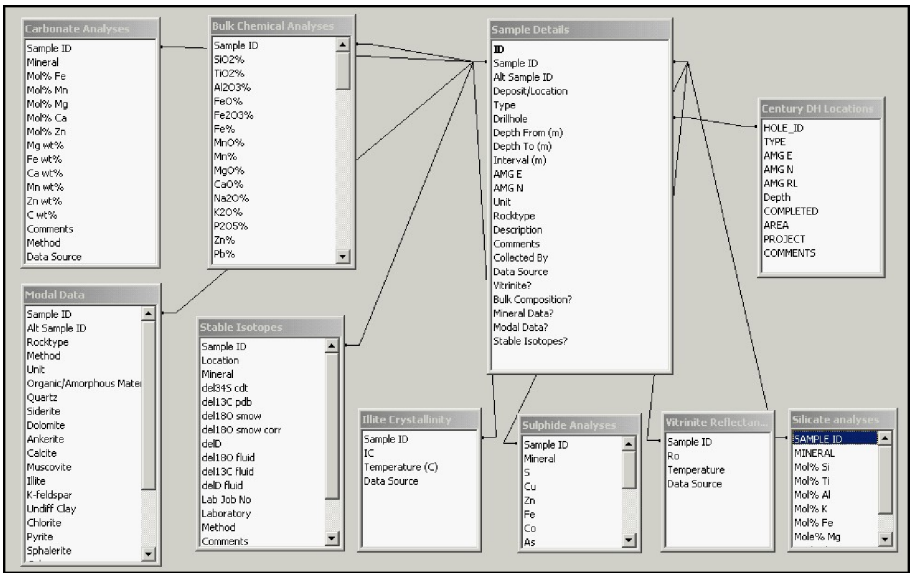

Figure A5-1. Tables in the Century database.

UnitCod	Description
100	Unit 1 siltstone/shale
140	Predominantly weakly mineralised silty shale
145	Siltstone interburden
150	Unit 1 shale (band 1)
155	Unit 1 siltstone/minor shale
160	Unit 1 shale (band 2)
165	Unit 1 siltstone
170	Unit 1 shale (band 3)
175	Unit 1 siltstone
180	Unit 1 shale (band 4 - high gn)
185	Unit 1 siltstone
190	Unit 1 shale (band 5)
195	Unit 1 siltstone
1MS	Shale and Siltstone - undifferentiated
1SH	Unit 1 Shale
1ST	Unit 1 Siltstone
200	Unit 2 shale
310	Unit 3.1
311	Zinc rich bit in 310
312	Zinc poor bit in 310
320	Unit 3.2
410	Unit 4.1 shale
420	Unit 4.2
430	Unit 4.3 shale
440	Unit 4.4
450	Unit 4.5 shale
460	Unit 4.6 shale
BCS	Pmh4 carbonaceous shale
CBX	Carbonate Breccia
CLS	limestone
FDR	Fault Disrupted Rock
HWB	Pmh5 sandstone, shale lenses
HWD	Pmh4 HW siltstone-shale
HWS	Pmh5 sandstone
LFW	Pmh4 Lower FW shale
SMU	Stratiform Mineralised Unit
SOIL	Soil & alluvium
UFHM	Upper Footwall Homer's Mudstone
UFW	Pmh4 Upper FW siltstone-shale
XXX	Core Loss

Table A5-3. Listing of rock-unit codes from the PCM-Zinifex database.

Drillhole	Zn	Zn%	Count
Amoco 83/1	53	0.01	22
Amoco 83/2	49	0.00	16
DD93LH439	33	0.00	1
DD94LH539	47	0.00	9
LH021	105559	10.56	29
LH023	51100	5.11	34
LH025	97013	9.70	63
LH031	98940	9.89	31
LH046	140578	14.06	9
LH054	232000	23.20	5
LH060	169783	16.98	6
LH065	139	0.01	7
LH090	156810	15.68	10
LH100	237714	23.77	7
LH129	40991	4.10	22
LH163	66688	6.67	8
LH164	85950	8.60	2
LH175			4
LH177	174667	17.47	6
LH179	662	0.07	6
LH195	51	0.01	68
LH198	116	0.01	39
LH203	62	0.01	24
LH205	170	0.02	20
LH206	52	0.01	4
LH210	99	0.01	12
LH229	16793	1.67	3
LH233	3749	0.37	9
LH234	605	0.06	17
LH319	25	0.00	1
LH355	15549	1.55	3
LH369	9511	0.95	6
LH412	39523	3.95	226
LH494	38442	3.84	216
Urapunga 3			32

Table A5-4. Research geochemical data for each sampled drillhole.

Stratigraphic nomenclature in some cases was modified to conform with the PCM/Zinifex conventions, listed below (Table A5-2). For stratigraphic units not in the Century mine area the unit notations of Andrews (1998) were used.

Chapter 6: Geochemical Modelling of the Wallaby Ore system, Yilgarn Block, Western Australia

James Cleverley, Nick Oliver And Placer Dome (Asia Pacific) Granny Smith

Predictive Mineral Discovery CRC & Economic Geology Research Unit, School of Earth Sciences, James Cook University, Townsville, QLD, Australia

*This work was originally presented as a poster (11 Oct 2004), as part of a **pmd*CRC open (type II) project on behalf of Placer Dome** Asia Pacific. We we would like to thank Susan Dreiberg and all the staff at the Granny Smith exploration office for arranging and financing a visit by James Cleverley in September 2004 and facilitating an earlier trip by Nick Oliver, Evgeniy Bastrakov, James Cleverley and Warren Potma. Scott Halley is thanked for providing us with PIMA datasets used in an inversion here.*

Abstract

Geochemical modeling using the HCh code along with geochemical analysis of pre-existing whole rock data has been used to help understand the genesis of the Wallaby gold system. Some limited petrography, including backscattered imaging, has also been completed.

The Wallaby gold system is hosted within a magnetite-dominant pipe structure closely related to the intrusion of a sequence of felsic stocks and dykes intruding mafic composition conglomerates which form part of the Wallby (late) basin. Early high temperature skarn formation related to the intrusion of the felsic bodies generated a magnetite-garnet assemblage which is responsible for the magnetic halo of the Wallaby system. Interaction of oxidized, SO_2-rich magmatic fluids with the country rock flowing down a temperature gradient was most likely responsible for the development of an albite-sericite assemblage (300ºC). This assemblage is not observed laterally from the Wallaby system because the preconditioning (magnetite) precluded much flow away from the focus of intrusion. However the cross-cutting, flat, white-mica assemblages are thought to be related to telescoping of the hydrothermal system back on itself causing low temperature alteration overprinting of the high temperature assemblage.

The felsic intrusions exsolved an oxidized, SO_2-CO_2-rich fluid which is manifest in the development of intrusive carapaces with carbonate alteration as well as high temperature 'magmatic' calcite-biotite veins. These structures carry low gold grades and implicate the melts, and in particular the CO_2-rich fluid, as a source of gold from outside the immediate system. The role of reduced, metamorphic fluids in equilibrium with the local host rock is still unknown, however it is likely that some proportion of this reduced fluid may have been involved at the time of lower temperature lode gold formation.

Introduction

Wallaby is surrounded by a broad thermal aureole style of alteration zonation extending a few km away from syenitic rocks in the core of the system (Fig. 6-1). Proximal magnetite alteration grades outwards to pyrrhotite- and chlorite-bearing assemblages in a mafic conglomerate sequence, the latter assemblages being difficult to distinguish from regional assemblages, at least from the information provided.

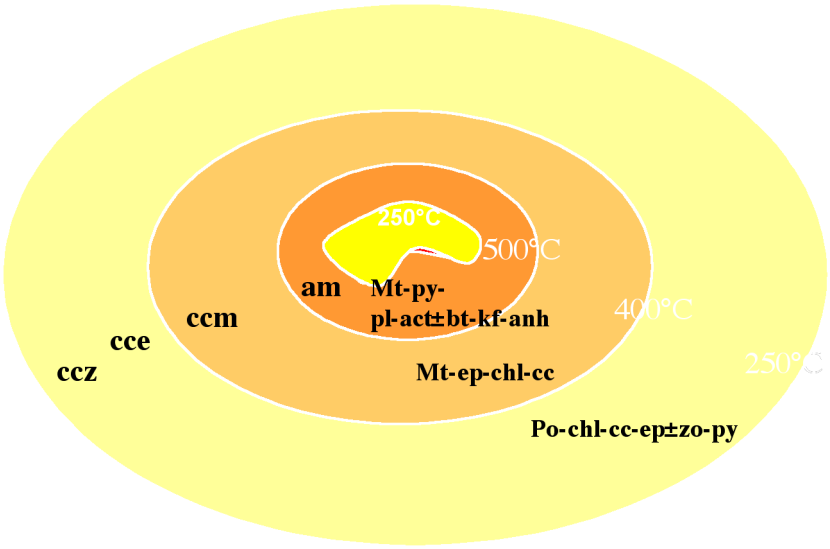

Figure 6-1: Cartoon of the Wallaby alteration system showing inferred temperatures of intrusion-related alteration. The zone acronyms are ccz = calcite-zoisite, cce = calcite-epidote, ccm = calcite-magnetite, am = actinolite-magnetite. The ore association appears to be a lower temperature overprint but the time gap between the intrusion-related alteration and the emplacement of the orebody has been disputed.

We attempt here to provide some model scenarios to test out a) whether the intrusion produced the observed zonation by fluid inflow, fluid outflow, or simple thermal heating, b) the extent to which the precursor intrusion-related alteration impacted on the nature and distribution of mineralization, and c) whether or not there is a reasonable basis for connecting the intrusion directly to the mineralization, for example, through some style of telescoping of the system as the temperatures waned. The geochemical modelling work presented here uses the software code HCh to simulate the interaction of rocks and fluids. In this example the following methodology was used:

1. Generate a "magmatic fluid" by equilibrating fluid with syenite at 550°C, let the fluid 'pick up' chemistry.
2. Use typical 'fresh' but greenschist metamorphosed rock as conglomerate wallrock.
3. Run simulations between magmatic fluid and greenschist conglomerate with temperature gradients and fluid-rock interaction

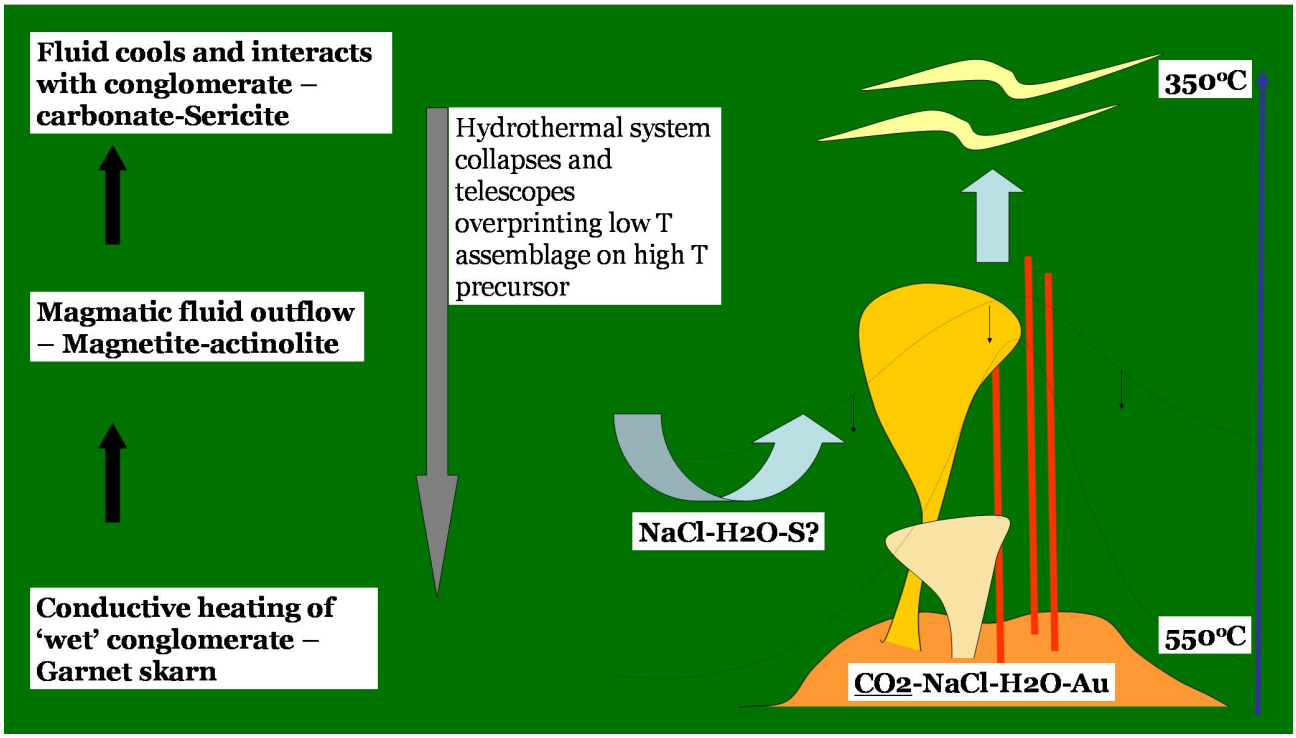

Figure 6-2: Conceptual model for Wallaby alteration simulations. Fluid outflows from syenite at 550°C and moves down a temperature gradient, interacting with greenschist facies conglomerate. HCh Figures (below) are snap shots of this model where the fluid has moved further down temperature.

What do the models predict?

We trialled several scenarios of up-T and down-T fluid flow (towards and away from the intrusion) as well as thermal-only models (no fluid flow), and by far the best results were produced with down-T fluid flow indicating that the intrusion caused the alteration via fluid flow out and up from the intrusion.

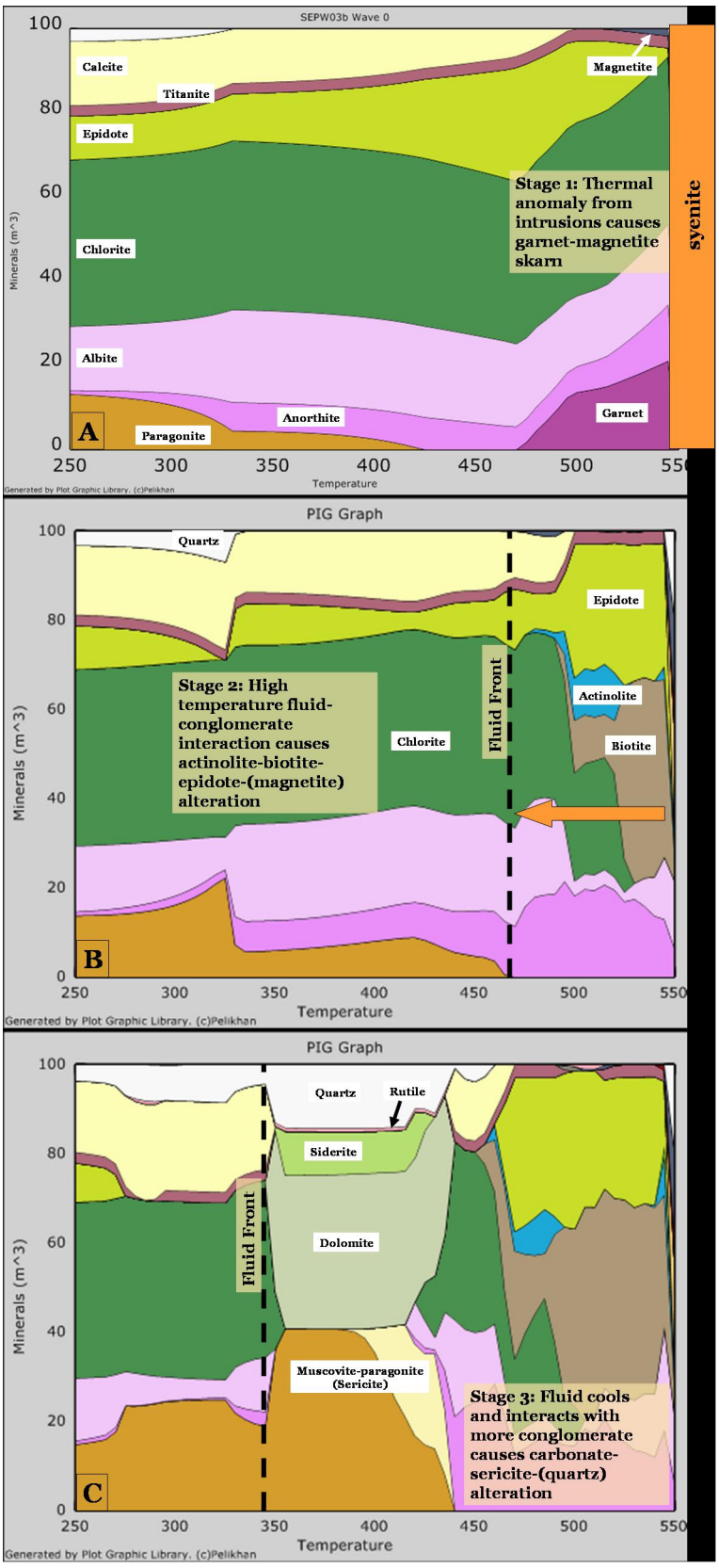

Figure 6-3: simulations of outwards fluid flow from the intrusion after an initial heating phase

A. Stage 1: Heating of the greenschist facies (chlorite-carbonate-mica-plagioclase) conglomerate from 250 to 550°C develops a hot (500-550°C) garnet assemblage with magnetite and some secondary epidote.

B. Stage 2: Fluid infiltration of the conglomerate at close to the intrusives (450-550°C) generates biotite-epidote and magnetite-actinolite.

C. Stage 3: As the fluid cools and interacts with more of the conglomerate it generates a quartz-carbonate-sericite (paragonite-muscovite) zone, which is similar to the ore host.

What does this mean?

- The skarn assemblage develops during the thermal stage but is destroyed during later fluid migration, as observed in the deposit.
- The ore host assemblage can be formed from cooled syenite fluid that has interacted with conglomerate.
- The simulated outflow could also indicate outflow in a vertical sense, such that the ore host develops as an overprint of early high temperature alteration as the hydrothermal system collapses (telescoping).

The fact that the simulations predicts distal carbonate-sericite alteration (which is not seen) may indicate that fluid is precluded from flowing outwards from the intrusive centre. This would mean that the flow path is dominated by the near vertical structures around the intrusive, and distal alteration occurs above the source of fluids.

The source and timing of sulphur and gold

Adding sulphur and gold to the fluid flowing out from the intrusion produced a set of results inconsistent with the observed relationships between the alteration and mineralization.

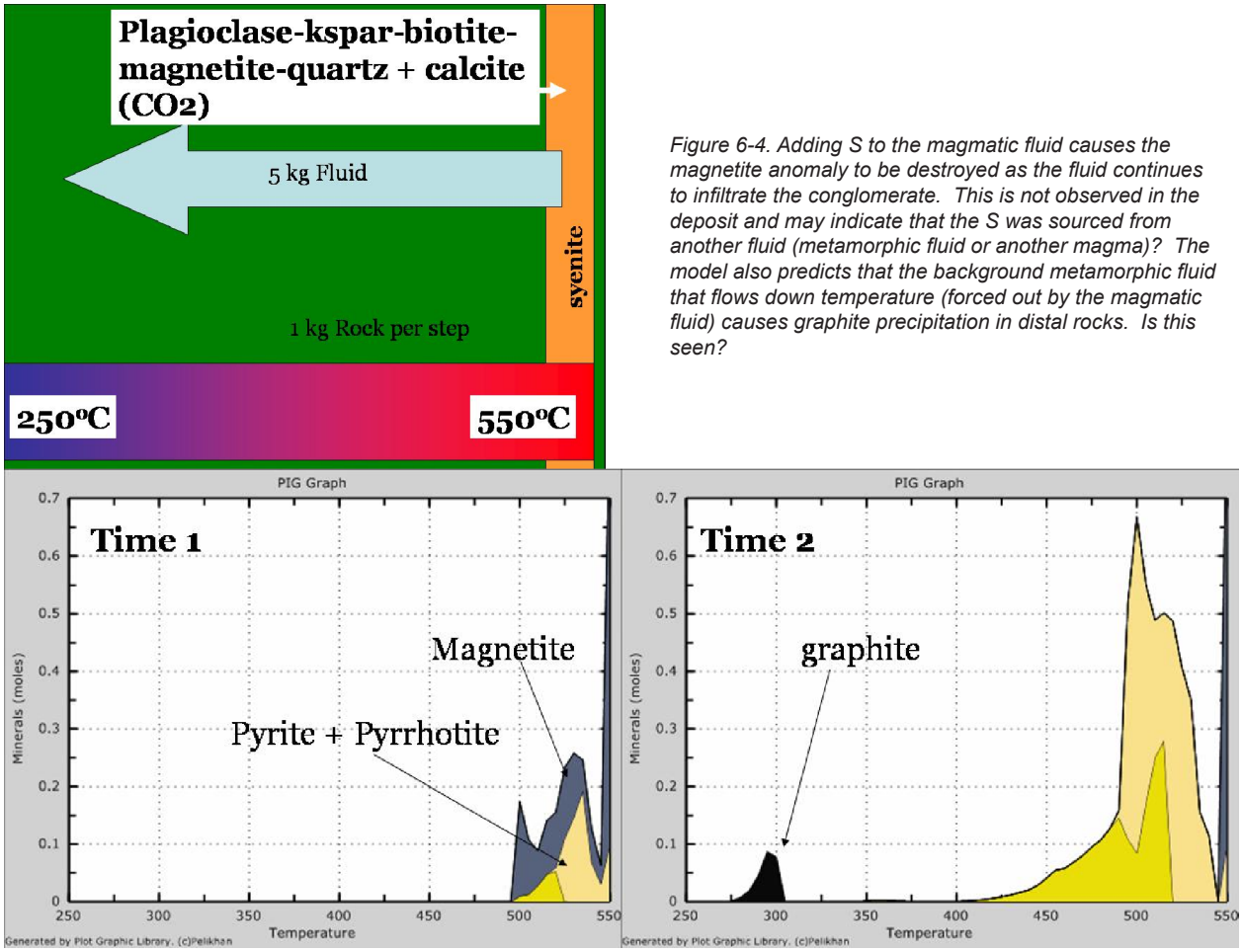

Figure 6-4. Adding S to the magmatic fluid causes the magnetite anomaly to be destroyed as the fluid continues to infiltrate the conglomerate. This is not observed in the deposit and may indicate that the S was sourced from another fluid (metamorphic fluid or another magma)? The model also predicts that the background metamorphic fluid that flows down temperature (forced out by the magmatic fluid) causes graphite precipitation in distal rocks. Is this seen?

Inverting to exploration datasets

We did an inversion of some of the model results to simulate a predicted PIMA response (Fig 6-5, below). This shows the change in PIMA wavelength based on the occurrence of paragonite and/or muscovite (using data courtesy of Scott Halley) in the ore host assemblage. A higher PIMA wavelength is inferred to reflect hotter conditions and therefore a likely proximity to a thermal source (e.g. granite, syenite). The PIMA reponse was processed after the model was run using the new PIG (data visualisation) software (***pmd****CRC* product).

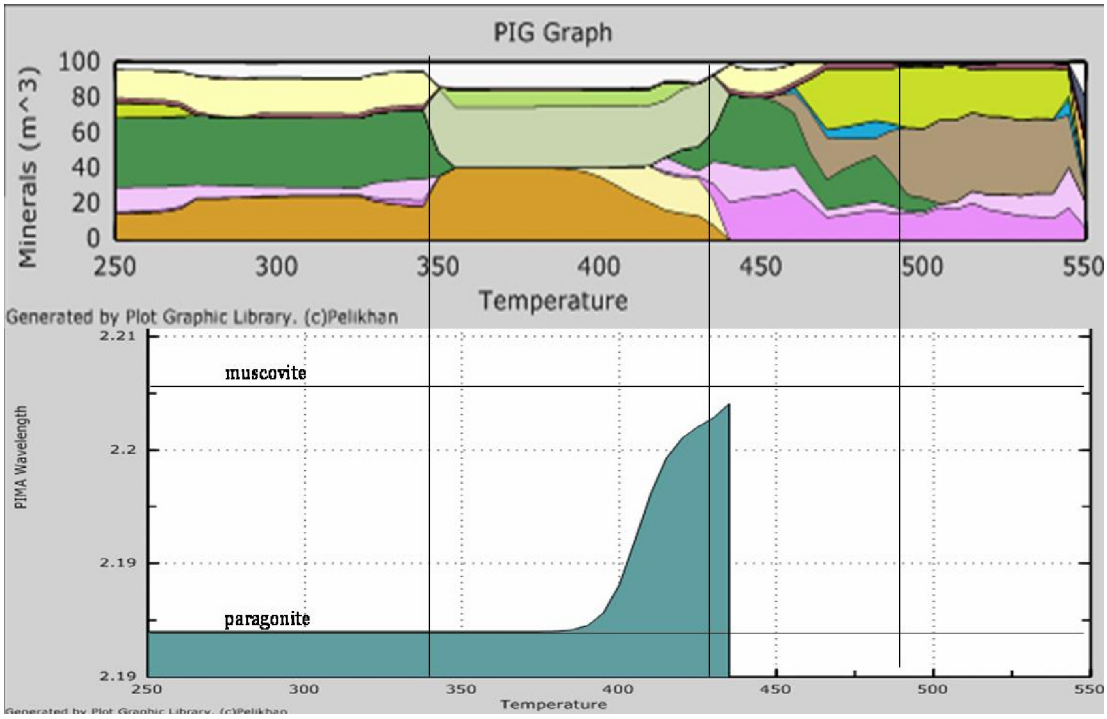

Figure 6-5. Adding S to the magmatic fluid causes the magnetite anomaly to be destroyed as the fluid continues to infiltrate the conglomerate. This is not observed in the deposit and may indicate that the S was sourced from another fluid (metamorphic fluid or another magma)? The model also predicts that the background metamorphic fluid that flows down temperature (forced out by the magmatic fluid) causes graphite precipitation in distal rocks. Is this seen?

Outcomes and further work

- The model predicts the correct assemblage but the wrong modal proportions (too much K-alteration). This is probably related to the estimate of the Na/K ratio in the magmatic fluid. Try some more Na magmatic fluid models.
- Need to better constrain the source of Au and S and are they really separate?
- Understand better the role of carbonatite and carbonate-rich melt derived fluids in the Wallaby system.
- The inversion from HCh simulations to geophysical responses (PIMA, seismic velocity, density and magnetics) can be better developed as this has the greatest impact for relating to the exploration dataset.

Chapter 7: Developing and Testing Chemical Modelling Codes

Michael Kühn

*Computational Geoscience, CSIRO EM, **pmd***CRC*

Introduction

The mission of the ***pmd***CRC* is to move the understanding of mineralising systems beyond the acquisition of information, towards analysis, integration and modelling across all scales. The research results presented in this final report of some sub-projects in F1-F2 for the period of June 2003 to February 2005 are dedicated to the development of new reactive transport simulation capabilities and their application to reverse-engineer existing ore deposits of specific regions and commodities and based on that, subsequently, in the mid term future, to produce a tool as well as understanding for predictive mineral discovery.

*"Many ore discoveries followed industry's use of the inversion and rapid interpretation of aeromagnetic geophysical data. Very little such utilisation has ever occurred with geochemistry, because there is a perception that it is 'disconnected from discovery'. Our project aims to change that perception. Our ambition is to break open the Pandora's Box of geochemistry and provide a 2D and 3D connection between remotely sensed geophysical and geochemical data, ore deposit models, and real exploration targets based on geochemical possibility and risk reduction." (Nick Oliver, F1-F2 Annual Report 2003, **pmd***CRC)*

This chapter consists of two major parts: (1) the code development, which is in this case the amendment of SHEMAT (Clauser 2003) with the geochemical simulation program PHREEQC (Parkhurst and Appelo 1999). Additionally the program UT2Chem has been developed to produce thermodynamic data bases for SHEMAT-PHREEC from UNITHERM (Shvarov and Bastrakov 1999). (2) The application of the new tools to terrane modelling across different length scales. Numerical studies shown by Kühn (2004) have shown already the applicability of SHEMAT for studies on different time scales.

Chemical codes development

SHEMAT-PHREEQC

SHEMAT (Simulator for HEat and MAss Transport) is an easy-to-use, general purpose reactive transport simulation code for a wide variety of thermal and hydrogeological problems in two and three dimensions. Specifically, SHEMAT solves coupled problems involving fluid flow, heat transfer, species transport, and chemical water-rock interaction in fluid-saturated porous media. It can handle a wide range of time scales. Therefore, it is useful to address both technical and geological processes. In particular, it offers special and attractive features for modelling steady-state and transient processes in hydro-geothermal reservoirs.

SHEMAT and Processing SHEMAT

SHEMAT in its present form evolved from a fully coupled flow and heat transport model (Clauser 1988) which had been developed from the isothermal USGS 3-D groundwater model of Trescott and Larson (Trescott 1975; Trescott and Larson 1977). Transport of dissolved species, geochemical reactions between the solid and fluid phases, extended coupling between the individual processes (most notably between porosity and permeability), and a convenient user interface (developed from Processing Modflow (Chiang and Kinzelbach 2001)) were added during several research projects funded by the German Science Foundation (DFG) under grant CL 121/7 and the German Federal Ministries for Education, Science, Research, and Technology (BMBF) under grant 032 69 95A-D and for Economics and Technology (BMWi) under grant 0327095 (Bartels et al. 2002; Kühn et al. 2002).

SHEMAT handles the following classes of problems:

- one individual process:
  - groundwater flow;
  - conductive heat transport;
  - diffusive species transport;

    - chemical reactions;
- two coupled processes:
    - groundwater flow combined with heat transport;
    - groundwater flow combined with species transport;
- three coupled processes:
    - groundwater flow combined with species transport and chemical reactions;
    - prescribed flow, species and heat transport combined with chemical reactions;
    - combined groundwater flow, heat and species transport, and chemical reactions.

SHEMAT uses a finite difference method to solve the partial differential equation. Three schemes are available for the spatial discretization of the advection term in the transport equations:

- a pure upwind scheme;
- the Il'in flux blending scheme;
- the Smolarkiewicz diffusion corrected upwind scheme.

The resulting system of equations can be solved explicitly, implicitly or semi-implicitly. For implicit and semi-implicit time-weighting the sets of linear equations are solved iteratively by the strongly implicit procedure (SIP, Weinstein et al. 1969).

Processing SHEMAT (PS) is a graphical user interface for the finite difference code SHEMAT. PS is based on an interface for MODFLOW, Processing MODFLOW version 5.0, by Chiang and Kinzelbach (2001). PS comes complete with a professional graphical pre- and post-processor, the 3-D finite difference fluid-flow, heat and species transport code SHEMAT, and the chemical reaction module, which is based on the program code PHRQPITZ (Plummer 1988).

PS checks the final models for potential problems prior to starting the simulation. PS can use the computer's entire available memory. The model grid can be shifted, rotated, and refined. Model data can be specified either for each finite-difference cell individually or for constant parameter zones. PS can import Processing Modflow (PM5) files. PS can read in geo-referenced raster graphics (bitmaps) and vector graphics (DXF or Line Maps) as background sitemaps. PS exports results into Surfer® and Tecplot® data files.

The results of a simulation are distributions in space and time of, for instance, hydraulic head, Darcy-velocity, temperature, species and mineral concentration, permeability, and porosity. The Result Viewer permits a visual check of the input data and simulation results. It can plot logs of selected parameters versus depth at defined locations of the model. The Permeability Estimator allows to infer the initial permeability of a given domain in the model from available supplementary data.

Expansion of SHEMAT and Processing SHEMAT

Linking between SHEMAT and PHREEQC

Within the framework of the F1-F2 project it was decided to finish the interface between SHEMAT and the geochemical simulation program PHREEQC (Parkhurst and Appelo 1999). This was pre-prepared by the author in his former position at the Technical University of Hamburg-Harburg. The new chemical module is additional to its built in chemistry based on PHRQPITZ (Plummer et al. 1988). The interface between SHEMAT and PHREEQC has been wanted due to several reasons:

- increase the valid temperature range above 150°C,
- enlarge the chemical system to enable the chemical processes of ore deposition and the use of UNITHERM data,
- reduce the computational time,
- provide a user-friendly program package for predictive mineral discovery,
- because additional features come with PHREEQC (kinetics, solid solutions, isotope fractionation).

The new coupling and interface is finishes and test simulations of fully coupled systems (Flow-Heat-

Transport-Reaction) were successful. The particular, simulated system is described in detail in Kühn and Schneider (2003). This benchmark showed that the new coupling to PHREEQC is twice as fast as the coupling to PHRQPITZ. SHEMAT-PHREEQC has then been used to perform reactive transport modelling in F1-F2 for the Mount Isa terrane (see below).

Development of Processing SHEMAT

The graphical user interface of SHEMAT, Processing SHEMAT, has been updated and amended according to the requirements of the new chemical module PHREEQC. A new chemical data set management system has been set up now so that the user can easily define different thermodynamic data sets for different models (see below 'Reader and Writer from UNITHERM').

A new data exporter for Processing SHEMAT has been programmed to rewrite SHEMAT simulation results into data files readable by MayaVi. The export function is accessible directly from Processing SHEMAT. The user is able to choose any 3D array to be exported (e.g. temperature, pressure, hydraulic head, fluid flow vectors or solutes and minerals incorporated in the model). There is also the functionality to calculate and export u◊grad(T) a measure for the supposedly, chemically most reactive areas of the system. This work is basic for the terrane modelling with SHEMAT to enable better interpretation of 3D modelling results.

Reader and writer from UNITHERM to any chemistry

To populate any geochemical simulation program with thermodynamic data from the UNITHERM data base requires a reader and writer which transfers the UNITHERM data into data sets readable by the particular program. The program called UT2Chem (Fig. 6-1) has been developed using Visual Basic. It is written in VB7 .NET. Necessary data are read from the System.txt and the logk.txt (both types: grid and path), which are produced by UT2K.

Data files can be transferred from UNITHERM to use them with i.e. the USGS stand alone geochemical simulation program PHREEQC. This is specifically important to provide high quality data sets for SHEMAT-PHREEQC the reactive transport model described above.

Because the chemical system of PHREEQC is based on primary as well as secondary master species a special workflow is necessary to produce data from UNITHERM. Firstly, four data sets have to be made with UT2Chem from UNITHERM which are secondly merged into one set of thermodynamic data (Fig. 6-1, right). The different data sets need to incorporate the following combination of redox species:

1. oxidised metals / oxidised anions
2. reduced metals / oxidised anions
3. reduced metals / reduced anions
4. oxidised metals / reduced anions

The limitation for the application of UT2Chem in combination with PHREEQC and / or SHEMAT-PHREEQC is that redox relevant species can so far only be handled in two states, one oxidised and one reduced. Intermediate redox potentials won't pass the combining process correctly of amalgamating four PHREEQC data sets into one.

The reader and writer UT2Chem also exports data set readable by the reactive transport model OS3D and preliminary procedures are in place to support the programs GWB, EQ3/6 and RST2D (Fig. 6-1, left).

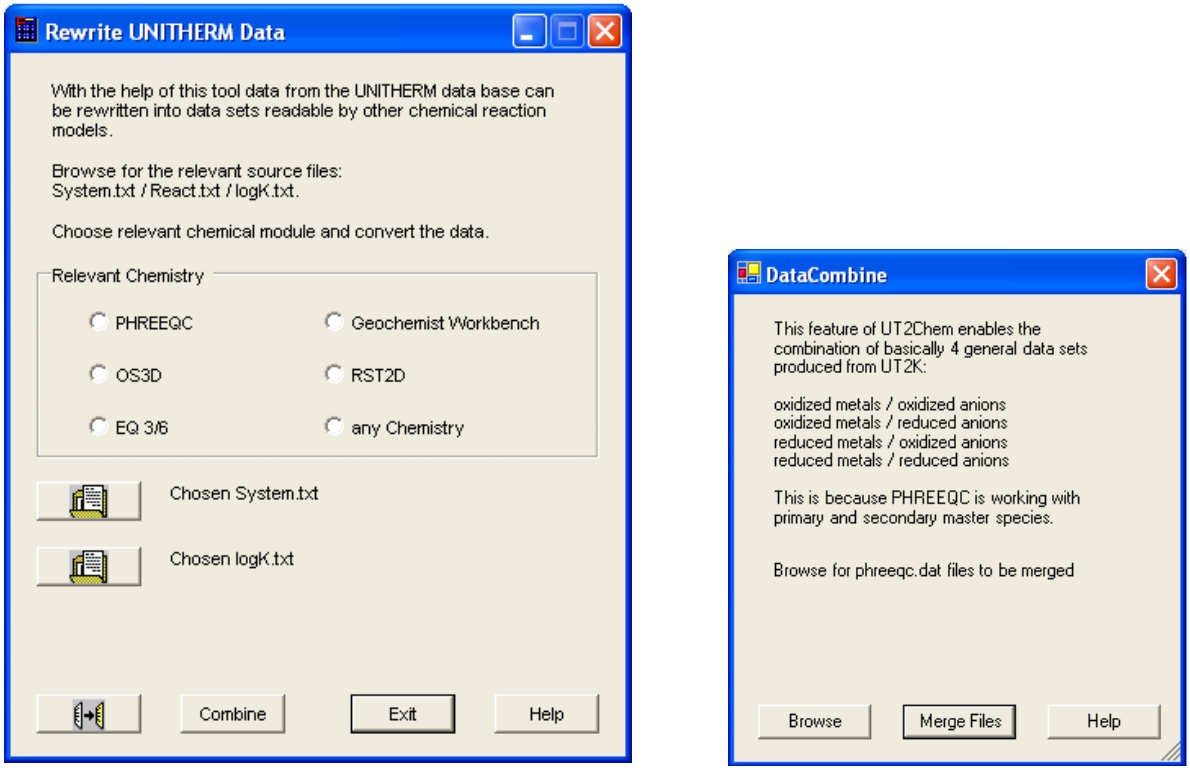

Figure 7-1. UT2Chem's main menu (left) and merging functionality for PHREEQC (right)

Terrane modelling on multiple scales using SHEMAT

The Mount Isa Inlier in Queensland (Fig. 7-2) hosts several giant ore deposits and is considered one of the most valuable regions for mineral resources in Australia (Solomon and Groves 1994). With its long history of exploration and mining, the region offers a great opportunity for investigating ore deposition due to availability of extensive geological, geophysical, hydrological, and chemical data. To predict the location of (as yet) undiscovered deposits requires an understanding of the coupled, physical and chemical processes involved in mineralisation. Such understanding may be gained through a combination of conceptual and quantitative models. Numerical modelling permits investigation of competing hypotheses concerning mineralisation, and can be used to reverse-engineer known deposits in order to guide future mineral exploration. Numerical models of the Mount Isa Copper and the Century Lead Zinc deposit have been performed with respect to the '5 Questions' (compare following section) and taking into account multiple length scales. Simulation results gained by applying the reactive transport code SHEMAT are described in the following.

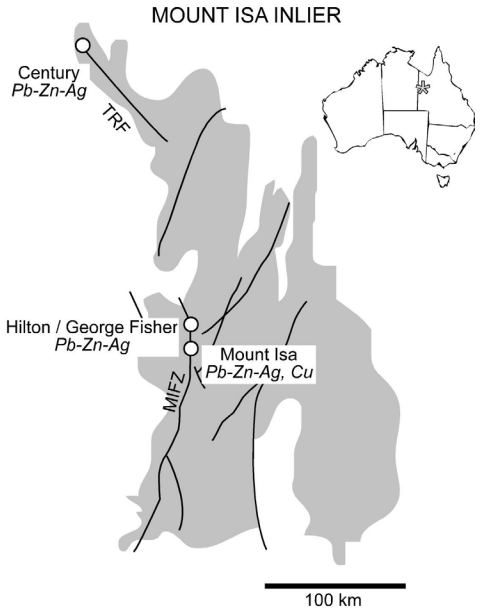

Figure 7-2. Location of Mount Isa, Hilton, George Fisher, and Century Mines in Mount Isa Inlier. Also shown are major fault systems, including Termite Range Fault (TRF), and Mount Isa Fault Zone (MIFZ).

5 Questions and hypotheses testing

Investigation of mineralisation in a particular area should begin by considering the following five questions (Ord et al. 2002):

1. What is the architecture of the mineralising system?
2. What is its geotectonic history?
3. What was the nature of the fluids associated with the mineralisation?
4. What processes were driving fluid flow on the scale of the system?
5. What was the mechanism for alteration and precipitation of the ore?

Qualitative answers to these questions lead the way to conceptual models, which in turn provide a framework for quantitative, numerical models.

Questions 1 and 2 investigating the structural and stratigraphic architecture and the geotectonic history of the system have been extensively examined by Gessner et al. (2005) in case of Mount Isa and by Ord et al. (2002) with regard to Century. These two studies provide the basis of this work. Answers to question number 3 about the nature of fluids associated with the mineralisation have been inferred from fluid inclusions (personal communication Andy Wilde, Monash University). The present investigation is concerned with question 4, regarding possible drivers for fluid flow and question 5, regarding the mechanism of ore deposition.

It is very important to note that numerical models are to be used to test and subsequently evaluate or falsify hypotheses of conceptual models built upon the '5 questions'. Numerical models should not be used to create hypotheses by themselves.

Simulation approach on multiple scales

As yet, the combination of all scales from regional down to micro scale is not feasible in numerical models. The relevant scales (Fig. 7-3) studying ore deposits reach down from the regional scale (~100 km) to the micro or thin section scale (~1cm). The idea is to finally provide constraints for smaller scale models from the larger scale and derive functionality from smaller scale models of processes which cannot be resolved in larger scale models, due to restrictions of discretization of the applied numerical mesh.

Within this study a couple of examples are given for numerical investigations on different scales (regional, deposit, thin section). The next goal, to come in the newly planned ***pmd****CRC* projects (I-new, F-new), is to include constraints or functionality in smaller scale or larger scale models, respectively.

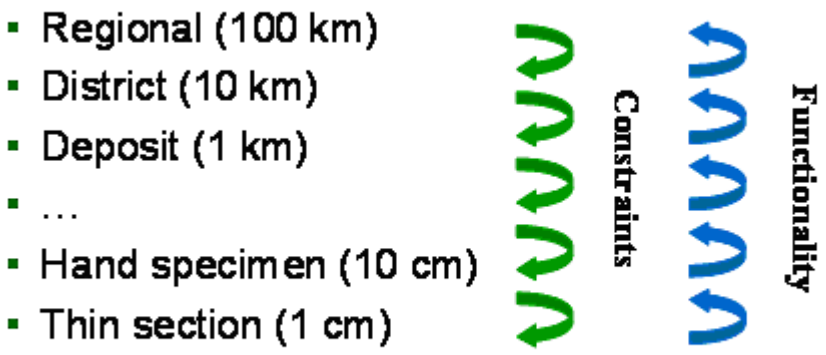

Figure 7-3. Numerical modelling on multiple scales to produce constraints for smaller scale models from larger scales and functionality for larger scale models from smaller scales.

Century – regional scale

The aim of the 'Century' sub-project in F1-F2 is to generate 'soft' models based on literature review and to compile key data. To investigate the hydrogeological and thermal regime, as a starting point, it has been decided to go on from the work of Ord et al. (2002). For that purpose existing FLAC3D models have been transferred into SHEMAT models. Model transfer and simulations are presented in the following.

Superimposed on the district geology the location of the modelled area is given in Fig. 7-4. The actual model simulated with SHEMAT had a size of 100 km in NW-SE direction and 50 km in SW-NE direction with a total depth of 25 km. Fig. 7-5 displays the integrated fault architecture with the first order Termite Range Fault (TRF) crossing the model from NW to SE.

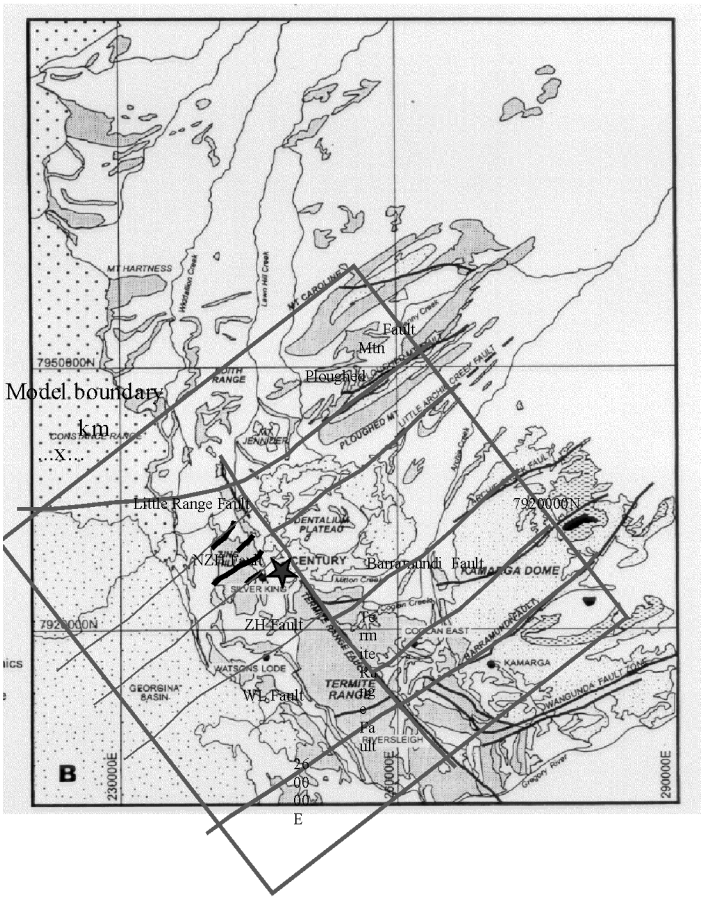

Figure 7-4. Location map of the Ord et al. (2002) Century model superimposed on the district geology map from Andrews (1998). The shown boundaries are 50 km x 50km. The model finally simulated is 25 km longer in NW as well as SE direction.

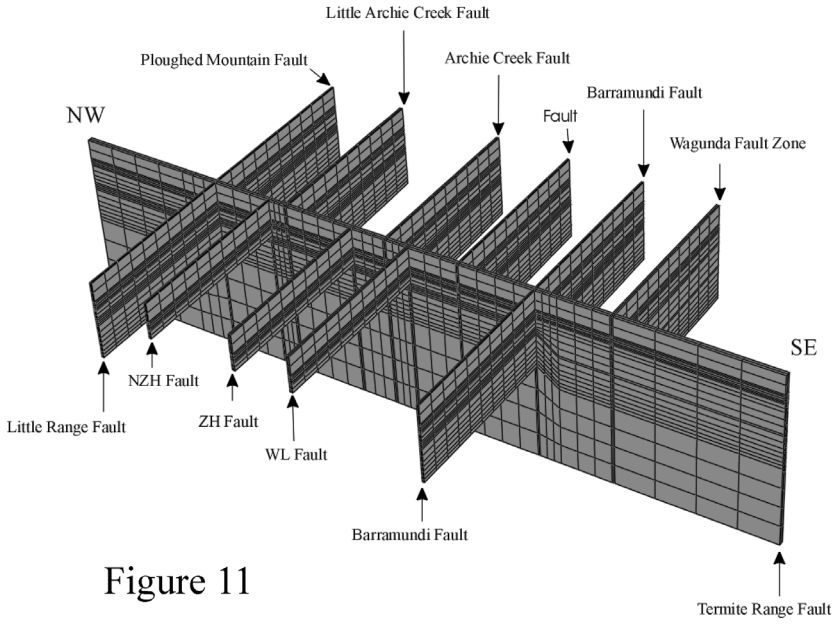

Figure 7-5. Architecture of faults. Exposed fault surfaces from Century 3D FLAC model showing stratigraphic geometries (Ord et al. 2002).

Model set up

The model mesh in SHEMAT needs to be structured, hexahedral and with all internal angles set to 90°. However, the grid of the existing Century model (Ord et al. 2002) is built also with angles deviating from 90°, which makes a direct transfer to SHEMAT difficult. Hence, the SHEMAT model has been 'drawn' from images of various cross-sections extracted from FLAC3D. Processing SHEMAT provides a feature with which a model can be built upon background maps which has been used here. Simplifications during the model transfer include neglecting specific geometrical features in the vicinity of the Termite Range Fault, namely the inclined and tapering layers of the North-East side of the model. After 'drawing' the geometry, rock properties are assigned manually to specify different permeability settings for further calculations with coupled heat and fluid flow processes.

The mesh needed refinement because the original mesh in FLAC3D, used by Ord et al. (2002) has just been used for mechanical deformation and fluid flow simulations. Those studies were carried out to locate areas in which hydrofracturing occurs what in turn produces fluid pathways. Numerical models dealing with fluid flow only are far more robust from the perspective that much higher fluid velocities can be applied on coarser meshes without numerical instabilities.

To allow in SHEMAT for conductive as well as advective heat transport the mesh was refined starting at the faults and increasing cell sizes by 20% from there. This has been done because Spitz and Moreno (1996) and Anderson and Woessner (1992) both pointed out that cell size changes have to be between 0.5 and 2 from one cell to the next. They also advice that the aspect ratios of the cells or elements of a mesh (ratio between delta x and delta y, or delta x and delta z, or delta y and delta z) should not exceed 1:10 or 10:1.

In addition to the application of both rules for set up of the SHEMAT model permeabilities of the water conducting units of the model where lowered to reduce fluid velocities and keep the temperature Peclet number within a stable range. The described refinements, applied to the original FLAC3D model now produce numerically stable results.

Investigation of flow and temperature fields

Different flow regimes in the Century regional system have been investigated to determine resulting fluid flow and thermal pattern. Five major flow regimes were investigated:

- Pure convection scenario
- Lateral flow through the Termite Range Fault (TRF),
- Vertical flow through the TRF,
- Lateral flow through Lady Loretta (LL),
- Lateral flow through LL combined with vertical flow through TRF.

Pure convection scenario: The first test was to investigate if convection evolves in the system with no forced fluid flow across the boundaries. The presence or absence of Rayleigh convection in fluid saturated porous media can be estimated with the dimensionless Rayleigh number (Ra). Ra represents the ratio of the buoyant forces, driving thermal convection, to the viscous forces, inhibiting fluid movement. As shown by Turcotte and Schubert (2002), linear stability analysis for the onset of thermal convection in a fluid-saturated porous layer heated from below yields the dimensionless Rayleigh number:

$$Ra = \frac{\alpha_f g \rho_f^2 c_w k H (T_1 - T_2)}{\mu \lambda_m} \qquad (1)$$

In Eq. (1) _f [K^{-1}] is the thermal expansion coefficient of water (subscript f = fluid), g [m s-2] the gravitational acceleration, _f [kg m^{-3}] the density of liquid water, cpf [J kg^{-1} K^{-1}] the isochoric heat capacity, k [m^2] the permeability, H [m] the characteristic height of the system, (T1 - T2) [K] the temperature difference across this height, _ [kg m^{-1} s^{-1}] the dynamic viscosity of water, and _m [J s^{-1} m^{-1} K^{-1}] the medium thermal conductivity. Above some critical Ra, the system is unstable, and free convection occurs. For an infinitely long and homogenous vertical 2D system with impermeable boundaries of constant temperature and a linear initial thermal gradient across the layer, free convection is expected when Ra exceeds 4p2 (Lapwood 1948).

Permeabilities assigned to TRF, all other faults, and the Lady Loretta (LL) formation was 5.0E-16 m^2. The thermal conductivity of the rocks has been uniformly defined with 3.35 [W m^{-1} K^{-1}]. The top temperature was 25°C and the bottom temperature was 775°C according to a geothermal gradient of 30 K per km depth. The actual Ra of a system like Century is calculated with averaged values of the temperature dependent properties used in Eq. (1). In this case Ra is determined to be 704 based on an average temperature of 400°C. Due to the height of the model of 25 km a large range of the temperature dependent properties is applicable. Ra at the top boundary for example calculates to be only 12. However, Ra is increasing with depth, due to increasing temperature, and the critical value is overstepped in a depth of around 4000 metres. Ra values towards depth increase above 1000. Hence, determination of Ra predicts free thermal convection for the Century system as it has been defined after Ord et al. (2002).

From Fig. 7-6 it can be seen that free thermal convection with 18-19 cells develops within TRF in accordance with a Rayleigh number above critical. Interesting to see is that the high permeable LL unit seems to cut short the heights of the system wherein convection occurs. Although the TRF extends from bottom to top of the model, convection solely occurs below Lady Loretta.

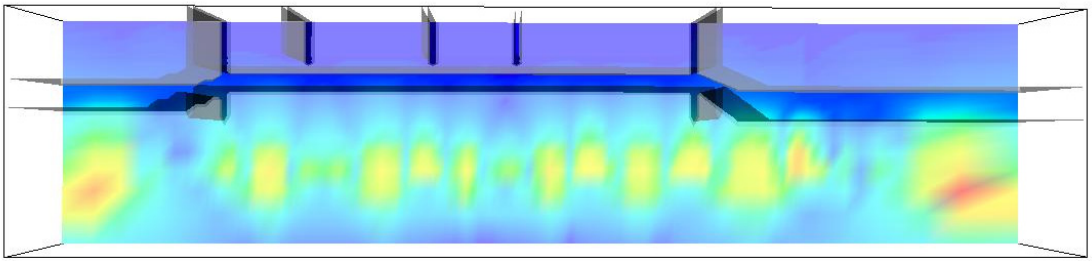

Figure 7-6. Velocity map within the Termite Range Fault (TRF) showing Darcy fluxes from 0.0 (dark blue) up to 5E-09 m s-1 (red). Grey planes are isosurfaces of high permeability. Convection occurs in TRF underneath the laterally high permeable Lady Loretta formation.

Lateral flow through Termite Range Fault

The effect of a forced fluid flow with 1.0E-09 m s-1 (Darcy flux) crossing the system through the entire height of the TRF (e.g. due to topographically driven flow) has been investigated with a different scenario. Velocity vectors in Fig. 7 display that convection is ongoing beside the flux from right to left through the system. Less convection cells are observed compared to the pure convection scenario shown above.

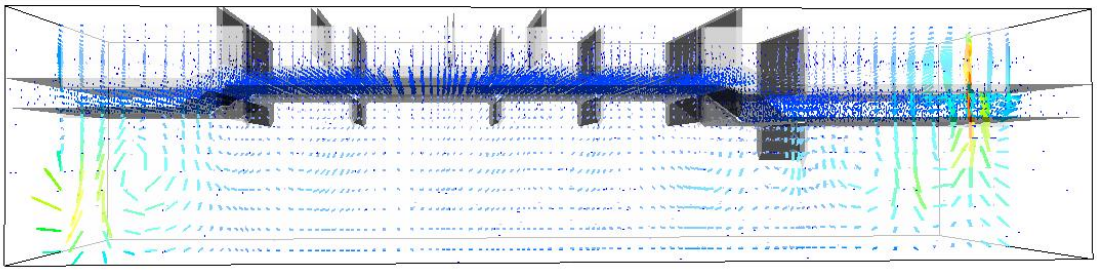

Figure 7-7. Fluid flow vectors within the Termite Range Fault (TRF) as they develop with lateral flow from right to left through TRF. Colors reflect Darcy fluxes from 1.0E-09 m s^{-1} (dark blue) to 1.1E-08 m s^{-1}(red).

Fluid flux through TRF from bottom to top

Another assumption in Ord et al. (2002) is that there might have been supply of water through TRF but from the bottom (Darcy flux 1.0E-09 m s^{-1}). The figures below show the results of the numerical simulations with flow into TRF at the bottom of the model and out of TRF at the top. It is only the forced upward flow which is observed in this model and any kind of free convection in TRF is suppressed. The temperature distribution changes significantly compared to the previous models due to the upwards directed flow. The isotherms within the system are identical to the initially applied geothermal gradient except for the area in and around TRF in which they are dragged up with increased temperatures in shallower depth. A closer look into the model along TRF (Fig. 7-8) reveals that due to the flow through TRF the faults perpendicular to it (secondary faults) are also activated.

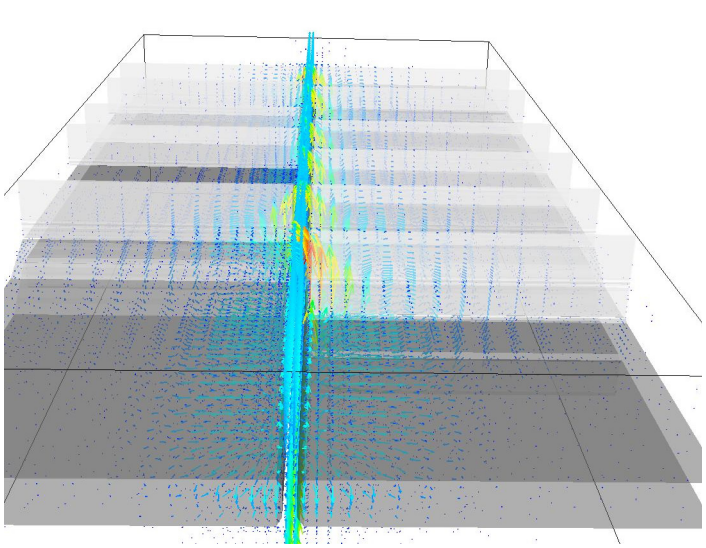

Figure 7-8. Fluid flow vectors viewed along the Termite Range Fault (TRF) from SE to NW. Flow through TRF initiates flow also in the secondary faults perpendicular to TRF.

Lateral flow through Lady Loretta (LL)

This conceptual model takes into account topographically driven lateral flow through LL (Darcy flux 1.0E-09 m s^{-1}) additional to any kind of convection which might form in TRF as shown above. Fig. 7-9 displays that additional to the forced flux through LL, free thermal convection is evolving within TRF. The fluid flow field is slightly inclined towards the left indicating the influence of the horizontal flow through LL. The number of convection cells (6-7) is significantly less compared to the case of pure convection.

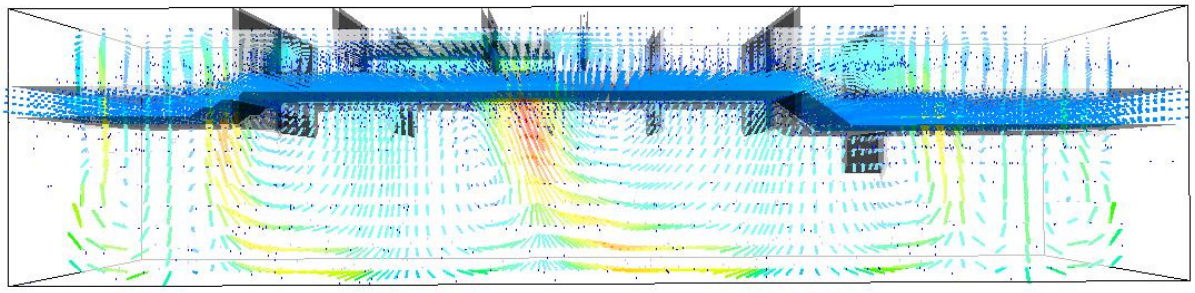

Figure 7-9. Fluid flow vectors within the Termite Range Fault (TRF) as they develop with lateral flow from right to left through the Lady Loretta formation (LL). Colors reflect Darcy fluxes from 1.0E-09 m s^{-1} (dark blue) to 1.5E-08 m s^{-1}(red).

It has to be noted that the thermal pattern in this case study is not fixed (no steady state reached) neither in space nor in time. The investigated time was 1 million years. The convection cells are migrating from SE to NW (right to left) through the model propelled by the lateral flow through LL. The conceptual set up of the experiment is given in Fig. 7-10 with the hydrofractured shale (Ord et al. 2002), the Lawn Hill formation, which is the host of the Century ore deposit.

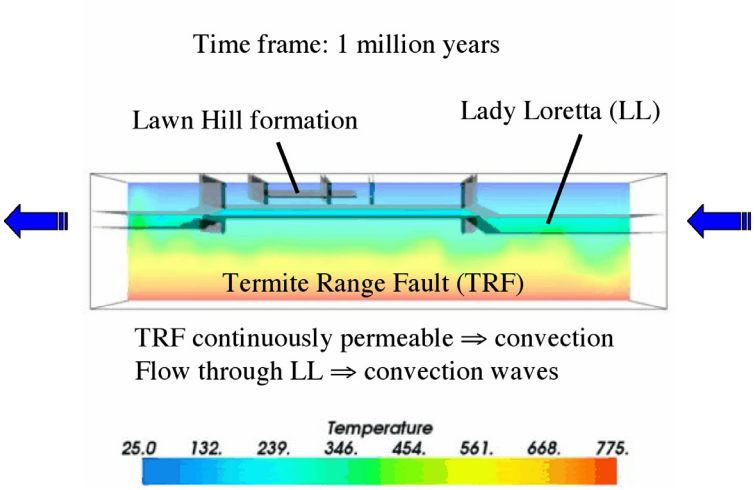

Figure 7-10. Conceptual set up of numerical experiment with convection in the Termite Range Fault (TRF) and forced fluid flow lateral through the Lady Loretta formation (LL). The Lawn Hill formation is the host of the Century deposit. Convection waves developing in TRF are propelled through the system from right to left propelled by the flux through LL.

Ord et al. (2002) assumed that thermal anomalies have been characteristic for the ore forming process. The temperature within the Lawn Hill formation is portrayed over time in Fig. 7-11. It is obvious that those temperature waves mentioned above lead to significant changes of temperature over time in the formation hosting the deposit.

As a result of the forced flux through Lady Loretta and the evolving convection in the system not only leads to temperature fluctuations but also to varying mixing ratios of different fluids in the Lawn Hill formation. Fluid scavenged from TRF has been observed to mix with fluid flowing along LL with time dependent mixing ratios.

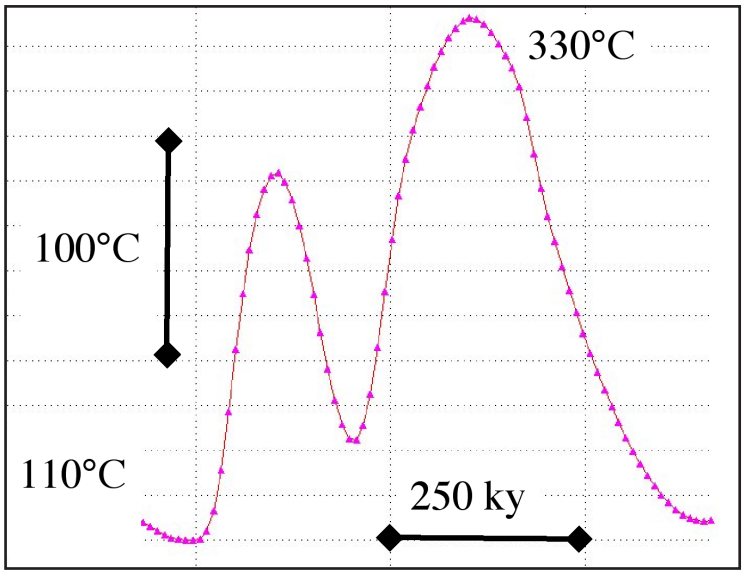

Figure 7-11. Time dependent thermal anomaly observed in the Lawn Hill formation.

Fluid flux through LL and bottom to top through TRF

The combination of both previous models, fluid flow through LL and upwards flow through TRF, has been investigated in the last conceptual model of the regional scale Century model. As before, convection in the TRF is completely suppressed by the upwards flow. The velocity vectors show (Fig. 7-12) that the upwards flow in TRF is bend towards the left hand side of the model because of the flow forced through LL. This results in a distinctive thermal signature, constant through time and space. The isotherms observed within the system are dragged up into TRF and show the initially applied geothermal gradient distal to TRF.

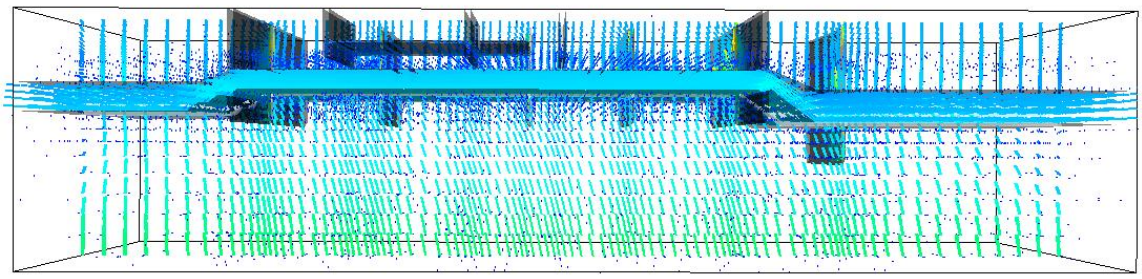

Figure 7-12. Fluid flow vectors within the Termite Range Fault (TRF) indicated the forced upward flow as they develop with additional lateral flow from right to left through the Lady Loretta formation (LL). Colors reflect Darcy fluxes from 1.0E-09 m s^{-1} (dark blue) to 5E-09 m s^{-1}(green).

Implications from conceptual hypotheses

The conceptual models about potential major flow regimes and how they have been set up in the numerical models via distinct boundary conditions has important effects for resulting fluid flow fields mutually coupled with the development of thermal pattern in the system:

- A continuous permeability throughout the entire depth of TRF, here 25 km, combined with a minimum permeability of around 1.0E-16 m^2 ensures that free thermal convection occurs within TRF.
- Lateral flow (Darcy flux 1.0E-09 m s^{-1}) through TRF reduces the number of convection cells developing within TRF.

- Vertical flow (Darcy flux 1.0E-09 m s^{-1}) through TRF from bottom to top suppresses any convection cell development. Fluid flow is activated in the second order faults perpendicular to TRF.
- Lateral flow (Darcy flux 1.0E-09 m s^{-1}) through LL combined with convection developing in TRF result in waves of thermal anomalies migrating through the system in the same direction. Those waves lead to thermal anomalies in the Lawn Hill formation varying with time.
- With combined lateral flow through LL and vertical flow through TRF any kind of convection is suppressed. Thermal anomalies are restricted to TRF and are constant in time and space.

Mount Isa – deposit scale

Location of the Mount Isa mine is shown in Fig. 7-2. The stratigraphic model of the Mount Isa mine scale architecture is generated from surfaces, which represent faults and stratigraphic contacts (Fig. 7-13, Gessner 2005). The Mount Isa Copper deposit, shown in silver-grey colour, is hosted in the matrix of the partly brecciated, steeply dipping and layered Urquhart shale, which bounds the complex-shaped Paroo fault.

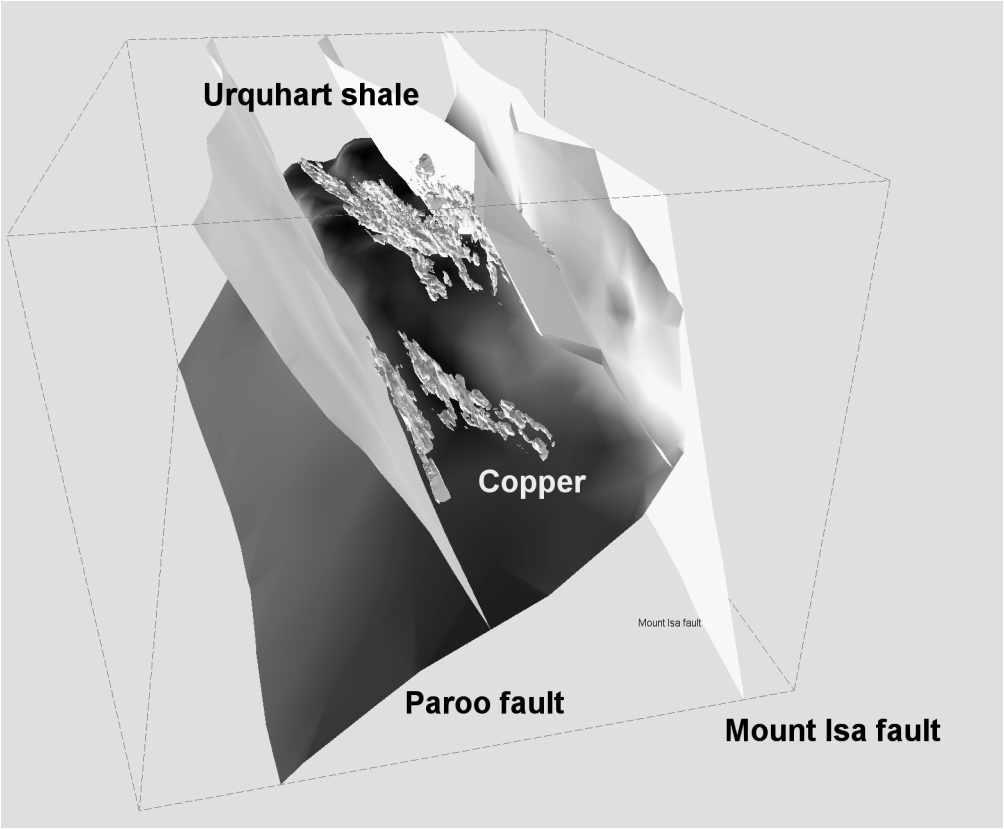

Figure 7-13. Geometry of the mine scale model. Surfaces shown are faults and stratigraphic boundaries. The Mount Isa Copper deposit (silver grey colour, Cu grade >2.5 %) is hosted in the matrix of the partly brecciated, steeply dipping and layered Urquhart shale, which bounds the complex-shaped Paroo fault. The bounding box of the faults measures 5429 m by 3734 m by 2974 m.

Gessner et al. (2005) showed that strength contrast of the layered rock and different orientations of rheological anisotropy controlled fracturing and brecciation. The layering within and between rock types results in heterogeneous and anisotropic deformation, which in turn influences the permeability distribution and creates a network of fluid pathways. These fractured zones with higher permeabilities than the surrounding rock mass are in this case the Mount Isa and Paroo fault zones and the partly brecciated Urquhart shale. Gessner et al. (2005) concluded that hydrothermal convection is a possible process that may have driven fluid flow under the assumption that pronounced deformation and partial fracturing of the Urquhart shale provided a high permeability zone close to the Paroo fault.

Numerical model

The numerical model (Fig. 7-14) has been built from the geological model shown in Fig. 7-13. The stratigraphic model of Mount Isa has been discretized for numerical simulations into 49 x 49 x 21 cells, each of them with a size of 124.45 m x 110.79 m x 141.6 m. The entire model measures 6098 m W-E direction, 5429 m in N-S, and 2974 m from top to bottom (a number of extended models have been set up which are described below).

The Mount Isa numerical model contains eight geological units (Table 7-1): the Eastern Creek Volcanics (ECV), the Lena quartzite which is actually a part of the ECV, the Moondarra siltstone, the Breakaway shale, the Native Bee siltstone, the Urquhart shale, the Kennedy-Spear siltstone, and finally the Paroo and Mount Isa faults. The Mount Isa fault is almost vertical running from top to bottom of the model and is aligned over the entire length of the model in north-south direction. Its thickness ranges from about 100 m to 300 m. The Paroo fault branches off the Mount Isa fault on its eastern side, half way up the model, and is dipping east. The Paroo fault has a different shape at the northern end of the model (Fig. 7-14A) compared to the southern end (Fig. 7-14B). The contact between the Mount Isa and Paroo faults and the dip angle of the Paroo fault also vary throughout the model. The Urquhart shale and all other stratigraphic units, forming the Mount Isa group, are in a similar steeply west-dipping position like the Mount Isa fault itself, all bounded in the oldest geological unit, the ECV. The Mount Isa group is a Middle Proterozoic series of carbon-rich siliciclastic sediments and carbonates.

Geological unit	Lithology	Permeability [m_]
Faults	-	7.5E-15
Kennedy Spear	Dolomitic siltstone	3.0E-16
Urquhart shale	Pyritic and dolomitic shale	1.5E-16 - 7.5E-15
Native Bee siltstone	Siltstone, shale	3.0E-16
Breakaway shale	Siliceous and carbonaceous shale	1.5E-16
Moondarra siltstone	Siltstone, shale	3.0E-16
Eastern Creek Volcanics	Metabasalt, metasediments	1.5E-16
Lena quartzite	Felspathic and quartz sandstone	1.5E-15
Low permeability patches	-	7.5E-18

Table 7-1. Lithologies (after Blake 1987) and intrinsic permeabilities of different rock types in the Mount Isa model

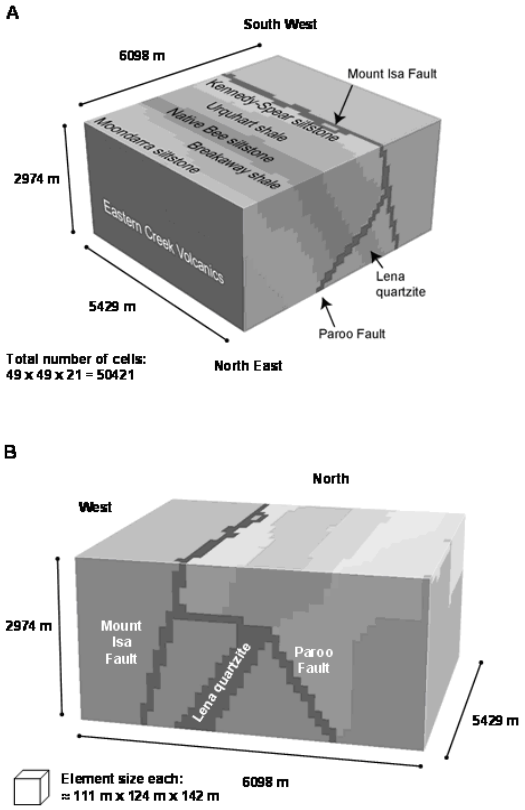

Figure 7-14 Numerical model of the Mount Isa three dimensional architecture built from the stratigraphic model (Fig. 7-13). The model domain is 6098 m W-E, 5429 m N-S, and 2974 m high, discretized into 50421 elements. Each element measures roughly 124 x 111 x 142 m. The stratigraphy is subdivided into eight geological units (Table 1). The Paroo fault branches from the Mount Isa fault on its eastern side, half way up the model, and is dipping east. The slope of the Paroo fault varies in shape at the northern end of the model (top) compared to the southern end (bottom).

The conceptual outline of the numerical model is shown in Fig. 7-15. Displayed are the major potential fluid pathways, the Mount Isa fault, the Paroo fault, and the Urquhart shale. Permeabilities assigned to the geological units are given in Table 7-1.

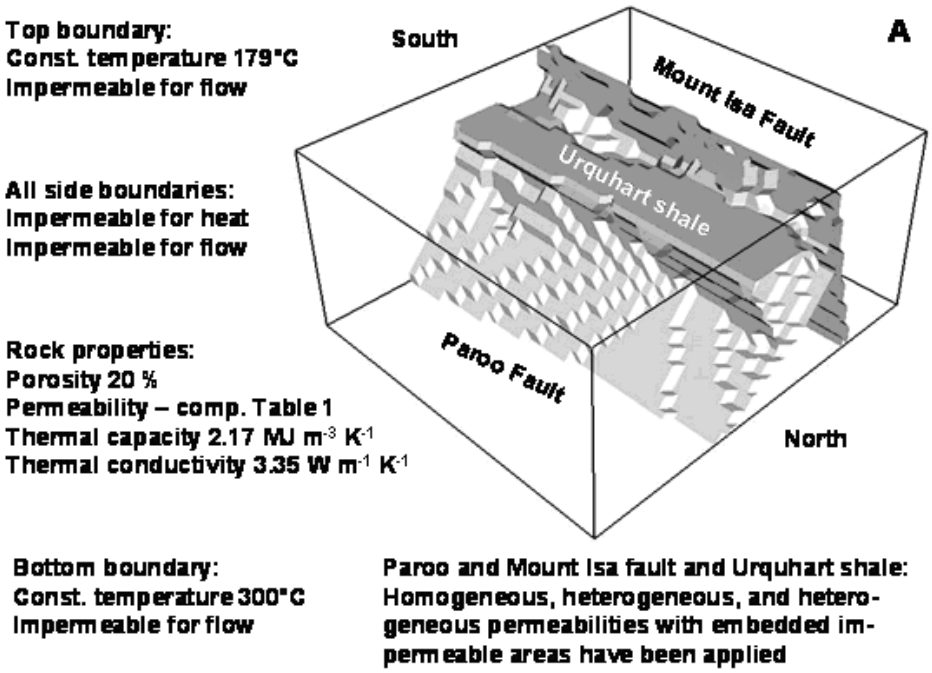

Figure 7-15. Conceptual outline of numerical studies with model properties and boundary conditions. Major units with significant hydraulic conductivity are the Mount Isa and Paroo faults and the partly brecciated Urquhart shale. Scenarios with homogeneous and heterogeneous permeability distributions as well as additional low permeability patches within those three geological units have been conducted. The system is heated from below and cooled from the top with constant temperature boundaries. All boundaries are impermeable for fluid flow.

Convection flow pattern with respect to Mount Isa

One part in solving the puzzle of reverse-engineering a mineralised system to understand ore depositional processes and subsequently to build predictive modelling capabilities is the determination of the fluid flow driver. Free thermal convection has been investigated in this study as a possible fluid flow driving process based on the findings of Gessner et al. (2005), who studied the structural and stratigraphic architecture and the geotectonic history of the hydrothermal system at Mount Isa.

The simulation package SHEMAT / Processing SHEMAT (Clauser 2003) has been applied to examine the effect of heterogenous permeability distributions on free Rayleigh convection around the Mount Isa mine. Two scales of permeability heterogeneity were investigated. Firstly heterogeneity introduced by stratigraphy and secondly different heterogeneous permeability distributions assigned to major geological structures. Furthermore, low permeability patches were defined within those stratigraphic units to account for even more complexity.

The architecture is characterized by the Mount Isa and Paroo fault zones and the partly brecciated and therefore highly permeable Urquhart shale. Faults and shale act as aquifers, controlling the fluid flow patterns, in a domain of surrounding rocks with otherwise low hydraulic conductivity.

It is impossible to accurately determine the Rayleigh number (Ra) for a model with complex geometries such as Mount Isa, because no analytical solution can be derived. However, from a simplified theory of Ra one could expect free thermal convection occurring in the Mount Isa fault plane (Ra 52) but not in the Paroo fault (Ra 35). The fact that one number is above and one below the critical Ra and yet convection occurs in both faults, underlines that numerical simulation of the hydraulic conditions in the Mount Isa system is essential to determine and understand if and under which circumstances free convection could have been a fluid flow driver. This study has focused on convection under consideration of heterogeneous permeability distributions, including application of low permeability patches along fluid pathways. The following

conclusions can be drawn from results of numerical simulations:

- Flow pattern and temperature distribution in a system with small-scale, uniform heterogeneity within stratigraphic units can be approximated by models with homogeneous permeability in each unit equal to the average permeability of the heterogeneous distribution.
- Increasing volumes of non-continuous permeability along fluid pathways, due to impermeable patches, first reverses the direction of convection (15 % vol.%) and finally shuts it down completely (30 vol.%).
- The dipping, wedge shaped portion of the brecciated and therefore permeable Urquhart shale governs fluid flow to an extent where it spatially attracts a convection cell, irrespective of the volume of adjacent permeable units (Fig. 7-16).
- Even in a complex and heterogeneous system with patches of low permeability along fluid pathways, the Rayleigh number can be used to determine whether free convection will occur or not.

These results emphasize that free convection in hydrothermal systems is highly sensitive to the 3D permeability distribution in the geological architecture, and that the fluid flow patterns can only be predicted using numerical methods.

Quartz body – field observations vs. numerical simulation

One distinct feature of the Mount Isa Fe-sulphide copper mineralising system is a massive silica body in the Urquhart shale (Fig. 7-17), which predates the copper deposit. Quartz occurs mainly as an infill in veins and breccias, suggesting high fracture permeability at the time of quartz formation. The combination of locally high fracture permeability and an inferred high geotherm may be sufficient for hydrothermal convection to occur on the scale of the mineralised system. Reactive transport simulation of the quartz rock alteration patterns has been used to test whether the convection scenario can reproduce the silicification observed in the field. This has been done in comparison with models in which topographically driven flow up the faults is the major fluid flow driving process.

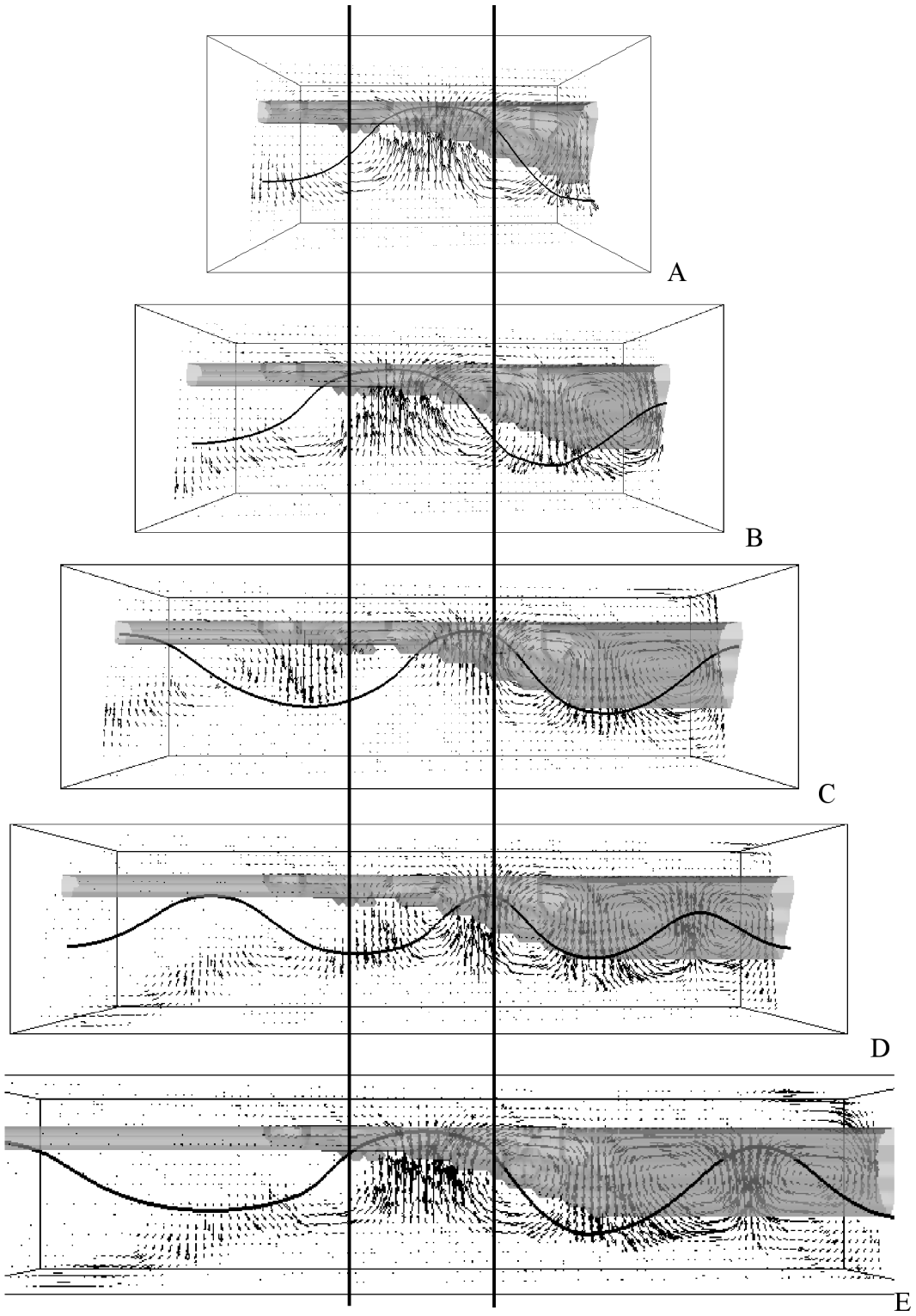

Figure 7-16. Comparison of flow patterns in the extended models with the reference model. Basis model has been extended North and South by roughly 1000, 2000, 3000, and 4000 m in each direction. Flow fields are displayed as vectors in a N-S vertical cut plane tracing apparent flow directions at the intersection between the Paroo fault and the Urquhart shale. The black line represents the 240°C isotherm within the vector cut plane. The dipping portion of the Urquhart shale (grey, for clarity the faults are not shown) attracts a clock wise turning convection cell.

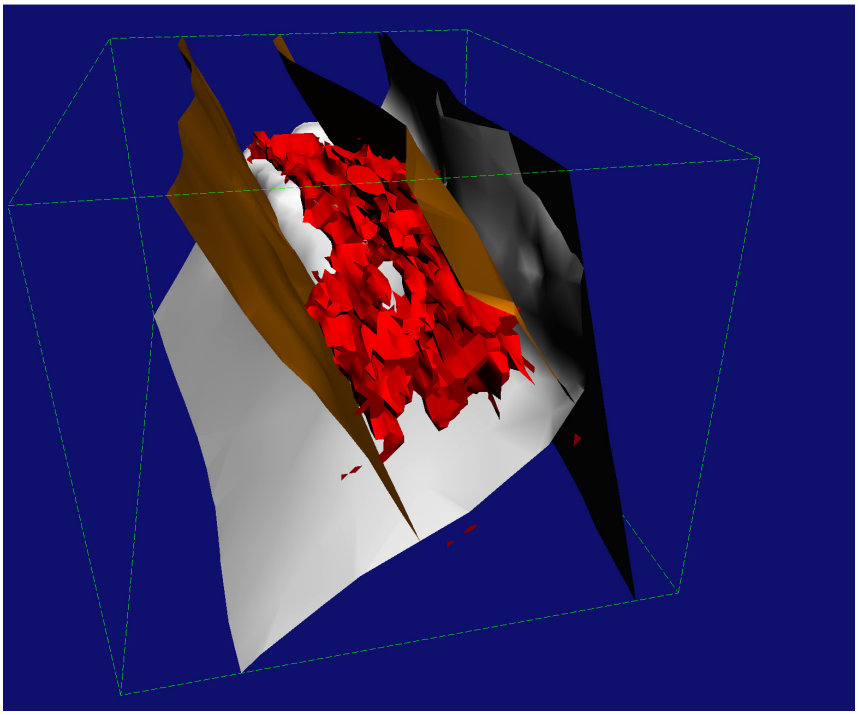

Figure 7-17. The silica body (red colour) is hosted in the matrix of the partly brecciated, steeply dipping and layered Urquhart shale, which bounds the complex-shaped Paroo fault.

As mentioned in the previous section permeability distribution is the controlling factor for convection and that in turn governs mineral alteration patterns. In Mount Isa a massive silica body occurs immediately above the Paroo fault, near the centre of the modelled architecture (Fig. 7-17). Reactive transport modelling has been applied to deepen the understanding of how the quartz body might have formed.

Fig. 7-18A refers to the convection scenario with homogeneous permeability distribution as described in Table 7-1 and displays a simulated silicification which is similar in shape, size, and location to the field observations (Fig. 7-17). The resulting quartz body of the second case study also with homogeneous permeability (Fig. 7-18B) but with forced flux as a fluid flow driver produces an even better match. Fig. 7-18C and Fig. 7-18D show the equivalent cases with heterogeneous permeability distribution in the faults and the Urquhart shale. It can be seen that only in the case of forced flux the resulting silicification provides a pattern still very similar to the real world. In the convection model with heterogeneous permeability distribution the silica body is cut into two with the major central part free of quartz precipitation. For the sake of completeness Fig. 7-18E underlines the fact that for an unbrecciated Urquhart shale with low permeability and resulting reversed convection there isn't any relevant quartz precipitation in the Urquhart shale at all. The last example Fig. 7-18F reflects the case with heterogeneous permeability distribution as well as 50 vol. % of impermeable patches along the fluid pathways for the forced flux scenario. It has to be noted that in this case free thermal convection is completely suppressed. Only forced flux is a relevant fluid flow driver in the Mount Isa system under these conditions. Even here a close match between numerical and field studies is observed.

It can be concluded that only one specific convection mode is capable of producing a quartz body in the Urquhart shale which is close to the field observations whereas any forced flux model produces a silicification very similar to it.

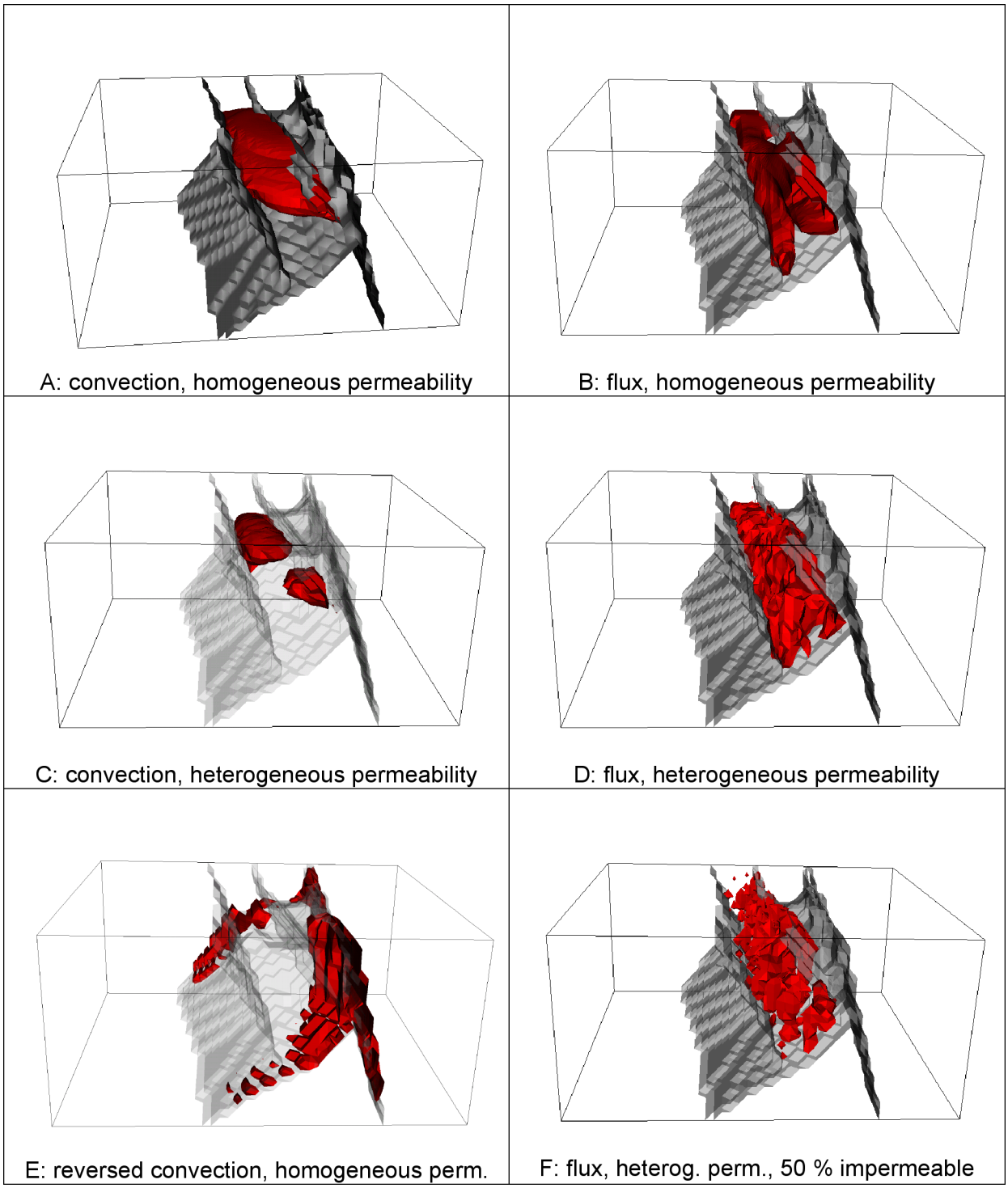

Figure 7-18 Quartz silica bodies determined from reactive transport simulations for varying permeability distributions (rows) and different fluid flow drivers (columns). Cases A and B refer to a homogeneous permeability distribution, C and D to a heterogeneous distribution, E to a homogeneous distribution but an unbrecciated Urquhart shale with low permeability, and F to a heterogeneous distribution with 50 vol. % of impermeable patches in the Urquhart shale. The left column shows the convection and the right column the forced flux scenarios.

Convection and fluid mixing

Two major hypotheses exist, which chemical process might have lead to the formation of the Mount Isa ore deposit. One potent mechanism for precipitating copper in the system is fluid mixing as demonstrated by reactor style geochemical modelling. Hence, a series of simulations based on the model with variable permeability distribution in the Urquhart shale (shown above) was focused on evolving fluid mixing ratios in the model domain and especially the Urquhart shale. Different scenarios of flow driven by hydraulic gradients, free thermal convection, or mixed convection processes were studied to determine the potential role of fluid mixing as major chemical mechanism resulting in ore deposition.

The model set up was as such that under varying flow regimes a basinal brine entered the domain from the top, through the Mount Isa fault, and / or two different basement brines flowed from the bottom into the system, one through the Parroo and the other through the Mount Isa fault. The model was initially filled with formation water (Fig. 7-19).

The particular monitoring point shown below is located in the centre of the Urquhart shale and round about 500 m down from the top and 500 m above the Paroo fault. It can be seen that after approximately 400,000 years the convection is in a steady state indicated by the temperature evolution shown in magenta. The formation fluid displayed in bright green is pushed away by the entering fluids until constant conditions are almost reached after 1 million years. Main contribution comes in this case from the basinal brine, in orange, with some 55%.

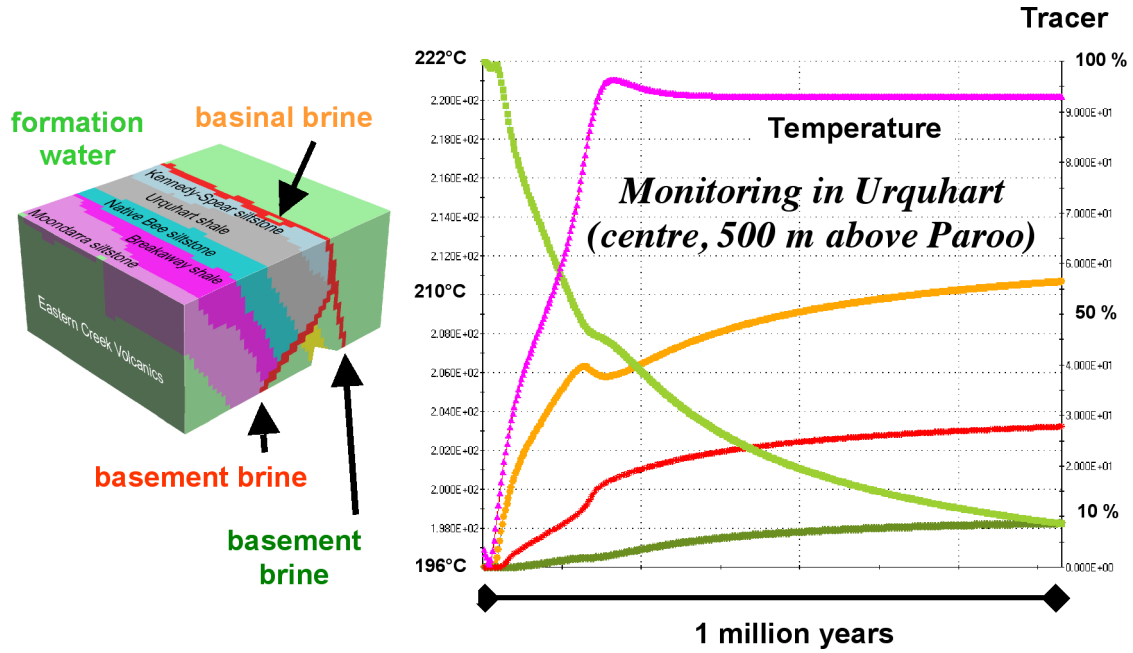

Figure 7-19 Monitoring of fluid mixing in the Urquhart shale during a time period of 1 million years. Two different basinal brines can enter the model from the bottom and a basinal brine from the top. The system is initially filled with formation water.

The main results of the fluid-mixing scenarios summarized from all simulations performed are:

- With convection the major flow direction, up the faults or down the faults controls the mixing ratios.
- Any time water is coming up Paroo the mixing ratios in the Urquhart shale are dominated by the basement fluid.
- The contribution of the basinal brine is up to 60%, when the major flow direction is downwards the Mount Isa fault.
- Without any convection, in case of fluid flow exceptionally forced from outside through the faults, no mixing can be observed in the Urquhart shale.

Chalcopyrite deposition due to basinal brine intrusion

The second potential mechanism of ore deposition is wall rock reaction. The hypothesis in this case is a copper bearing basinal brine intruding the model from the top (personal communication Anyd Wilde). A cross section from the central part of the Mount Isa 3D model has been cut out and applied to 2D reactive transport simulations. The configuration with a fluid pathway for the basinal brine, coming from the top of the model,

through the upper part of the Mount Isa fault and the Paroo fault (bottom part of Mount Isa fault impermeable, closed for fluid flow) is as shown in Fig. 7-20.

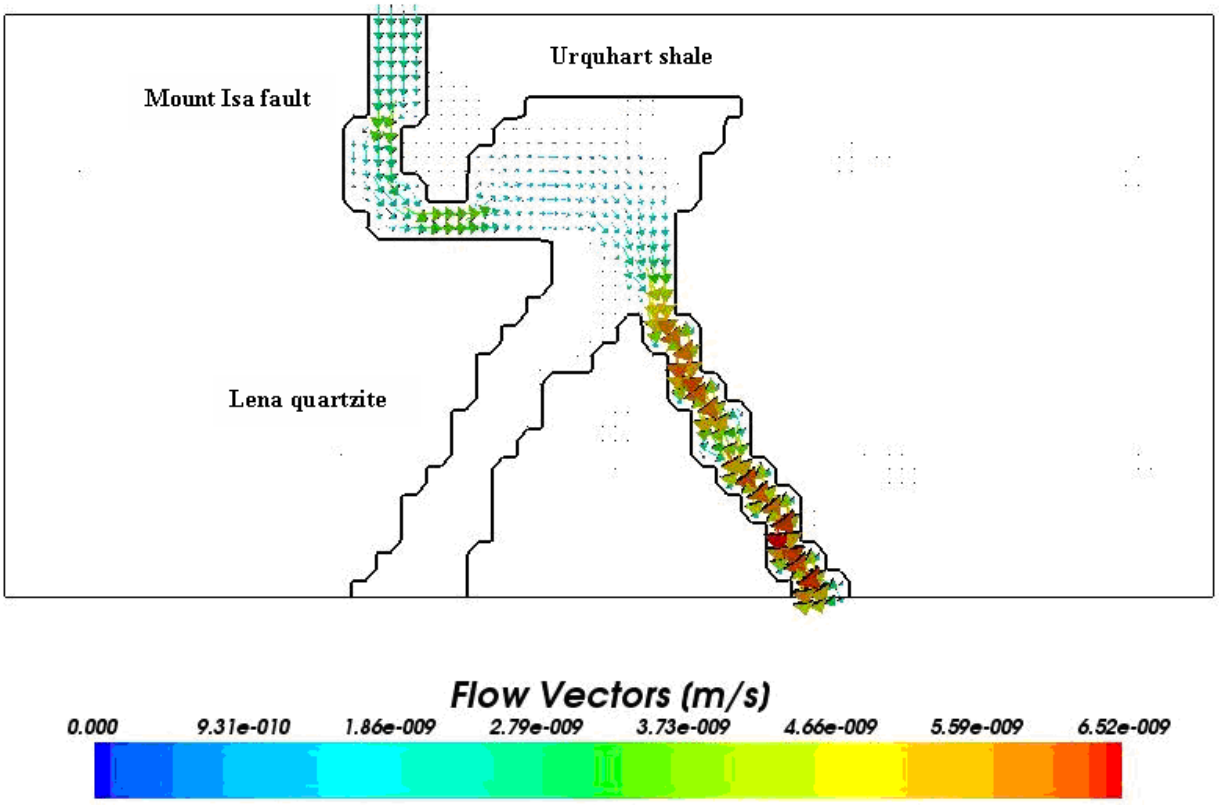

Figure 7-20. Central cross section cut out of the 3D Mount Isa model with basinal brine entering the system from the top and flowing down the Mount Isa fault, through the brecciated parts of the Urquhart shale and down the Paroo fault. The black line represents the isosurface of medium permeability delineating the faults, the Urquhart shale, and the Lena quartzite.

The resulting flow field of the model shows how the basinal brine enters the system through the Mount Isa fault and partly flushes the Urquhart shale on its way through the model. This is the result of permeability initialisation with 7.5E-15 m2 in the Mount Isa and Paroo fault as well as in the brecciated Urquhart shale in the part adjacent to the Paroo fault. From there the permeability in the Urquhart shale is decreasing, away from the fault towards the top of the model. Permeability is decreasing down to country rock values of 1.5E-16 m2. The black lines mark a medium permeability of 1.3E-15 m2 which includes the faults, parts of the Urquhart shale, and the Lena quartzite. The lower part of the Mount Isa fault has been defined impermeable to get the flow mainly through the Paroo fault and the Urquhart shale.

The mineral assemblage of the reactive transport model has been defined following Waring (1990) with a composition of supposedly unaltered Urquhart shale:

- quartz / ankerite / chlorite / k-feldspar (>10%)
- pyrite / calcite / graphite / albite (<10%)

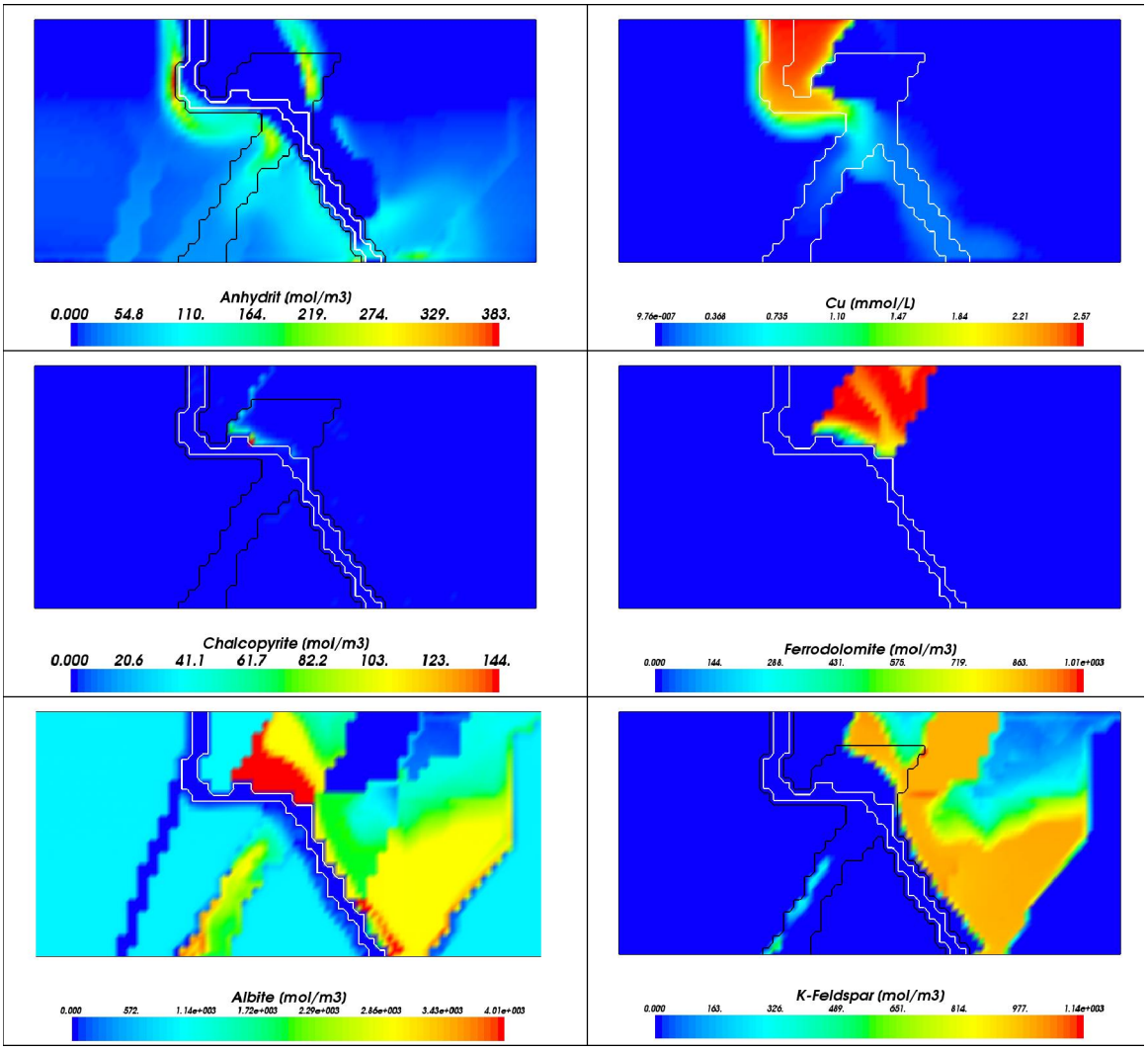

Figure 7-21. Mineral alteration pattern after 100,000 years of copper bearing basinal brine intrusion into the Urquhart shale through Mount Isa and Paroo fault. Anhydrite reflects the redox gradient between the basinal brine and the basement brine (formation water). Chalcopyrite precipitates in the Urquhart shale while ferrodolomite (ankerite) is dissolved. Albitization is observed while K-feldspar is dissolved.

A couple of potential precipitates following water-rock interactions between the basinal brine and the unaltered Urquhart shale have been determined via batch reaction calculations. As a result the following mineral assemblage has been defined to be in permanent thermodynamic equilibrium with the fluids in the system:

- albite / anhydrite / calcite / chalcopyrite / chlorite / dolomite / ferrodolomite / graphite / K-feldspar / kaolinite / magnetite / muscovite / phlogopite / pyrite / quartz / talc

Potential precipitates are initialised with zero amounts. Initially abundant minerals are defined, according to the reactive alteration index philosophy, with 1000 mol m-3 (Quartz 10,000). The “Rock Alteration Index” (RAI) provides a measure of rock alteration with regard to a mineral phase being dissolved or precipitated within the investigated system. For that purpose same amounts of minerals are initially defined disregarding the exact mineral rock composition. Mineral amounts above the initial one display precipitation and below dissolution.

The model was run for roughly 100,000 years. The resulting mineralisation pattern show that anhydrite precipitates on the fringes of the flowing to the stagnant system where intruding basinal brine and the formation water, the basement brine, get to meet each other and mix (Fig. 7-21, top left). The white lines mark the permable faults and the black line areas of medium permeability. The anhydrite mineralisation pattern represents a redox gradient because the basinal brine is oxidized and the basement brine is reduced. After the first 100,000 years the copper concentration is high as in the basinal brine down to the Urquhart shale (Fig. 7-21, top right). Chalcopyrite has precipitated in the Urquhart shale close to the Paroo fault and

along the boundary to the Kennedy Spear siltstone (Fig. 7-21, centre left). Albite has precipitated in the area up to medium permeabilities in the Urquhart shale (Fig. 7-21, bottom left) on the expense of K-feldspar which has been dissolved (Fig. 7-21, bottom right). There are no significant amounts of dolomite observed in the Urquhart shale and ferrodolomite (ankerite, Fig. 7-21, centre right) is dissolved as well as calcite is precipitated.

Mount Isa – thin section scale

This generic experiment investigates the idea that an ion, a water molecule, or even a small package of mineralised solution can only react with one mineral at a time because it can only be at one location at a time. In “normal” reactive transport simulation space a specific but averaged mineral assemblage is considered for one model element or cell of finite size. We homogenise in that way a big bunch of rock because we are forced to quite coarse discretization to have applicable numbers of cells for our simulations. However, the history of a water package getting into contact with distinct minerals in a certain sequence might be important to understand the chemistry of the ore mineralisation process.

The model described here is on the scale of 1 cm by 3 cm and discretized into 1 mm by 1 mm cells. Taking the mineral composition of the unaltered Urquhart as determined by Waring (1990) and based on a random distribution the model elements have been assigned to distinct minerals:

- 30 % quartz (dark blue color)
- 32 % ankerite (ferrodolomite, green)
- 15 % chlorite (red)
- 12 % K-feldspar (magenta)
- 5 % pyrite (dark green brownish)
- 2 % calcite (light blue)
- 1 % graphite (turquoise)
- 3 % albite (grey)

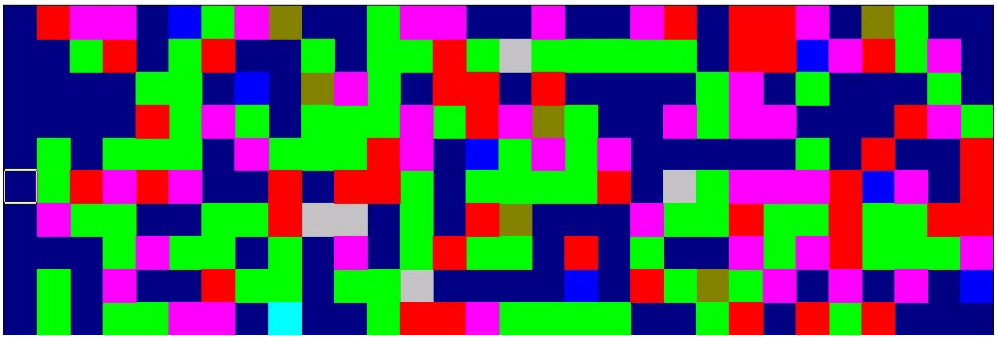

Figure 7-22. Thin section scale model of 3 cm by 1cm with cell sizes of 1 mm by 1 mm with a random distribution of mineral amounts after Waring (1990).

The fluid is send through the model, from the left end to the right, with a Darcy flux of 1.0E-06 m s^{-1}. The temperature has been kept constant at 200°C because it is assumed that on a cm scale the temperature does not change significantly and to concentrate on purely chemical gradients across the model.

After 0.1 days the copper reaction front can be seen half way through the model. The non-reactive tracer (not shown here) has just reached the outlet of the core after this period of time. Due to the reaction processes between the incoming basinal brine, the rock, and the previously abundant basement brine the chemical reaction front is retarded compared to the pure transport of non-reacting substances. The copper concentration is shown in contour colours from zero (blue) to maximum basinal brine Cu contents (red).

The initial and final distribution of the mineral phases is shown below in Fig. 7-25. The red contour color refers to the maximum concentration (as indicated). An initial abundance of 100 mol m^{-3} has been arbitrarily chosen to reflect the rock alteration index. The blue color shows an amount of zero of the specific mineral. Like the models on the deposit scale the thin section scale investigated here shows albitization on the

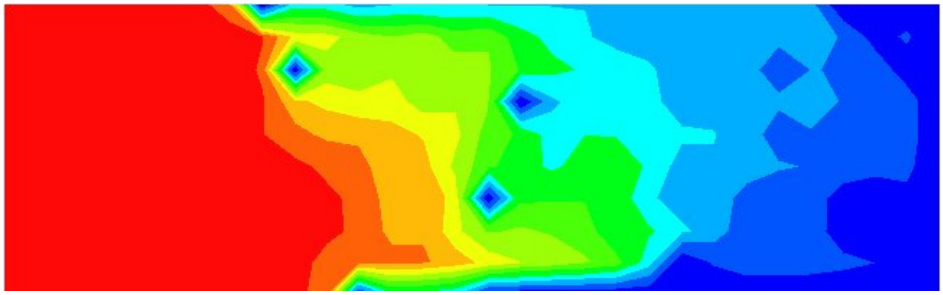

Figure 7-23. Copper reaction front with Cu concentrations from 0.0 mmol L^{-1} (dark blue) up to the concentration within the intruding basinal brine of 2.5 mmol L^{-1} (red). Pyrite is a sink for copper and highest concentrations of chalcopyrite are produced there. The copper front cannot move on until pyrite is completely dissolved.

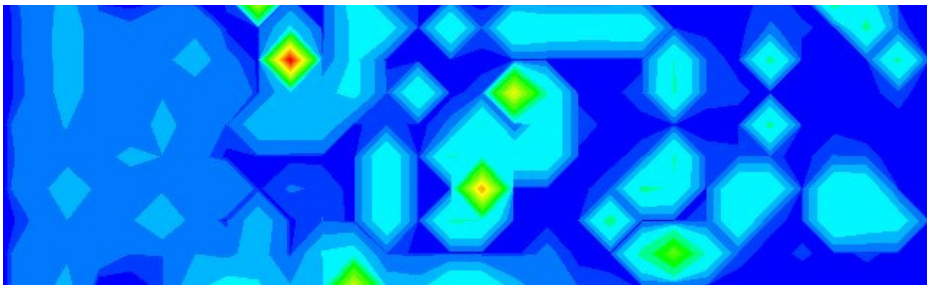

Figure 7-24. Resulting chalcopyrite concentration. Highest concentrations (23.2 mol m-3, red) are observed where pyrite was abundant (Fig. 7-22).

expense of K-feldspar dissolution (Fig. 7-25). Ferrodolomite (ankerite) abundant with initially 32% is unstable and dissolves with regard to the formation water, the basement brine. At the thin section inlet (left hand side) ferrodolomite remains as defined. In contrast, calcite is stable with regard to the basement brine and

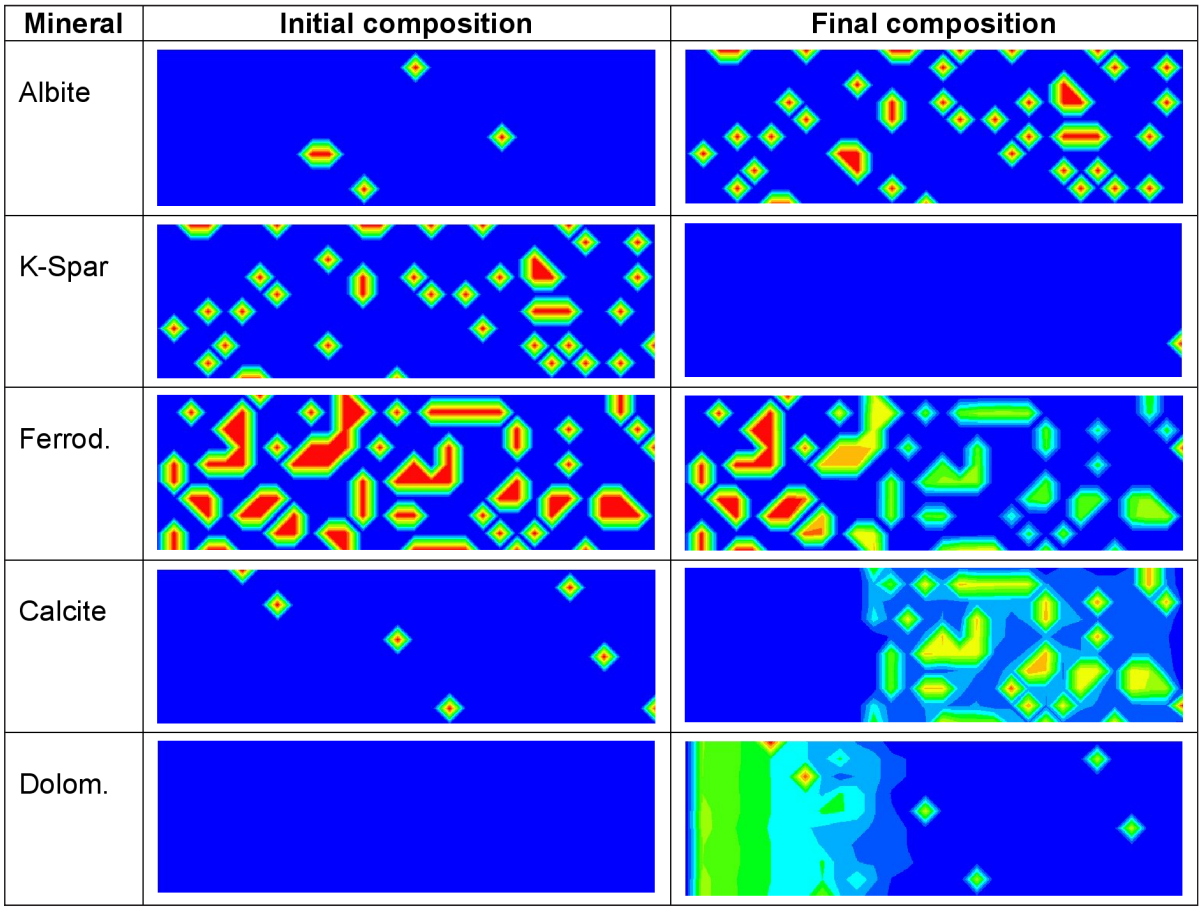

Figure 7-25. Mineral alteration pattern in comparison to the initial mineral abundance for the thin section scale model (3 cm x 1 cm).

precipitates towards the outlet of the core whereas the initially abundant amount of 2% is dissolved at the inlet. At the same time dolomite precipitates in the area of the thin section which is dominated by the intruding basinal brine.

Summary

Following the mission of the ***pmd**CRC* to move the understanding of mineralising systems beyond the acquisition of information and especially towards numerical modelling across all scales the interface between SHEMAT (Clauser 2003) and PHREEQC (Parkhurst and Appelo 1999) has been finished within the sub-project 'Codes Development' of F1-F2. The code SHEMAT-PHREEQC offers now the capability to study reactive transport processes relevant for ore deposition. This new tool has been equipped with thermodynamic data transferred from UNITHERM (Shvarov and Bastrakov 1999) via the newly developed code UT2Chem.

SHEMAT and SHEMAT-PHREEQC have been applied for fluid flow and heat transport modelling as well as reactive transport on the terranes of Century and Mount Isa. It has been shown how modelling on different scales (regional, deposit, and thin section scale) can be applied to test various hypotheses. Following the '5 questions' (Ord et al. 2002) numerical experiments have been performed to specifically investigate what processes were driving fluid flow and what the mechanism of ore deposition was.

With the conceptual models of Century on the regional scale (100 km x 50 km x 25 km) it has been shown that a continuous permeability throughout the entire depth of the Termite Range Fault (TRF) combined with a minimum permeability of around 1.0E-16 m^2 ensures that free thermal convection occurs within TRF. Lateral flow (Darcy flux 1.0E-09 m s^{-1}) through TRF reduces the number of convection cells developing within TRF. Vertical flow (Darcy flux 1.0E-09 m s^{-1}) through TRF from bottom to top suppresses any convection cell development. Fluid flow is also activated in the second order faults perpendicular to TRF. Lateral flow (Darcy flux 1.0E-09 m s^{-1}) through LL combined with convection developing in TRF result in waves of thermal anomalies migrating through the system in the same direction. Those waves lead to thermal anomalies in the Lawn Hill formation varying with time. With combined lateral flow through LL and vertical flow through TRF any kind of convection is suppressed. Thermal anomalies are restricted to TRF and are constant in time and space.

The study of Mount Isa on the deposit scale (6098 m x 5429 m x 2974 m) has focused on convection under consideration of heterogeneous permeability distributions. It was shown that flow pattern and temperature distribution in a system with small-scale, uniform heterogeneity within stratigraphic units can be approximated by models with homogeneous permeability in each unit equal to the average permeability of the heterogeneous distribution. Increasing volumes of non-continuous permeability along fluid pathways, due to impermeable patches, first reverses the direction of convection (15% vol.%) and finally shuts it down completely (30 vol.%). The dipping, wedge shaped portion of the brecciated and therefore permeable Urquhart shale governs fluid flow to an extent where it spatially attracts a convection cell, irrespective of the volume of adjacent permeable units.

One distinct feature of the Mount Isa mineralising system is a massive silica body in the Urquhart shale. Quartz occurs here mainly as an infill in veins and breccias. Further reactive transport simulations on the deposit scale reveal that only one specific mode of free thermal convection is capable of producing a quartz body in the Urquhart shale which is close to the field observations whereas any forced flux model produces a silicification very similar to it.

In a 2D study, with a cross section cut out of the 3D Mount Isa system, the intrusion of basinal brine through the top of the Mount Isa fault has been investigated to understand mineral alteration pattern better and to work out the mineral precipitation process of chalcopyrite. Chalcopyrite has been observed to precipitate in the Urquhart shale close to the Paroo fault. Albite has precipitated in the area up to medium permeabilities in the Urquhart shale on the expense of K-feldspar which has been dissolved.

Models on the thin section scale (3 cm x 1 cm) have been conducted to investigate the chemical process of mineral precipitation. This generic experiment investigates the idea that a mineralised solution can only react with one mineral at a time because it can only be at one location at a time. The micro scale simulations show a thermodynamic importance of pyrite. Pyrite is a sink for copper coming from the intruding basinal brine and produces the highest grades. The copper reaction front is only able to move on when pyrite has been entirely dissolved. This is why the reaction front trails behind the front of non-reactive tracers.

Reverse-engineering of existing ore deposits of specific regions and commodities is of major importance to subsequently produce a tool as well as an understanding for predictive mineral discovery.

References

Anderson MP, Woessner WW (1992) Applied Groundwater modelling. Simulation of flow and advective transport. Academic Press, London, 381 pp

Andrews SJ (1998) Stratigraphy and depositional setting of the upper McNamara Group, Lawn Hills region, Northwest Queensland. Economic Geology and the Bulletin of the Society of Economic Geologists 93, 1132–1152.

Bartels J, Kühn M, Schneider W, Clauser C, Pape H, Meyn, V, Lajczak I (2002) Core flooding laboratory experiment validates numerical simulation of induced permeability change in reservoir sandstone. Geophysical Research Letter 29(9), 10.1029/2002GL014901

Blake DH (1987) Geology of the Mount Isa Inlier and environs, Queensland and Northern Territory. BMR Bulletin, Geol. Geophys. Aust. 225: 83p

Chiang WH, Kinzelbach W (2001) 3D-Groundeater Modeling with PMWIN. Springer Verlag, Berlin

Clauser C (1988) Untersuchungen zur Trennung der konduktiven und konvektiven Anteile im Wärmetransport in einem Sedimentbecken am Beispiel des Oberrheintalgrabens. Doctoral Dissertation, Tech. Univ. Berlin, Fortschritt-Berichte VDI 19(28), VDI Verlag, Düsseldorf

Clauser C (2003) SHEMAT and Processing SHEMAT – Numerical simulation of reactive flow in hot aquifers, Springer Publishers, Heidelberg

Gessner K, Jones PA, Wilde AR (2005) Numerical models of strain localisation and fracturing in re-lation to hydrothermal mineralisation at Mount Isa, Australia. In: Buiter S, Schreuers G (eds) Geological Society Special Publications (submitted)

Kühn M (2004) Reactive Flow Modeling of Hydrothermal Systems. Lecture Notes in Earth Sciences 103, Springer Publishers, Heidelberg (Eng.D. thesis)

Kühn M, Bartels J, Pape H, Schneider W, Clauser C (2002) Modeling chemical brine-rock interaction in geothermal reservoirs. In: Stober I, Bucher K (eds), Water Rock Interaction, Kluwer Academic Publishers, Dordrecht, pp 147-169

Kühn M, Schneider W (2003) Injection well with reaction kinetics. In: Clauser C (ed) Numerical simulation of reactive flow in hot aquifers - SHEMAT and Processing SHEMAT, Springer Publishers, Heidelberg, pp 253-262

Lapwood ER (1948) Convection of fluids in a porous medium. Proceedings of the Cambridge Philosophical Society 44: 508-521

Ord A, Hobbs BE, Zhang Y, Broadbent GC, Brown M, Willetts G, Sorjonen-Ward P, Walshe JL, Zhao C (2002) Geodynamic modelling of the Century deposit, Mt Isa Province, Queensland, Australian Journal of Earth Science 49: 1011-1039

Parkhurst DL, Appelo CAJ (1999) User's guide to PHREEQC (version 2)--A computer program for speciation, batch-reaction, one-dimensional transport, and inverse geo-chemical calculations: U.S. Geological Survey Water-Resources Investigations Report 99-4259

Plummer LN, Parkhurst DL, Fleming GW, Dunkle SA (1988) A computer program incorporating Pitzer's equations for calculation of geochemical reactions in brines: U.S. Geological Survey Water-Resources Investigations Report 88-4153, 310 p.

Shvarov YV, Bastrakov EN (1999) HCh: a software package for geochemical equilibrium modelling (User's guide). Australian Geological Survey Organisation, Record 1999/25

Solomon M, Groves DI (1994) The geology and origin of Australia's mineral deposits. Oxford Mono-graphs on Geology and Geophysics, 28: 951 p

Spitz K, Moreno J (1996) A practical guide to Groundwater and Solute Transport Modelling. John Wiley & Sons Inc, New York, 461 pp

Trescott PC (1975) Documentation of Finite Difference Model for Simulation of Three-Dimensional Ground-Water Flow. U. S. Geol Survey Open File Rep 75-438, U. S. Geol Survey, Reston Va

Trescott PC, Larson SP (1977) Solution of the three-dimensional groundwater flow equations by using the strongly implicit procedure. J Hydrol 35: 49-60

Turcotte D, Schubert GL (2002) Geodynamics (2nd Edition): Cambridge, UK, Cambridge University Press: 456 pp

Waring CL (1990) Genesis of the Mt. Isa Cu Ore System. Department of Earth Sciences, Monash University, Clayton, Victoria (Ph.D. Thesis)

Weinstein HG, Stone HL, Kwan TV (1969) Iterative Procedure for Solution of Systems of Parabolic and Elliptic Equations in Three Dimensions. Industrial and Engineering Chemistry Fundamentals 8(2): 281-287

Chapter 8: Introduction to Thermodynamic Utilities

Evgeniy N. Bastrakov, James S. Cleverley and Nicholas H.S. Oliver

In addition to the terrain-based geochemical modeling undertaken by the F1-2 group, we developed a number of databases, utilities, and graphics packages to improve the access to and interconnections between diverse modeling programs and datasets.

These packages include:

FreeGs: a web-enabled thermodynamic database system initially based on the Unitherm dataset from HCh, and designed so that anyone using the Gibbs minimization approach to geochemical modeling can access the power of this large dataset. The FreeGs database stores data on thermodynamic properties of geologically important substances (minerals, gases and aqueous species). Currently it is the central core of all geochemical modeling in the ***pmd****CRC*. The database is complemented by an on-line "thermodynamic calculator" to derive some pressure-temperature dependent thermodynamic parameters from the stored values. During the second stage of ***pmd****CRC* the FreeGs system will be converted in a web service to serve data in multiple formats for a number of different geochemical modeling programs. The FreeGs system is part of the Virtual Centre for Geofluids and Thermodynamic data located at the Geoscience Australia web site:

http://www.ga.gov.au/minerals/research/methodology/geofluids/index.jsp

The Virtual centre for Geofluids has been developed in collaboration with the M4 database project.

2 Phase field developments: the challenging area of fluid unmixing is crucial to understand processes involved in lode-gold style deposits and IOCG deposits. The capacity to do this has been limited by the simplistic model for the two phase field assumed by users of the off-the-shelf geochemical modeling codes including HCh. The project has continued beyond the life of the F1-2 project and good progress has been made.

UT2K and K2GWB: these utilities were developed initially to allow users of Geochemists Workbench to access the Unitherm database, thus extending the range of possible P and T for modeling to the conditions covered by HCh users, i.e. 5 kb and 1000°C. The work since expanded to allow any 'log K'-based package to communicate with the Unitherm database, particularly including the SHEMAT code.

PIG: this is a graphics tool designed to speed up and greatly improve the appearance of output data from HCh. It has been particularly useful as a presentation tool for workshops, which otherwise previously required cumbersome exporting of HCh outputs into Excel.

ELF: This is a package that uses a template-style approach to HCh modeling. The user selects options from a variety of drop-down menus, HCh calculations are performed in the background, and outputs can be easily tabulated. It is intended to use for training and for HCh modeling where there are a large number of similar calculations required.

FreeGs: web-enabled thermodynamic database for modeling of geochemical processes

E.N. Bastrakov[1], Yu. Shvarov[2], L. Wyborn[1], S. Girvan[1], P. Scheffer[1], J. Cleverley[3], D. C. "Bear" McPhail[4]

*[1] Geoscience Australia & **pmd***CRC; [2] Moscow State University &**pmd***CRC; [3] James Cook University & **pmd***CRC; [4] Australian National University & CRC LEME*

The following information (with minor amendments) is based on the description of the FreeGs system available from the Virtual Centre for Geofluids and Thermodynamic Data located at the Geoscience Australia

web site:

http://www.ga.gov.au/minerals/research/methodology/geofluids/freegs_about.jsp

Up-to-date specifications of the FreeGs database system can be found from this site.

Summary

Using multiple computer packages for modeling geochemical processes requires standardisation of the thermodynamic data underpinning such calculations. This is especially true for work in a “virtual” collaborative environment, where remote researchers, with different skill sets and levels of thermodynamic literacy, work on the same or similar problems. Standardisation is hindered by multiple sources of recommended thermodynamic data, disparities in speciation models, different models for extrapolation of thermodynamic properties, and program-specific database formats. This situation often precludes the choice of the best (or the favourite) package for the problem at hand, or a comparison between performances of different packages on the basis of common data. The problem is further exacerbated by the tendency to collect and modify data on personal computers, resulting in multiple mutated data sets of variable quality and consistency. To overcome this problem, we have initiated the development of the FreeGs web-enabled database of thermodynamic properties hosted at Geoscience Australia. FreeGs aims to provide a single authoritative source available in real time to remote modeling applications via the Internet. This is one of the core activities of the Fluids and Modeling programs of the Predictive Mineral Discovery Cooperative Research Centre (***pmd**CRC*.) The initial FreeGs concept was suggested by the desktop UNITHERM database system that offers considerable flexibility in the choice of the data formats and integrated algorithms (Shvarov, 1999; Shvarov & Bastrakov, 1999). FreeGs contains mineral, gas, and aqueous species parameters that permit calculation of thermodynamic properties in a wide range of geological temperatures and pressures (0–1000°C, 1–5000 bar). It follows the main principle “multiple choices to multiple users”. There is a choice of the depth of the database interrogation (“casual” or “novice” user vs an expert); the choice of the data versions (“recommended” values for the species of interest vs all the available data); a choice of the available extrapolation models (equations of state); and a choice of formats of the output data. Storage and access to primary FreeGs data are already available via Web forms and reports.

An on-line software integrated with the FreeGs database (“FreeGs thermodynamic calculator”) enables users to calculate thermodynamic properties of species and chemical reactions at high T&P (eg, _g(T,P) or log Kr(T,P)).

The next step is development of a web-feature service (WFS) that will enable users to calculate thermodynamic properties of species and chemical reactions at high T&P and output the recalculated data to clients computers and applications using XML. To ensure effective database maintenance, a group of experts will remotely contribute to FreeGs via the Web. This group compiles the data from literature and e-datasets, evaluates their quality and ensures their reasonable consistency, and makes them available via web forms and reports. This part of the project is run in collaboration with the Cooperative Research Centre for Landscape, Environment and Minerals (CRC LEME) to guarantee the seamless integration between low- and high-temperature geochemical modeling.

The provided summary is based on Bastrakov et al. (2005) and Bastrakov et al. (2004).

FreeGs project, *pmd***CRC*, and geochemical community

FreeGs assists in meeting one of the long-term objectives for the ***pmd**CRC*: to create a computational environment to simulate the 4D evolution of mineral systems. An integral part of such simulation is modeling of geochemical processes over a wide range of temperatures and pressures.

Although primarily serving the ***pmd**CRC*, we believe that FreeGs can benefit the wider geochemical community. Most of FreeGs thermodynamic data can be interrogated by the general public. In turn, we expect that the ***pmd**CRC* will benefit from feedback and contributions by the external geochemical community.

The ultimate vision of FreeGs is as an online collaborative tool for exchange of thermodynamic data between interested geochemists.

FreeGs data

The initial FreeGs concept was inspired by the desktop UNITHERM database system for the HCh package for geochemical modeling. UNITHERM offers considerable flexibility in the choice of the data formats and integrated algorithms for calculation of thermodynamic properties (Shvarov, 1999; Shvarov & Bastrakov, 1999).

FreeGs contains mineral, gas, and aqueous species parameters that permit calculation of thermodynamic properties over a wide range of geological temperatures and pressures (0–1000°C, 1–5000 bar). The initial set of thermodynamic models and calculation algorithms implemented in FreeGs were selectively extracted from UNITHERM. This set will be extended beyond the current UNITHERM capabilities within the second half of the ***pmd****CRC*.

Though FreeGs aims to provide a single authoritative source of thermodynamic data for the ***pmd****CRC* community, it follows the main principle of "multiple choices to multiple users". There are choices of

- the depth of the database interrogation ("casual" or "novice" user vs an "expert")
- the data versions ("recommended" values for the species of interest vs all the available data)
- the available extrapolation models (equations of state)
- formats of the output data (yet to be implemented)

FreeGs is NOT a self-consistent database of thermodynamic properties, nor is internal consistency the goal of the project, though we will strive for a "reasonable" consistency wherever possible. The values that we recommended for the ***pmd****CRC* community are "reasonable" from a modeler's point of view (i.e., they reproduce the natural or experimental equilibria to the satisfaction of the maintenance team). For an external user, we leave the choice of the selected datasets and responsibility for this choice entirely to himself/herself.

The overall maintenance, access, and development concept has similarities with the Common Thermodynamic Database Project (CTDP) at the Paris School of Mines (Van der Lee, 2004), though the latter renders a compilation of selected thermodynamic properties of chemical reactions with all exploitable data available up to 300°C. Similar to CDTP, the constants and values in FreeGs are not forcibly certified, and a confidence-level is attributed instead.

FreeGs implementation stages

FreeGs is being implemented in the following stages:

Completed:

- Implementation of the database and the web-based database maintenance system – Completed February 2004
- Database population and maintenance – Ongoing, with the goal to include all major thermodynamic datasets for geochemistry by June 2006
- Implementation of algorithms to calculate selected thermodynamic properties of database species (eg, apparent free energies of formation and log K values of chemical reactions) at high temperatures and pressures – Completed August 2004 (release of Beta version)

On-going within the second stage of the ***pmd****CRC* (within the Modeling module):

- Database population and maintenance – Ongoing, with the goal to include all major thermodynamic datasets for geochemistry by June 2006
- Implementation of a web service (WFS) that will enable users to output the "primary" and recalculated data (eg, _g(T,P) or log Kr(T,P)) to clients computers and applications using XML – December 2006

Vision for the FreeGs Database

The ultimate vision for the FreeGs web services can be summarized by the following picture that illustrates the "seamless" access to primary and "derivative" FreeGs data using the FreeGs web service:

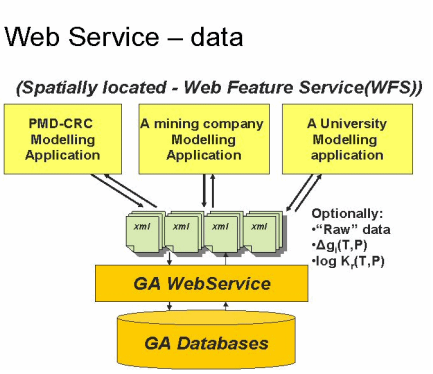

FreeGs team

During the first stage of the ***pmd*CRC***, the FreeGs development team was as follows:

- Concept – E. Bastrakov[1], Yu. Shvarov[2], L. Wyborn[1]
- Programming: S. Girvan[1], P. Scheffer[1], Yu. Shvarov
- Database content maintenance team – E. Bastrakov, J. Cleverley[3], D. C. "Bear" McPhail[4]
- Database custodian at Geoscience Australia – E. Bastrakov

[1] Geoscience Australia & ***pmd*CRC***; [2] Moscow State University & ***pmd*CRC***; [3] James Cook University & ***pmd*CRC***; [4] Australian National University & CRC LEME

FreeGs is considered to be an "open" project with the intent of bringing together the researchers involved in modeling of geochemical processes over a wide range of temperatures and pressures. We encourage external users interested in using this system to send us their constructive suggestions, bug reports, data and computational algorithms that they might want to share.

In addition, they can join the database maintenance team with direct access to data entry and editing forms.

Project partners

Beyond ***pmd*CRC***, the current FreeGs partners are:

- LEME (The Cooperative Research Centre for Landscape Environments and Mineral Exploration) at the Australian National University
- Metals and Solutions (HyDAC) group at the South Australian Museum, University of Adelaide, and CSIRO

References

Bastrakov, E., Shvarov, Y., Girvan, S., Cleverley, J., and Wyborn, L., 2004, FreeGs: web-enabled thermodynamic database for modeling of geochemical processes, in McPhie, J., and McGoldrick, P., editors, Dynamic Earth: Past, present and future. Abstracts of the 17th Australian Geological Convention, Hobart, Tasmania, Australia. February 8-13, No 73, p. 52.

Bastrakov, E., Shvarov, Y., Girvan, S., Cleverley, J., McPhail, D., and Wyborn, L. A. I., 2005, FreeGs: a web-enabled thermodynamic database for geochemical modeling: Geochimica et Cosmochimica Acta: Goldschmidt conference abstracts 2005, v. 69, No. 10, Supplement 1, 15 May 2005, p. A845.

Shvarov, Y. V., 1999, Algorithmization of the numerical equilibrium modeling of dynamic geochemical processes: Geochemistry International, v. 37, 6, p. 571-576.

Shvarov, Y. V., and Bastrakov, E. N., 1999, HCh: a software package for geochemical equilibrium modeling. User's Guide: Australian Geological Survey Organisation, Record 1999/25, 61 p.

Van der Lee, J., 2004, Common Thermodynamic Database Project, http://ctdp.ensmp.fr/index.html

Chapter 9: Improvements in modelling the two-phase field for H_2O-CO_2-CH_4±NaCl fluids

Evgeniy N. Bastrakov and Yuri Shvarov

Summary

Two fundamental problems are associated with modelling hydrothermal fluids containing high concentrations of gas components: (1) changes in the solvent properties, and (2) effects of fluid immiscibility (fluid phases separation). Both effects will significantly affect solubilities of ore components, and cannot be disregarded (e.g., Akinfiev and Zotov, 1999 and references therein; Bowers, 1991 and references therein). Multi-purpose off-the-shelf geochemical modelling packages do not allow to take these processes into account properly. Thus we attempted to develop an add-on module for the HCh package for geochemical modelling as a proof-of-concept for one of the possible approaches – incorporation of the improved Peng-Robinson equation of state for calculation of the activity coefficients of the volatile species both in the gas and liquid phases into a free energy minimisation program (Gibbs; Shvarov, 1999).

The results are partially successful and require a follow-up research in the second stage of the ***pmd****CRC*. Interim results were initially reported in Bastrakov and Shvarov (2004).

Introduction

One of the activities of the Fluids module of the ***pmd****CRC* is to improve calculation capabilities of the available geochemical packages to address the modelling problems pertinent to the specific ***pmd****CRC* goals. An example of such a problem is modelling of mobilization, transport, and deposition of metals in gas-rich (e.g., Xgas > 5 mol%) water-salt fluids. This is especially important for understanding of the processes controlling the distribution of the Yilgarn lode gold deposits, as well as the distribution of ore at the deposit scale (e.g., Mernagh et al., 2005).

Overall, lode gold deposits were emplaced over a substantial range in pressure-temperature (PT) conditions (200 to > 600˚C, < 1 to 4 kbar). Despite this diversity, the ore-forming fluids exhibit similar characteristics: they are near neutral, low salinity (3 to 7 wt% NaCl equivalent) H_2O-CO_2±CH_4 fluids (5 to 25 mol% CO_2+CH_4), with redox conditions often near the aqueous CO_2/CH_4 buffer. Quite frequently, these fluids underwent separation of a generic supercritical H_2O-CO_2±CH_4-salt fluid into essentially aqueous phase and CO_2-rich gas, resulting in liquid-gas fractionation of components controlling gold solubility (e.g., H_2, H_2S).

The Problem

Two fundamental problems are associated with modelling fluids containing high concentrations of gas components: (1) changes in the solvent properties, e.g., the dielectric constant of the mixed water-gas fluids (Akinfiev and Zotov, 1999 and references therein), and (2) effects of fluid immiscibility (Bowers, 1991). Both effects will significantly affect solubilities of ore components, including gold (Akinfiev and Zotov, 1999; Bowers, 1991).

Despite the numerous equations-of-state (EOS) available in the geochemical literature (see Bakker, 2003 for a comprehensive list of references), there is no unified and numerically-effective approach that allows accurate simultaneous simulation of supercritical fluid densities, sub-critical immiscibility, and solubility of minerals in multi-component geochemical fluids. The problem with many EOS is that they are tuned for particular chemical systems, do not allow incorporation of additional chemical components, and are quite complicated in nature, containing numerous empirically-fitted cross-interaction parameters (e.g., Duan et al., 2003). This precludes their ready extension into multi-component systems and incorporation in popular codes for mass-transfer geochemical modelling. The main goal of the current sub-project was to develop numerical algorithms for calculation of activity coefficients of fluid components in supercritical and heterogeneous fluid mixtures for incorporation into one of the popular packages for geochemical modelling, HCh (Shvarov, 1999). Subsequently, these algorithms can be incorporated into other modelling packages of the ***pmd****CRC* modelling framework.

Suggested approach

The main issue is the merger of the "symmetrical" description of the two-phase fluids (as provided by some gas EOS), with non-symmetrical description provided by conventional geochemical packages (i.e., essentially water-rich fluid with the dedicated precise EOS for water versus the gas phase with a special "gas"-oriented EOS). The latter approach cannot adequately address the changes in the activity coefficients of the liquid water and the dissolved gases in a gas-rich liquid phase; this makes reproduction of the phase equilibria impossible in a significant area of the PTX compositional space even for simple systems.

A resolution of this problem was suggested by Bowers (1991) who suggested using a "gas" equation of state to calculate fluid densities and activity coefficients of "liquid" water and the dissolved gases in the mixed fluid; these activities then can be plugged back into the "liquid" phase defined according to the modified Helgeson-Kirkham-Flowers model. A number of authors (e.g., Bowers, 1991; Akinfiev and Zotov, 1999) used this approach for supercritical fluid mixtures applying modified versions of the Redlich-Kwong equation of state. However, they have not attempted to extend this approach to reproduce the phase immiscibility boundaries within their modelling software. For example, Bowers (1991) had to use empirical polynomial fitting of the H_2O-CO_2 solvus as a function of pressure in her version of EQ3/6 software.

In this study, we have attempted to assess the feasibility of the application of the improved Peng-Robinson equation of state (Stryjek and Vera, 1986) for the description of supercritical and two-phase fluids in the water-gas systems for geological problems. This equation is well known in chemical engineering and was developed specifically to reproduce liquid-gas equilibria. The Peng-Robinson-Stryjek-Vera EOS is attractive because it is simple, general, and provides a potential for incorporating new gas components with minimum knowledge of the gas cross-interaction parameters.

Implementation

Most up-to-date versions of HCh allow users to create their own add-on dynamic link libraries (dll) for calculation of activity coefficients of components of the specified solution phases. Thus, we have developed a module (PRSV_aq.dll) that complements the free energy minimisation solver of HCh, Gibbs, and calculates the activity coefficients of the specified components of the liquid phase (e.g., H_2O(aq) and the dissolved gases such as CO_2(aq)) according to the Peng-Robinson-Stryjek-Vera EOS. The latest version of the module developed within the F1-2 project utilizes (1) either the cross-interaction parameters automatically calculated from the geometric mixing rules using the data for pure gases, or (2) can include one binary interaction parameter. The latter implementation is sufficient for testing the module against experimental data for binary water-gas systems.

Current Results

The approach was tested against the available experimental data on the H_2O-CO_2 (Figures 9-1, 9-2), and H_2O-CH_4 systems.

As can be seen from the figures, we have managed to improve the performance of HCh in modelling water-

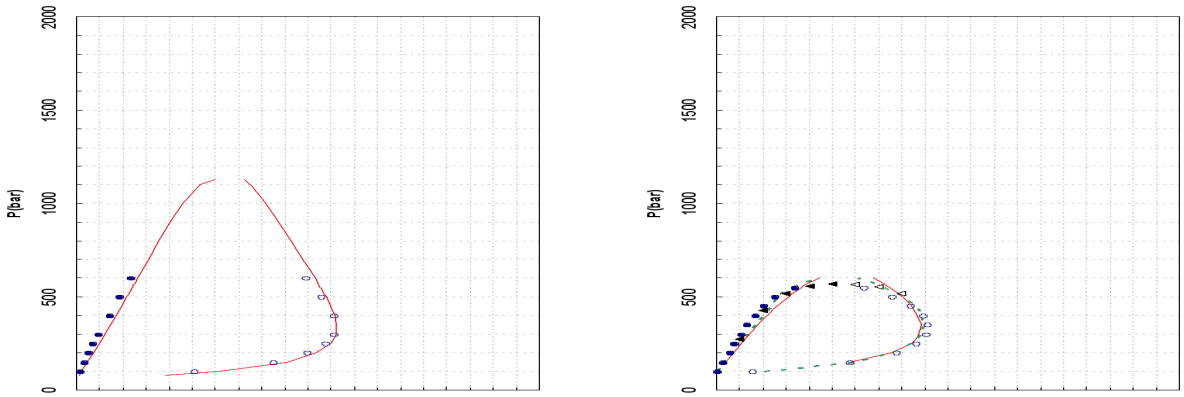

Figure 9-1. Isotherms showing the compositions of gas and liquid phases in the system H_2O-CO_2,: calculated (lines, k_{ij}=0.05) vs experimental (points) results. The filled symbols represent data for the "aqueous" liquid phase, and open symbols – data for the gas phase; Experimental data: circles – Takenouchi and Kennedy (1964); triangles – Blenkoe et al. (2001). (a) 275°C; (b) 300°C. The dotted line is calculated with a comprehensive EOS of the program GEOFLUIDS referenced in Duan et al. (2003).

gas mixtures, and reproduce the main features of the water-gas diagrams. The software now reproduces the H_2O-CO_2 solvus over a wide range of PT parameters. The current performance cannot match the accuracy of the published EOS specifically tuned for the H_2O-CO_2±CH_4±NaCl system, but demonstrates some promise of the suggested method. Though the topology of the diagrams is reasonably reproduced adopting a simplified approach (using the geometric mixing rules based on the data for pure gases), introduction of an additional empirical parameter (binary interaction coefficient) significantly improves the prediction (see Figures, calculations with the binary interaction parameter k_{ij} = 0.05). In fact, in case of the H_2O-CO_2 system, the quality of the gas-liquid solvus prediction can be as good as the solvus calculated with the multi-parameter EOS of Duan et al. (2003).

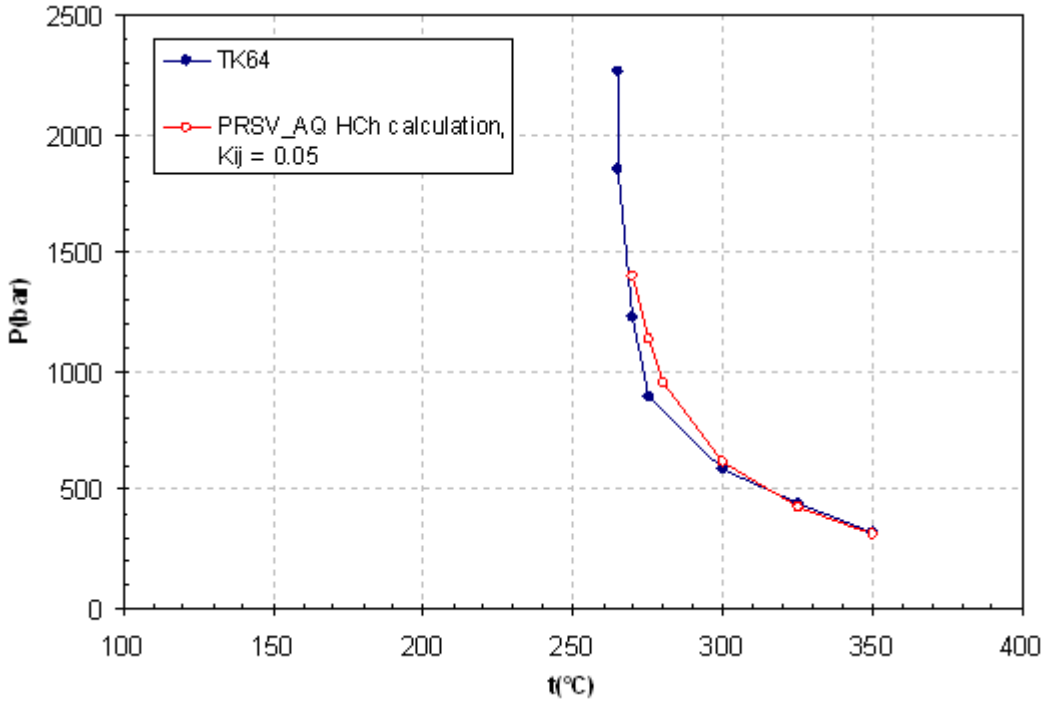

Figure 9-2. PT projection of the part of the critical curve of the system H_2O-CO_2 (calculated vs experimental results). Experimental data are from Takenouchi and Kennedy (1964).

Identified problems

Despite the initial apparent success achieved for the definition of the solvus of water-gas systems like H_2O-CO_2, H_2O-CH_4 and similar, subsequent testing revealed two problems:

1. Currently, the Gibbs minimization code of the HCh package fails to reproduce the water-gas solvus for some compositional ranges. This problem is related to the shape of the free energy surface of the water-gas mixture.
2. Attempts to use “the dual approach” to define activity coefficients of different types of aqueous species via different models (i.e., the PRSV EOS for water plus the dissolved gases, and the Debye-Hückel equation for the ionic solutes) in salt-bearing aqueous solution fail to reproduce the liquid-gas solvuses correctly and consistently.

Conclusions

In spite of the promise of the suggested approach, the way forward is probably in adopting only one activity coefficient model for all types of the dissolved species in the aqueous phase. This might be another modification of the Peng-Robinson-Stryjek-Vera EOS that would incorporate terms to account for electrostatic interaction between solute species. Some examples can be found in the chemical engineering literature.

Both problems will be investigated within the second half of the ***pmd****CRC* in collaboration with external partners.

References

Akinfiev, N. and Zotov, A., 1999. Thermodynamic description of equilibria in mixed fluids (H_2O-non-polar gas) over a wide range of temperature (25–700°C) and pressure (1–5000 bars). Geochimica et Cosmochimica Acta, 63, 2025-2041.

Bakker, R. J., 2003. Package FLUIDS 1. Computer programs for analysis of fluid inclusion data and for modelling bulk fluid properties. Chemical Geology, 194, 3-23.

Bastrakov, E., and Shvarov, Y., 2004, The two-phase problem of modelling complex fluids, in Barnicoat, A. C., and Korsch, R. J., eds., Predictive Mineral Discovery Cooperative Research Centre - Extended Abstracts from the June 2004 Conference. Geoscience Australia, Record 2004/09, p. 13-16.

Blencoe, J. G.,Naney, M. T. and Anovitz, M. L., 2001. The CO_2-H_2O system: III. A new experimental method for determining liquid-vapor equilibria at high subcritical temperatures. American Mineralogist, 86, 1100–1111.

Bowers, T. S., 1991. The deposition of gold and other metals: pressure-indiced fluid immiscibility and associated stable isotope signatures. Geochimica et Cosmochimica Acta, 55, 2417-2434.

Duan, Z., Moller, N. and Weare, J. H., 2003. Equations of state for the NaCl-H_2O-CH_4 system and the NaCl-H2O-CO2-CH4 system; phase equilibria and volumetric properties above 573 K. Geochimica et Cosmochimica Acta, 67, 671-680.

Mernagh, T. P., Bastrakov, E., and Wyborn, L., 2005, A comparison of some chemical processes of ore precipitation, in Orogenic and Intrusion-Related Gold Mineral Systems., Structure, Tectonics and Ore Mineralisation Processes (STOMP) Abstracts Volume, EGRU Contribution No.64, p. 89.

Shvarov, Yu., 1999. Algorithmization of the numerical equilibrium modelling of dynamic geochemical processes. Geochemistry International, 37, 571-576.

Stryjek, R. and Vera, J. H., 1986. PRSV: An improved Peng-Robinson equation of state for pure compounds and mixtures. Canadian Journal of Chemical Engineering, 64, 323-333.

Takenouchi, S. and Kennedy, G. C., 1964. The binary system H_2O-CO_2 at high temperatures and pressures. American Journal of Science, 262, 1055–1074.

Tödheide, K. and Franck, E.U., 1963. Das Zweiphasengebiet und die kritische Kurve im System Kohlendioxyd-Wasser bis zu Drucken von 3500 bar. Zeitschrift für Physikalische Chemie Neue Folge, 37, 387–401.

Chapter 10: Productive Interactive Graphics (PIG)

James S. Cleverley[1], Andrew Dent[2] & Robert Woodcock[2]

[1.] ***pmd**CRC at JCU*
[2.] ***pmd**CRC at CSIRO*

Introduction

Productive Interactive Graphics (PIG) is a data visualization package for plotting, reformatting and recalculating the results from HCh models. PIG has recently been used in industry interactive workshops (1-on-1) with live "what if" modelling, results viewed as meaningful plots and instant feedback. Version 1.0 of this package (April 2004) is available to members and sponsors of the ***pmd**CRC*. Details and the downloadable software can be found under the F1/2 pages of the TWiki at:

https://pmdtwiki.arrc.csiro.au/twiki/bin/view/Pmdcrc/PigVersion1

PIG is designed to improve the access to, and interpretation of HCh modeling results. This process also enables the modelling results to be delivered to industry partners in a format that find useful (i.e. mineral modes rather than moles). More importantly PIG has enabled the use of HCh modelling capabilities in one-on-one modelling workshops with industry by speeding up the visualisation of the results of models and creating aesthetic plots quickly. Research use also benefits with the improved time to produce plots and explore all aspects of the geochemical modelling results.

The Development Team

The PIG concept was initiated and scoped by James Cleverley (JCU) and the main software development work was undertaken by Andy Dent and Rob Woodcock (CSIRO Perth). Projects F1/2 and M2 funded the development work. The project began in early 2003 with software engineering starting in September, and version 1.0 was released on the TWiki in April 2004 for general testing by all HCh users. Extra fixes and functionality based on comments received have been added.

What's New in PIG1?

PIG offers the user more than just "plotting the data". The software includes a full recalculation function that enables the results to be recast as different units, or plotting complex functions (i.e. Na/Na+K). There is also a user defined function that allows for custom equations to be used in plotting. Key features of version 1 include:

- Plot data as lines, stacked and normal area fills, stacked and normal bar plots (1 bar per step)
- Use standardised or random colour pallets
- Click labelling of graphs
- Full unit recalculations from the basic HCh units, including volumes and masses
- Log10, Ln, linear and delta (change in) graphs
- Plot selections or full data, minerals, aqueous, and element concentrations
- User defined and customised data plotting
- Easily plot 1D sections from 2D data grids
- Export graphs to wide range of image formats or "save to clipboard" for use in presentations
- Fully control graph formats (labels, fonts etc).

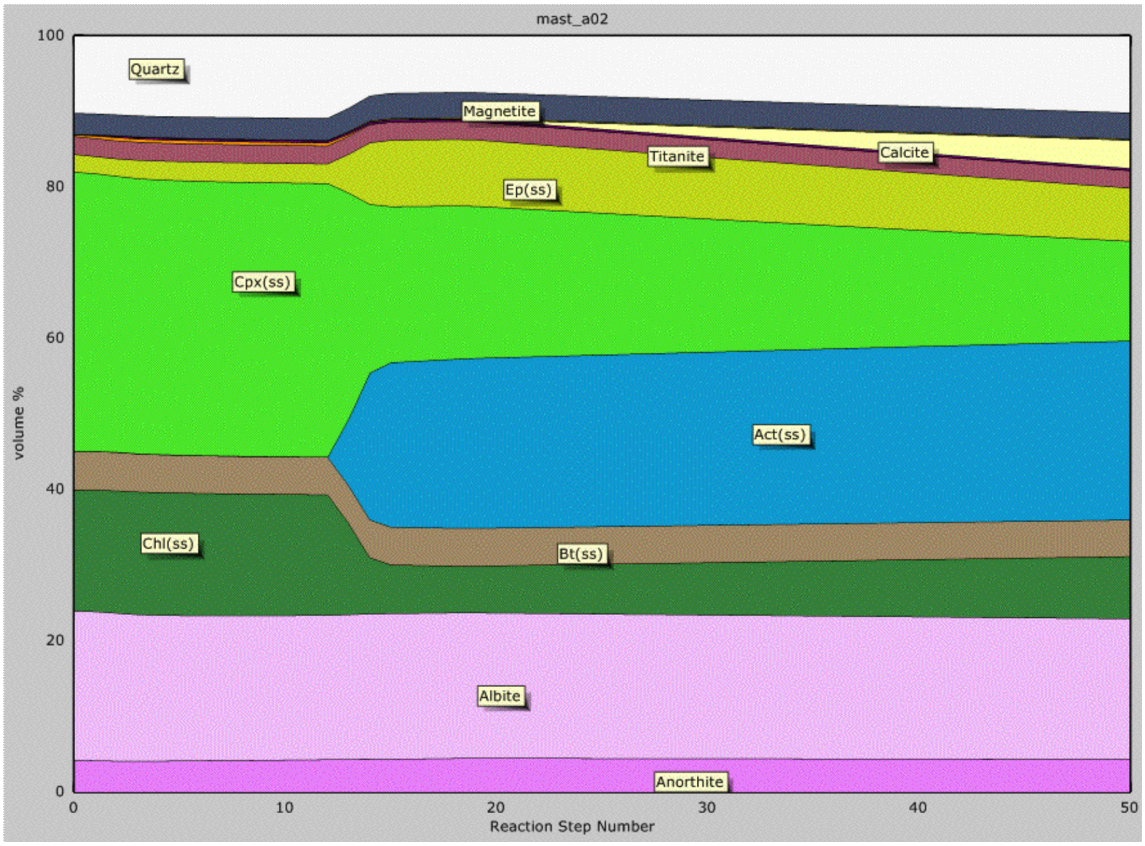

Figure 10-1. Example of a normalised stacked modal mineral plot from PIG showing point and click labels for minerals.

Industry Impact of PIG

PIG allows quick and easy presentation of modelling results in easy to understand format and with the highest impact data units. The software is already proving its worth in the speed of data delivery and the ability to run live 1-to-1 “what if scenarios” with the key exploration geologists. The application of PIG during a live 1-to-1 workshop with AngloGold Ashanti in Brazil (G11 project) in August 2004 was highly successful and allowed real time progress to be made where this was not possible previously.

Future Developments

Building on the sucessful development and implementation of PIG version 1, plans are already in process for version 2. New features will be dedicated to the visualisation of data in 2D and include new “click-box” style formats that allow users to view the spatial distribution of minerals or mineral assemblages from 2D grid results. This development is part of the ***pmd*CRC*** commitment to developing better methods to present and deliver data and results to the industry sponsors.

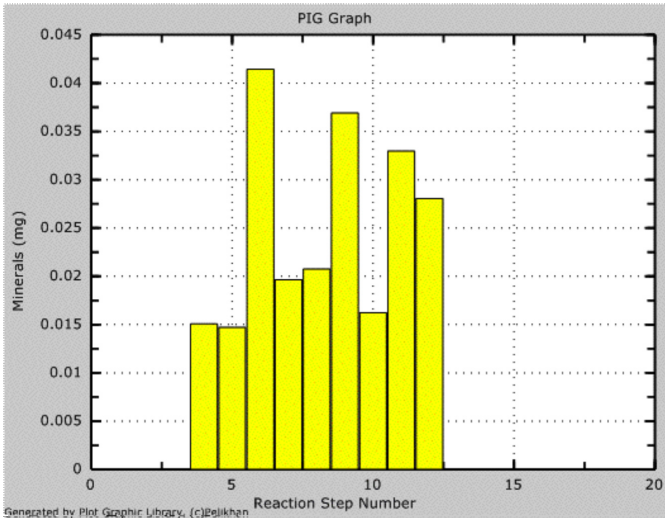

Figure 10-2. Predicted gold distribution and grade. Generation of these plots is almost instantaneous and they can be quickly compared with other plots from the same model.

Chapter 11: Elf - a geochemical modelling tool for economic and exploration geologists and geology students

Bastrakov, E. N., Shvarov, Y., Cleverley, J. S., Fox, N. P., and Oliver, N. H. S.

This paper is modified from:
Bastrakov, E., Shvarov, Y., Cleverley, J., Fox, N., and Oliver, N., 2005, Elf: a geochemical modelling tool for economic and exploration geologists, Structure, Tectonics and Ore Mineralisation Processes (STOMP) Abstracts Volume, EGRU Contribution No.64, p. 8.

Summary

The program Elf has been developed as a user-friendly tool for geochemical modelling (Bastrakov et al., 2005). It is aimed at two target audiences:

- Geologists and geology students without previous experience in geochemical modelling
- Geochemists solving a number of routine tasks involving significant amount of calculations for similar problems using different system compositions

The program is based on the HCh package for geochemical modelling (Shvarov, 1999; Shvarov and Bastrakov, 1999). It requires components of the HCh package pre-installed on your computer. However, it does not require a complete HCh package. Also, usage of Elf itself does not assume any knowledge of the HCh package or skills in its application.

The user does not need to prepare modelling files other then files containing compositions of rocks, aqueous solutions, and gases. Even in the latter case, the program is supplied with a number of reference compositions that can be used for generic modelling exercises.

Introduction

Geochemical modelling of ore-forming systems has been practiced for more than 30 years (Helgeson, 1971). Within this time, a number of “standard” fluid-rock interaction models have been developed by academic researches and have become widespread in the economic geology literature. These models have been applied to ore-forming processes with different degrees of success; though still confined by the limitations of physical chemistry, they can be undoubtedly useful (e.g., Heinrich et al., 1996), as demonstrated by other chapters of the current report.

However, the uptake of geochemical modelling by the mineral exploration industry has been rather limited. Two obvious reasons are: (1) insufficient literacy of the majority of geologists to set up and run geochemical models; and (2) user-interface deficiencies of the geochemical modelling packages that are generally oriented towards highly-specialised experts. This circle was broken in the hydrogeological, environmental, and geothermal specialties, where the software market is large and the value of geochemical modelling is historically well appreciated. This resulted in the advent of user-friendly software packages like Geochemist’s Workbench® (Bethke, 1996). Economic geology, with its enormous ranges of pressures, temperatures, and ranges of fluid compositions, was generally left untouched by these developments.

Questions asked by economic and exploration geologists are often very straightforward, eg,: “Provided a chemical model complied by an expert is reasonable and within its limitations, what would happen if I react fluid A with rock B according to a popular scenario C?” This means that a significant number of popular models in typical chemical systems do not need to be re-invented or re-coded for each modelling run. What is required is software that allows the user to readily adopt these models for the constraints pertinent to his or her specific problem.

To address this issue, we have developed a software “handbook” for geochemical modelling, Elf. Elf is based on the core components of the geochemical modelling package HCh (Shvarov & Bastrakov, 1999). HCh is well suited for a number of geological problems routinely solved by economic geologists, and the predictive mineral discovery CRC has selected it as its primary geochemical modelling tool.

The program specifications have been compiled via interactive consultations with the ***pmd**CRC* modeling stakeholders from academia and industry.

Main features

The main program features are as follows:

- Pre-defined chemical systems hidden behind its interface. These systems, optimised for work with the aqueous phase and “pure” minerals ± solid solutions ± gas phase, include 18 chemical elements (13 “petrogenic” elements + 5 “economic” elements, H-O-C-Cl-S-Na-K-Ca-Mg-Fe-Si-Al-Ti-Ag-Au-Cu-Pb-Zn)
- Predefined set of popular geochemical models (modelling scenarios)
- Predefined set of reference compositions of rocks, aqueous solutions, and gases
- Flexibility in defining compositions of rocks, aqueous solutions, and gases via:
  - Interactive dialog data entry
  - Recycling of calculation results
  - Filtered import of data from geochemical databases
- Spreadsheet-oriented output of results into database-style tab-delimited text files

The default chemical system files can be amended by an experienced HCh user if necessary, provided a complete HCh package is installed on user’s system.

A summary of Elf specifications and the working files structure are found in documentation that accompanies the installed program.

The following figure illustrates the main Elf interface for competing routing geochemical modelling tasks.

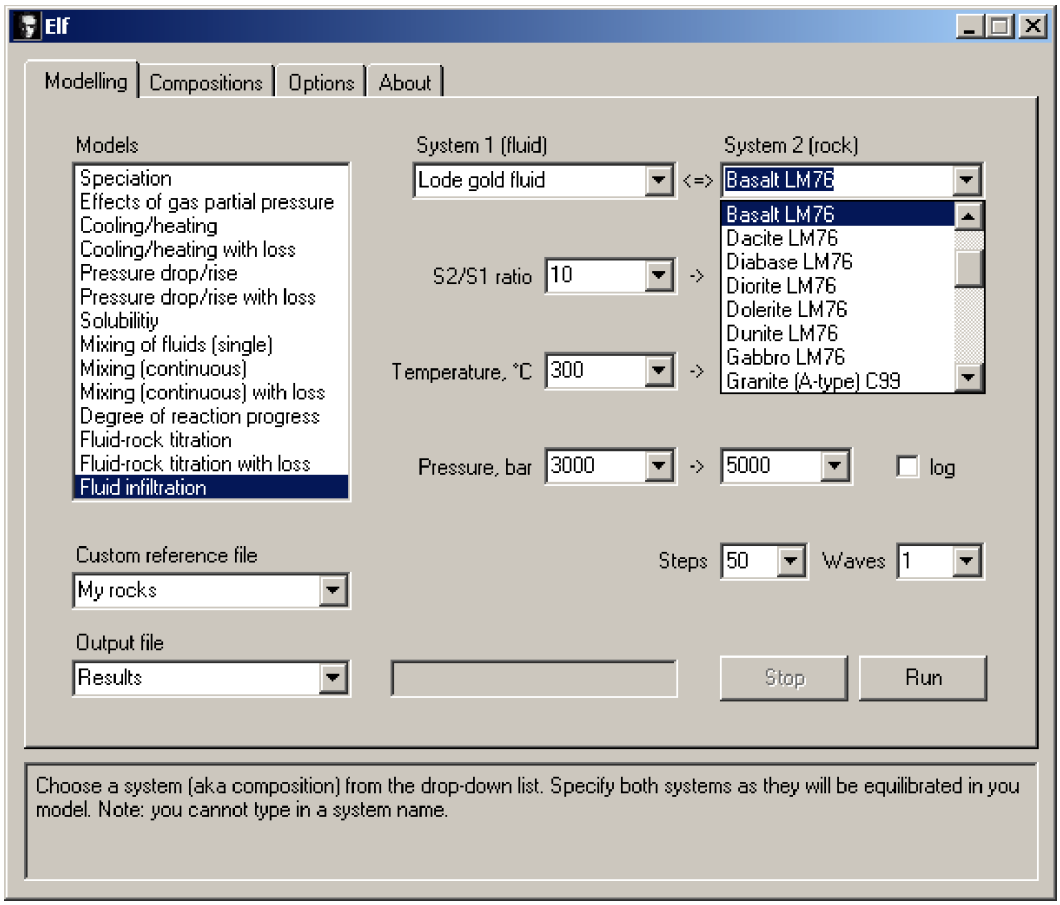

Figure 11-1. Main Elf user interface.

The output tab-delimited text files of results can be read by any text editor or a spreadsheet program. Currently, visualisation of results is achieved using Excel or a similar program; Integration with the PIG software for visualisation of the HCh modeling results has been scoped and will be implemented down the track.

Current status

Completed:

- The initial version of the program was released for ***pmd****CRC* in March 2005
- The program is currently employed by a number of ***pmd****CRC* projects

The "proof-of-the-concept" testing suggests that Elf can be used as an efficient tool for introduction to geochemical modeling; However, its use by geologists and geology students without previous experience in geochemical modelling is constrained by the degree of their overall understanding of hydrothermal geochemistry.

Further developments within the second stage of the ***pmd****CRC* (within the Modeling module):

- Additional compilation of standard reference compositions
- Integration with the PIG visualisation software
- Batch processing for a selection of reference compositions in a true modelling mode (subject to time availability)

References

Bastrakov, E., Shvarov, Y., Cleverley, J., Fox, N., and Oliver, N., 2005, Elf: a geochemical modelling tool for economic and exploration geologists, Structure, Tectonics and Ore Mineralisation Processes (STOMP) Abstracts Volume, EGRU Contribution No.64, p. 8.

Bethke, C., 1996, Geochemical reaction modeling; concepts and applications: New York, Oxford University Press, 397 p.

Heinrich, C. A., Walshe, J. L. & Harrold, B. P., 1996, Chemical mass transfer modelling of ore-forming hydrothermal systems: current practice and problems, Ore Geology Reviews, 10, 319-338.

Helgeson, H., 1971, Kinetics of mass transfer among silicates and aqueous solutions, Geochimica et Cosmochimica Acta, 35, 421-469.

Shvarov, Yu. V., 1999, Algorithmization of the numerical equilibrium modelling of dynamic geochemical processes: Geochemistry International, v. 37, p. 571-576.

Shvarov, Yu. V. & Bastrakov, E. N., 1999, HCh: a software package for geochemical equilibrium modelling, User's Guide. Australian Geological Survey Organisation, Record 1999/25, 61 p.

Appendix: List of Digital Appendices

Use the links below to open the supporting digital data relating to the F1/2 project. Where the supply of material would contravene copyright, the full reference is given.

Annual Reports

Annual Report 2002

Annual Report 2003

Annnual Report 2004

Quarterly Reports

F1 Quarterly Reports

September 2002 Quarterly Report

December 2002 Quarterly Report

March 2003 Quarterly Report

September 2003 Quarterly Report

F2 Quarterly Reports

December 2002 Quarterly Report

March 2003 Quarterly Report

F1/2 Quarterly Reports

September 2003 Quarterly Report

December 2003 Quarterly Report

March 2004 Quarterly Report

September 2004 Quarterly Report

December 2004 Quarterly Report

Annual Review, 2002 (Canberra)

Presentations

F1 presentation

F2 presentation

Posters

F1 poster

Annual Review, 2003 (Perth)

Presentations

Fluids overview presentation (Nick Oliver)

Posters
Fluids posters (multi-page pdf file)

Annual Conference, 2004 (Barossa Valley, SA)
Abstracts & Presentations

Bastrakov E.N. & Shvarov Y.V., 2004. The two-phase problem of modelling complex fluids. *In: Barnicoat, A.C. & Korsch R. J. eds. Predictive mineral discovery Cooperative Research Centre - Extended Abstracts from the June 2004 Conference*. Geoscience Australia Record 2004/09.

Link to abstract Link to presentation

Kühn M., Alt-Epping P., Gessner K. and Wilde A., 2004. Application of reactive transport modelling to the Mount Isa copper mineralised system, 2004. *In*: *Barnicoat, A.C. & Korsch R. J. eds. Predictive mineral discovery Cooperative Research Centre - Extended Abstracts from the June 2004 Conference*. Geoscience Australia Record 2004/09.

Link to abstract Link to presentation

External Conference Abstracts
Australian Geological Congress 2004 (Hobart, Tasmania)
Bastrakov, E.N., Shvarov, Y.V., Girvan, S.W., Cleverley, J.S. and Wyborn, L.A.I., 2004. FreeGs: Web-enabled thermodynamic database for modeling of geochemical processes. *In: J. McPhie and P. McGoldrick eds. Dynamic Earth: Past, present and future, 17th Australian Geological Convention, Hobart, 8-13 February 2004. Geological Society of Australia Abstracts*, **73**, pp. 52.

SEG2004: Exploration under cover (Perth, WA)
Cleverley J.S., Oliver N.H.S. and Bastrakov E.N., 2004. Geochemical modelling tools in predictive mineral discovery. *In: Muhling J., Goldfarb R., Vielreicher N., Bierlein F., Stumpfl E., Groves D.I and Kenworth S., eds. 2004. SEG 2004 Predictive Mineral Discovery Under Cover; Extended Abstracts.* Centre for Global Metallogeny, The University of Western Australia. Publication No. **33**. pp. 6-11.

Oliver N.H.S., Cleverley J.S., and Bastrakov E.N., 2004. Modelling hydrothermal systems: A future for exploration geochemistry. *In: Muhling J., Goldfarb R., Vielreicher N., Bierlein F., Stumpfl E., Groves D.I and Kenworth S., eds. 2004. SEG 2004 Predictive Mineral Discovery Under Cover; Extended Abstracts.* Centre for Global Metallogeny, The University of Western Australia. Publication No. **33***.* pp 62-66.

Goldschmidt International Geochemistry Conference 2004 (Copenhagen, Denmark)
Cleverley, J.S., Oliver, N.H.S. and Bastrakov E.N., 2004. Reactor style modelling of fluid-rock infiltration and interaction using the HCh software package. Goldschmidt Geochemistry 2004 Conference, Copenhagen, Denmark, 5-11 June 2004. *Geochimica et Cosmochimica Acta,* **68**, No. 11S, pp. A187

Oliver N.H.S, Cleverley J.S, and Bastrakov E.N., 2004. Geochemical simulation of veining and an explanation for bulk mass transfer in fractured rocks. Goldschmidt Geochemistry 2004 Conference, Copenhagen, Denmark, 5-11 June 2004. *Geochimica et Cosmochimica Acta,* **68**

Goldschmidt International Geochemistry Conference 2005 (Moscow, Idaho)
Bastrakov E.N., Shvarov Y.V., Girvan S.W., Cleverley J.S., McPhail D. and Wyborn L.A.I, 2005. FreeGs: A web-enabled thermodynamic database for geochemical modelling. *In: Geochimica et Cosmochimica Act:* Goldschmidt International Geochemistry Conference , Abstracts **69** (10) suppl 1pp. A845.

Gordon Conference 2005
Cleverley J.S., 2005. Volatile (CO_2-H_2O-Cl) transfer between the mantle and upper crust: Brecciation, magmatism and Fe-oxide copper-gold deposits.

STOMP - Structure, Tectonics and Ore Mineralisation Processes 2005
Bastrakov E., Shvarov Y.V., Cleverley J.S., Fox N. and Oliver N.H.S., 2005. Elf: A Geochemical Modelling Toolfor Economic and Exploration Geologists

Fisher L.A., Kendrick M.A. and Mustard R., 2005. Noble and halogen evidence for the source of mineralising fluids in the Osborne IOCG deposit, Mt Isa Inlier, Australia

Cleverley J.S. and Oliver N.H.S, 2005. Crustal Scale Volatile Transfer: Melts and Breccias in the Mount Isa Terrain.

Kuhn M., 2005. Hypothesis testing applying reactive transport simulation with respect to the Mount Isa Copper ore deposit.

Journal Articles
Cleverley J.S. and Bastrakov E.N., 2004. K2GWB: utility for generating thermodynamic data files for The Geochemists Workbench at 0-1000ºC and 1-5000 bars from UT2K and the UNITHERM database. Computers and Geoscience.

Cleverley, J.S. and Oliver, N.H.S., 2004. Equilibrium Dynamic Modelling of fluid-rock interaction concepts using HCh: Examples from K-alteration in Fe-oxide Cu-Au systems. Geofluids, (in review).

Oliver N.H.S, Cleverley J.S., Mark G., Pollard P.J., Fu B., Marshall L.J., Rubenach M.J., Williams P.J. and Baker T., 2004. Modelling the role of Sodic Alteration in the Genesis of Iron Oxide-Coppre-Gold Depsoits, Eastern Mount Isa Block, Australia. *Economic Geology,* **90**, pp.1145-1176.

General Presentations
Kühn et al, 2003. Century - Reactive transport modelling presentation

F1-2 team, 2003. Numerical modelling in Predictive Mineral Discovery: Geochemical Models

Yilgarn PDT Delivery Workshop December 2004
Cleverley J.S & Olver N.H.S, 2004. Geochemical models (and preliminary geophysical correlations) pertinent to magmatic contriubtions to ore system hydrology at Wallaby & elsewhere in the Yilgarn

Mt Isa PDT Delivery Workshop March 2005
Cleverley J.S. & Olver N.H.S, 2005. Fluids project: Applied Geochemical Modelling - The Ernest Henry System

Oliver et al., 2005. From source to sink: evolution of fluid systems in the Eastern Succession

Courses
Cleverley J.S. & Olver N.H.S., 2005. JCU/EGRU/CRC Masters Program at JCU. Geochemical Modelling

Cleverley J.S., 2005. STOMP conference shortcourse: Application of Geochemical modelling to Minerals Exploration